The role of the secretory pathway for the mammalian circadian clock

Inaugural-Dissertation

to obtain the academic degree

Doctor rerum naturalium (Dr. rer. nat.)

submitted to the Department of Biology, Chemistry and Pharmacy
of Freie Universität Berlin

by

Dipl. Biochem. Sebastian Jäschke

from Berlin

2017

This thesis was conducted from 2012 to 2017,
supervised by Prof. Dr. rer. nat. Achim Kramer,
at the Laboratory of Chronobiology,
Institute for Medical Immunology,
Charité - Universitätsmedizin Berlin

1st Reviewer: Prof. Dr. rer. nat. Achim Kramer,
Charité - Universitätsmedizin Berlin

2nd Reviewer: Prof. Dr. rer. nat. Florian Heyd,
Freie Universität Berlin

Date of the disputation:
16th of February 2018

Contents

Figures

Tables

List of Appendices

Summary

Circadian clocks are ubiquitous timekeeping mechanisms that are present in all species and have evolved to adapt organisms to a changing environment with a 24-hour light-dark cycle. The circadian network is constructed in a hierarchical manner, with the suprachiasmatic nucleus (SCN) as the master clock in the brain which synchronises slave oscillators in the periphery through humoral signals, temperature cycles and feeding-fasting rhythms. Together, the circadian oscillators regulate a variety of physiological, metabolic and behavioural processes throughout the body. How cell-autonomous circadian clocks in peripheral tissue resist exogenous fluctuations in synchronising signals and keep a stable phase and period coherence is so far unknown. Over the years, intercellular coupling involving secreted paracrine signalling molecules has been proposed, but its existence is highly debated.

Here, we show for the first time that the secretory pathway is important for the generation of normal circadian rhythms. Using RNA interference and pharmacological inhibitors, we perturbed early stages of vesicular protein transport, which led to a drastic lengthening of the circadian period and a reduction in the circadian rhythms' amplitude. Further, we collected evidence that the anterograde protein transport is the most important route for the circadian clock through genetic rescue experiments. This strengthens our hypothesis that secreted signalling molecules and an unperturbed expression of signalling receptors at the cell surface are necessary for normal clock function.

Furthermore, we provide evidence that secreted signalling molecules directly affect the circadian oscillator. Application of conditioned medium from U-2 OS cells immediately phase-shifted circadian rhythms and caused an induction of CRE-mediated transcription. We speculate that unknown signalling molecules activate immediate early genes, a common pathway to integrate timing information into the clock. Finally, we report a direct connection between a cell culture's density and its circadian clock's coupling strength. Low cell density with consequently low concentrations of secreted signalling molecules led to circadian oscillations with longer periods and severely decreased amplitudes. These effects can be rescued using wild-type, but not secretion-deficient U-2 OS cells. This further highlights the importance of the secretory pathway and the presence of paracrine signalling molecules for circadian period and phase coherence through coupling in peripheral tissues.

Zusammenfassung

Zirkadiane Uhren sind allgegenwärtig und in nahezu jeder Spezies zu finden. Sie haben sich evolutionär entwickelt, um Organismen eine Anpassung an den 24 Stunden Licht-Dunkel-Zyklus zu ermöglichen. Das zirkadiane Netzwerk ist hierarchisch aufgebaut mit dem Nucleus suprachiasmaticus (SCN) als Hauptuhr an der Spitze, welcher die Oszillatoren in den peripheren Organen durch lösliche Faktoren im Blut, Temperaturzyklen und tageszeitlich gesteuerte Nahrungsaufnahme synchronisiert. Zusammen steuern die zirkadianen Uhren eine Vielzahl an physiologischen und metabolischen Prozessen im Körper sowie unsere Aktivitäts- und Ruhephasen. Wie zellautonome, zirkadiane Uhren in peripheren Geweben sich vor störenden Fluktuationen in exogenen Synchronisationsfaktoren schützen um eine stabile, zirkadiane Periode und Phase zu bewahren, ist bisher nicht ausreichend aufgeklärt. In den vergangenen Jahren wurde in diesem Zusammenhang über die Existenz von interzellulärer Kopplung der zirkadianen Uhren spekuliert, aufrecht erhalten durch sekretierte, parakrine Faktoren.

Im Rahmen dieser Doktorarbeit zeigen wir erstmalig die Wichtigkeit des sekretorischen Transportweges für die zirkadiane Uhr. Durch den Einsatz von RNA-Interferenz und pharmakologischen Inhibitoren störten wir den vesikulären Transport zwischen Golgi und ER, was zu einer drastischen Periodenverlängerung und einer Verringerung der Amplitude des zirkadianen Oszillators führte. Darüber hinaus, konnten wir zeigen, dass vor allem der anterograde Proteintransport wichtig für 24-Stunden Rhythmen ist. Dies bestärkt uns in dem Glauben, dass die Sekretion von Signalmolekülen und die unveränderte Expression von Oberflächenrezeptoren für die Aufrechterhaltung von zirkadianen Oszillationen notwendig sind.

Zusätzlich liefern wir Hinweise darauf, dass sekretierte Signalmoleküle den zirkadianen Oszillator direkt beeinflussen. Die Applikation konditionierten Mediums von U-2 OS Zellen bewirkte eine sofortige Phasenverschiebung in der Expression von Leuchtkäfer-Luziferase in U-2 OS Reporterzellen. Zudem beobachteten wir eine Aktivierung von CRE-vermittelter Genexpression nach Zugabe von konditioniertem Medium. Wir vermuten, dass über diesen Signalweg die Transkription von „immediate early genes“ induziert wird, welche auch bei der Integration von anderen externen Signalen in den zirkadianen Oszillator eine zentrale Rolle spielen. Abschließend verknüpfen wir die Dichte mit der Kopplungsstärke einer Zellkultur. Bei abnehmender

Zellzahl und damit einhergehender Reduktion von sekretierten Faktoren verlängert sich die Periode und verringert sich die Amplitude zirkadianer Rhythmen. Diese Effekte können durch die Zugabe von wild-typ Zellen, nicht jedoch durch sekretionsdefiziente Zellen wieder umgekehrt werden. Diese Erkenntnisse betonen abermals die Wichtigkeit des sekretorischen Transportwegs und einer ausreichenden Menge an sekretierten Signalmolekülen für die Aufrechterhaltung von stabilen zirkadianen Perioden und Phasen durch die Kopplung zirkadianer Oszillatoren in peripheren Geweben.

1 Introduction

1.1 Biological rhythms as ubiquitous timekeeping systems from an evolutionary perspective

All life on planet Earth is subject to constant changes in its environment. Some of these changes are single events and unpredictable other changes reoccur on a periodic basis and can, therefore, be anticipated. The most prominent rhythms in our nature are the daily cycles of light and dark caused by the counter clockwise rotation of the Earth around its own axis and the annual cycles of seasons generated by the orbiting of the Earth around the sun. As a result, all living organisms experience daily changes in temperature, humidity and exposure to ultra violet (UV) light. Anticipation of rather than reaction to these changes reduces the organism's energy costs as it replaces an unfavourable constant production of metabolites and enzymes with an adapted production regulated in a time-of-day-dependent manner. Today, it is widely believed throughout scientific circles that circadian rhythms emerged for evolutionary reasons and advanced further under selective pressure. Intriguingly, circadian rhythms can be found in any organism investigated ranging from cyanobacteria[1] to fungi[2], plants[3], fish[4], insects[5] up to mammals[6]. This ubiquity further strengthens the hypothesis of an evolutionary benefit.

One of the first supporters of this hypothesis was Collin Pittendrigh arguing in his "escape-from-light" theory, that early organisms developed the first timekeeping mechanisms to protect their fragile DNA from the damaging UV light[7]. Furthermore, he reasoned, that the "necessity to avoid reactions that would proceed spontaneously at physiological temperatures" advanced and shaped the circadian clock. One example is the fixation of nitrogen in cyanobacteria that takes place at night timely-separated from the photosynthesis to protect the enzymes necessary for nitrogen fixation from the destructive effects of oxygen[8]. Finally, circadian rhythms not only control and regulate intrinsic processes but translate beneficially on a behaviourally level as well. For instance, animals have adjusted their active and resting phases according to the availability of food, the risk of encountering predators and the likelihood of mating.

In 2004, Carl Johnson and colleagues were the first ones to show that the adaptation of cyanobacteria to the exogenous light-dark-cycle had indeed a fitness value.

They subjected cyanobacterial strains with differing clock properties to varying light-dark cycles and let them grow in competition. As expected the strains that adapted to the 24-hour biological rhythm outgrew clock-impaired competitors under 24-hour light-dark-cycles[9]. Further, clock-impaired strains that showed an internal free-running period of 22 or 30 hours that grew in resonance with the exogenous light-dark cycle (LD11:11 or LD15:15) outgrew the wildtype strains that adapted to the 24-hour light-dark-cycle. In 2016 Michaela Hau and colleagues tested the hypothesis that "natural selection should favour circadian systems that operate in resonance with the external cycle" and monitored the survival and reproduction rate of six individual mouse populations[9]. These populations were all off-spring from two Ck1ε^{tau} - heterozygote parents following the Mendelian distribution, a known mutation which shortens the circadian period by two hours for each affected allele. Again, the organisms adapted to the environmental light-dark-cycle showed an increased fitness with higher adult survival rates and advanced juvenile recruitment. The frequency of the mutated *tau* allele decreased from 49% in the beginning to 20% in the end over a period of 14 month, exhibiting natural selection against the unfavourable mutation.

1.1.1 History of chronobiology

First observations of daily rhythms in behaviour can be traced back more than two millennia into the year 400 BC. Back then, Androsthenes described the time of day dependent leaf movements of the tamarind tree, *Tamarindus indicus*, during the marches of Alexander the Great[10]. At that time, there were no evidence towards an endogenous timekeeping mechanism and it was not experimentally tested until the 18th century. In 1729, the French astronomer Jean Jacques d'Ortous de Mairan was the first scientist to document experiments on daily leaf movements on the heliotrope plant, *Mimosa pudica*[11]. He noted that the plant's leaves opened during the day and closed at night, keeping this rhythm even in constant darkness without light as an environmental cue. The findings were reproduced independently by various scientists in the years to come and excluded temperature fluctuations as a potential *zeitgeber*[12,13]. Fascinated by the idea that flowers could tell the time of day, the Swedish botanist Carolus Linnaeus proposed a flower clock consisting of plants that would all open and close their leaves at different specific times

of days[14]. In 1832, De Candolle was the first scientist to measure the free-running period of *Mimosa pudica*'s leaf movement under constant conditions. Furthermore, he observed that the inherited rhythm could be inverted by reversing the light-dark-cycle[15]. In 1875, Pfeffer doubted his earlier colleagues' results and proposed leakage of daylight into the otherwise dark room as an important environmental cue. However, his own work erased his doubts and he published many works on endogenous diurnal rhythms[16]. His hypothesis was supported by Charles Darwin who published his book "On the Power of Movement in Plants", emphasising the inherent nature of diurnal periodicity[17]. But early work in chronobiology was not limited to observations regarding leaf movement. For instance, in 1894 A. Kiesel described persisting pigmentation cycles of anthropoids in the absence of light-dark alterations[18]. The first person to coin the term "circadian rhythm" in the context of intrinsic biological timekeeping mechanism was Franz Halberg in 1959, the founder of the chronobiology laboratories at Minnesota University and author of hundreds of scientific publications on circadian rhythms[19]. The first milestone in unrevealing the genes involved in circadian rhythm generation was taken in 1971 by Ronald Konopka and Seymour Benzer who were working with the fruit fly *Drosophila melanogaster*. They identified a gene in a mutagenesis screen which was later called the *period (per)* gene and when mutated led to an altered circadian period or arrhythmicity in locomotor activity[5]. Subsequently, in 1984, Jeffrey Hall, Michael Rosbash and Michael Young succeeded in isolating the *period* gene. For their great discovery they were rewarded the 2017 Nobel Prize in Physiology or Medicine.

1.1.2 Rhythms and biological clocks

The online dictionary Merriam Webster (www.Merriam-webster.com/dictionary) defines the term "biological clock" as follows:

> "*An inherent timing mechanism in a living system that is inferred to exist in order to explain the timing of periodicity of various behaviours and physiological states and processes."*

From a chronobiologist's point of view this definition emphasises nicely the necessity of the time keeping mechanism to be endogenous and inherited. Nonetheless,

the definition does not mention additional requirements for such an intrinsic oscillator to become a functional biological clock. Firstly, it is important to receive and process information from the outside to react to changes in the environment. Secondly, the reception of exogenous information can only be integrated into the system within a narrow range close to the original frequency of the oscillator. This prevents the oscillator from becoming too susceptible to external stimuli. Thirdly, the intrinsic time-keeping machinery keeps running with stable phase and period even in the absence of external stimuli and under constant conditions. This is called entrainment to the external zeitgeber cycle. Finally, the biological clock does not only explain the timing of behaviour and physiological states. In fact, the clock actively drives behaviour and physiology and, therefore, intrinsic timing information are forwarded to operators which control output processes (for a schematic overview, see **Figure 1-1**).

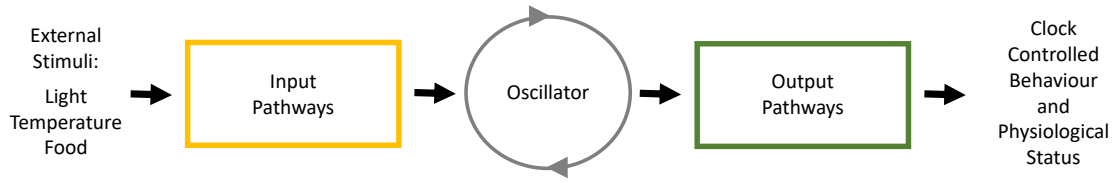

Figure 1-1: Schematic design of biological timekeeping systems. A biological clock consists of three important components: an input pathway (yellow), an oscillator (grey), and an output pathway (green). Endogenous signals such as light, food and temperature act as *zeitgeber* (German; literal translation time-giver). They are detected by the organism's input pathway receptors, processed and forwarded to the central oscillator which integrates the time information into its oscillation. The sustained rhythm is used to anticipate reoccurring exogenous events and translates into rhythmic output of transcriptional and translational events regulating behavioural and physiological processes.

Biological clocks evolved to anticipate rhythmic occurrences in the environment. When we talk about rhythms we refer to highly repetitive oscillations that can be described by well-defined parameters such as period, amplitude, phase and damping. The period of an oscillation represents the time it takes to complete a full cycle (for instance the time it takes from peak to peak or nadir to nadir). The amplitude describes the maximal deflection of an oscillator and the phase is defined as the time difference between a reference point (e.g. the beginning of the oscillation) and an arbitrary point of interest. The damping describes the decrease of amplitude over time in a non-self-sustained oscillation. As stressed previously, naturally occurring rhythms are highly diverse and their cycles range from seconds to years. Accordingly, these biological rhythms are anticipated by different biological clocks and termed by the time it takes to complete one

circle: ultradian, circadian and infradian. Ultradian (lat. ultra dies = “beyond a day” which refers to the frequency) rhythms cycle with short periods under 24 hours. For instance, sleep research refers to the 90-120 minutes long sleep stages of humans as ultradian rhythms. In contrast, infradian (lat. infra dies = “below a day”) rhythms cycle with periods longer than 24 hours. Examples for infradian rhythms are the menstrual cycle or the seasonal cycle. The probably best and most intensively studied rhythms are circadian (lat. circa dies = “about a day”) rhythms that show a period of roughly one day. Over the last century certain criteria were established to distinguish a circadian clock from a diurnal rhythm or a time-of-day-dependent fluctuation:

1. A circadian clock is a self-sustained, inherited oscillation with a period of approximately 24 hours and persists under constant conditions without contribution from environmental *zeitgebers*. Without an exogenous stimulus, the oscillation free-runs. Depending on the intrinsic period, the free-running oscillation might shift out of phase with the superior *zeitgeber* cycle that was previously forced onto it.
2. A circadian clock can be influenced by environmental cues – so called *zeitgebers*. If the environmental cues reoccur in a rhythmic fashion, the oscillator can be synchronized or entrained to the new rhythm over time.
3. A circadian clock is temperature-compensated. It allows the period of the oscillation to remain constant independent of the ambient temperature.

Diurnal rhythms or time-of-day-dependent variations to not encompass these characteristics. They are highly dependent on the environmental zeitgebers reoccurring in a 24-hour schedule and disappear under constant conditions.

1.2 The organization of the mammalian timekeeping system

Circadian clocks are found in almost every tissue and cell throughout the mammalian organism where they drive and modulate physiological and metabolic

functions. 2-10 % of all gene transcripts are rhythmic in peripheral tissues and their rhythmic expression is dependent on local as well as systemic timing cues[20–22]. To keep all the different oscillators synchronized in a coherent phase, the circadian timekeeping system is constructed as a hierarchical multi-oscillator network, with the suprachiasmatic nucleus (SCN) as the central pacemaker at the top that actuates the slave oscillators in the periphery (see **Figure 1-2**). As the master clock, the SCN receives and processes external timing signals, so called *zeitgeber*, and projects this information to other brain regions and the periphery via multiple output pathways. Additionally, peripheral clocks integrate local timing information in order to adjust to metabolic and physiological changes[23,24].

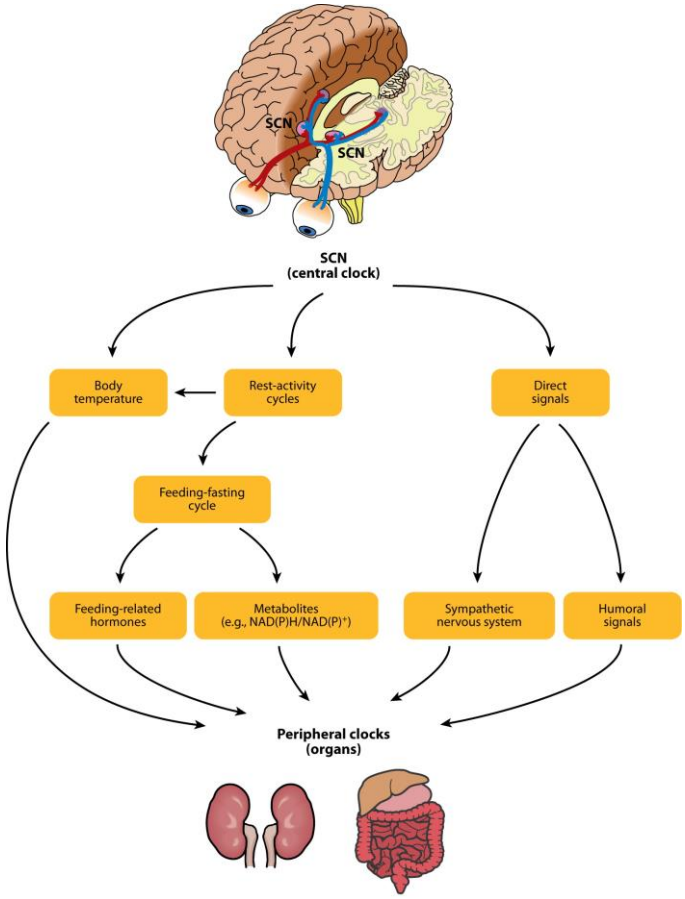

Figure 1-2: The organization of the mammalian time keeping system. The mammalian time keeping system is organized in a hierarchical manner with the SCN as the master clock at the top. Light as the dominant timing cue is perceived through the retina and the retinohypothalamic tract (RHT) and processed in the 20.000 densely packed neurons of the SCN. SCN input information is forwarded to the periphery via several direct and indirect pathways which include innervation by the nervous system, humoral signals, body temperature as wells as rest-activity cycles, feeding-fasting cycles and metabolites (modified from "The Mammalian Circadian Timing System: Organization and Coordination of Central and Peripheral Clocks" by C. Dibner, U. Schibler and U. Albrecht [25]).

1.2.1 The mammalian cellular circadian clock

In mammals, cellular circadian rhythmicity of SCN neurons as well as peripheral cells is achieved through a cell-autonomous autoregulatory transcriptional-translational feedback network (see **Figure 1-3**). The main circuit comprises the transcriptional activators brain and muscle aryl hydrocarbon receptor nuclear translocator-like protein 1 (BMAL1) and circadian locomotor output cycles protein kaput (CLOCK) that dimerize via their basic helix-loop-helix domain and their Per-Arnt-Sim (PAS) domains in the nucleus[26]. As the BMAL1/CLOCK heterodimers bind to E-box containing promotor regions, they positively regulate the transcription of *period1*, *period2* and *period3* (*Per1*, *Per2*, and *Per3*) and *cryptochrome1* and *cryptochrome2* (*Cry1* and *Cry2*) genes[27]. In the cytoplasm, PER and CRY proteins are post-translationally modified and accumulate over time to form oligomeric complexes[28]. With a critical delay, the PER/CRY protein complexes translocate into the nucleus to inhibit CLOCK/BMAL1 transactivation thereby shutting down their own transcription[29–31]. As the protein levels of the negative regulators decline, CLOCK/BMAL1 protein level rise again and start a new cycle. To add more robustness to the circadian transcriptional-translational network, additional loops are intertwined with the core circuit. Most prominent is the second negative transcriptional-translational feedback loop involving REV-ERBα and RORα. The transcription of *Rev-erbα* and *Rorα* are tightly controlled by the positive regulation of the BMAL1/CLOCK heterodimer[32]. The translated proteins are shuttled into the nucleus where they compete for binding to REV-ERB/ROR responsive elements (RREs) in the *Bmal1* promotor region[33,34]. While RORα acts as a positive regulator of *Bmal1* expression, REV-ERBα represses *Bmal1* transcription once bound to the RREs and BMAL1 protein level decrease[35,36]. Other stabilizing loops of the circadian network involve the proteins DBP, HLF, TEF, E4BP4, DEC1 and DEC2 which were shown to be under the transcriptional control of BMAL1/CLOCK. Protein stability and degradation represent additional level of circadian clock regulation. Often, protein turnover rates are determined by tightly regulated post-translational modifications. In the case of PER1 and PER2, phosphorylation by casein kinases 1δ and 1ε (CKIδ/ε) are necessary for subcellular localization but can also lead to the recruitment of the F-box protein β-TrCP or SCF ubiquitin E3 ligase that targets PER proteins for proteasomal degradation[37,38]. CRY1 and CRY2 stability are dependent on the competitive binding of two proteins of the SCF ubiquitin E3 ligases - FBXL3 and its paralog FBXL21[39].

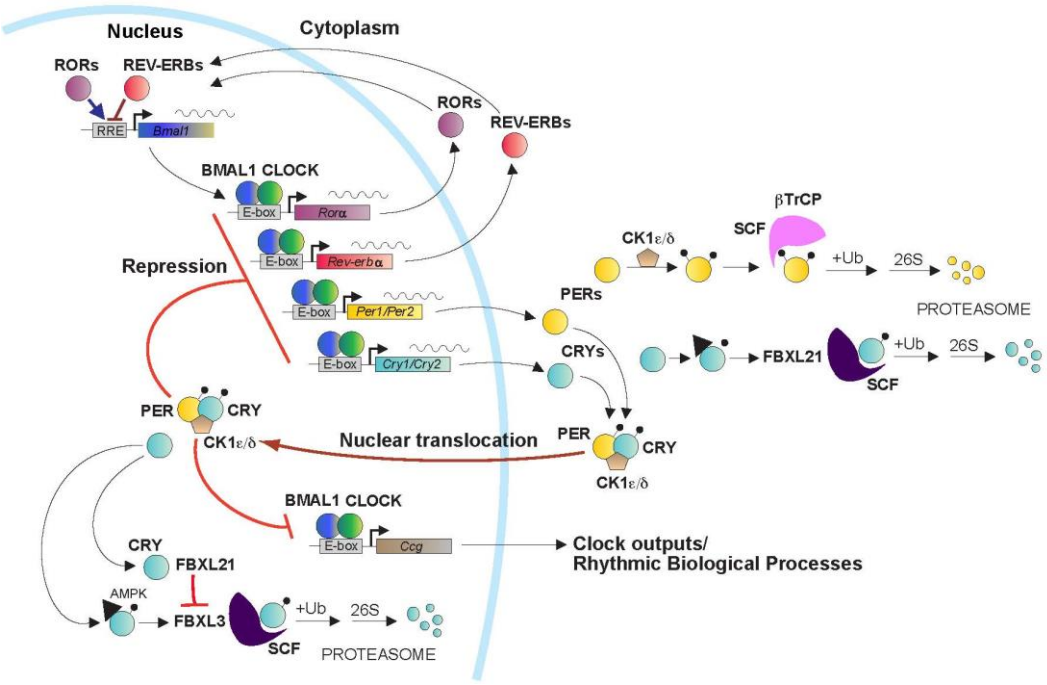

Figure 1-3: Current model of the cellular circadian clockwork in mammals. The mammalian circadian clockwork is comprised of interlocked transcriptional-translational feedback loops. The two transcriptional activators BMAL1 and CLOCK form heterodimeric complexes in the nucleus and bind to enhancer sequences so called E-boxes in the promotor regions of their target genes such as *Per* and *Cry* genes. Translation happens in the cytoplasm where PER and CRY proteins accumulate over time and form oligomeric complexes with kinases like CK1 ε/δ. Their half-life depends on post-translational modifications which can either increase their stability and lead to nuclear translocation after a critical delay or target them for proteasomal degradation mediated by βTrCP or FBXL21. In the nucleus, PER and CRY complexes inhibit BMAL1/CLOCK transactivation thereby shutting down their own transcription. The inhibitory complex is stabilized by FBXL21, which protects CRY proteins from FBXL3-mediated degradation. Consequently, nuclear PER/CRY level in the nucleus fall, BMAL1/CLOCK levels rise and the cycle can start over. To add more robustness to the system, a second circuit comprising *Rev-erbs* and *Rors* is intertwined which is BMAL1/CLOCK driven, too. After translocation to the nucleus, REV-ERBs and RORs compete upon binding to ROR-response elements (RRE) in the *Bmal1* promotor region, driving circadian *Bmal1* transcription (adapted from *http://www.utsouthwestern.edu/labs/takahashi-joseph/research/circadian-clock.html*).

The FBXL3 protein is almost exclusively expressed in the nucleus where it regulates nuclear CRY1 and CRY2 protein levels. There, FBXL3 binds to cryptochromes that were phosphorylated by AMP kinase and polyubiquitinates them, targeting CRY1 and CRY2 for rapid proteasomal degradation. FBXL21 is found in the cytoplasm as well as in the nucleus and shows much stronger binding affinities towards cryptochrome proteins than its paralog FBXL3, concurrently possessing a less efficient intrinsic E3 ligase activity. While there is no competition with FBXL3 in the cytoplasm, FBXL21 regulates cryptochrome levels by slowly promoting their degradation[40]. In the nucleus, FBXL21 stabilizes CRY1 and CRY2 by counterbalancing FBXL3 actions. FBXL21

blocks the FBXL3 interaction site, thus protecting the cryptochrome proteins from FBXL3 promoted ubiquitination and degradation.

1.2.2 The suprachiasmatic nucleus and its role as the central pacemaker

The suprachiasmatic nucleus is a paired, wing-shaped brain region in the hypothalamus located directly above the optic chiasm. The SCN is comprised of approximately 20.000 densely packed neurons. Each unilateral SCN can be divided into two distinct structures: the ventral core region which adjoins the optic chiasm and directly receives input from the intrinsically photosensitive retinal ganglion cells (ipRGC) and the shell region which encloses the core region and receives input from the core neurons[41]. The SCN neurons can be further distinguished by the specific signalling molecules they contain or secrete, by their response to light information and the areas they project to. The core neurons secrete predominantly vasoactive intestinal polypeptide (VIP), calretinin, neurotensin and gastrin releasing peptide (GRP)[41–44]. The shell neurons are enriched in arginine vasopressin (AVP), angiotensin II and met-enkephelin[41,45,46]. Furthermore, most of the SCN neurons contain gamma-aminobutyric acid (GABA) or glutamate[47,48]. To communicate and forward output signals SCN neurons can directly innervate structures in the hypothalamus, the thalamus and the forebrain[49,50]. AVP and VIP positive neurons are the most extensively studied examples of innervating neurons, and it has been shown that often both types of neurons innervate the same target tissue[41,50,51]. Finally, subclasses of neurons respond differently to changes in light. The core that receives direct light input from the ipRGCs displays light-induced gene expression and re-entrains faster than the SCN shell which leads to intra-SCN desynchrony and may contribute to phenomena like jet-lag[52,53].

The SCN`s function as the central pacemaker was first established in the early 1970`s by studies of lesions and transplants in rodents. Lesions of the SCN resulted in complete loss of behavioural and endocrinal circadian rhythms[54,55]. The loss of circadian rhythms could be partially restored by transplantation of embryonic SNC tissue but not by transplantation of fully developed SCNs[56]. Using either wild-type or mutant rodent strains displaying abnormally short circadian periods, known as the tau-mutation, resulting circadian oscillation after transplantation were determined by the donor SCN and not by the SCN-lesioned host[57]. The circadian rhythm could also be restored by

embryonic SCN tissue encapsulated in a semipermeable polymeric sheath, suggesting the involvement of secreted, diffusible synchronisation factors in rhythm transmission to adjacent brain regions[58].

Input pathways of the SCN

To entrain the master pacemaker to external timing cues the SCN receives and processes input from three different input pathways – the retinohypothalamic tract (RHT), the geniculohypothalamic tract (GHT), and serotonergic (5HT) input from the dorsal raphe nucleus (DRN) and median raphe nucleus (MRN). Timing information for the SCN in the form of light, one of the strongest *zeitgebers*, is detected by the non-visual melanopsin producing photoreceptors, termed intrinsically photosensitive retinal ganglion cells (ipRGC), in the inner retina of the eye[59,60]. Additionally, the non-visual light input received from image forming rods and cones is mediated by the ipRGCs and only mammals with a complete loss of rods, cones and ipRGCs show no photic entrainment[61–63]. The temporal responsiveness of the SCN to light varies throughout the day and, therefore, modulates the light's phase resetting and phase shifting capacity[64]. The ipRGC's axons project directly to the ventrolateral SCN core via the retinohypothalamic tract where the electrophysiological signal is transformed into a chemical signal by the synaptic release of glutamate and pituitary adenylate cyclase-activating polypeptide (PACAP)[65]. PACAP carries out modulatory functions enhancing the effect of glutamate[66]. The excitatory neurotransmitter glutamate depolarizes the membrane which leads to an influx of calcium ions and the activation of multiple signalling pathways culminating in the expression of clock genes, the expression of immediate early genes and the induction of chromatin remodelling[67–72]. To be more specific, the most extensively studied signalling pathway involves the activation of the MAPK/ERK pathway, which leads to the phosphorylation of cAMP response element–binding (CREB) protein[73–75]. Phosphorylated CREB binds to cAMP binding elements (CREs) located in the promotor regions of their target genes, leading to the activation of their transcription[76]. *Per1* and *Per2* genes contain one CRE in their promotors which allows a BMAL1/CLOCK heterodimer independent activation via light that leads to direct alterations of the circadian phase[77,78]. The importance of *Per1* and *Per2* induction for changes in the circadian phase in response to light is still under debate since

contradicting results were reported. On one hand, studies with *Per1*/*Per2* knockout mice or antisense nucleotides targeting *Per1* described impaired or abolished phase shifting and resetting[79–82]. On the other hand it was shown that neither *c-Fos* nor *Per1* are necessary for entrainment to light[67].

Signal processing and coupling in the SCN

The SCN works as a multi-oscillator network of coupled neurons to achieve phase coherency and similar circadian periods. In dispersed cell cultures, the SCN cells lose intercellular communication and slowly desynchronize[44]. Although some of the SCN neurons show random and spontaneous action potentials during the day with a close to 24-hour rhythm, which might demonstrate the origin of circadian rhythms, most SCN neurons exhibit a broad range of circadian periods that vary from 20 to 30 hours and as a result a broadly distributed range of phase relationships[83,84]. The circadian periods and their phase relationships are preserved in the individual single cell even when their neuronal firing is inhibited by tetrodotoxin (TTX)[44]. In dispersed cell cultures with low densities approximately 60 % of all neurons show circadian rhythmicity but only 30 % show detectable circadian rhythmicity in complete isolation[85]. These findings suggest that the generation of circadian rhythms in SCN neurons is cell-autonomous and does not rely on rhythmic neuronal firing or synaptic input from neighbouring cells but that cell-cell communication is probably important for synchrony, high-amplitude oscillations and phase coherence[86].

In contrast to dispersed neuronal cell cultures, neurons from intact SCN tissue exhibit high-amplitude circadian rhythms with extremely precise circadian periods and coherent circadian phases due to intercellular coupling[43]. When isolated and cultured as unperturbed slices, SCN neurons remain synchronized and show undamped tissue-rhythms for weeks. Additionally, the coupled SCN population is less susceptible to disruptions of the circadian clock. SCN rhythms persist in the presence of clock gene mutations that lead to arrhythmic phenotypes at the single cell level[87]. The reason for this are multiple communication pathways including synaptic signalling, chemical molecules and direct cell-cell interactions via gap-junctions. At first, synaptic signalling was discussed as one of the main synchronizing mechanism because blocking Na^+-dependent synaptic transmission using TTX severely decreases the synchrony of SCN neurons[86].

Today, it is known that the SCN relies on additional synchronizing pathways as SCN timekeeping can be detected in the absence of Na^+ - and Ca^{2+} - dependent synaptic transmission, and embryonic SCN tissue shows metabolic circadian rhythms even before synaptogenesis is terminated[88–92]. Therefore, it was postulated that soluble chemical synchronizing factors might be involved in paracrine signalling assembling a cell-cell communication network with neighbouring cells. VIP, AVP, GABA and GRP were proposed to function as paracrine coupling factors in addition to their function as intercellular core-to-shell signalling molecules. VIP was the most interesting candidate since VIP positive axons project to almost every SCN regions and the VIP receptor VPAC2 is ubiquitously expressed in SCN neurons[93,94]. Furthermore, VIP as well as its receptor show circadian expression level *in vitro* and *in vivo*[95–97]. Given that the VIP signalling cascade increases cAMP level - which leads to an induction of phosphorylated CREB culminating in activation of immediate early genes - VIP release can directly modulate the circadian clock and its output pathways (see 1.2.1.1) [98]. Moreover, studies in mice under constant darkness showed that the loss of VIP signalling decreases circadian rhythmicity in behaviour, leaving the animals arrhythmic or with low-amplitude rhythms[99,100]. Taken together, VIP is an established modulator of the clock and its loss has extensive consequences for the oscillations in behaviour and physiology. AVP is another potential coupling factor which is rhythmically expressed in the SCN *in vitro* and *in vivo*[101–104]. Two out of three AVP receptors (V_{1a} and V_{1b}) are highly expressed in the SCN and can modulate internal cellular calcium levels[105]. AVP is believed to function predominantly as an output signal and was shown to augment rhythmicity in corticosterone release, melatonin secretion and sleep[106–108]. Consistent with its role for circadian output, the application of AVP does not phase-shift the SCN of wild-type mice *in vitro* or *in vivo*. Interestingly, transgenic rodents lacking AVP receptors in the SCN re-entrain almost instantly to new light regimes, which suggest impaired coupling of the SCN neuronal network and establishes an additional role of AVP in setting the pace of re-entrainment[86]. Next, it was argued that GABA could function as a possible coupling factor since not only GABA is ubiquitously expressed throughout the SCN but also the $GABA_A$ receptor and the $GABA_B$ receptor[109,110]. Further, GABA signalling shows circadian rhythmicity in the SCN tissue and regulates its neuronal activity, photic signalling and output pathways to the periphery[111–113]. GABA application was shown to synchronize electrical firing rates of dispersed SCN neurons and functions as a resetting signal in core-to-shell signal transmission in intact SCN tissue[114,115]. Since VIP is such a

strong synchronization factor, the effects of GABA are barely detectable in the presence of VIP. In transgenic animals lacking VIP, SCN neurons desynchronize after GABA application, which mitigates GABA's role as a sole coupling factor [116]. In fact, it was proposed that VIP signalling and $GABA_A$ signalling act together in an antagonistic or cooperative manner depending on the network state. Finally, GRP was brought up as a secreted coupling factor in the SCN due to its rhythmic expression level which can be controlled by light[117,118]. Moreover, the GRP receptor, known better as bombesin 2 (BB2), is rhythmically expressed as well[119]. Application of GRP can induce phase shifts in locomotor activity *in vivo* and shift SCN oscillations *in vitro* in a comparable manner as VIP and light[120,121]. The effects on the circadian phase are most likely induced by activated CREB signalling and immediate early gene expression. In SCN slices of VIP knockout animals, GRP can enhance the circadian oscillations and antagonists of BB2 can attenuate circadian rhythmicity[122]. These findings point towards a coupling function of GRP which is probably masked under physiological conditions by the strong coupling effects of VIP.

Gap junctions and their direct cell-cell communications constitute the third mechanism implicated in coupling of SCN neurons. Gap junctions allow the direct exchange of small diffusible molecules through channels in the cell membrane. Results from pharmacological experiments with octanol and halothane suggest that communication via gap junctions can influence circadian rhythmicity in the SCN[123]. Furthermore, there is evidence that neuronal gap junction protein connexin 36 is important for electrical coupling as transgenic animals lacking the protein show reduced amplitudes in activity rhythms[124].

Output pathways of the SCN

The SCN forwards its received and processed timing information through output pathways to the slave oscillators in peripheral tissues. In the last decades, more and more has evidence emerged that the master clock in the brain does not use a single output pathway, but instead communicates with the periphery via a combination of autonomic innervation, endocrine signalling, core body temperature and local signals resulting from locomotor behaviour.

The SCN uses the parasympathetic as well as the sympathetic nervous system to transmit entrainment signals. The autonomic nervous system forwards timing information from the SCN via the paraventricular nucleus superior cervical ganglia (PVN-SCG) pathway directly to peripheral oscillators in the submandibular salivary glands and the liver, influencing saliva protein production and plasma glucose levels[125–127]. Furthermore, the SCN controls the adrenal as well as the pineal cortex function. For instance, it has been shown that the adrenal gland receives photic input by sympathetic innervation modulating the sensitivity to adrenocorticotropic hormone (ACTH) and regulating glucocorticoid production and release[128,129].

Several different hormones and polypeptides have been described to function as SCN output signals. Alongside GABA and glutamate, two prominent neurotransmitters in intra-SCN communication, AVP, VIP, cardiolipin-like cytokine, transforming growth factor α and prokineticin 2 (PK2) were implicated to contain synchronizing properties and some were shown to exhibit rhythmic transcription and translation. One of the most intensively studied candidates is PK2 whose expression pattern can be shifted by light input[130]. Many brain areas which are known to receive input from the parasympathetic as well as the sympathetic nervous system show cyclic PK2 mRNA expression and exogenous application of PK2 alters wheel running and feeding behaviour[131,132]. Nevertheless, PK2 does not function as an exclusive output factor with synchronising properties since mutated mice lacking either the protein or the corresponding receptor still show dampened circadian locomotor activities[133,134]. This suggests that additional output signals can sustain rhythmic behaviour.

Another group of well-studied output signals are glucocorticoids. It is well established that mammals show rhythmic glucocorticoid levels, for instance in cortisol, which peak during the morning hours right before the beginning of the active phase and constantly decrease throughout the day with the lowest level during the late evening hours prior to the inactive phase[135,136]. Rhythmic glucocorticoid levels are generated by input signals form the autonomic nervous system and rhythmic production of the corticotropin releasing hormone CRH resulting in cyclic release of the adrenocorticotropic hormone (ACTH). In conjunction with the adrenal gland clock, the ACTH regulates the rhythmic production of glucocorticoids and their distribution to the periphery via the blood stream[129]. Glucocorticoid analogues like Dexamethasone provide strong entrainment information and can re-set the circadian clock in peripheral organs like liver, kidney and heart as well as mammalian primary cell culture[137]. Presumably, they act through

glucocorticoid-response elements that were identified in the promotor region of core clock genes *Bmal1*, *Cry1*, *Per1* and *Per2*[138–140]. Furthermore, there are probably more - yet unidentified - diffusible synchronising factors in the blood stream. For instance, Gerber et al. reported an entrainment factor that regulates diurnal changes in actin dynamics resulting in rhythmic translocation of the SRF coactivator Myocardin-related transcription factor-B (MRTF-β) from the cytosol to the nucleus. Together, SRF and MRTF-β rhythmically activate immediate early genes like *Per2* which alters the circadian phase[141].

A third strong output pathway of the SCN is rhythmic variation in the organism's core body temperature. The SCN as the central pacemaker is relatively resistant to temperature cycles, which makes time-of-day-dependent changes in body temperature an important entrainment signal for the periphery. It was shown, that the core body temperature is driven by the circadian clock and is under the direct control of the SCN. In contrast to the master clock, peripheral oscillators like liver, kidney, lungs and fibroblasts are extremely sensitive to temperature changes and even low-amplitude temperature rhythms are sufficient to synchronize and entrain them[142,143]. Heat-shock factor 1 (HSF1) is a temperature driven transcription factor that shows a highly rhythmic expression level in peripheral organs and can modulate clock gene expression by binding to heat-shock factor binding elements in the promotor regions of target genes, for instance *Per2*[144,145]. Additionally, the cyclic body temperature can directly influence the abundance of proteins such as cold-inducible RNA-binding protein through modulation of the splicing efficiency, showing another regulatory way of gene expression *in vitro* and *in vivo*[146].

1.2.3 Circadian clocks in peripheral organs

Robust circadian oscillations in mRNA expression level and/or protein abundance are present in cultured cells and almost all peripheral tissues ranging from heart through lung, kidney, muscle, spleen, and stomach, to corneal and the immune system related tissues[137,147,148]. The only exceptions are murine testis and the thymus. For both organs, there are contradicting results reporting either no circadian rhythms or 12-hour ultradian rhythms under certain conditions[149,150]. The observed underlying molecular mechanism

of the peripheral circadian oscillators is similar to the one identified in murine SCN tissue and is comprised of delayed and interlocked transcriptional-translational feedback loops using the same set of core clock genes (see **1.2.1**). One important difference is the clock paralogue NPAS2, that is exclusively expressed in the brain and is not detectable in peripheral tissues[151,152]. Further genome-wide transcriptome analysis, notably in liver, spleen, and muscles, revealed that key enzymes for tissue specific processes are under clock regulation. Depending on the study, it is reported that peripheral circadian oscillators control the rhythmic expression of up to 10 % of all known genes with minimal overlap between different tissues[20–22]. These findings highlight the importance of temporal control of key physiological and metabolic processes in each unique tissue, including detoxification, carbohydrate and lipid metabolism, urine production and parameters of the cardiovascular system like blood-pressure[153–156].

Until the last decade, it was widely accepted that peripheral tissue explants do not display self-sustained, long-lasting circadian oscillations but damp out rapidly after a few circadian cycles. This view was challenged when Yoo and colleagues published their results on *Per2*-promotor driven *luciferase (Per2_luc)* expression in lung and liver slices that lasted up to 20 circadian cycles without resynchronisation[148]. Nevertheless, input from the master clock in the SCN is still necessary to achieve phase coherence between multiple peripheral organs or even between hepatocytes of liver explants, as SCN-lesioned animals show prominent phase differences[157]. Further support for robust peripheral oscillators comes from observation on the single cell level. Circadian rhythms monitored in cultured rat fibroblasts are comparable to rhythms in single SCN neurons, as their oscillations persist throughout their lifetime. They are resilient to changes in temperature, changes in transcription rate and cell division processes[158,159].

Input pathways and synchronization of peripheral organs

As summarized above (see **1.2.2**), the SCN is the master pacemaker of the organism and synchronises peripheral tissues using direct and indirect synchronising signals to achieve phase coherence throughout the body. Innervation through the parasympathetic as well as the sympathetic nervous system and the rhythmical secretion of synchronising molecules directly affect peripheral oscillators forcing them in synchrony. Body temperature changes and feeding-fasting cycles are examples of indirect

timing cues to enforce phase coherence as they are strongly dependent on the animal's sleep-wake-cycle under the control of the SCN. Nevertheless, it is widely accepted that temperature cycles and rhythmic availability of food are one of the strongest *zeitgeber* signals for the peripheral oscillators[24,143]. In wild-type animals that are fed ad libitum, the feeding-fasting cycles are in synchrony with the SCN controlled activity cycles leading to a positive reinforcement of circadian oscillations in the periphery. Under conditions where food is restricted to the daytime (the period when animals normally rest), the animal will start to entrain to the new feeding schedule and anticipate the food with an increase in activity and body temperature[160,161]. Accordingly, some but not all peripheral organs will re-entrain to the new feeding regime and, in consequence, will shift their rhythmic gene expression and uncouple their circadian clock from the SCN clock[24,162]. In SCN-lesioned animals lacking the dominant timing cue light that is perceived through the retina and forwarded to the SCN, the availability of food can take on pace-making functions, synchronising the peripheral oscillators to achieve phase coherence once completely entrained to the (new) feeding-fasting cycle[163,164]. Stunningly, animals can entrain to food as the sole *zeitgeber* even in the absence of a functional clock as Bmal1$^{-/-}$ mice are still able to adapt to restricted feeding[165]. These findings imply that some components of the circadian clock are under the direct control of the metabolism and are sufficient to drive circadian oscillations and control clock output pathways.

Coupling in peripheral organs

In the SCN, coupling confers robustness to the central pacemaker by ensuring a strong phase and period coherence between single SCN neurons and protecting the master oscillator against external noise. Therefore, SCN explants in isolation show self-sustained, persistent rhythms for 30 circadian cycles and more. In contrast, coupling in peripheral tissue is still under debate and experimental outcomes are said to be dependent on the overall experimental setup and the chosen culture conditions. Early studies with *ex vivo* tissue cultures reported a rapid dampening of *Per1*promotor -driven *luciferase* rhythms in liver, lungs, and skeleton muscle after two to seven circadian cycles[147]. The bioluminescence rhythms could be re-initiated through a medium change suggesting rapid desynchronization of the individual cells. Additionally, the majority of rhythmically expressed genes in the liver damp out or lose their rhythmic expression pattern completely

without input from the SCN within two days[22]. Both findings strongly argue for uncoupled oscillators in peripheral tissues which depends on SCN input to maintain high-amplitude rhythms with intercellular phase coherence. In contrast, Yoo and colleagues detected long-lasting and only slightly damped PER2::LUC rhythms in liver, lung, kidney, cornea and pituitary over at least 20 consecutive days (see **Figure 1-4A)**[148]. The persistent oscillations of peripheral tissue were detectable in SCN lesioned animals, too, but with lost phase coherence between examined organs as wells as among multiple scrutinised animals[148]. Another study partially confirmed the findings of Yoo, reporting *in vivo* PER2::LUC rhythms in SCN lesioned animals one month after surgery although with stable phase and period relationships[166]. Strikingly, the results could even be verified in the living animal, using real-time luciferase recordings. SCN lesioned animals that showed arrhythmic locomotor activity for one month exhibited robust *Bmal1*-promotor driven *luciferase* rhythms in the liver under restricted feeding conditions that could be phase shifted by reversed feeding-fasting cycles and persisted under *ad libitum* feeding for several days without detectable dampening (see **Figure 1-4B**)[167]. *Ex vivo* liver and kidney tissue from mouse embryos as early as day 13 showed robust circadian rhythms persisting for at least seven days, although the organs had not been fully developed yet (see **Figure 1-4C**)[168]. In addition, there is evidence supporting coupling in the periphery from primary cell culture experiments. PER2::LUC fibroblasts cultivated in low density exhibit reduced numbers of rhythmic cells and damped, low-amplitude oscillations. The phenotype can be rescued by the addition of non-bioluminescent feeder cells or conditioned medium from high density cultures[169]. In primary hepatocytes maintained in 2D culture, local intercellular communication of circadian information between adjacent cells was detected[170]. Although no evidence was found for the exchange of circadian period information between adjacent hepatocytes of wild-type animals and liver specific clock mutant animals, a weak and more local coupling in cultured cell clusters was detected resulting in higher phase coherence which might stabilise circadian rhythmicity (see **Figure 1-4D**). Together, these findings propose gap-junction-dependent and/or paracrine signalling of unidentified, secreted signalling molecules that boost circadian rhythmicity, supposedly by keeping the culture in synchrony and, thereby, increasing phase coherence of cultured cells.

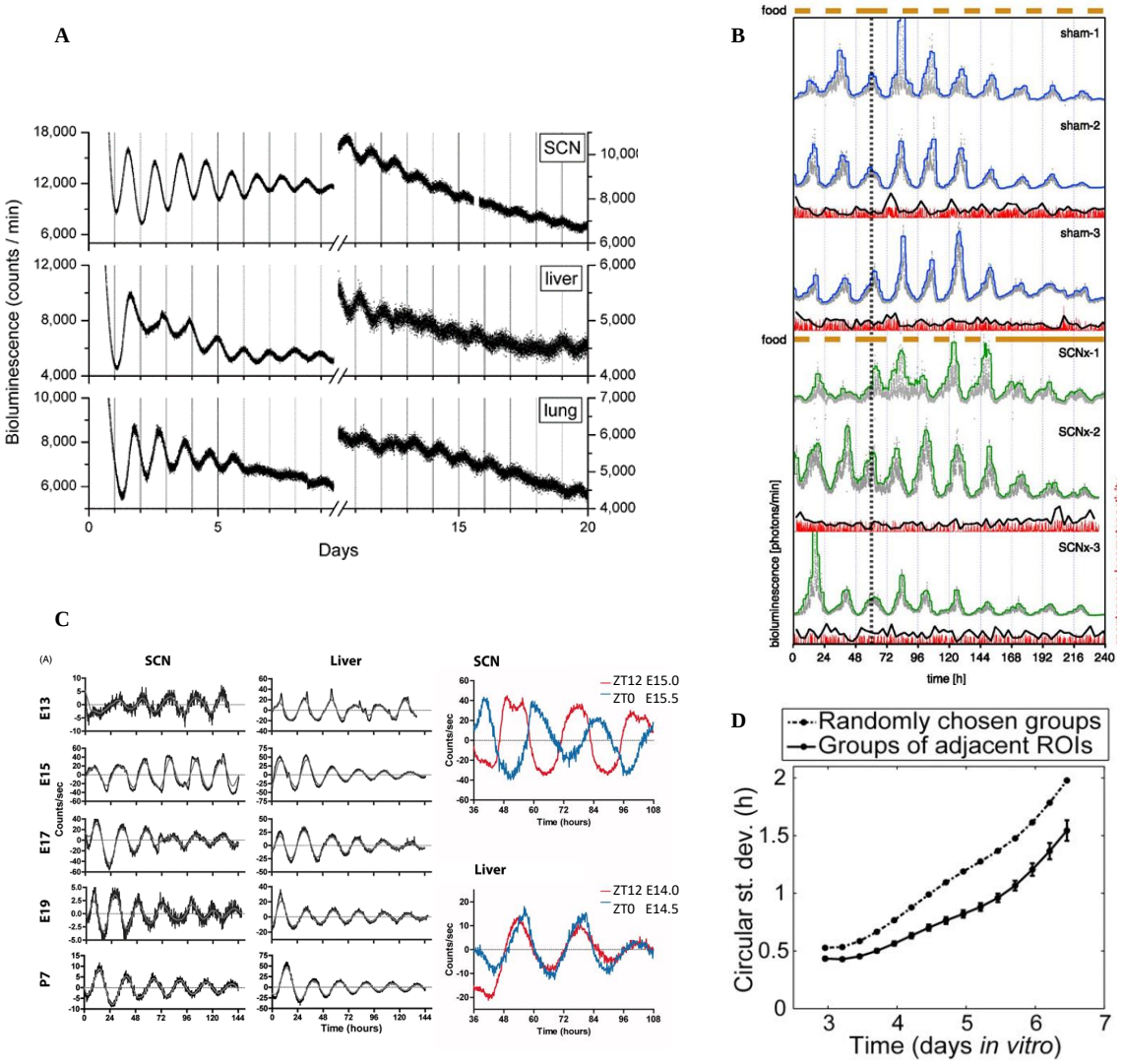

Figure 1-4: Several studies provide compelling evidence for coupling in peripheral tissues. A) SCN and peripheral tissues from PER2::LUC mice were harvested and cultured for at least 20 days, recoding bioluminescence rhythms. The circadian oscillations persist for the whole time in culture without external re-synchronisation, although they exhibit a progressive dampening over time. **B)** Sham-operated and SCN lesioned animals were monitored for 28 days to confirm arrhythmic locomotor activity (in the SCN lesioned animals) and fed during the night time to entrain them to feeding-fasting cycles. An osmotic pump providing luciferin was implanted in the intraperitoneal cavity and the animals were transduced with *Adv-Bmal1-luc* reporter vectors to record liver bioluminescence rhythms in real-time. Bioluminescence rhythms in the liver of SCN lesioned animals could be phase-shifted, changing the feeding regime. Rhythms persisted for several days with minor dampening compared to the sham-operated animals. **C)** SCN and liver tissues from PER2::LUC mice embryos were harvested at different developmental stages and cultured for at least seven days, recording bioluminescence rhythms. Strong circadian rhythms were detected from E13 on that persisted without further external stimuli for at least seven days. Time of harvest did not re-set the circadian phase in liver tissue, but in the SCN, which suggests that the monitored rhythms did not occur due to resynchronisation during harvesting procedure. **D)** Primary hepatocytes taken from PER2::LUC mice were maintained in 2D cultures and bioluminescence rhythms were monitored over seven days. Analysis of the circadian phase of either seven adjacent or seven randomly chosen hepatocytes revealed smaller phase differences for neighbouring cells at all time points, suggesting stronger phase coherence.

1.3 The vesicular protein transport along the secretory pathway

1.3.1 The cellular compartmentalization and the secretory pathway

Eukaryotic as well as prokaryotic cells are surrounded by a semi-permeable membrane which separates their interior from the outside environment. The membrane barrier ensures the integrity of the encapsulated interior while its semi-permeability allows for an exchange of ions, metabolites and macromolecules with the surrounding milieu either in a controlled fashion or through passive diffusion. Further, additional membrane-enclosed structures developed in eukaryotes (e.g. the nucleus, the endoplasmic reticulum (ER), the mitochondria as well as the Golgi, endosomes and lysosomes) and in prokaryotes (e.g. the geomagnetic-field sensing magnetosomes or carboxysomes)[171,172]. These organelles are separated cellular compartments with a distinct biochemical and enzymatic composition designed to carry out specific functions.

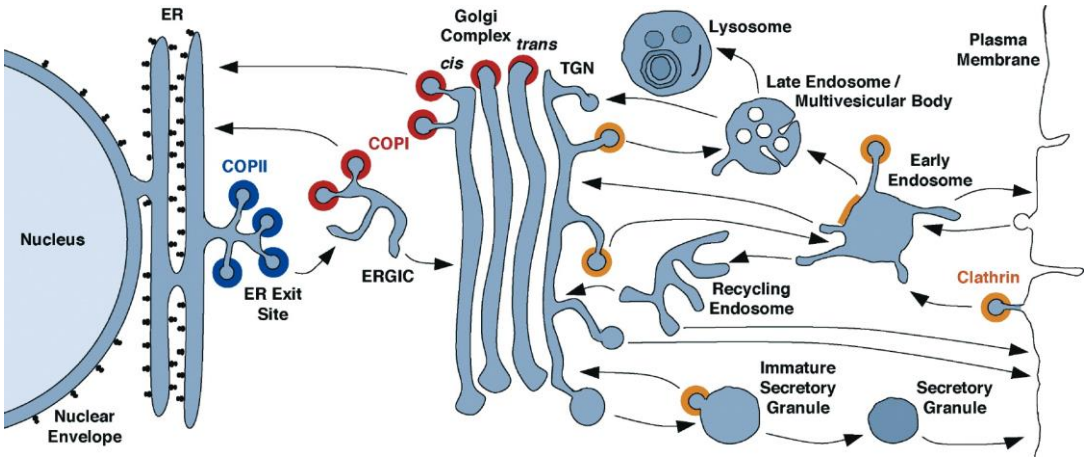

Figure 1-5: Vesicle-mediated transport along the secretory pathway. Newly synthesised secretory or membrane associated proteins are transported from the endoplasmic reticulum to the plasma membrane or the destined target compartment by specialised protein coated vesicles. Shortly, after translation into the ER lumen, the proteins go through extensive folding and quality control processes before they start their journey and are packaged into COPII coated vesicles at ER exit sites (highlighted in blue). COPII vesicles run along microtubules to the ERGIC or the cis-Golgi membrane, fuse with the compartment membrane and release their cargo into the corresponding lumen. If proteins are correctly folded in the ER lumen, they will progress through the Golgi to be packed into clathrin coated vesicles at the trans-Golgi. Otherwise, misfolded proteins are recognized by chaperons and retrieval receptors, sorted into COPI coated vesicles at the cis-Golgi membrane and recycled to the ER (depicted in red). Clathrin-coated vesicles carry out the transport steps between the trans-Golgi network, endosomes, lysosomes and the plasma membrane, relying on a variety of adaptor proteins associated with cargo sorting and vesicle targeting (depicted in yellow). Additionally, clathrin-coated vesicles are involved in endocytosis at the plasma membrane (adapted from "The mechanisms of vesicle budding and fusion" by JS. Bonifacino and BS. Glick [173])

For instance, the mitochondrial respiratory chain relies on a complex series of reduction and oxidation reactions, establishing an electrochemical proton gradient at the inner mitochondrial membrane which drives ATP production[174]. Moreover, the ER, the Golgi, endosomes and lysosomes represent independent check-points for proteins designed to be secreted to the extracellular environment. To assure the organelle's integrity and function, the presence of signalling receptors at the plasma membrane and the proper secretion of signalling molecules and enzymes is necessary, as well as a tightly regulated transport of lipids, membrane proteins and soluble proteins between organelles and the plasma membrane. Small vesicles carry out this function continuously cycling between membrane-enclosed organelles and the cell surface (see **Figure 1-5**). The sorting of cargo into the transport vesicles is coupled with quality control mechanisms as the sorting signals often reside in the proteins themselves or rely on interaction with additional molecules[175–178].

1.3.2 Secretory protein translocation and maturation in eukaryotes

The early secretory pathway is comprised of three distinct organelles: the endoplasmic reticulum, the Golgi apparatus and the ER-Golgi-intermediated compartment (ERGIC) located between these two compartments. The ER is the entry point into the vesicular transport network for newly synthesized proteins. The translocation from the cytoplasm into the ER can occur either co-translationally or post-translationally, although in higher eukaryotes co-translational translocation is used almost exclusively and post-translational translocation occurs only for short polypeptides that cannot be recognized co-translationally by the signal recognition particle (SRP) (see **Figure 1-6**)[179]. In the former case, protein synthesis and translocation into the ER lumen happen simultaneously, in the latter case protein synthesis is carried out completely in the cytoplasm and the unfolded protein is translocated into the lumen afterwards. Both pathways depend on four sequential steps. First, the growing protein chain needs to be identified and successfully targeted to the ER. Second, the nascent protein chain must interact with the ER translocation machinery that guides the peptide to the ER pore for future translocation. Third, the translocation machinery facilitates the actual import event into the ER lumen, or the ER membrane in case of integral membrane proteins. Finally,

the polypeptide chain is folded by chaperones and maturates in the ER lumen. The co-translational translocation process occurs when the hydrophobic signal sequence or the transmembrane sequence of the nascent protein chain is translated and recognized by the SRP. Upon binding of the SRP, the translation process is significantly slowed down, allowing the ribosome to diffuse to the ER membrane where the SRP is bound by its receptor and the ribosome by ER membrane proteins.

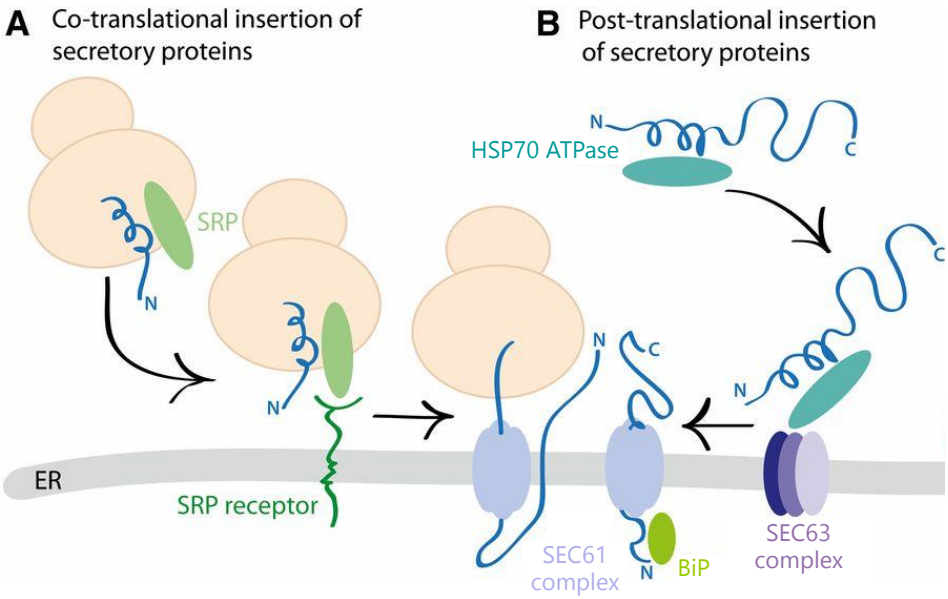

Figure 1-6: Co-translational translocation, post-translational translocation and GET-mediated insertion of secretory proteins in mammals. A) The signal recognition particle identifies a hydrophobic signal sequence on a nascent protein chain during translation, binds to it and stalls the ongoing polypeptide synthesis. The ribosome is targeted to the ER membrane by the SRP, where the complex is bound to the SRP receptor and correctly positioned for co-translational membrane insertion. **B)** The hydrophobic protein chain is recognized by a cytosolic HSP70 ATPase, kept in an unfolded translocation competent state and targeted to the ER membrane bound SEC63 complex. The SEC61 complex forms an aqueous passage for co-translational as well as post-translational translocation. SEC63 and BiP (a luminal HSP70 ATPase) enable an ATP dependent directed movement through the channel (modified from "Secretory protein biogenesis and traffic in the early secretory pathway" by Charles Barlowe and Elizabeth Miller [180]).

The binding of the SRP receptor triggers GTP-hydrolysis and therefore the dissociation of the SRP from the ribosome-nascent chain complex. Translation continues into the ER lumen through an aqueous channel formed by SEC61[181,182]. Protein-ribosome interactions help to position the ribosome with the growing nascent polypeptide chain at the ER pore[182–184]. Once positioned at the ER pore, co-translationally targeted proteins are pushed in by protein chain elongation. Additional help in protein chain translocation is provided by SEC63, BiP (identified as Kar2 in yeast) and the translocating chain-associated membrane protein (TRAM)[185]. Post-translational translocation often occurs when the nascent protein chain is soluble, less hydrophobic or - in the case of mammals

- very short [186,187]. Cytosolic chaperons termed HSP70 ATPases identify the hydrophobic polypeptides, keep them in an unfolded translocation competent state and target the fully translated protein to the ER membrane where it binds to ER residential proteins[188–191]. The nascent polypeptide chain is recognized by the SEC63 complex that changes its conformational state and thereby forwards information to the SEC61 and BiP/Kar2. The ER pore opens, allowing the polypeptide to span the channel, interact with BiP/Kar2 and be pulled through the channel in an ATP-dependent manner[192]. A third post-translational, SEC61 independent translocation pathway to the ER has been identified that relies on additional soluble and membrane bound factors[193–195]. The ribosome disguises the hydrophobic transmembrane region of integral membrane proteins and C-terminally anchored proteins until the protein translation is terminated thereby preventing the SRP dependent recognition. In mammals, the HSP40-HSP70 chaperone complex as well as the cytosolic ATPase ASNA1 binds to the membrane (anchored) protein, preventing its folding and keeping it in a translocation competent state[196,197]. In mammalian cell-free assays TRC40 was identified. TRC40 shares a high sequence identity with Get3, a former identified yeast protein, and is believed to be involved in the insertion of hydrophobic sequences of tail-anchored and integral membrane proteins[197]. In yeast the Sgt2-Get4-Get5 complex, as set of nonessential genes, delivers the bound, tail-anchored protein to the soluble Get3 which loads the protein onto an integral membrane complex consisting of Get1 and Get2. Together Get1, Get2 and Get3 insert the hydrophobic segment into the membrane.

Upon entering the ER lumen, signal sequences often form hairpin structures which are cleaved off by signal peptidase and broken down by signal peptide-peptidases complex concomitantly with translocation[198]. The cleavage of the signal peptide is regarded as the first major step of protein maturation. Since the nascent polypeptide chains are translocated through the SEC61 complex in a predominantly unfolded state, the peptide conformation allows for early recognition of consensus Asn-S-Ser/Thr sequences containing the asparagine destined for N-linked glycosylation through the oligosaccharyltransferase complex (OST). The OST transfers an oligosaccharide, the $Glc_3Man_9GlcNAc_2$ glycan *en bloc* to the asparagine of most consensus sites. It is widely believed that the attachment of the 14-residue oligosaccharide assists in protein folding and protein quality control to manage misfolded proteins[199,200]. The initially transferred oligosaccharide is sequentially processed by α-glucosidase 1 and 2 facilitating chaperone assisted protein folding. UDP-glucose:glycoprotein glucosyltransferase (UGGT) in

collaboration with calnexin reviews protein folding and can add additional glucose residues in order to keep the protein in a repetitive folding cycle[201]. When the protein chain is finally folded correctly the α-mannosidase removes the terminal mannosyl-residue which allows the ER export and further processing in the Golgi. But N-linked glycosylation is not the only post-translational modification that newly synthesized proteins undergo. Additionally, mannose residues can be attached to Ser/Thr residues via O-linked glycosylation that is carried out by the protein O-mannosyltransferases (Pmts). O-linked glycosylation is required for cell wall structure and cell morphology[202]. Furthermore, most secretory proteins form disulfide bonds in the oxidizing environment of the ER lumen that enables correct protein folding and stable tertiary structures.

1.3.3 COPII vesicle biogenesis and cargo sorting at the ER membrane

The export of lipids, membrane proteins and soluble cargo at the ER membrane in mammalian cells is well described[203]. In contrast to lower eukaryotes like *Saccharomyces cerevisiae*, COPII vesicle formation cannot occur throughout the ER but is restricted to specialised zones termed ER exit sites (ERES)[204]. The ERES are enriched in COPII proteins, the core components of the ER exit machinery that direct the budding event at the membrane (see **Figure 1-7**) [205]. The multi-subunit protein complex is not only responsible for the structural support of budding vesicles but is furthermore involved in accumulation and sorting of the vesicle cargo, the bending of the ER membrane, and the scission event. In mammalian cells, multiple isoforms of each COPII subunit (except SEC13) were identified which suggests differential roles in COPII assembly and cargo selection[206–209]. COPII vesicle biogenesis is initiated through the activation of the small RAS-like GTPase SAR1 by the ER resident guanine nucleotide exchange factor (GEF) SEC12 that performs the GDP to GTP exchange[211]. Upon exchange of GDP to GTP an N-terminal amphipathic α-helix element of SAR1 is exposed and inserts concomitantly into the membrane[212,213]. The insertion leads to a displacement of the lipid head-groups and promotes an initial membrane curvature[212,213]. Then, the membrane-associated, activated SAR1 recruits the hetero-dimeric SEC23/SEC24 protein complex and binds to the SEC23 protein. Together, they form the pre-budding complex, stabilizing the randomly appearing membrane curvatures[205]. Additionally, TMED10 and TMED2,

members of the p24 family interact with SEC23 to strengthen the interaction[214]. The heterodimeric SEC24/SEC23 complex shows binding affinities for various cargo molecules and is implicated in active cargo sorting[215,216]. Biochemical as well as structural studies identified the presence of three independent signal binding sites within the SEC24 protein that interact amongst others with SNARE proteins important for vesicle tethering and fusion[217]. Furthermore, ER export of membrane-bound and soluble proteins is enabled by distinct export signals within the amino acid sequence.

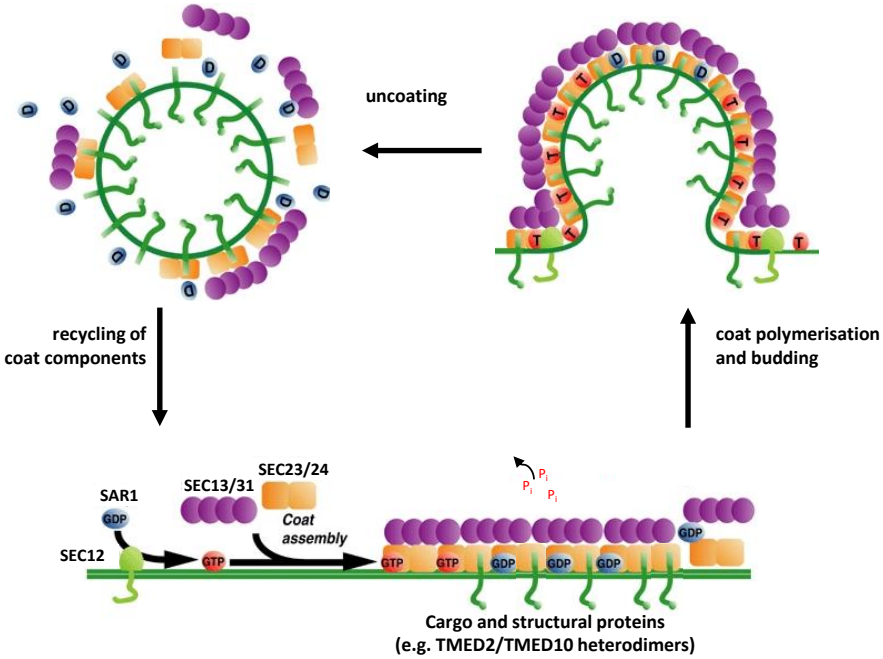

Figure 1-7: COPII vesicle biogenesis at ER exit sites. Membrane associated GEF SEC12 recruits SAR1 in its inactive GDP-bound form to ER exit sites. By catalysing the GDP to GTP exchange SAR1 is activated and the exposed amphipathic N-terminal helix is inserted into the membrane. SEC23/24 heterodimers bind to activated SAR1 molecules as well as selected cargo receptors as TMED2/TMED10 forming the inner layer of the COPII vesicle coat. Next, hetero-tetramers of SEC13 and SEC31 are recruited and bind to SEC24 molecules building up the outer layer of the protein coat. Polymerization of the SEC13/SEC31 tetramers further induces membrane curvature and maturation of the vesicle which gets pitched off the membrane through SAR1 actions. GTP-hydrolysis of GTP-SAR1 promotes vesicle uncoating and recycling of vesicle coat components (modified from "GTP/GDP exchange by Sec12 enables COPII vesicle bud formation on synthetic liposomes" by E. Futai, S. Hamamoto, L. Orci and R. Schenkman [210]).

Cargo proteins are selectively captured and 3- to 50-fold enriched in COPII vesicles, either through direct binding to the COPII coat proteins via the exposed cytoplasmic region or through interactions with specific transmembrane cargo receptors/adaptors molecules[218]. The group of transmembrane proteins is recognized either by their di-acidic D/ExD/E with x representing any amino acid residue, by a tyrosine containing motif closely located to the membrane proximal region or by a di-

hydrophobic motif (e.g. FF or LL) near the C-terminus. The latter is best understood in the p24 family proteins which and was shown to directly interact with SEC23[214,219–221]. Mutating the described SEC23 binding region of the p24 family member's cytoplasmic tail by exchanging the di-hydrophobic FF motif to AA diminishes SEC23 binding drastically[214]. The export of soluble luminal cargo, for instance blood coagulation factors, relies on the interaction with membrane spanning cargo receptors like ERGIC-53 linking the cargo to COPII subunits[222,223]. GPI-anchored proteins without an amino acid exposed to the cytoplasm also lean on adaptor proteins. TMED2/TMED10 heterodimers were shown to interact with GPI-anchored cargo to facilitate successful ER export[224,225]. In addition to their defined role of actively sorting the cargo into the vesicle, adaptor proteins are also implicated in containing sorting signals for downstream compartments and masking ER retention signals.

Next, SEC13/SEC31 hetero-tetramers comprised of two SEC13 proteins and two SEC31 proteins are recruited to the pre-budding complex, forming the outer layer of the COPII coat[226]. They are said to cross-link pre-budding complexes and bring forward membrane curvature by linking the SEC23/SEC24 complexes to clusters, further deforming the ER membrane. Finally, the budding vesicle is cut from the ER membrane, presumably by SAR1 and its N-terminal amphipathic α-helix element[212,213]. Vesicles are transported along microtubules to the ERGIC and further to the cis-Golgi by interacting with dynein, which was shown to be recruited by SEC23/SEC24[227]. After the completed budding from the donor membrane, COPII vesicles strip their coat in an uncoating event including SAR1 GTP hydrolysis[228]. To fuse with the acceptor membrane some proteins which are required for tethering and recognition stay associated with the vesicle. Subsequently, v-SNARE proteins on the engaging vesicle interact with t-SNARE proteins at the cis-Golgi membrane to direct the vesicle to its destination and promote the final membrane fusion[229–232]. The encapsulated content for the ER-derived vesicle is concurrently released into the Golgi lumen.

1.3.4 COPI-mediated retrograde protein transport

Most of the ER-derived proteins are further post-translationally modified and folded as they proceed through the Golgi lumen eventually leaving the Golgi apparatus at the trans-Golgi network. However, the proteins involved in COPII vesicle targeting and fusion as well as cargo receptors that are necessary for quality control and ER export must be recycled back to the ER to be available for the next round of transportation[233]. Furthermore, misfolded and partially folded proteins are redirected to the ER to resolve quality control issues[234]. Finally, residential ER proteins escape the compartment from time to time as they are accidentally sorted into COPII vesicles. The cis-Golgi H/KDEL receptor recognizes the escaped proteins, binds them and returns them to the ER[235,236]. The carriers responsible for facilitating the needed retrograde protein transport were first purified from a cell-free system using cis-Golgi enriched membranes, cytosol and hydrolysis-resistant GTPγS in 1989[237]. Analysis of theses coated carriers and subsequent studies identified seven protein subunits building up the outer and inner protein coat of the vesicle[238]. The proteins β-, γ-, δ- and ζ-COP are organized as the heteroquatrameric F-subcomplex whereas α-, β'- and ε-COP comprise the heterotetrameric B-subcomplex[239]. Comparable to the COPII protein subunits, multiple isoforms with varying cellular distributions and quantities of γ-COP and ζ-COP exist, suggesting differential roles in assembly and cargo sorting[240,241]. The COPI vesicle biogenesis is initiated by the recruitment of ARF1-GDP a small GTPase of the Ras superfamily to the cis-Golgi membrane (see **Figure 1-8**)[242]. There, ARF1-GDP as well as the activated form ARF1-GTP binds to the cytosolic tails of TMED10/TMED2, two members of the p24 superfamily, implying that the heterodimer facilitates the initial recruitment step[243]. Next, a GEF containing a Sec7 domain catalyses the exchange of GDP to GTP, which induces a conformational change exposing the myristoylated amphipathic N-terminal helix which stably inserts ARF1 into the membrane and triggers the dissociation of ARF1-GTP from the TMED10/TMED2 heterodimer[243–247]. GBF1 is the GEF associated in large quantities with the cis-Golgi membrane and was shown to be predominantly involved in COPI biogenesis or more precisely in ARF1's exchange of GDP to GTP[244]. Moreover, ARF1-GTP dimerizes with another ARF1 molecule driving not only coat recruitment but starting to deform the Golgi membrane inducing positive curvature[248,249]. Upon ARF1 activation coatomer proteins are recruited to the membrane. Subsequent studies revealed that ARF1 initially interacts with the trunk domains of β- and γ-COP opening a binding site for δ-

COP[250–252]. Additionally, TMED10 and TMED2 exhibit binding properties towards the trunk domains of γ-COP and α-COP, contributing directly to vesicle formation by triggering coat polymerization[253].

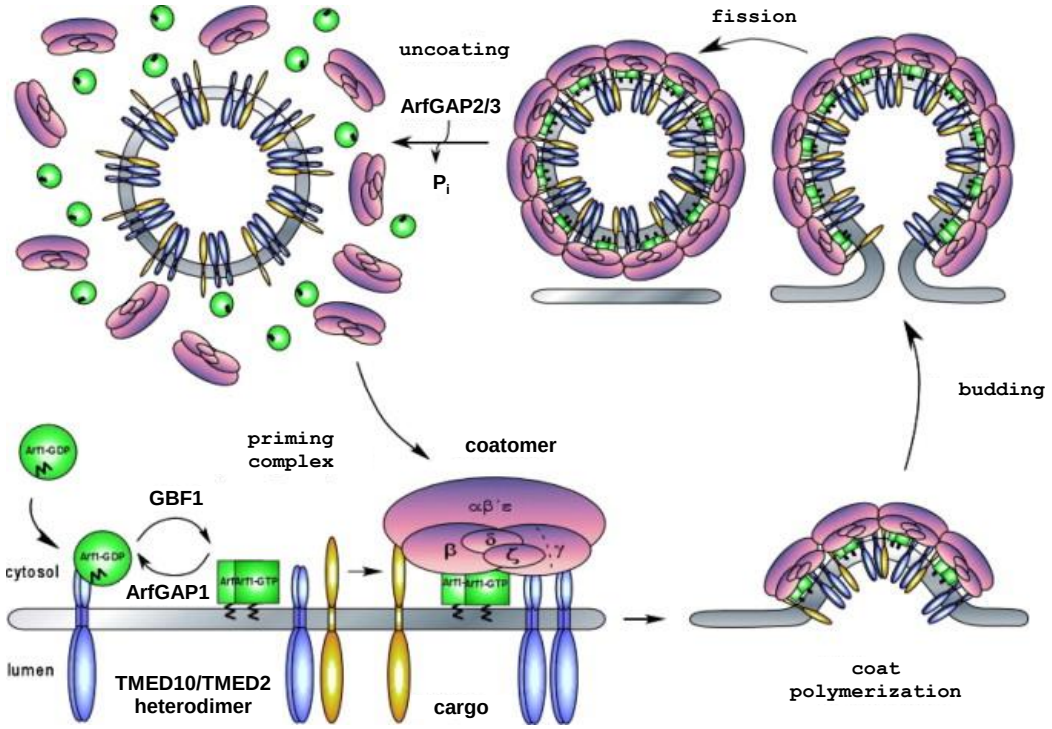

Figure 1-8: COPI vesicle biogenesis at the cis-Golgi membrane. ARF1-GDP is recruited by TMED10/TMED2 heterodimers located at the cis-Golgi membrane. The guanine nucleotide exchange factor GBF1 catalyses the exchange from GDP to GTP, inducing a conformational change in ARF1. A myristoylated amphipathic N-terminal helix becomes exposed and ARF-GTP is anchored in the Golgi membrane inducing membrane bending. Coatomer proteins are recruited to the budding site, interacting with ARF1, p24 superfamily members and cargo molecules building up an inner and outer vesicle coat that polymerizes and grows. As the curvature of the cis-Golgi membrane progresses ARF1 pinches off the budding vesicle which becomes uncoated in the cytoplasm due to ArfGAP driven GTP hydrolysis (adapted from "The COPI system: Molecular mechanism and function" by R.Beck, M. Ravet, F.T. Wieland and D. Cassel [254]).

Before the budding vesicle is released from the donor membrane, soluble and membrane bound cargo is sorted into the vesicle. ER-resident proteins or COPII machinery often display a C-terminal KDEL sequence that prevents them from being secreted and targets them back to the ER[255]. The KDEL sequence is recognised and bound by KDEL receptors. ERD2 was the first KDEL receptor identified in yeast and subsequent studies identified three human isoforms[235,256]. Upon ligand binding the KDEL receptors forms homodimers which interact with ARF1 and coatomer subunits thereby contributing to vesicle formation[257]. Today, it is believed that KDEL receptors bind their target proteins in the low pH environment of the Golgi, are transported back to the ER and

release the bound proteins due to the higher pH in the ER lumen[258]. This allows the empty receptor to be recycled back to the Golgi for another round of transportation. Retrograde transport of membrane or membrane-bound proteins highly depends on the C-terminal dilysine-motif K(X)KXX[259]. Proteins displaying the dilysine-motif can directly interact with the B-subcomplex consisting of α-, β'- and ε-COP and therefore be actively sorted in COPI vesicles[260]. Another coatomer binding signal mainly identified in the transmembrane proteins of the p24 superfamily members like TMED10 and TMED2 is the consensus sequence FFXX(KR)(KR)X_n n≥2, whose coatomer binding properties are said to rely on the dilysine-motif in cooperation with the diphenylalanine-motif[239]. The dilysine-motif was shown to interact with the B-subcomplex, whereas the diphenylalanine-motif exhibit binding strength to the F-subcomplex. Since contradicting results are published by multiple groups regarding the importance of the diphenylalanine-motif in the FFXX(KR)(KR)X_n n≥2 for COPI vesicle biogenesis, the crucial retrograde transport signal encoded in the p24 family members is still under debate[214,239,261–263].

With advancing cargo sorting, the coatomer protein lattice growth and increasing numbers of ARF1-GTP molecules are concentrated at the site of the budding vesicle. Hence, the ARF1 myristoylated amphipathic N-terminal helix dependent deformation of the cis-Golgi membrane progresses supposedly supported by BFA-induced ADP-ribosylation substrates (BARS) and endophilin B implicated in further shaping vesicle membranes and driving vesicle fission[264,265]. Additionally, the enrichment of phosphatic acid (PA) and diacylglycerol (DAG) on budding sites is believed to further support the membrane bending[266]. Recent studies showed that vesicle fission is independent of GTP hydrolysis. Nonetheless, the exact mechanism of vesicle release of the cis-Golgi membrane remains elusive[267]. The uncoating event of COPI vesicles necessary for fusion with acceptor membranes takes place after the COPI vesicle is pinched off and is facilitated by ArfGAP1 (ADP-ribosylation factor GTPase activating protein1) and ArfGAP2/3. ArfGAPS are recruited to the budding vesicle during coat formation and were shown to directly interact with coatomer subunits and cargo proteins. The primary role of ArfGAP1 is the hydrolysis of GTP of ARF1 and its activity is increased by positive membrane curvature. ArfGAP2/3's activity is uninfluenced by membrane curvature but is highly dependent on coatomer binding and drives ARF1-GTP hydrolysis as well. Although all three GAPs are viewed as non-essential components for COPI vesicle biogenesis, and single knockouts are considered non-lethal they are enriched in COPI vesicles and experimental findings support their role in vesicle uncoating.

1.3.5 Intra-Golgi transport: the two existing models

Newly synthesised proteins targeted for secretion or integration in membranes enter at the cis-Golgi interface, proceed through the three to nine stacked Golgi cisternae and leave the Golgi by being sorted into clathrin-coated vesicles at the trans-Golgi network[268]. As they pass through the Golgi apparatus, the cargo molecules are classified, sorted and post-translationally modified. Glycosidases and over 150 different glycosyltransferases subsequently trim, modify and/or rebuild the O-linked polysaccharide tree during this process[269]. To fulfil their part in a temporally and spatially organized manner, the Golgi cisternae's protein distribution as well as their lipid composition are inhomogeneous and can serve as a marker to discriminate between cis-, medial- and trans-Golgi cisternea[269,270]. Yet, how proteins and lipids are sorted and transported across the Golgi complex remains elusive, and vesicular transport, tubular extension, compartment fusion and compartment maturation are implied to be involved[203,271–274]. Various models are under debate since each can only partially explain the experimental results. Nonetheless, two main models have been developed over the years: the vesicular transport model and the cisternal maturation model[275,276].

The vesicular transport model was postulated by Farquhar and Palade in the early 80's of the 20th century. It suggested that the individual Golgi cisternae are stable compartments and that cargo transport through the Golgi complex relies on small protein-coated vesicles. The identification of COPI and COPII coated vesicles and their involvement in anterograde and retrograde vesicular transport strongly supported the vesicular transport model[277–279]. However, emerging evidence that COPI vesicles were lacking anterograde transport signals[280], that secretory cargo was excluded rather than enriched in COPI vesicles[281], and difficulties to explain large cargo transport[276] as well as the formation of tubular structures between Golgi cisternae cast doubt onto the vesicular transport model.

The cisternal progression/maturation model was proposed for the first time in the 50's by Grasse and co-workers and was updated multiple times to incorporate new experimental results[282,283]. The model postulates that ER-derived vesicles fuse at the cis-Golgi interface to build up Golgi cisternae which subsequently progress to the trans side where the cisternae disintegrate into post-Golgi carriers. Thereby, the cisternae act as anterograde carriers without assistance of additional membrane derived vesicles. Once cargo is incorporated into the cisternae it is transported and modified as it progresses

through the Golgi to the TGN. Golgi resident enzymes and lipids are retained and transported in a retrograde fashion through COPI vesicles, avoiding constant protein loss due to maturation[280,284–286]. The model is supported through the detection of some Golgi resident proteins in COPI vesicles (although their concentration is still under debate) and live-cell imaging demonstrating actual cisternae maturation[287,288]. In contrast, several studies questioned the sorting of Golgi resident proteins in COPI vesicles, contradicting one of the key assumptions of the model[289]. Furthermore, the model lacks an explanation how cargo molecules can show different transport kinetics through the Golgi compartment, as they are expected to progress through the cisternae simultaneously.

1.3.6 Trans-Golgi sorting and transport to the plasma membrane

The trans-Golgi is the sorting machinery of the cell, keeping track of the influx and exit of multiple cargos. Newly synthesised proteins from the cis-Golgi as well as proteins endocytosed at the plasma membrane are either transported to their target organelle or transported to the plasma membrane to be secreted. Interestingly, multiple transport pathways emerged to ensure specific protein targeting to their destination, involving different carriers, adapter proteins and sorting signals. The different pathways comprise the constitutive/default pathway, the selective endosomal pathway that is sub-divided into the transport to the apical or basolateral surface, and the regulated secretory pathway[290]. Nevertheless, the TGN-to-plasma-membrane transport routes have not been understood completely, yet. How these carriers are recruited, regulated and recycled is still under debate, and scientific working groups have published contradicting evidence.

By default, secretory proteins are targeted from the TGN-membrane to the plasma membrane in large pleiomorphic tubular structures as well as secretory vesicles and exit in a default, bulk-flow like fashion[291]. The anterograde movement of the pleiomorphic tubular structures seems to be dependent on dynamin-2, the kinesin-based motors, and the microtubule cytoskeleton[291–293]. The protein coat that envelops the TGN-derived vesicles in the constitutive pathway remains elusive, but several non-clathrin-coat-like proteins like p62, p200 and p230 have been identified in larger amounts at the TGN-membrane forming vesicles and were shown to be involved in vesicle formation in cell-free systems, as well[293–295].

Secretory cargo that does not exit the TGN network in a bulk-flow fashion relies on transport signals to be sorted into distinct vesicular carriers that target secretory granules, the endosome/lysosome system or the basolateral/apical surface directly. Furthermore, it is widely believed that endosome/lysosome targeted vesicles can use the endosomal compartment as an additional sorting station to transport their cargo further to either the apical or the basolateral side in polarized cells[296]. However, there is no evidence for such distinction in non-polarized cells until this assumption was challenged when two analogous transport routes with distinct sorting signals were identified in non-polarized cells like fibroblasts[297–299]. The molecular transport machinery involved in delivering proteins to endosomes and beyond is well characterized and relies on specific lipid compositions, ARF1, the clathrin protein coat, adaptor proteins (AP) and Golgi-localising, γ-adaptin ear homology, ARF-bindning proteins (GGAs). The vesical biogenesis is similar to the process reported for COPI and COPII vesicle formation. A family member of the small GTPases, ARF1, is recruited to the trans-Golgi network (or endosomes) and activated by BIG1/2-dependent exchange from GDP to GTP. It then initiates the vesicle biogenesis by insertion of the myristoylated amphipathic N-terminal helix into the membrane[300,301]. Together with the highly enriched membrane lipid phosphatidylinositol 4-monophosphat (PI4P), ARF1 synergistically promotes the binding of GGAs and the adaptor protein AP-1 to the trans-GOLGI network, which are implied to function in clathrin coat binding and cargo sorting[302–306].

So far, multiple sorting signals for the basolateral and apical side of the plasma were identified. In general, basolateral sorting of cargo molecules is facilitated by short signal sequences in the cytoplasmic domain. Two tyrosine-based sorting motifs, YXXØ and NPXY, were first identified in the low-density lipoprotein receptor (LDLR) and were intensively studied in the following years[307,308]. Additionally, the di-leucine motif found for instance in the Fc receptor represents a second broad group of basolateral sorting signals[309]. Finally, a sorting motif comprising a single leucine was proposed and studied in Emmprin[310]. Interestingly, NPXY is the only sorting motif that was shown to directly interact with the clathrin coat[311]. The other basolateral transport signals rely on the interaction with AP-1 or GGAs to be sorted into clathrin-coated vesicles and their transport to the basolateral side[312]. In contrast, apical transport signals have proven to be more difficult to decipher. Often, the actual transport motif is presented in extra-cytoplasmic and membrane-associated domains. The first apical transport signal identified was the posttranslational addition of glycosylphosphatidylinositol to proteins

anchoring it to membranes in MDCK cell and other epithelia cell lines[313,314]. Furthermore, evidence points to the involvement of N- and O-glycosylation on proteins in the apical sorting [315,316]. Removal of the glycosylation can trap the modified proteins in the TGN or alter their cellular distribution[317]. Today, apical sorting signals are considered to be hierarchically weaker than their basolateral counterparts, tested through blockage or removal of the basolateral signal sequence and subsequent detection of the investigated protein at the apical cell side[318,319].

During the cargo sorting process, lipid-binding and lipid-modifying proteins are recruited to the vesicular budding site, advancing the membrane curvature. Many of these proteins contain one of two conserved domains believed to possess membrane deforming properties: the Epsin N-terminal homology/AP180 N-terminal homology (ENTH/ANTH) domain and the Bin-amphiphysin-Rvs161/167p (BAR) domain[320–322]. EpsinR, containing an AP-1 and GGA2-binding motif and interaction sides for SNARE proteins, as well as Amphiphysin, a protein known to promote membrane tabulation, are two well characterized examples of the large group of membrane deforming proteins that are involved in clathrin-coated vesicle formation and present at the trans-Golgi membrane[320,323]. The deformed membrane is stabilized by the recruitment of the clathrin-coat. The coat consists of polymerized clathrin triskelia, each made up by three clathrin-heavy chains and three clathrin-light chains, assembling into hexagons and pentagons at the membrane[324]. The progressing membrane deformation, the action of different actin skeleton binding proteins and the large GTPase dynamin participate in the last steps of vesicle scission[325,326]. Dynamin assembles as an oligomeric complex at the vesicle neck, forming a spiral-like structure before it pinches the budding vesicle from the donor membrane in a GTP hydrolysing fission step[327,328]. Once the vesicle is constricted from the donor membrane, the clathrin coat is disassembled into the monomeric triskelia through the heat shock cognate 70 (HSC70) and its co-factor auxilin[329,330].

1.4 Aim of the study

The precisely controlled distribution of lipids, proteins and lipid-anchored proteins assembling into the membrane of various cellular organelles and the plasma membrane as well as the inter- and intracellular communication via receptors and signalling molecules are crucial for normal cellular function and depend on the secretory pathway. The correct temporal and spatial organisation of the secretory pathway largely contributes to cellular physiology in health and disease, among other things, by regulating intracellular signal transduction and transmitting input and output signals of the circadian clock, thereby regulating multiple cellular key pathways. In order to get a better understanding of coupling, intensive work investigating neuronal communication in the SCN has been done. Despite this, it is largely unknown and still under debate if coupling processes even actually exist in the periphery, what molecular components are involved, and what the implications for output signals of coupling in peripheral tissues are.

In the first part of the study, we aim to assess the contribution of vesicular protein transport to the generation of normal circadian rhythms in human osteosarcoma cell cultures as a model for peripheral tissues. To this end, we use RNAi-mediated knockdown constructs and pharmacological inhibitors blocking different important transport steps along the secretory pathway and monitor the effects on the circadian clock. By controlling for cell toxicity effects and off-target effects like unfolded protein response, we hope to directly link observed changes in circadian rhythmicity to the genetic and pharmacological perturbation.

In the second part of the study, we design experiments to investigate the influence of the secretory pathway on the intercellular communication of human osteosarcoma cells in order to maintain a stable period and high amplitude rhythmicity. To this end, we establish purification and enrichment protocols for conditioned medium and aim to discover paracrine signalling molecules which directly affect circadian oscillations, potentially revealing an undiscovered input pathway. Additionally, we intend to explore whether there is a connection between cell density in culture and robustness of the circadian oscillations by seeding varying numbers of human osteosarcoma cells and monitoring the *Bmal1*-promotor driven *luciferase* rhythms. Finally, we investigate the effects of secreted paracrine signalling molecules on circadian dynamics by

supplementing low density cell cultures with non-luminescent feeder cells to promote normal circadian periods and high amplitude rhythms.

The secretory pathway and the circadian clock are two crucial cellular processes that, to our knowledge, have not been directly connected so far. Here, we would like to provide first evidence that unperturbed vesicular transport events are important for normal clock function *in vitro*. Furthermore, we will collect data that may support the idea that signalling molecules are secreted into the exterior of the cell. We believe that their concentration is directly dependent on the capacity of the secretory pathway and the number of secreting cells and that it can directly influence the circadian oscillator. Taken together, this work would highlight the importance of the vesicular protein transport pathway for the circadian clock and deliver further support for coupling in peripheral tissue.

2 Material and Methods

2.1 Material

2.1.1 Cell lines

U-2 OS cells

The U-2 OS cells were provided as a kind gift of AG Hagemeier, Charité Berlin, Germany, originally purchased from the American Type Culture Collection (ATCC)[331].

Organism:	*Homo Sapiens*, human
Tissue:	bone
Disease:	osteosarcoma
Origin:	15-year-old Caucasian female
Morphology:	epithelial
Growth properties:	Adherent, contact inhibited growth
Culture Conditions:	DMEM medium, 10% v/v FBS, 37°C and 5% CO_2
Subcultivation ratio:	1:3 to 1:5 subcultivation ratio, two to three times a week
Reporter:	Stable expression of a 0.9 kB Bmal1 promotor fragment driving a firefly luciferase[332]
	Stable expression of a 0.5 kB Per2 promotor fragment driving a firefly luciferase[333]
	Stable expression of a full length Per2 promotor driving a firefly luciferase (kind gift of by Neta Tuvia)
	Stable expression of seven SRE cis-acting enhancer elements in front of a minimal promotor driving a firefly luciferase[3]
	Stable expression of seven CRE cis-acting enhancer elements in front of a minimal promotor driving a firefly luciferase (kind gift of by Neta Tuvia)

HEK293

The HEK293 cell line was purchased from ATCC[334].

Organism:	*Homo Sapiens*, human
Tissue:	Embryonic kidney
Morphology:	epithelial
Growth properties:	adherent
Origin:	foetus
Culture Conditions:	DMEM medium, 10% v/v FBS, 37°C and 5% CO_2
Subcultivation ratio:	1:6 to 1:12 subcultivation ratio, two to three times a week

HEK293T

The HEK293T cell line was purchased from ATCC[335].

Organism:	*Homo Sapiens*, human
Tissue:	Embryonic kidney
Morphology:	epithelial
Growth properties:	adherent
Origin:	foetus
Culture Conditions:	DMEM medium, 10% v/v FBS, 37°C and 5% CO_2
Subcultivation ratio:	1:6 to 1:12 subcultivation ratio, two to three times a week

2.1.2 Cell culture medium composition

Cell culture medium	Composition
Culture Medium (CM)	500 ml DMEM, high Glucose 10 % (v/v) FBS 1 % (v/v) Streptomycin/Penicillin 25 mM HEPES

Cell culture medium	Composition
Culture Medium, phenol-red free, serum-free	500 ml DMEM, high glucose, phenolred-free 1 % (v/v) Streptomycin/Penicillin
Culture Medium for bioluminescence measurement	500 ml DMEM, high glucose, phenolred-free 10 % (v/v) FBS 1 % (v/v) Streptomycin/Penicillin 250 µM D-Luciferin
Culture Medium for bioluminescence measurement without FBS	500 ml DMEM, high glucose, phenolred-free 1 % (v/v) Streptomycin/Penicillin 250 µM D-Luciferin
Freezing medium	90 % (v/v) FBS 10 % (v/v) dimethyl sulfoxide (DMSO)

2.1.3 Bacteria cells

Bacterial strains	Source	Genotype
E. coli DH10β	Thermo Fisher Scientific	F^- mcrA Δ(mrr-hsdRMS-mcrBC) ϕ80lacZΔM15 ΔlacX74 recA1 endA1 araD139 Δ (ara, leu)7697 galU galK λ- rpsL nupG /pMON14272 /pMON7124
E. coli DH5α	Thermo Fisher Scientific	F^- Φ80*lac*ZΔM15 Δ(*lac*ZYA-*arg*F) U169 *rec*A1 *end*A1 *hsd*R17(r_k^-, m_k^+) *pho*A *sup*E44 *thi*-1 *gyr*A96 *rel*A1 λ^-
E. coli TOP10	Thermo Fisher Scientific	F- *mcrA* Δ(*mrr-hsd*RMS-*mcr*BC) Φ80*lac*ZΔM15 Δ *lac*X74 *rec*A1 *ara*D139 Δ(*araleu*)7697 *gal*U *gal*K *rps*L (StrR) *end*A1 *nup*G
E. coli XL1blue	Stratagene	F´ *proA*$^+$*B*$^+$ *lacI*^{q} Δ*(lacZ)M15 zzf::Tn10* (Tet^R) */ fhuA2*Δ*(argF-lacZ)U169 phoA glnV44 Φ80Δ(lacZ)M15 gyrA96 recA1 relA1 endA1 thi-1 hsdR17*

2.1.4 Bacteria medium composition

Bacteria culture medium	Composition
LB-Medium	10 g NaCl 10 g Bactotryptone 5 g yeast extract 12.5 g agar ad 1 l aq. dest sterilize

2.1.5 Chemicals

All chemicals were purchased from the following companies:

Company	Location
Sigma-Aldrich	Taufkirchen, Germany
Carl Roth GmbH + Co. KG	Karlsruhe, Germany
Becton Dickinson (BD)	Heidelberg, Germany
AppliChem	Darmstadt, Germany
Merck Chemicals GmbH	Darmstadt, Germany
Serva	Heidelberg, Germany
Fluka	Buchs, Switzerland

2.1.6 Consumables and plastics

All consumables and plastics were purchased from the following companies (see **2.1.21** for additional information on special consumables and plastics).

Company	Location
Sarstedt	Nümbrecht, Germany
Becton Dickinson (BD)	Heidelberg, Germany

Company	Location
Merck Chemicals GmbH	Darmstadt, Germany
VWR International GmbH	Darmstadt, Germany
Biozym Scientific GmbH	Hessisch Oldendorf, Germany
Thermo Fisher Scientific	Darmstadt, Germany

2.1.7 Reagents

Reagent	Supplier	Product number
β-mercaptoethanol	Carl Roth	4227.1
bovine serum albumin (BSA)	Sigma-Aldrich	A7030
dexamethasone (stock 1 mM in EtOH)	Sigma-Aldrich	D4902
dimethyl sulfoxide (DMSO)	AppliChem	A3672
D-Luciferin (stock 0.1 mM in CM)	PJK	102112
dNTP Mix 10 mM	Thermo Fisher Scientific	611352
ethidium bromide	Carl Roth	2218.1
fetal bovine serum (FBS)	Thermo Fisher Scientific	10106-169
HPLC water	Carl Roth	A511.2
Lipofectamine2000	Thermo Fisher Scientific	11668019
NuPAGE 10-15 % SDS poly acrylamide gel	Thermo Fisher Scientific	NP0335PK2
NuPAGE sample buffer (4x)	Thermo Fisher Scientific	NP0007
nitrocellulose membrane protan BA85, pore size 0.45 µM	Schleicher and Schuell	10401196
Oligo (dT)12-16	Thermo Fisher Scientific	18418012
Orange Load. Dye (6x)	Thermo Fisher Scientific	R0631

Reagent	Supplier	Product number
Poly-D-lysine	Sigma-Aldrich	P6407
ProLong Diamond Antifade Moutant with DAPI	Thermo Fisher Scientific	P36966
protamine sulfate	Sigma-Aldrich	P3369
protease inhibitor cocktail	Sigma-Aldrich	P8340
random hexamers	Thermo Fisher Scientific	SO1492
Resazurin	R & D systems	AR002
SuperSignal West Pico Chemiluminescent substrate	Thermo Fisher Scientific	34080
SYBR green master mix	Thermo Fisher Scientific	K0364
trypan blue	Sigma-Aldrich	T8154
Trypsin/EDTA (1 x), 0.5 g/l trypsin	Lonza Biozym	882

2.1.8 Enzymes

Enzyme	Supplier	Product number
CIP – alkaline phosphatase, calf intestinal, 10.000 U/ml	New England Biolabs	M0290S
DNA Polymerase I, large (Klenow) fragment, 5.000 U/ml	New England Biolabs	M0210L
PureLink DNAse, 3 U/µl	Invitrogen	12185-010
M-MLV Reverse Transcriptase, 200 U/µl	Thermo Fisher Scientific	28025-021
LR-Clonase enzyme mix, 20 reactions	Thermo Fisher Scientific	11791-019
T4 Ligase (FastLink Ligase Kit), 2 U/µl	Biozym Scientific GmbH	133600 (LK6201H)

Restriction Enzyme	Supplier	Product number
AgeI, 5 U/µl	New England Biolabs	R0552S
BamHI, 20 U/µl	New England Biolabs	R0136S
BlpI, 10 U/µl	New England Biolabs	R0585S
BsgI, 5 U/µl	New England Biolabs	R0559S
BsrGI, 10 U/µl	New England Biolabs	R0575S
DpnI, 20 U/µl	New England Biolabs	R0176S
EcoRI, 20 U/µl	New England Biolabs	R0101S
EcoRV, 20 U/µl	New England Biolabs	R0195S
HindIII, 20 U/µl	New England Biolabs	R0104S
NotI, 10 U/µl	New England Biolabs	R0189S
SacI, 20 U/µl	New England Biolabs	R0156S
SacII, 20 U/µl	New England Biolabs	R0157S
XhoI, 20 U/µl	New England Biolabs	R0146S

Polymerase	Supplier	Product number
Deep Vent DNA Polymerase, 2.000 U/ml	New England Biolabs	M0258S
Phusion High-Fidelity DNA Polymerase, 2 U/µl	Thermo Fisher Scientific	F-530L
Platinum Pfx DNA Polymerase, 2 U/µl	Thermo Fisher Scientific	11708-013

2.1.9 DNA und protein standards

Reagent	Supplier	Product number
100 bp DNA ladder	New England Biolabs	N3231
1 kb DNA ladder	New England Biolabs	N3232
Magic Mark XP	Thermo Fisher Scientific	LC5602
Spectra multi-color broad range	Thermo Fisher Scientific	26634

2.1.10 Buffers and media

Self-made buffers and media

Buffer or medium	Composition
Bicinchonic acid assay (BCA) solution A	2 % (w/v) Na2CO3 1 % (w/v) BCA-Na2 0.95 % (w/v) NaHCO3 0.4 % (w/v) NaOH 0.16 % (w/v) Na2-tartrat x 2 H_2O solved in aq. dest.; pH 11.25 (NaOH)
Bicinchonic acid assay (BCA) solution B	4 % (w/v) CuSO4 x 5 H2O
Blocking Solution for Western Blots	1 x TBS 0.05 % Tween® 20 5 % (w/v) skim milk
Coomassie staining solution	45 % (v/v) MeOH 10 % (v/v) CH_3COOH (100%) 0.25 % (w/v) Coomassie Blue R250/L
Coomassie de-staining solution	30 % (v/v) MeOH 10 % (v/v) CH_3COOH (100%)
Ethidium bromide solution	2 µg/ml Ethidium bromide in aq. Dest

Buffer or medium	Composition
Formaldehyde solution	1x PBS 3.7 % formaldehyde
HEPES	1 M HEPES solved in aq. dest.; pH 7.2 (NaOH); sterile filtered
LB-Agar	10 g NaCl 10 g Bactotryptone 5 g yeast extract ad 1 l aq. dest sterilize
Permeabilization solution	1x PBS 0.1 % Triton X 0.5 % goat serum
10x Phosphate-buffered saline (PBS)	1.37 M NaCl 27 mM KCl 100 mM Na2HPO4 20 mM NaH2PO4 solved in aq. dest.; pH 7.2 (NaOH); dilute to 1x PBS before use sterilize
Radioimmunoprecipitation assay buffer (RIPA)	1 % (w/v) Igepal CA-630 0.5 % (w/v) sodium deoxicholat 0.1 % (w/v) sodium dodecyl sulfate (SDS) solved in 1 x PBS; sterile filtered
SDS-solution	10% (w/v) sodium dodecyl sulfate (SDS) solved in aq. dest.
SDS tris-glycine running buffer	0.25 M tris-base 1.92 M glycine 1 % (w/v) SDS solved in aq. dest.; pH 8.3; dilute to 1x SDS-TGR buffer before use

Buffer or medium	Composition
SDS transfer buffer	1 x SDS tris-glycine running buffer 20 % (v/v) MeOH
Separation gel buffer	1.5 M tris-base solved in aq. dest.; pH 8.8
Stacking gel buffer	0.5 M Tris-HCl solved in aq. dest.; pH 6.8
10 x Tris-buffered saline (TBS)	1.37 M NaCl 100 mM tris-base solved in aq. dest.; pH 7.3; sterilize dilute to 1x TBS before use
5x Tris-borate-EDTA-buffer (TBE)	54 g tris-base 27.5 g boric acid 20 ml of 0.5 M EDTA (pH 8.0) ad 1 l aq. dest. dilute to 1x TBE before use
50x Tris-acetate-EDTA-buffer (TAE)	2 M tris-base 50 mM EDTA 1 M 100 % acetic acid solved in aq. dest.; pH 8.5 dilute to 1x TAE before use

Commercially available buffers and media

Buffer or Medium	Supplier	Product number
DMEM, high glucose	Thermo Fisher Scientific	41965-062
DMEM, high glucose, phenolred-free	Thermo Fisher Scientific	21063-045
HEPES buffer solution, 1M	Thermo Fisher Scientific	15630-080

Buffer or Medium	Supplier	Product number
New England Biolabs buffer 1-4	New England Biolabs	B7001S, B7002S, B7003S, B7004S
New England Biolabs CutSmart® Buffer	New England Biolabs	B7204S
NuPAGE MES SDS running buffer (20x)	Thermo Fisher Scientific	NP0002
NuPAGE transfer buffer (20x)	Thermo Fisher Scientific	NP00061
Opti-MEM Reduced Serum Medium	Thermo Fisher Scientific	31985-047

2.1.11 Pharmacological Inhibitors

Inhibitor	Supplier	Product number
Eeyarestatin	Biomol	Cay10012609-5
CI-976	Sigma	C3743-5MG
FLI-06	Sigma	SML0975-5MG
Golgicide A	Sigma	G0923-5MG
Exo 1	Sigma	E8280-5MG
Exo 2	Sigma	E7159-5MG
AG1478	Sigma	T4182-1MG
Brefeldin A	Sigma	B7651-5MG
LM 11	Enamine	Z1037336016
Pitstop 1	Abcam	ab120685
Pitstop 2	Abcam	ab120687
Dynasore	Biomol	Cay14062-5
MiTMAB	R&D Systems	4224/10

Inhibitor	Supplier	Product number
ZCL278	VWR	BVIS2466-5
Vacuolin	Millipore	673000-10MG
16D10	Hit2Lead	# 5175347
GW4869	Sigma	D1692-5MG
A5	Hit2Lead	# 5431942
Tunicamycin	Biomol	Cay11445-5
Deoxynojirimycin	Biomol	BVT-0112-M005
Castanospermine	Biomol	Cay11313-5
Deoxymannojirimycin	Sigma	D9160-1MG
Swainsonine	Sigma	Cay16860-1

2.1.12 Antibiotics

Antibiotic	Supplier	Product number
Streptomycin/Penicillin (100x)	Thermo Fisher Scientific	15140-122
Ampicillin	Carl Roth	K029.2
Kanamycin	Carl Roth	T832.4
Puromycin	Sigma-Aldrich	P9620-10 ml
Blasticidin	Thermo Fisher Scientific	R210-01
Zeocin	Thermo Fisher Scientific	R250-01

2.1.13 Antibodies

Primary antibodies

Target	Source	Supplier	Product number	Dilution
α-TMED10 (human)	rabbit, polyclonal	Kindly provided by Felix Wieland, BZH Heidelberg		1:10.000
α-βACTIN, clone AC-15 (human)	mouse, monoclonal	Sigma-Aldrich	A5441	1:100.000
α-GM130 (human)	rabbit, monoclonal	Epitomics	1837-1	1:200
α-V5-tag	mouse, monoclonal	Thermo Fisher Scientific	R96025	1:5.000
α-GFP	mouse, monoclonal	Santa Cruz	SC-9996	1:1000
α-tGFP	rabbit, polyclonal	Evrogen	AB513	1:20.000

Secondary antibodies

Target	Source	Supplier	Product number	Dilution
α-mouse IgG-HRP	goat	Santa Cruz	sc-2005	1:1000
α-rabbit IgG-HRP	donkey	Santa Cruz	sc-2305	1:1000
α-rabbit-Alexa488	goat	Thermo Fisher Scientific	A-11034	1:200
α-rabbit-Alexa594	goat	Thermo Fisher Scientific	A-11037	1:200

2.1.14 Gene Synthesis

Gene synthesis was ordered from Eurofins MWG Operon.

Name	Sequence (5′ → 3′)
TMED10 lacking the luminal domain	CCAACTTTGTACAAAAAAGCAGGCTCCGCGGCCGCCCCCT TCACCATGTCTGGTTTGTCTGGCCCACCAGCCCGGCGCGG CCCTTTTCCGTTAGCGTTGCTGCTTTTGTTCCTGCTCGGCC CCAGATTGGTCCTTGCCATCACCGGTGCCGCTGAATTCCG GGTCCTATACTTCAGCATCTTTTCAATGTTCTGTCTCATTG GACTAGCTACCTGGCAGGTCTTCTACCTGCGACGCTTCTT CAAGGCCAAGAAATTGATTGAGTAAGGGTGGGCGCGCCG ACCCAGCTTTCTTGTACAAAGTTG

2.1.15 Primers and Oligos

All primers were designed using GENtle and Primer Blast. The melting temperature was calculated using GENtle. All primers were orders from Eurofins MWG Operon.

Sequencing primers

Primer name	Sequence (5′ → 3′)
Seq GBF1 2	GCTGCTCTTCACAAGGTT
Seq GBF1 3	GCTGACAGTGGCCCTTG
Seq GBF1 4	CATCAGCCCTGCAGATGT
Seq GBF1 5	GAGGAAGCTGTTGACTCT
Seq GBF1 6	GAATGTGCTGCTTCATCG
Seq GBF1 7	CTCATGAAGGCTCTGGTC
Seq GBF1 8	CCTGATCAATCAATACAG
M13 FW	GTAAAACGACGGCCAGT
M13 RV	CAGGAAACAGCTATGAC

Mutagenesis primers

Mutagenesis primers were designed as described in the QuikChange Site - Directed Mutagenesis Kit and ordered from Eurofins MWG Operon.

Primer name	Sequence (5′ → 3′)
hTMED10 FF->AA FW	GTCTTCTACCTGCGACGCGCCGCCAAGGCCAAGAAATTG ATTGAG
hTMED10 KK->SS FW	GTCTTCTACCTGCGACGCTTCTTCAAGGCCTCGTCATTG ATTGAG
hTMED10 FF->AA RV	CTCAATCAATTTCTTGGCCTTGGCGGCGCGTCGCAGGTA GAAGAC
hTMED10 KK->SS RV	CTCAATCAATGACGAGGCCTTGAAGAAGCGTCGCAGGTA GAAGAC

Amplification primers

Primer name	Sequence (5′ → 3′)
hARF1 FW (TOPO)	CACCATGGGGAACATCTTCGCCAA
NΔ17-hARF1 FW (TOPO)	CACCATGCGCATCCTCATGGTGG
hARF1 RV m St	TCACTTCTGGTTCCGGAGCTGATT
hARF1 RV w/o St	CTTCTGGTTCCGGAGCTGATTGG
AgeI-EGFP FW	TGGCCACCGGTATGGTGAGCAAGGGCGAG
EGFP-EcoRI RV	GGCCGAATTCCTTGTACAGCTCGTCCATG
hGBF1 FW (TOPO)	CACCATGGTGGATAAGAATATTTACATCATTCAAG

Primer name	Sequence (5′ → 3′)
hGBF1 RV w St	TTAGTTGACCTCAGAGGTGGG
hGBF1 RV w/o St	GTTGACCTCAGAGGTGGGTAT
hTMED2 FW (TOPO)	CACCATGGTGACGCTTGCTGAA
hTMED2 RV w St	TTAAACAACTCTCCGGACTTCAAAAAATCTC
hTMED2 RV w/o St	AACAACTCTCCGGACTTCAAAAAATCTCT
hTMED10 FW (TOPO)	CACCATGTCTGGTTTGTCTGG
hTMED10 RV m St	TTACTCAATCAATTTCTTGGCCTTGAA
hTMED10 RV w/o St	CTCAATCAATTTCTTGGCCTTGAAGAA
hXBP1 FW	TTACGAGAGAAAACTCATGGCC
hXBP1 RV	GGGTCCAAGTTGTCCAGAATGC

2.1.16 quantitative real-time polymerase chain reaction (qRT-PCR) primers

All qRT-PCR primers were either ordered from Quiagen as QuantiTected Primer Assays or from Eurofins MWG Operon as unmodified oligos.

Target	Product number	Sequence (5′ → 3′)
hGAPDH FW		TGCACCACCAACTGCTTAGC
hGAPDH RV		ACAGTCTTCTGGGTGGCAGTG
hSEC13	QT00027657	
hGBF1	QT00042399	
hTMED2	QT00013195	

Target	Product number	Sequence (5′ → 3′)
hTMED10	QT00012656	
hBMAL1	QT00011844	
hCLOCK	QT00054481	
hREVERB-α	QT00000413	
hDBP1	QT00055755	
hPER1	QT00069265	
hPER2 FW		CACCAAATTGTTTGTTCCAGG
hPER2 RV		AACCGAATGGGAGAATAGTCG
hCRY1	QT00025067	
hTMED10 oLD PP10 FW		TCAGCATCTTTTCAATGTTCTGTC
hTMED10 oLD PP10 RV		AAGAAGCGTCGCAGGTGAAA
hDNAJC3	QT00011284	
hHERPUD1	QT00026418	
hFOS	QT00007070	

2.1.17 PCR-amplified coding sequences (CDS)

All coding sequences used in this study were verified by restriction enzyme digestion and sanger sequencing.

Coding sequence	Entrez Gene ID	Origin
TMED10	10972	PCR-amplified from an oligo-dT transcribed cDNA library from U-2 OS cells
TMED2	10959	PCR-amplified from an oligo-dT transcribed cDNA library from U-2 OS cells

Coding sequence	Entrez Gene ID	Origin
eGFP		PCR-amplified from an pGIPZ-ns lentiviral expression vector
ARF1	375	PCR-amplified from an pcDNA3.1 expression vector (Kindly provided by Michael Krauß, FMP Berlin)

2.1.18 RNAi constructs

Target	Product number	Sense sequence (5′ → 3′)
GBF1_1	V2LHS_33647	GCCAG AAGAT TGAAG CTGA
GBF1_2	V2LHS_33649	GACAC TAAGT CTCTG CTTA
SEC13_1	V2LHS_265275	GAAGT AAAGA AGATC AACA
SEC13_2	V3LHS_406089	CGGAG ATGCT TTGTA ATCT
TMED2_1	V2LHS_78727	CTCAA ACACT GTAAG TGAA
TMED2_2	V2LHS_258384	CTGAT GATCC CAACT CAGA
TMED10_1	V2LHS_78397	CTTTC AGAAT CTATT GTTA
TMED10_2	V2LHS_78399	GGGCT TCCAT TCTAG TTCT
TMED10_3	V3LHS_411690	AGAGT CACCT ATGACA AAA
TMED10_4	V3LHS_411689	ACCTA CACCC AACAA GTCA
TMED10_5	V3LHS_381637	GCAAA AGTTG AGAAG CTCA

Target	Product number	Sense sequence (5′ → 3′)
TMED10_6	V3LHS_381638	CCTTT CAGAA TCTAT TGTT
TMED10_7	V3LHS_261717	CAAAT GTTGA GAAAG TCTA
TMED10_8	V3LHS_78396	CCAAG AAATT GATTG AGTA
TMED10_9	V3LHS_411688	TGGAT GTGAC ACCTC ATAA
TMED10_10	V3LHS_381636	ACGAA GAGAT TGCAA AAGT
Non-silencing	RHS4346	ATCTC GCTTG GGCGA GAGTA AG

2.1.19 Vector Backbones

Vector backbone	Supplier/Source	Purpose
pENTR/D-TOPO	Thermo Fisher Scientific	TOPO-cloning, shuttling vector
pcdnaDEST 40	Thermo Fisher Scientific	Expression-vector
pLenti6-Dest-V5	Thermo Fisher Scientific	Expression-vector, V5-tag
pLenti6-Dest-Venus	Thermo Fisher Scientific	Expression-vector, venus-tag
pGIPZ	GE Dharmacon,	Expression-vector for shRNA
pMD2G	Addgene	Expression-vector, coding for viral envelope
psPAX	Addgene	Expression-vector, coding for viral packaging machinery
pEX-A	Eurofins MWG Operon	Delivery of gene synthesis

2.1.20 Kits

Name of the kit	Supplier	Product number
CalPhos Mammalian Transfection kit	Clontech Laboratories	631312
Fast-Link DNA Ligation kit	Biozym	133625
Gateway LRClonase® II Enzyme mix	Thermo Fisher Scientific	11791020
MycoAlert detection kit	Lonza	LT07-418
QIAEX II gel extraction kit	QIAGEN	20021
QuikChange Site - Directed Mutagenesis Kit	Agilent Technologies	200518
PureLink HiPure Plasmid Filter Midiprep kit	Thermo Fisher Scientific	K210015
pENTR/D-TOPO Cloning kit	Thermo Fisher Scientific	K240020
PureLink Quick Mini kit	Thermo Fisher Scientific	K210011
PureLink RNA Mini kit	Thermo Fisher Scientific	12183018A

2.1.21 Equipment und electronic devices

Product name	Description	Supplier
agarose gel chamber		Febikon Biometra
ALPS 50	manual heat sealer	Thermo Fisher Scientific
Amicon Ultra 15 mL centrifugal filters	Protein purification and concentration filter	Merck
Biometra Tadvanced	PCR machine	Biometra
C1000 Touch	thermal Cycler	Bio-Rad Laboratories
CFX96	qRT-PCR cycler	Bio-Rad Laboratories

Product name	Description	Supplier
ChemoCam Imager 3.2	imaging station	INTAS
centrifuges (5810R, 5424R, 5415D)		Eppendorf
Consort E143	electrophoresis power supply	Sigma-Aldrich
Filtropur S 0.45	virus supernatant filtration	Sarstedt
GFL 3032	shaking incubator	GFL
Hera cell 150	incubator	Thermo Fisher Scientific
Hera cell 150i	incubator	Thermo Fisher Scientific
Herasafe (S1)	biosafety cabinet	Thermo Fisher Scientific
Herasafe KS class II (S2)	biosafety cabinet	Thermo Fisher Scientific
Infinite F200 pro	microplate reader	Tecan
LumiCycle	luminometer	Antimetrics
Leica DMIL LED Fluo	fluorescence microscope	Leica
NanoDrop 2000c	determination of DNA and RNA concentration	Thermo Fisher Scientific
Neubauer chamber	cell counting chamber	Karl Hecht GmbH & CoKG
Lab pH meter inoLab, pH7110	pH meter	WTW
Leica TC SP8 (63x oil immersion objective)	confocal microscope	Leica
Liquidator96	Multipipette, 96 well format	Steinbrenner
microwave		Bosch
MultiSCREEN HTS	96 well plates for lentiviral filtration	Merck
pipettes (1-1000 µl)		Eppendorf Gilson
pipettes, multichannel		Eppendorf
(5-300 µL)		Thermo Fisher Scientific

Product name	Description	Supplier
Rainin AutoRep E	electronic multistep pipette	Rainin
standard power pack P25	electrophoresis power supply	Biometra
Unitwist RT	rocking table shaker	UniEquip
tabletop centrifuge		NeoLab
TC dish 35 x, Nunclon	cell culture dishes, LumiCycle	Thermo Fisher Scientific
Thriller	thermal shaker	VWR
TopCount	luminometer	PerkinElmer
Uno thermal cycler	PCR machine	VWR
UV trans illuminator		Konrad Benda
Vortex Genie 2		Scientific Industries, Inc.
Whatman gel blotting paper		Schleicher and Schuell
White micro well 96F, Nunclon delta	white 96 well plates, TopCount luminometer assay	Thermo Fisher Scientific
XCell SureLock Mini-Cell	electrophoresis system	ThermoFisher Scientific

2.1.22 Software

Software	Source/Supplier
CFX Manager	Bio-Rad Laboratories
ChronoStar 2.0	in-house developed; S. Lorenzen, B. Maier
GENtle	open source (M. Mankske, University of Cologne)
ImageJ 1.44p	open source (National Institute of Health)
Irfanview	open source (Irfan Skiljan)
LAS X Software	Leica
Matlab 7.0	Mathwoks

2.1.23 Databases and online tools

Database	Homepage
Ensemble genome browser	http://www.ensembl.org/index.html
Circa DB - circadian expression profiles data base	http://circadb.hogeneschlab.org/
National Center for Biotechnology Information	http://www.ncbi.nlm.nih.gov/
UniProt	http://www.uniprot.org/
Primer Blast - NCBI	https://www.ncbi.nlm.nih.gov/tools/primer-blast/

2.2 Methods

2.2.1 Cell culture procedures and assays

Cultivation and passaging of mammalian cells

Aliquots of U-2 OS cells and HEK293T cells were thawed every 8. Once thawed, cells were cultured in CM at 37°C and 5% CO_2 in humid atmosphere. During this time, the cells were passaged twice or thrice a week at a 90% confluency. To do so, cells were rinsed once with pre-warmed 1x phosphate buffered saline (PBS) prior to enzymatic detachment using a trypsin/EDTA solution for 10 minutes at 37°C. The detached cells were completely dispersed in CM by pipetting up and down trice and then split at appropriate ratios. All cultured cells were tested on mycoplasma in regular intervals using the luciferase-based MycoAlert detection kit (Lonza).

Determination of cell number and seeding of cells

To estimate the cell number in an enzymatically detached cell suspension an aliquot of 10 µl was mixed with trypan blue at a 1:1 ratio. Then, the coloured cell suspension was introduced into the Neubauer cell chamber and unstained cells in the four big squares were counted. The number of living cells was calculated using equation (1):

$$cell\ number\ [cells\ /\ ml] = \frac{cell\ count\ x\ dilution\ factor\ x\ 10000}{counted\ squares} \quad (1)$$

The cell suspension was diluted in CM to suit the experimental setup and cells were seeded in appropriate volumes.

Freezing and thawing of mammalian cells

To freeze cells for long term storage, confluent U-2 OS cells or HEK293T cells were detached, dispersed and counted as described previously (see *Cultivation and*

passaging of mammalian cells and *Determination of cell number and seeding of cells*) Subsequently the cells were spun down at 300g and 4°C for 10 minutes and the supernatant was aspirated. The U-2 OS cell pellet or HEK293T cell pellet was resuspended in freezing medium at a concentration of $2x10^6$ or $1x10^6$ respectively, aliquoted and, then, slowly cooled down to -20°C in an isopropanol bath. For long term storage, the aliquots were transferred to the liquid nitrogen storage tank.

Thawing of cell was accomplished by prewarming a frozen vial of approximately $2x10^6$ human U-2 OS cells or $1x10^6$ human HEK293T cells in a water bath at 37°C for two minutes. The thawed cells were transferred to 12 ml of complete medium (CM) in a $75cm^2$ cell culture flask. After 24 hours, the medium was exchanged with fresh complete medium to take off the DMSO containing freezing medium.

Transient transfection of mammalian cells

Transient transfection of U2OS cells or HEK293T cells was carried out using either Lipofectamin2000 or the CalPhos Mammalian Transfection kit respectively, according to the manufacturer's manual.

Very briefly, cells were seeded one day prior to transfection at a density that led to a 90% confluent culture 24 hours later. When using Lipofectamin2000 the transfection reagent as well as the plasmid DNA were mixed in Opti-MEM, incubated for 30 minutes at room temperature and then applied to the cells after aspiration of the culture medium. The next day the cell culture supernatant was exchanged to CM and follow-up experiments could be carried out.

When cells were transiently transfected with the CalPhos Mammalian Transfection kit a pre-mixed solution of DNA and calcium was slowly added to an 2xHBS solution. During the 30-minute incubation time at room temperature the culture medium was exchanged to increase transfection efficiency and, then, the transfection reaction was directly added to the culture medium. The next day the medium was exchanged and follow-up experiments could be carried out.

Lentivirus production in HEK293T cells

Production of lentivirus in HEK293T cells was carried out as described in the standard operating procedure (**Supplemental Figure C 1**).

Briefly, HEK293T cells were transiently transfected with equimolar amounts of psPAX2 (coding for the viral packaging machinery), pMD2.G (coding for the viral envelope) and the expression plasmid using the CalPhos Mammalian Transfection kit according to the manufacturer's manual. After 24 hours, the culture medium was exchanged. On the two consecutive days, the viral particle containing supernatant was collected in a 50-ml reaction tube and stored at 4°C on ice until filtration through a 0.45 µM filter unit. Filtered virus particles were either used directly for lentiviral transduction of mammalian cell culture or stored at -80°C for future experiments.

Lentiviral transduction of mammalian cells

Mammalian cells were detached using an trypsin/EDTA solution (see *Cultivation and passaging of mammalian cells*), counted (*see Determination of cell number and seeding of cells*) and diluted to a density of 20.000 cells/cm^2. The filtered lentivirus containing supernatant was added in an equivalent volume in the presence of 8 µg/ml protamine sulfate. Incubation was carried out for at least a day under standard conditions before the cell culture medium was exchanged.

Selection of transfected or transduced cells

Transfected or transduced cells were selected by supplementing the cell culture medium with the appropriate antibiotic. Puromycin was used in a concentration of 10 µg/ml for at least three consecutive days. Blasticidin was used in a concentration of 10 µg/ml for at least seven consecutive days and the cells were detached every 2-3 days using an EDTA/Trypsin solution to increase the selection efficiency.

Immunofluorescence staining

U-2 OS cells were transduced with pGIPZ knockdown constructs containing a silenced tGFP (see *Lentiviral transduction of mammalian cells* and **2.2.6**) and selected as described previously (see *Selection of transfected or transduced cells*). Then, the transduced cells were seeded onto poly-D-lysine coated glass coverslips in two different densities and incubated for 24 hours to allow proper attachment. 24 hours later, the U-2 OS cells were rinsed once with pre-warmed PBS and fixed with 3.7 % formaldehyde solution for 15 minutes in a wet chamber. Afterwards, the cells were washed thrice with pre-warmed PBS, blocked, and permeabilised, incubating them with permeabilization solution for one hour at room-temperature. Primary antibody rabbit-anti-GM130 was diluted 1:200 in permeabilization solution and applied for two hours at room temperature. After intensive washing with pre-warmed PBS, the secondary antibody goat-anti-rabbit-Alexa488 (or goat-anti-rabbit-Alexa594) was diluted 1:200 in permeabilization solution and applied for one hour at room temperature. The permeabilization solution was washed away intensively with prewarmed PBS, cells were rinsed once with aqua dest. and dried at room temperature. The coverslips were transferred onto coverglasses using mounting medium and dried overnight before imaging.

Pharmacological treatments

Every purchased pharmacological compound was dissolved in the appropriate solvent as recommended by the manufacturer's manual and stored at -20°C. For pharmacological perturbation experiments, cells were grown to confluence and prepared for bioluminescence measurement (see *Bioluminescence recordings*). Right before the start of the measurement the cell culture medium was supplemented with the indicated concentration of the pharmakon. The maximum solvent concentration of either DMSO or ethanol was thereby limited to 2%.

Cell vitality assay

Cell vitality was determined by using a fluorescence based Resazurin cell vitality assay according to the manufacture's manual. Briefly, cell cultures were supplemented with 10% Resazurin and incubated 2-4 hours at 37°C. Red fluorescence was measured at an excitation wavelength of 535 nm and an emission wavelength of 590 nm using the Infinite F200 pro (Tecan). The measured red fluorescence values were either normalized to non-silencing controls, solvent controls or untreated cells. A result higher than 0.75 was considered as vital.

Preparation and enrichment of conditioned Medium

Conditioned medium was prepared from U-2 OS wild-type cells. Briefly, the cells were seeded at a low density of 15.000 cells/cm^2 with no cell-cell-contact and cultured for two days under normal cell culture conditions. At approximately 50% confluency, the cells were rinsed thrice with 1xPBS and once with serum and phenol red free DMEM prior to a one-day cultivation in serum and phenol red free DMEM supplemented with 250 µM D-Luciferin.

The conditioned medium was decanted into a 50-ml reaction tube, spun at 4000g and 4°C for 15 minutes and transferred through a 0.2 µM filter unit. To concentrate the conditioned medium, up to 12 ml of the sample were added to an Amicon Ultra filter device and spun at 4000g and 4°C for 20 minutes, repeatedly, until all sample was passed. The concentrated conditioned medium was withdrawn from the Amicon Ultra filter device and stored in a reaction tube at 4°C for up to one hour.

2.2.2 Imaging Methods

Bioluminescence recordings

Mammalian cells used for bioluminescence recordings were either harbouring a *Bmal1*- or a *Per2*-promotor driven *luciferase* construct or were expressing a Per2::Luc-fusion protein. They were seeded and grown to confluency in white 96-well plates

(TopCount) or in Nunc 35-mm dishes (Lumicycle or LumiBoxes). In preparation for the measurement, the cells were synchronized with 1 µM Dexamethasone for 30 minutes, rinsed twice with pre-warmed 1xPBS and supplied with serum- and phenol red free DMEM supplemented with 250 µM D-Luciferin (and additional pharmaceutical compounds dependant on the experimental setup). To prevent evaporation of the media, the cell culture plates and dishes were sealed prior to the start of measurement. The cellular bioluminescence was recorded over a period of five to seven days in either one of three devices: TopCount (PerkinElmer), Lumicycle (Actimetrics) or LumiBoxes.

Bioluminescence recordings – conditioned medium induced phase shifts

U-2 OS cells used for conditioned medium induced phase shift experiments were harbouring a *Bmal1*- or a *Per2*-promotor driven *luciferase* construct. They were seeded and grown to confluency in white 96-well plates (TopCount). In preparation for the measurement, the cells were synchronized with 1 µM Dexamethasone for 30 minutes, rinsed thrice with pre-warmed 1xPBS and supplied with serum and phenol red free DMEM supplemented with 250 µM D-Luciferin. To prevent evaporation of the media, the cell culture plates were sealed prior to the start of measurement. Approximately 4-6 hours after the first peak of the bioluminescence signal, the cell culture medium was withdrawn with a multi-channel pipette and replaced by enriched conditioned medium (see *Preparation and enrichment of conditioned Medium*). The plate was sealed and the bioluminescence recording was continued.

Bioluminescence recordings – conditioned medium induced CRE and SRE activation

U-2 OS cells used for conditioned medium induced CRE activation experiments were harbouring a reporter construct containing a 7xCRE cis-element or a 7xSRE cis-element fused in front of a minimal promotor driven *luciferase*. In preparation for the measurement, the cells were rinsed thrice with pre-warmed 1xPBS and supplied with serum and phenol red free DMEM supplemented with 250 µM D-Luciferin. To prevent

evaporation of the media, the cell culture plates were sealed prior to the start of measurement. Over the course of one day, the bioluminescence signal declined to a signal corresponding to the minimal promotor activity. At that point, the cell culture medium was withdrawn with a multi-channel pipette and replaced by enriched conditioned medium (see *Preparation and enrichment of conditioned Medium*). The plate was sealed and the bioluminescence recording was continued.

Fluorescence microscopy

Fixed cells were imaged with a Leica TC SP8 using a × 63 magnification oil immersion objective. Images were processed using ImageJ free software.

2.2.3 Protein assays

Cellular protein extraction

U-2 OS cells or HEK293T cells were grown to full confluency, rinsed once with ice-cold 1xPBS and lysed in either RIPA or CO-IP buffer supplemented with 1:100 protease inhibitor cocktail. The cell lysis reaction took place at 4°C for 30 Minutes on a rocking shaker. Afterwards, the cells were scraped from the cell culture dish, transferred to a reaction tube on ice for another 30 minutes and mixed by vortexing every 5-10 minutes. To remove DNA and cell debris, the cell lysate was spun at 4°C and 15000g for at least 30 minutes. Then, the cleared supernatant was collected for use in further experiments or stored at -20°C.

Determination of protein concentrations in whole cell protein lysates using a bicinchoninic acid (BCA) assay

Bovine serum albumin (BSA) was used to setup a standard curve ranging from 0 mg/ml up to 10 mg/ml to in the corresponding cell lysis buffer supplemented with 1:100

protease inhibitor cocktail. 5 µl of either the standard or the protein lysate were transferred to a clear 96-well plate and mixed with 200 µl of a prepared BCA solution consisting of BCA solution A and BCA solution B in a ratio of 1:50. The samples were incubated for 30 minutes at 37°C and the absorbance was measured in the Infinite F200 pro Tecan reader at 560 nm. Using the BSA standard curve the corresponding protein concentrations were calculated.

SDS polyacrylamide gel electrophoreses (PAGE)

The polyacrylamide gel used for the SDS-PAGE was either self-prepared (see **Table 2-1**) or purchased from Thermo Fisher Scientific. The prepared protein lysates (see *Cellular protein extraction*) were supplemented with 4x NUPAGE-buffer containing 0.8% β-mercaptoethanol, boiled at 95°C for 10 minutes and cooled down on ice. Subsequently, the samples were loaded on the gel and it was run either at 120 V (self-prepared gel) or 200 V (Life technology) for 60-120 minutes till the bromphenol dye front reached the end of the gel.

Table 2-1: Composition of the 12% polyacrylamide gel

Separating gel		Stacking gel	
Acrylamide/Bis-acrylamide 30%	2 ml	Acrylamide/Bis-acrylamide 30%	0.4 ml
Separating gel buffer	1.5 ml	Stacking gel buffer	0.65 ml
ddH_2O	2.4 ml	ddH_2O	1.9 ml
SDS 10%	60 µl	SDS 10%	30 µl
APS 10%	30 µl	APS 10%	15 µl
TEMED	3 µl	TEMED	3 µl

Western blot

The separated proteins were transferred from the polyacrylamide gel onto a nitrocellulose membrane using the wet blotting technique. Shortly, the polyacrylamide gel and the nitrocellulose membrane were stacked in a blotting cassette and the proteins

were transferred at 400 mA for 180 minutes under cooling conditions. Afterwards, the membrane was blocked in TBS-T supplemented with 5% skim milk at room temperature for one hour on a rocking shaker. The primary antibody was diluted accordingly (see **2.1.13)** and the membrane was incubated with the primary antibody overnight at 4°C. The next morning, the membrane was rinsed thrice with 1xTBS-T and the diluted secondary antibody was applied to the membrane for one hour at room temperature on a rocking shaker. Prior to detection, the membrane was rinsed thrice with 1xTBS-T. Using the Super Signal West Pico Luminescent Substrate, the bound antibodies were detected in the ChemoCam Imager 3.2.

Coomassie staining of polyacrylamide gels

The Coomassie staining was performed with the Stain NuPAGE Novex Bis-Tris Gel kit according to the manufacturer's manual. Briefly, the gel was incubated with the fixing solution for 10 minutes, rinsed once with deionized water and then stained with staining solution for three hours. Afterwards, the staining solution was decanted and replaced with either 200 ml deionized water or destaining solution for twelve hours.

2.2.4 RNA and DNA assays

RNA preparation from U-2 OS and HEK293 cells

The cells were rinsed once with ice-cold 1xPBS and then either frozen at -80°C until the day of processing or kept on ice and processed right away. RNA preparation was performed with the PureLink RNA mini kit according to the manufacturer's manual using centrifugation and an on-column DNase treatment. The purified RNA was eluted in an appropriate volume of deionized water and stored on ice for determination of yield and purity. Long-time storage was carried out at -80°C.

Determination of DNA and RNA concentration, yield and purity

The concentration, yield and purity of RNA and DNA was determines using the nanodrop2000c device according to the manufacturer's manual.

Reverse transcription of whole cell RNA

To reversely transcribe 0.25-2 µg RNA a two-step protocol was carried out. Firstly, the purified RNA was mixed with deionized water, dNTPs and primers and heated to 70°C and chilled immediately afterwards to melt secondary structures in the RNA and to prevent them from reforming. Depending on the planned assays either random hexamers or oligo-dT were selected as primers. Then, M-MLV reverse transcription buffer, DTT, RNase inhibitor and the M-MLV reverse transcriptase were added to the reaction and the cDNA synthesis PCR program was executed as followed:

Table 2-2: Sample preparation and PCR protocol for cDNA synthesis.

Step 1:

Sample composition		PCR protocol	
total RNA (0.5 – 2 µg)	variable	5 minutes	70 °C
ddH_2O	ad 28.25 µl		
dNTPs (10 mM)	1 µl		
random hexamers (20 µM)	5 µl		
or			
oligo-dT (100 pM)	1 µl		

Step 2:

Sample composition		PCR protocol	
ddH_2O	ad 39.25 µl	10 minutes	25 °C
5x first strand reaction buffer	5 µl	50 minutes	37 °C
		15 minutes	70 °C
RNase inhibitor 40 U/µl	0.5 µl	∞	4 °C
M-MLV reverse transcriptase 200 U/µl	0.25 µl		

For expression analysis via qRT-PCR, the synthesised cDNA was diluted 1:4 – 1:10 in deionized water depending on the initial amount of RNA and stored at -20 °C for further experiments. For detection of specific mRNA splice variants via poly acrylamide gel electrophoreses, the synthesised cDNA was mixed 1:6 with 6x Orange Loading Dye and stored at -20 °C.

Quantitative real-time polymerase chain reaction (qRT-PCR)

To determine gene expression levels quantitative real-time polymerase chain reaction were set up using the Maxima SYBR Green qPCR Master Mix. The primers were either ordered at Quiagen or designed with the online tool primer-blast, https://www.ncbi.nlm.nih.gov/tools/primer-blast/. The sample preparation and the qRT-PCR were performed accordingly to the manufacturer's manual. The suggested sample composition and the PCR protocol were setup as listed below:

Table 2-3: Sample composition and PCR protocol for qRT-PCR.

Sample composition		PCR protocol		
diluted cDNA	8 µl		2 minutes	50 °C
primers	2 µl		10 minutes	95 °C
Maxima SYBR Green qPCR Master Mix 2x	10 µl		15 seconds	95 °C
		40x cycles	1 minute + plate read	60 °C

DNA polyacrylamide gel electrophoresis

The polyacrylamide gel used for the DNA-PAGE was prepared as following (see **Table 2-4**). The samples supplemented with 1x Orange Loading Dye were loaded on the gel and it was run at 80 V for 45-60 minutes in 1x TBE buffer.

Table 2-4: Composition of the 12% and 8% polyacrylamide gel.

12 % polyacrylamide gel (for 2 gels)		8 % polyacrylamide gel (for 2 gels)	
Acrylamide/Bis-acrylamide 30%	4.8 ml	Acrylamide/Bis-acrylamide 30%	3.2 ml
ddH_2O	4.8 ml	ddH_2O	6.4 ml
5x TBE buffer	2.4 ml	5x TBE buffer	2.4 ml
APS 10%	200 µl	APS 10%	200 µl
TEMED	10 µl	TEMED	10 µl

To detect the separated DNA bands the gels were stained in ethidium bromide solution for 15 minutes, rinsed three times with deionized water and, then, analysed under UV light.

Cultivation, growth and long-term storage of bacterial cells

Isolated colonies of bacterial cells were obtained by streaking bacterial cells of long-term storage glycerine cultures or freshly transformed bacterial cell cultures on LB-agar plates supplemented with the appropriate antibiotic. The streak cultures were incubated at 37°C overnight. Using an inoculation loop, isolated colonies were transferred to 5 ml (mini-culture) or 50 ml (midi-culture) liquid LB-media supplemented with the appropriate antibiotic and incubated at 37°C on a horizontal shaker for 14-20 hours. Streak culture plates were stored at 4°C up to 4 weeks.

For plasmid DNA preparation, the bacterial cells were spun down at room temperature and 3000g for 3 minutes and the supernatant was aspirated.

For long-term storage, freshly prepared liquid bacterial culture and sterile glycerol were mixed in equivalent volumes, cooled down on ice for an hour and then transferred to cryo-cultivation at -80°C.

Plasmid DNA preparation from bacterial cells

Plasmid DNA preparation was performed with the PureLink plasmid DNA extraction kit according to the manufacturer's manual using centrifugation. Depending on the bacterial culture volume either the mini, midi or maxi kit was used. DNA was eluted in an appropriate volume of deionized water.

Polymerase chain reaction (PCR)

Depending on the DNA template, one out of three different polymerases was selected. The Deep Vent DNA polymerase was used for the amplification of short DNA segments from plasmid DNA. The Phusion High-Fidelity DNA polymerase and the Platinum Pfx DNA polymerase were chosen for amplifications of DNA segments from genomic DNA or complex cDNA, which was reversely transcribed from whole cell RNA, using oligo-dT primer. The samples were prepared and polymerase chain reaction carried out as described below (see **Table 2-5).**

Table 2-5: Sample composition and PCR protocol for the Deep Vent DNA polymerase, the Pfx DNA polymerase and the Phusion High Fidelity DNA Polymerase.

Sample composition	
Deep Vent Reaction buffer (10x)	5 µl
dNTPs (10 mM)	1 µl
Forward Primer (10 µM)	1 µl
Reverse Primer (10 µM)	1 µl
Deep Vent polymerase 2 U/µL	0.5 µl
Template DNA (50 ng)	variable
ddH_2O	Ad 50 µl

PCR program		
5 minutes		95 °C
40x cycles	30 seconds	95 °C
	30 seconds	55 °C
	1 minute /kbp	72 °C
∞		4 °C

Sample composition	
Pfx reaction buffer (10x)	5 µl
dNTPs (10 mM)	1.5 µl
Forward Primer (10 µM)	2 µl
Reverse Primer (10 µM)	2 µl
Pfx DNA polymerase 2 U/µL	0.5 µl
$MgSO_4$	1 µl
Template DNA (50 ng)	variable
ddH_2O	Ad 50 µl

PCR program		
5 minutes		95 °C
40x cycles	30 seconds	95 °C
	30 seconds	55 °C
	1 minute /kbp	72 °C
5 minutes		72 °C
∞		4 °C

Sample composition	
High fidelity buffer (10x)	5 µl
dNTPs (10 mM)	1 µl
Forward Primer (10 µM)	2 µl
Reverse Primer (10 µM)	2 µl
Phusion High fidelity DNA polymerase 2 U/µL	0.25 µl
Template DNA (25 – 50 ng)	variable
ddH_2O	Ad 50 µl

PCR program		
2 minutes		95 °C
40x cycles	30 seconds	95 °C
	30 seconds	55 °C
	30 seconds /kbp	72 °C
10 minutes		72 °C
∞		4 °C

Side-directed mutagenesis PCR

The side directed mutagenesis PCR was performed using the QuickChange Site-directed mutagenesis kit accordingly to the manufacturer's manual. The primers were designed as proposed in the manual and ordered at Eurofins MWG. The suggested sample composition and the PCR protocol were setup as listed below:

Table 2-6: Sample composition and PCR protocol for site-directed mutagenesis.

Sample composition		PCR program		
Pfu reaction buffer (10x)	5 µl	1 minutes		95 °C
dNTPs (10 mM)	1 µl		30 seconds	95 °C
Forward Primer (10 µM)	1 µl	15-18x cycles	1 minute	55 °C
Reverse Primer (10 µM)	1 µl		1 minute /kbp	T_m
Pfu DNA polymerase 2.5 U/µL	1 µl	∞		4 °C
Template DNA (25-50 ng)	variable			
ddH_2O	Ad 50 µl			

T_m was calculated using the equation (2), where N equals the primer length in bases:

$$T_m = 81.5 + 0.41 \times (\%GC) - \frac{675}{N} - \%\, mismatch \quad (2)$$

The mutated DNA was digested with Dpn I at 37°C for one hour prior to transformation into chemically competent XL1-Blue bacteria cells (see **2.1.3**). The sequence was verified by restriction enzyme digestion and Sanger sequencing.

Restriction enzyme digestion

Purified plasmid DNA was verified or prepared for further cloning steps by restriction enzyme digestion. Therefore, the DNA was diluted in deionized water, mixed with the appropriate buffer, BSA and restriction enzyme, according to the manufacturer's manual, and incubated for at least one hour. If a closed plasmid was linearized for further

cloning using restriction enzyme digestion, the sample was treated twice with 1 µl CIP for 30 minutes at 37°C to dephosphorylate the sticky ends of the fragment and prevent recirculation.

To stop the digestion reaction, the sample was either supplemented with 6x Orange Loading Dye or the enzyme was heat inactivated as proposed by the manufacturer.

Agarose gel electrophoreses

To verify the result of the restriction enzyme digestion or to analyse purified plasmid DNA, the sample was supplemented with 6x Orange Loading Dye and separated by size, using agarose gel electrophorese. Depending on the DNA fragment of interest an 0.8% (>2000 bp), 1% (500 bp - 2000 bp) or 2% (< 800 bp) agarose gel was used. The gel was run for 45 minutes in a 1xTAE and analysed using the ChemoCam Imager 3.2.

DNA purification from agarose gels

The DNA fragment of interest was cut from the agarose gel with a scalpel and transferred to a 1.5-ml reaction tube. The purification was carried out using the Qiaex II extraction kit according to the manufacturer's manual. The DNA was eluted in 10-30 µl deionized water.

Sequencing of purified DNA

Purified DNA samples were sent to Source Bioscience (Berlin) for Sanger sequencing. The samples were prepared as recommended by the service provider:

- 5 µl of purified DNA, 100 ng/µl
- or 5 µl of purified PCR-product, 1 ng/µl per 100 bp
- 5 µl sequencing primer per reaction, 3.2 pmol/µl

Ligation of DNA fragments

Purified DNA fragments were ligated using the Fast-Link DNA ligation kit according to the manufacture's manual. The ligase reaction was incubated at room temperature for at least 10 minutes.

Table 2-7: Sample composition for the Fast-Link ligase reaction.

Ligation reaction	
10x Fast Link ligation buffer	1 µl
ATP (10 mM)	1 µl
Purified linearized vector 30 ng/µl	1 µl
Purified DNA fragment 30 ng/µl	5 µl
Fast-Link ligase	0.5 µl
deionized water	1.5 µl

Directional TOPO-cloning

The DNA sequence of interest was PCR-amplified from a vector or another DNA fragment with an appropriate primer pair, the forward primer possessing a CACC-overhang at the 5'end. The PCR product was purified by agarose gel electrophoreses (see *Agarose gel electrophoreses*DNA polyacrylamide gel electrophoresis) and subsequent DNA gel extraction using Qiaex II (see *DNA purification from agarose gels*). The directional TOPO cloning step was carried out with the pENTR Directional TOPO cloning kit (Thermo Fisher Scientific) according to the manufacturer's protocol. The reaction was incubated for 30 minutes at room-temperature prior to transformation of the pENTR vector into chemically competent cells.

Gateway-cloning

The LR recombination reaction between an attL-containing entry clone and n attR-containing destination vector was performed using the Gateway LRClonase II Enzyme Mix (Thermo Fisher Scientific). The entry clone, the destination vector and the LRClonase II Enzyme were mixed in a reaction tube and incubated at room-temperature for one hour.

Table 2-8: Sample composition for the Gateway LRClonase reaction.

Gateway LRClonase II reaction	
Entry clone	1 µl
Destination vector	1 µl
LRClonase II Enzyme	0.5 µl

Next, 0.3 µl of proteinase K were added to the sample and incubated for 10 minutes at 37°C prior to transformation of the destination vector into chemically competent cells.

Transformation of chemically competent cells

One vial of chemically competent cells per transformation reaction (see **2.1.3**) was thawed at 4°C on ice for ten minutes and then mixed with 1-4 µl of a TOPO-cloning or Gateway-cloning reaction sample (or 50-100 ng plasmid-DNA in case of a retransformation reaction). The sample was incubated at 4°C on ice for 30 minutes prior to a 60 second heat-shock treatment at 42°C. Afterwards, the cells were cooled at 4°C on ice for two minutes, supplemented with 500 µl of S.O.C-medium or LB-medium and, then, incubated at 37°C for 45 minutes on a rocking thermal mixer. The transformed bacterial cells were transferred to LB-agar plates containing the appropriate antibiotic and incubated at 37°C over night.

2.2.5 Cloning of the plasmid: pENTR-TMED10oLD plasmid

First, we had the *TMED10* gene lacking the luminal domain synthesised at Eurofins MGW operon (see **2.1.14)**. We substituted *TMED10*'s luminal domain with a AgeI and an EcoRI restriction side which enabled us later in the cloning process to insert the open reading frame of turbo *gfp*.

The ordered gene synthesis was delivered in the pEX-A vector with 3'- and 5'-flanking BsrgI restriction sites. Subsequently, we cut the pEX-A vector as well as the empty pENTR vector using BsrgI according to the manufacture's manual. The pENTR vector backbone and the cut-out gene synthesis were separated on an 2% and an 1% agarose gel respectively, purified, using the Qiaex II extraction kit, and ligated, using the Fast-Link DNA ligation kit. Next, the pENTR-TMED10oLD plasmid was introduced into chemically competent cells, purified with the PureLink plasmid Mini DNA extraction kit and digested with ApaI and SacII to confirm the right orientation of the insertion. To insert the turbo *gfp* open reading frame, we PCR amplified turbo *gfp* from the pLenti6-*tgfp* vector using a forward primer containing a 5' AgeI restriction side and a reverse primer containing a 3' EcoRI restriction side. Afterwards the pENTR-TMED10oLD and the amplified turbo *gfp* were digested using AgeI and EcoRI according to the manufacture's manual. The pENTR vector backbone and the amplified *tgfp* were separated on an 1% agarose gel, purified using the Qiaex II extraction kit and ligated using the Fast-Link DNA ligation kit. The constructed vector was introduced into chemically competent cells, purified with the PureLink plasmid Mini DNA extraction kit and the sequence was verified by restriction enzyme digestion and Sanger sequencing.

2.2.6 *Gfp*-silencing in pGIPZ-knockdown constructs

The pGIPZ-vector contains a human cytomegalovirus promotor driving the expression of *tgfp*. The expression of *tgfp* interfered with additional fluorophores in experiments using fluorescently tagged antibodies or fluorescent fusion proteins. To overcome this obstacle, we created a non-functional tGFP by introducing a frame shift into the *tgfp* open reading frame. In more detail, the pGIPZ vector was digested by the restriction enzyme BlpI cutting 175 bp downstream of the *tgfp* start side. The emerging

sticky ends of the linearized pGIPZ vector were filled up using the Klenow polymerase according to the manufacturer's protocol. The blunt end vector was separated on a 1% agarose gel, purified using the Qiaex II extraction kit and re-ligated using the Fast-Link DNA ligation kit. To verify the successful frame shift, restriction enzyme digestion and Sanger sequencing were performed.

2.2.7 Analysis of bioluminescence recordings

Bioluminescence recordings were analysed, using the in-house developed software chronostar2.0 by Stephan Lorenzen, Freie Univerisität Berlin, Berlin, Germany. First, the obtained raw data were trend-eliminated through division by their 24-hour running average. Then, sine waves were fitted to the trend-eliminated data and circadian parameters were assessed. The software uses the following equation for sine wave fitting:

$$y = amp(24) \times 2^{(-(0.5-damp)\times t)} \times \cos\left(\frac{t-phase}{per} \times 2 \times \pi\right) \quad (3)$$

amp (24):	circadian amplitude after 24 hours
damp:	damping
per:	period

3 Results

3.1 RNAi-mediated knockdown of genes associated with vesicular protein transport identified transport events between the ER and the Golgi to be crucial for normal circadian rhythms

Cellular vesicular protein transport can be divided into three important parts: ER to Golgi transport, intra-Golgi transport and transport from the trans-Golgi network to the target location which can either be a cellular organelle or the plasma membrane. It is plausible that interference with one of these precisely timed and controlled events may lead to a disruption or dysregulation of multiple cellular processes including the circadian clock. Our previous work has shown that genetic perturbation during the early stages of vesicular protein transport led to altered circadian rhythms with prolonged circadian periods (Bert Maier, unpublished Data; Sebastian Jäschke, diploma thesis: "Modulation des zirkadianen Uhrwerks durch "Golgi-Apparat" und "Vesikulärer Transport" assoziierte Gene"). To test whether depletion of genes associated with Golgi- and vesicular transport alters circadian rhythmicity and to verify previous findings, RNAi interference was used to knock-down mRNA level of genes involved in early protein transport events and circadian parameters were assessed. To this end, four different short-hairpin RNAs targeting Golgi-associated genes and one non-silencing (ns) control plasmid were selected and lentivirally transduced into U-2 OS reporter cells harbouring a *Bmal1*-promotor driven *luciferase* construct. The transduced cells were selected, synchronized, and, then, monitored over a period of five consecutive days in the LumiCycle device. After the measurement was terminated, the cellular RNA was extracted, reversely transcribed to cDNA and mRNA level were determined using quantitative real-time polymerase chain reaction (qRT-PCR) to evaluate the knock-down efficiency.

When *TMED10* and *TMED2* transcript levels, coding for integral membrane proteins involved in COPI and COPII vesicle formation, were reduced through shRNA constructs, the circadian period was drastically lengthened by 5.0 ± 0.3 and 3.9 ± 0.6 hours respectively (see **Figure 3-1A** and **Table 3-1).** Additionally, the overall luciferase activity was significantly increased by 201 ± 13% and 153 ± 27%. The amplitudes of the

fitted sine waves were slightly reduced in both cases. Furthermore, the decrease in *TMED10* and *TMED2* mRNA levels resulted in higher dampening of the oscillations. Upon reduction of *GBF1* transcript level, coding for a GEF important for the formation of COPI vesicles, the circadian period slightly lengthened by 1.5 ± 0.3 hours. The amplitude and damping parameter of the fitted sine wave as well as the overall luciferase activity were not significantly altered compared to non-silencing controls. The knockdown of *SEC13* transcript level, coding for an essential coat component of the COPII vesicle, resulted in a strong period lengthening effect of 3.4 ± 0.3 hours. This period phenotype was accompanied by a reduced amplitude, a significant higher damping of 0.6 ± 0.1, and an overall increase of luciferase activity by 158 ± 13%.

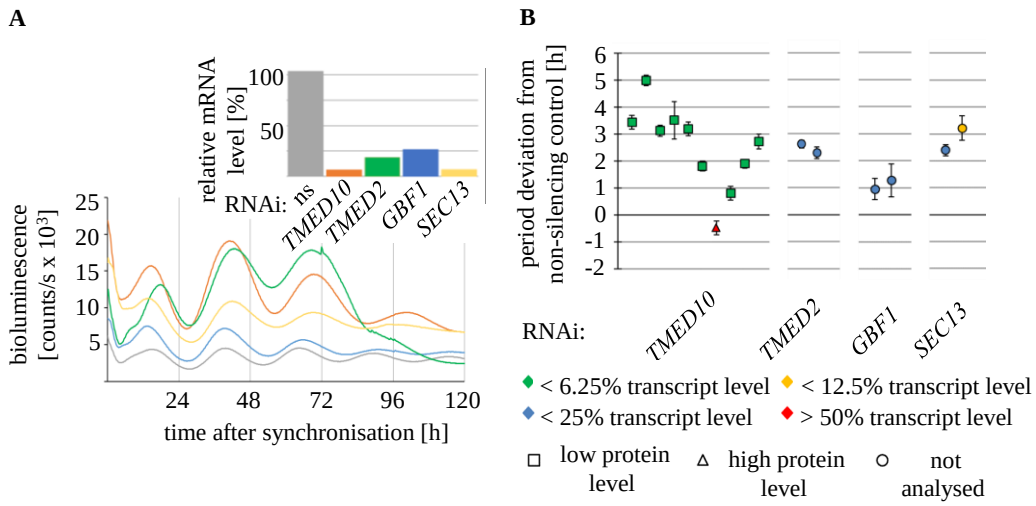

Figure 3-1: Genetic perturbation of Golgi associated components lengthened the circadian period of human osteosarcoma cells. U-2 OS cells harbouring a *Bmal1*-promotor driven *luciferase* reporter construct were transduced with either a non-silencing control construct or RNAi knockdown constructs targeting *TMED10*, *TMED2*, *GBF1* or *SEC13* and synchronised with dexamethasone. **A)** Depicted are representative bioluminescence recordings. The inlay shows the corresponding mRNA levels [%] upon knockdown. **B)** Bioluminescence data were fitted to sine waves using chronostar2.0 and the circadian parameters were assessed. Depicted are the circadian period deviations relative to non-silencing controls for each knockdown condition as well as the determined mRNA and protein levels using qRT-PCR and western blot. Each symbol represents one individual shRNA construct (n = 2-3 individual recordings with three biological replicates, mean ± SD).

To summarise, RNAi-mediated knockdown of *SEC13*, *GBF1*, *TMED2* and *TMED10* transcripts resulted in the perturbance of normal circadian clock function, showing strong period lengthening effects. Therefore, we could strengthen our hypothesis that an unperturbed protein transport machinery is necessary for the circadian clock to function.

Table 3-1: Genetic perturbation of early vesicular protein transport led to altered circadian oscillations. The bioluminescence data of **Figure 3-A** were fitted to sine waves and the circadian parameters were assessed. Summarised are the changes in circadian oscillations compared to non-silencing controls (ns-cntr), Per: period, dev.: deviation, Damp: damping, Luc: Luciferase (n = 3 biological replicates of the same shRNA construct, mean ± SD; Student's T-Test: * $p < 0.01$, ** $p < 0.001$)

shRNA construct	Per dev. from ns-cntr [h]	Rel. amp dev. from ns-cntr	Damp dev. from ns-cntr	Lue activity dev. from ns-cntr [%]
TMED10 #1	5.0 ± 0.3 **	-0.05 ± 0.03	0.15 ± 0.05 *	201 ± 13 **
TMED2 #1	3.9 ± 0.6 **	-0.13 ± 0.03 *	0.21 ± 0.14	153 ± 27 *
GBF1 #1	1.5 ± 0.3 *	0.04 ± 0.10	0.28 ± 0.13	8 ± 35
SEC13 #1	3.4 ± 0.3 **	-0.11 ± 0.03 *	0.55 ± 0.08 **	158 ± 13 **

To ensure that the observed period lengthening effect is connected to the reduction of the above-mentioned transcripts and not a result to off-target effects, additional shRNA constructs for each gene were selected. Since the RNAi-mediated knockdown of all tested genes associated with the vesicular transport affected the circadian period in the previous set of experiments, we focused on this parameter in the current one. Moreover, we wondered if the strong period lengthening phenotype is correlated with reduced mRNA and protein levels. We tested at least one additional shRNA constructs for each gene with a different target sequences. To test the extent of the shRNA-mediated depletion on protein level, cells were cultured independently following the same protocol and harvested on the second day of bioluminescence measurement for whole cell protein extraction. The protein samples were analysed, carrying out polyacrylamide gel electrophoreses followed by western blot analysis.

Nine out of ten tested shRNA constructs targeting *TMED10* lengthened the period (see **Figure 3-1B**). On average, the knockdown of *TMED10* transcripts caused a prolongation of the circadian cycle by 2.8 ± 1.2 hours, in which the period lengthening effect of the different constructs ranged from 0.8 ± 0.2 up to 5.0 ± 0.2 hours. The tenth construct (#7) led to a period shortening. Overall, the observed effects coincided nicely with the mRNA and protein levels. Every shRNA construct that prolonged the circadian cycle showed a reduced *TMED10* transcript level down to 6.25% or less leaving the translated protein barely detectable in the western blot (see **Supplemental Figure A 1**).

However, we could not find a strong correlation between effect strength and transcript level. The shRNA #7 that showed no period lengthening effect, exhibited only low knockdown efficiency with a remaining mRNA level above 50%. The translated protein was detected in the western blot showing half of the non-silencing control's signal intensity.

The depletion of *TMED2* resulted in a longer circadian cycle for both constructs tested with a period deviation from non-silencing controls of 2.6 ± 0.2 and 2.3 ± 0.2 hours. The corresponding *TMED2* transcript levels were successfully reduced below 25%. Upon depletion of *GBF1* the circadian period was lengthened by 1.0 ± 0.4 and 1.3 ± 0.6 hours. The phenotype was correlated with reduced transcript levels below 25%. Finally, the decrease in *SEC13* expression prolonged the circadian period by 2.4 ± 0.2 and 3.2 ± 0.5 hours. The *SEC13* mRNA levels were decreased to under 25% and 12.5%, respectively. Since we had no antibodies to detect TMED2, GBF1 or SEC13 proteins, we were unable to correlate the reduced transcript levels with their corresponding protein levels. Given the results for the TMED10 protein levels upon transcript reduction, we assume a reduction in TMED2, GBF1 and SEC13 protein level, as well.

In conclusion, the detected period lengthening effects were related to the knockdown of the target genes. Additional constructs showed high reproducibility. The results suggest a link between the knockdown efficiency and the observed period lengthening effect, although a quantitative correlation could not be found in the TMED10 dataset. However, the reduced transcript levels were nicely reflected in the lowered protein levels. All in all, we could strengthen our hypothesis that an unperturbed protein transport machinery is necessary for the circadian clock.

3.1.1 Overexpression of TMED10 and TMED2 in a shRNA-mediated knockdown background restored normal circadian function

shRNAs are believed to be highly specific due to their complementary target sequences. To test, whether the period lengthening phenotypes observed in previous experiments were due to the intended knockdown, we conducted genetic rescue experiments to restore normal circadian function.

To this end, we lentivirally transduced U-2 OS cells harbouring a *Bmal1*-promotor driven *luciferase* construct with either non-silencing control plasmids or shRNA targeting *TMED10* or *TMED2* transcripts. The shRNA constructs selected for this set of experiments had their complementary binding sequence in their target gene's 3'UTR, allowing the concurrent ectopic overexpression of the gene's coding sequence (CDS). After selection with puromycin the stable knockdown cells were lentivirally transduced with the corresponding overexpression plasmid or a control plasmid expressing *green-fluorescent protein* (*gfp*) and selected with blasticidin. Dexamethasone was used to synchronize the U-2 OS cells and the bioluminescence was monitored over five days in the LumiCycle device or the TopCount device. The data set was analysed with chronostar2.0 and the circadian parameters were assessed. After the bioluminescence recording was terminated, the cellular RNA was purified, reversely transcribed and the relative mRNA determined using qRT-PCR.

The overexpression of *TMED10* or *TMED2* in cells stably expressing the corresponding shRNA construct rescued the phenotype and restored normal circadian rhythmicity (see **Figure 3-2**). In more detail, the 13-fold overexpression of *TMED10* in a non-silencing control background showed a slightly shorter period by -0.5 ± 0.2 hours. U-2 OS cells transduced with a shRNA construct targeting the 3'UTR of *TMED10* exhibited the previously observed longer period of 4.5 ± 0.6 hours compared to non-silencing controls. The determined period phenotype correlated nicely with the residual mRNA levels of 9.8%. The overexpression of a *gfp*-control plasmid in the knockdown background did neither alter the circadian period (4.4 ± 1.2 hours) nor the *TMED10* mRNA level (11.3%) to a substantial manner. However, the expression of a plasmid containing coding sequence of *TMED10* led to an elevation of *TMED10* mRNA by a factor of 46 ± 0.6 and, more interestingly, restored the normal circadian period. Upon overexpression, the period lengthening effect was rescued in these cells and the determined period matched the one observed in non-silencing control cells (-0.03 ± 0.03 hours). The six-fold overexpression of *TMED2* in non-silencing control cells did not alter the circadian period, exhibiting a period of -0.1 ± 0.1 hours compared to control cells. As expected, the RNAi-mediated decrease in *TMED2* transcripts targeting the 3'UTR region resulted in a 4.1 ± 0.5 hours longer circadian cycle accompanied by reduced relative mRNA levels of 9.4%. The *gfp*-overexpression showed a relative *TMED2*-mRNA expression of 12.5% along with a shorter period of 3.5 ± 0.02 hours.

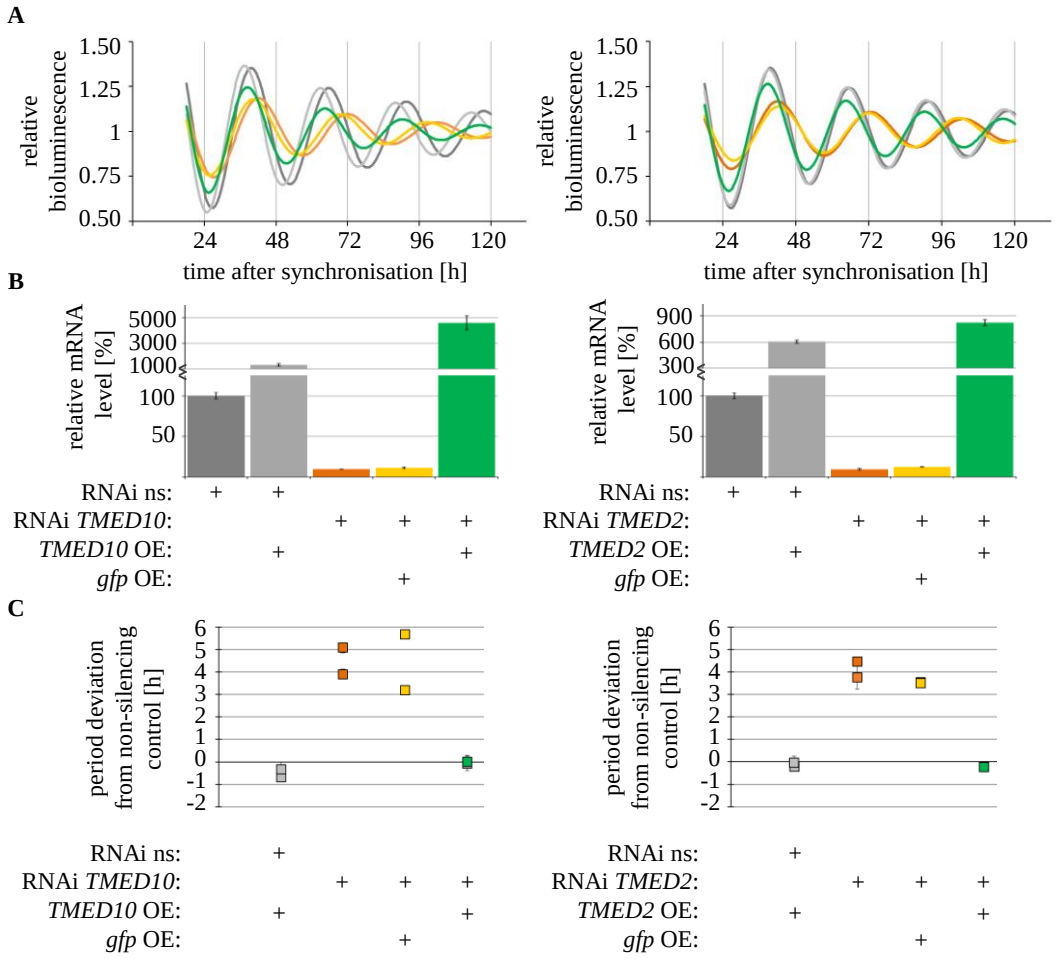

Figure 3-2: The RNAi-mediated *TMED10* and *TMED2* knockdown phenotypes were rescued through constitutive overexpression in human osteosarcoma cells. Firstly, U-2 OS cells harbouring a *Bmal1*-promotor driven *luciferase* reporter construct cells were transduced with either a non-silencing control construct or RNAi constructs targeting *TMED10* or *TMED2* and selected, following a second transduction with either a *gfp* control plasmid or the corresponding *TMED10* or *TMED2* overexpression (OE) construct. After synchronisation with dexamethasone, bioluminescence was recorded for five days and sine waves were fitted to the data set using chronostar2.0. **A)** Depicted are representative detrended bioluminescence data of a *TMED10* and *TMED2* rescue experiment with **B)** the corresponding mRNA levels [%] upon knockdown and overexpression (mean ± variance). **C)** Shown are the period deviations from non-silencing controls [h] (n = 2 individual recordings with 3 biological replicates, mean ± variance).

The apparent shorting of the circadian cycle might be a result of the reduced knockdown efficiency. Still, the ectopic overexpression of *TMED2* in the *TMED2* depleted cells rescued the period phenotype completely. The cells displayed normal circadian oscillations with a period of -0.2 ± 0.02 hours compared to the non-silencing control cells and an eight-fold higher relative mRNA level.

Together, the constitutive overexpression of *TMED10* as well as *TMED2* in the corresponding knockdown background was sufficient to rescue normal circadian oscillations with periods close to 24-hours. Therefore, we could strengthen our hypothesis

that the observed period phenotype was not caused by off-target effects. *TMED10* and *TMED2* gene expression were identified to be necessary for normal circadian function. The underlying mechanisms how these two proteins affect circadian rhythmicity are to be investigated.

3.1.2 Reduction of transcript levels of Golgi associated genes did not lead to cell death

In previous studies conducted in our lab, we observed that cell death might be accompanied by period lengthening effects, probably due to attenuation of transcription and translation. To rule out the possibility that the observed period lengthening effect was caused by starting cell death rather than the interference with ER to Golgi transport events necessary for the circadian clock to function, we analysed the cell vitality upon genetic perturbation. To this end, we lentivirally transduced U-2 OS reporter cells either with a non-silencing control construct or RNAi constructs targeting *TMED10*, *TMED2*, *GBF1* or *SEC13* in five individual 96-well plates and carried out the selection procedure. For five consecutive days, we supplemented the cell culture medium of one 96-well plate with 10 % Resazurin solution for four hours and measured the conversion of the non-fluorescent Resazurin to the red-fluorescent Resorufin as a marker for unimpaired metabolic activity and redox potential as expected in vital cells.

The reduced expression of *TMED10*, *TMED2*, *GBF1* or *SEC13* did not induce cell death in the first five days of a bioluminescence measurement (see **Figure 3-3**). Over time, the knockdown of *TMED10*, *TMED2*, *GBF1* or *SEC13* transcript levels reduced the fluorescence signal by up to 25 %. However, the fluorescence signal never fell below 75 % of the signal detected in non-silencing control cells. In contrast, application of the inhibitor BFA in toxic concentrations, which interferes with COPI and COPII vesicle biogenesis, rapidly reduced cell vitality, resulting in fluorescence signals near the assay background (see **Supplemental Figure A 2**). Surprisingly, U-2 OS cells treated with RNAi constructs targeting *TMED10* exhibited the highest fluorescence signal of all RNAi-treated cells analysed. This finding was unexpected as we obtained the best knockdown efficiencies and the most pronounced circadian phenotypes in these cells in previous experiments.

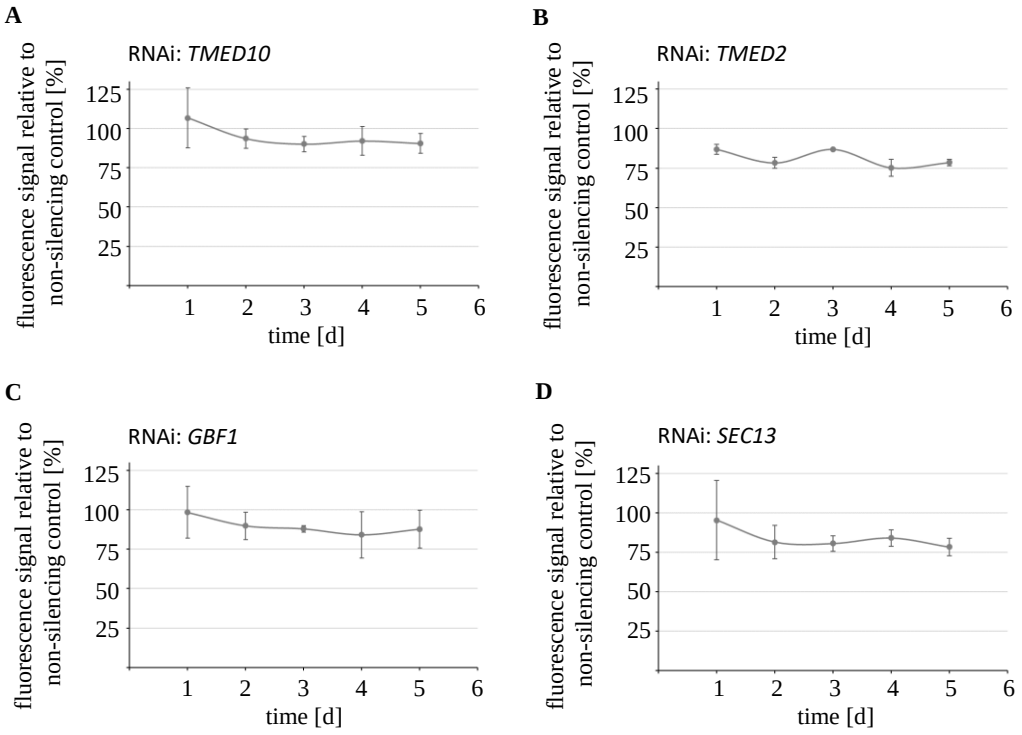

Figure 3-3: The RNAi-mediated knockdown of Golgi associated genes did not induce cell death. In five individual 96-well plates, U-2 OS cells harbouring a *Bmal1*-promotor driven *luciferase* reporter construct were lentivirally transduced with either a non-silencing control construct or RNAi constructs targeting **A)** *TMED10*, **B)** *TMED2*, **C)** *GBF1* or **D)** *SEC13* and selected. After synchronisation with dexamethasone, cells were treated as cells prepared for bioluminescence recordings. Every 24 hours the cell culture medium of one plate was supplemented with 10 % Resazurin and incubated for four hours before the fluorescence signal was measured. Depicted are the fluorescence values relative to the non-silencing controls of each individual plate (n = 3 individual recordings with 4 biological replicates – except TMED2 with n = 2, mean ± SD).

Taken together, our findings indicated that the knockdown of transcript levels of Golgi associated genes only slightly affected the overall metabolic activity. Nevertheless, we found no indication for substantial cell death. Furthermore, we could not find any evidence that the circadian phenotype and the cell vitality were directly linked.

3.1.3 Knockdowns of Golgi associated genes disrupted Golgi integrity

In literature, genetic and pharmacological interferences with early stages of vesicular protein transport are often described to change Golgi morphology and disrupt transport events between ER and Golgi[336–339]. Both phenotypes are tightly linked, since the integrity of the Golgi is highly dependent on the continuous fusion and scission of

membrane vesicles. Hence, we investigated the possibility that the RNAi-mediated knockdown of Golgi associated genes resulted in decreased Golgi integrity comparable to previous reports.

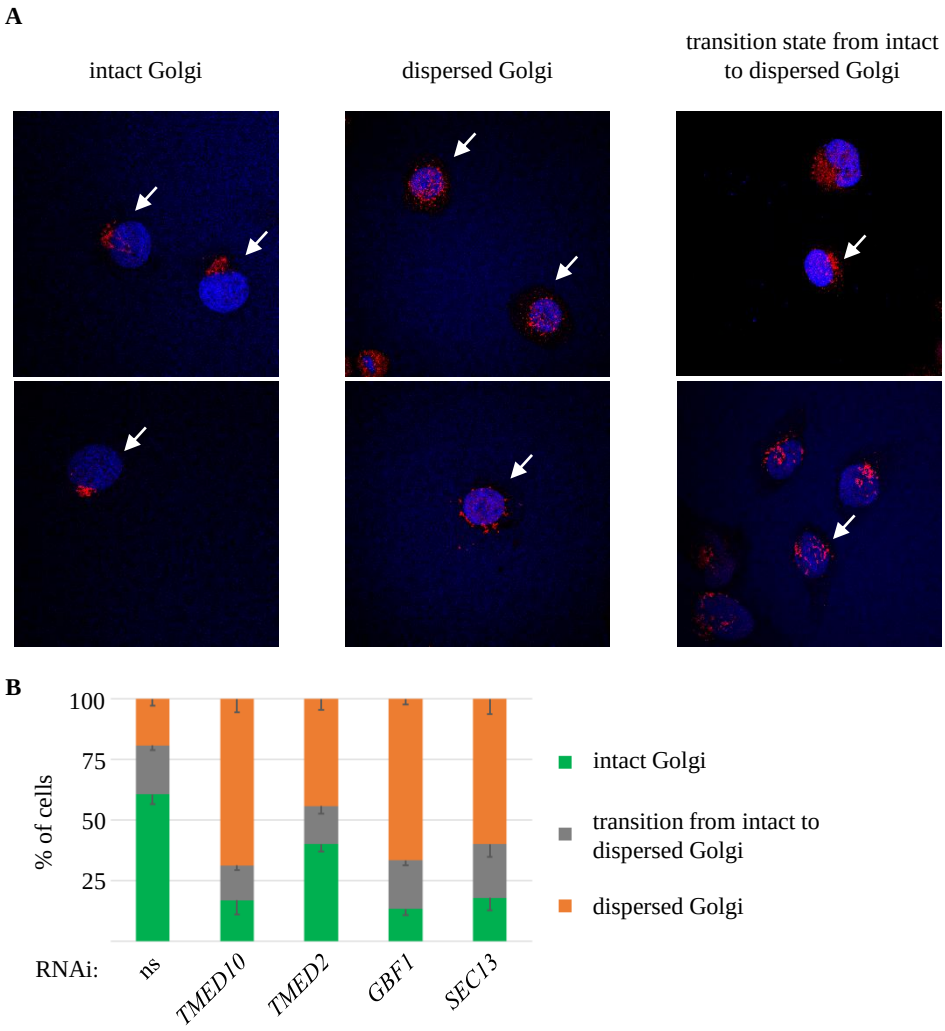

Figure 3-4: RNAi-mediated knockdown of Golgi associated genes disrupted Golgi integrity. U-2 OS cells harbouring a *Bmal1*-promotor driven *luciferase* reporter construct were lentivirally transduced with either a non-silencing control plasmid or RNAi constructs targeting *TMED10*, *TMED2*, *GBF1* or *SEC13*. After selection, cells were stained with Hoechst solution (blue) and antibodies against GM130 (red) labelling the nucleus and the Golgi respectively. Fluorescence microscopy was used to analyse Golgi morphology. Six people were asked to blindly score the images, discriminating between the three different Golgi states: intact, transition from intact to dispersed and dispersed. **A)** Shown are representative immunofluorescence pictures with white arrowheads pointing to the cells scored as indicated by all six analysts. **B)** Shown are the mean percentage of cells with Golgi morphology scored as intact (green), transition from intact to dispersed (grey) and dispersed (orange). (one experiment with 27-47 cells per condition, see **Supplemental Figure A 3** for second experiment with 40-80 cells per conditions, Golgi morphology scoring performed by six individuals with scientific education, mean ± SEM)

To test this hypothesis, we lentivirally transduced U-2 OS cells harbouring a *Bmal*1-promotor driven *luciferase* reporter construct with the shRNA constructs that were previously used to study the effects of RNAi-mediated knockdown on circadian oscillations. To avoid interferences between the plasmid's encoded *gfp* and the fluorescent antibodies, a frame shift was generated within the plasmid's *gfp* open reading frame (see **2.2.6**). The transduced cells were selected, fixed, and stained with Hoechst solution and fluorescent antibodies against GM130 labelling the nucleus and Golgi respectively. Fluorescence microscopy was used to evaluate the Golgi morphology and, therefore, the changes induced by genetic perturbation.

The knockdown of *TMED2*, *TMED10*, *GBF1* and *SEC13* transcripts drastically decreased the number of cells with an intact Golgi apparatus and increased the number of cells exhibiting a dispersed or dissolved Golgi compared to non-silencing control cells (see **Figure 3-4** and **Supplemental Figure A 3**).

In more depth, the control cells showed an intact Golgi in 61 ± 4% of the cells, a dispersed Golgi in 19 ± 3% of the cells and an in-between state in 20 ± 2% of the cells, suggesting that the lentiviral transduction procedure leads to a slight damage of the Golgi apparatus already. The RNAi-mediated knockdown of *TMED2* transcripts resulted in an intact Golgi only in 40 ± 3% of all cells analysed and a completely dispersed Golgi in 44 ± 4% of all cells, doubling the number of cells with severely decreased Golgi integrity. The effects on Golgi morphology in a *TMED10*, *GBF1* or *SEC13* depleted cell were even more pronounced. Under these conditions only 17 ± 8%, 13 ± 2% and 18 ± 4% of all cells featured an intact Golgi, respectively. In fact, the reduction of *TMED10* transcripts evoked a completely dispersed Golgi in 69 ± 8% of all analysed cells, displaying the most drastic effects, closely followed by the reduction of *GBF1* transcripts (67 ± 2% of all cells) and the reduction of *SEC13* transcripts (60 ± 5% of all cells).

Taken together, these results implied strong negative repercussions on the Golgi integrity and the vesicular protein transport machinery upon RNAi-mediated knockdown of Golgi associated genes. The number of cells displaying a dispersed Golgi apparatus increased significantly upon transcript reduction, suggesting an impaired protein transport in all four cases. Therefore, we speculated that the observed period lengthening phenotypes were caused by interferences with the vesicular protein transport.

3.1.4 Genetic perturbation of genes associated with vesicular protein transport resulted in altered clock gene transcript levels and low amplitude oscillations

Next, we asked whether there are direct effects of the genetic perturbation of the early vesicular protein transport pathway on circadian gene expression. To answer this question, we analysed clock gene transcript levels upon *TMED10* depletion over a time course of 40 hours. For this purpose, we selected *TMED10* shRNA construct #2 for the knockdown, because it led to the strongest period lengthening phenotype, prolonging the circadian cycle by 5.0 ± 0.2 hours. U-2 OS reporter cells harbouring a *Bmal1*-promotor driven *luciferase* construct were lentivirally transduced either with a non-silencing control construct or the *TMED10* shRNA #2. The transduced cells were selected and synchronized. Subsequently, the cells were harvested in four-hour intervals over a time course of 40 hours starting 24 hours after synchronisation. The cellular RNA was extracted, reversely transcribed to cDNA and clock gene mRNA levels as well as *TMED10* mRNA levels were determined using qRT-PCR.

Upon knockdown of *TMED10* transcripts (see **Supplemental Figure A 4**), six out of seven tested clock genes showed altered oscillations in their mRNA levels compared to non-silencing controls (see **Figure 3-5**). They cycled with an estimated circadian period of roughly 28 hours. *CLOCK* was the only clock gene whose transcript level was unaffected by the decrease in *TMED10* expression. CLOCK's interaction partner BMAL1 showed a prolonged circadian cycle of its transcript, therefore the expression level peaked and troughed four to eight hours later compared to controls. Additionally, the amplitude of *BMAL1* transcript level was severely reduced. *NR1D1 (*also known as REV-ERBα), a E-box gene directly dependent on BMAL1/CLOCK heterodimerization, shows overall reduced transcript levels. The time of day dependent variations in *NR1D1* transcript level seemed almost abolished due to a highly-reduced amplitude. The peak and nadir times were shifted as well by four to eight hours. The observed alterations resulted probably from the changes in *BMAL1* transcript level.

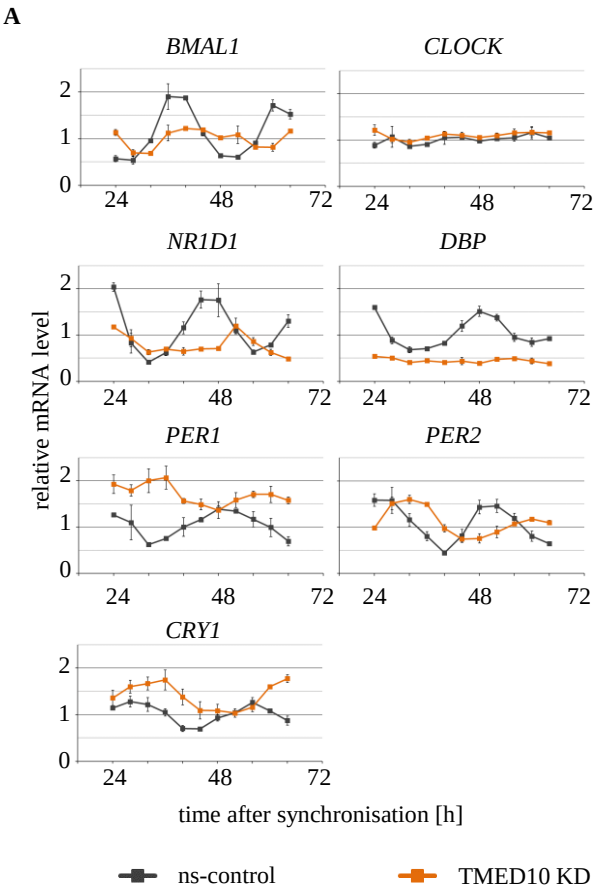

Figure 3-5: Genetic perturbation of *TMED10* severely disrupted the circadian clock in human osteosarcoma cells. U-2 OS cells harbouring a *Bmal1*-promotor driven *luciferase* reporter construct were transduced with either a non-silencing control construct or an RNAi construct targeting *TMED10*. 24 hours after synchronization with dexamethasone cells were harvested in 4-hour intervals over 40 hours and total RNA was extracted. Depicted are clock gene expression levels upon *TMED10* depletion compared to control determined by qRT-PCR. The mean clock gene expression level in non-silencing control cells was set to one (n = 3 dishes per time point and condition, mean ± SD).

DBP, another E-box controlled gene, lost circadian rhythmicity completely. The mRNA peak and nadir times could not be determined due to low amplitude rhythms, and the overall expression levels were reduced drastically. In contrast to *NR1D1* and *DBP*, the overall mRNA levels of *PER1* and *CRY1* were elevated. However, the amplitude of the oscillation stayed unaffected. The *PER2* mRNA expression level as well as the amplitude of the oscillation were not changed upon *TMED10* knockdown.

To conclude, genetic perturbation of vesicular protein transport disrupted normal circadian clock function, altering the mRNA expression pattern of six out of seven clock genes. Upon reduction of *TMED10* expression, the clock gene expression levels oscillated with a lengthened circadian period comparable to the one observed in bioluminescence recordings. Moreover, the reduction of the clock gene expressions' amplitude and their

changed overall expression levels could be interpreted as reduced clock robustness. Direct output genes like *DBP* exhibited the most severe effects, losing circadian rhythmicity completely accompanied by reduced expression levels.

3.2 Pharmacological interference with the vesicular protein transport pathway confirmed the importance of unperturbed ER to Golgi transport for normal circadian oscillations

3.2.1 An inhibitor screen identified ER to Golgi transport, endocytosis at the plasma membrane and N-glycosylation to be important for proper clock function

Having collected strong evidence that early vesicular protein transport is important for the circadian clock, we asked ourselves whether later steps of the vesicular protein transport might also play an important role, undetected by previous studies and genetic perturbation experiments (Bert Maier, unpublished data)[333]. To investigate this question and strengthen our previous findings, we chose pharmacological perturbation to block important steps along the vesicular protein transport pathway and monitored the effects on circadian oscillations.

In total, 23 pharmacological inhibitors (see **2.1.11**) were selected, inhibiting different steps of the vesicular pathway, ranging from ER exit sites to transport between ER and Golgi, N-glycosylation, trans-Golgi network trafficking, and finally transport events at the plasma membrane[340]. They were applied at concentrations of 50 µM and 5 µM to confluent U-2 OS reporter cells harbouring a *Bmal1*-promotor driven *luciferase* construct after synchronisation with dexamethasone. The bioluminescence was monitored over seven days and the time series was fitted to sine waves, using the chronostar2.0 software. After the measurement, the cell vitality was verified using a Resazurin based assay.

Inhibitors blocking vesicular protein transport had severe effects on the circadian clock (see **Figure 3-6A**). Eight out of 23 tested inhibitors showed strong period lengthening effects between 2.3 ± 0.4 and 11.0 ± 0.6 hours and one out of 23 inhibitors exhibited a subtle period shortening of 1.5 ± 0.7 hours upon application of 50 µM of inhibitor. Eeyarestatin damaged the cells to an extent that no bioluminescence signal was

detectable after day two, rendering data analysis impossible. Note, it has been described that six out of the nine inhibitors showing an effect, more specific FLI-06, Golgicide A (Gol A), Exo I, Exo II, AG1478, and Brefeldin A (BFA), perturb early stages of the vesicular protein transport pathway, Pitstop II interferes with endocytosis and exocytosis events at the plasma membrane, 16D10 blocks a V-ATpase at endosomes, and Tunicamycin inhibits the GlcNAc transferase. In addition to the pronounced effect on the circadian period, the application of the inhibitors resulted in reduced cell vitality in seven out of nine cases. Only U-2 OS cells treated with Exo I or Exo II exhibited unimpaired cell vitality at concentrations of 50 µM and 5 µM. Six out of 23 tested inhibitors showed period lengthening effects between 2.4 ± 0.7 and 14.8 ± 0.5 hours upon application of 5 µM of inhibitor. Eeyarestatin's effect on cell vitality was less pronounced so that data analysis was possible and the inhibitor showed period lengthening effects. In contrast, Exo I, Exo II and Pitstop II no longer lengthened the circadian cycle at this concentration. Again, most inhibitors perturbed early steps of the transport pathway. As observed in the higher concentration, the cell vitality was reduced in five out of six cases, although to a minor extend. We observed a correlation between the period lengthening effect and the low cell vitality in the past. Therefore, it is possible that the effects described were at least partially caused by cell damage.

To summarize, the use of 23 inhibitors blocking different steps along the vesicular protein transport pathway verified the importance of an unimpaired early transport between the ER and the Golgi. Seven out of 23 inhibitors showed strong effects on the circadian period. Furthermore, the inhibitor screen identified events at the plasma membrane and in the N-glycosylation process to be important for the circadian clock.

Since in all assays cell vitality was impaired, we chose to titrate the inhibitors down to non-toxic concentrations as circadian phenotypes that occur independent of impaired cell vitality would further strengthen our results. It has been reported that Eeyarestatin successfully blocks ER associated protein degradation (ERAD) and induces ER stress, which could influence the circadian clock. FLI-06 inhibits NOTCH signalling as a known side effect. In addition to Tunicamycins inhibitory effect on the N-glycosylation pathway, the compound is implicated in cell cycle arrest and ER stress induction. All three inhibitors were excluded from further studies due to their unwelcomed off-target effects despite their potential. Brefeldin A, Exo I and II, Golgicide A, AG1478 and Pitstop II were especially interesting, since no off-target effects were known from the literature.

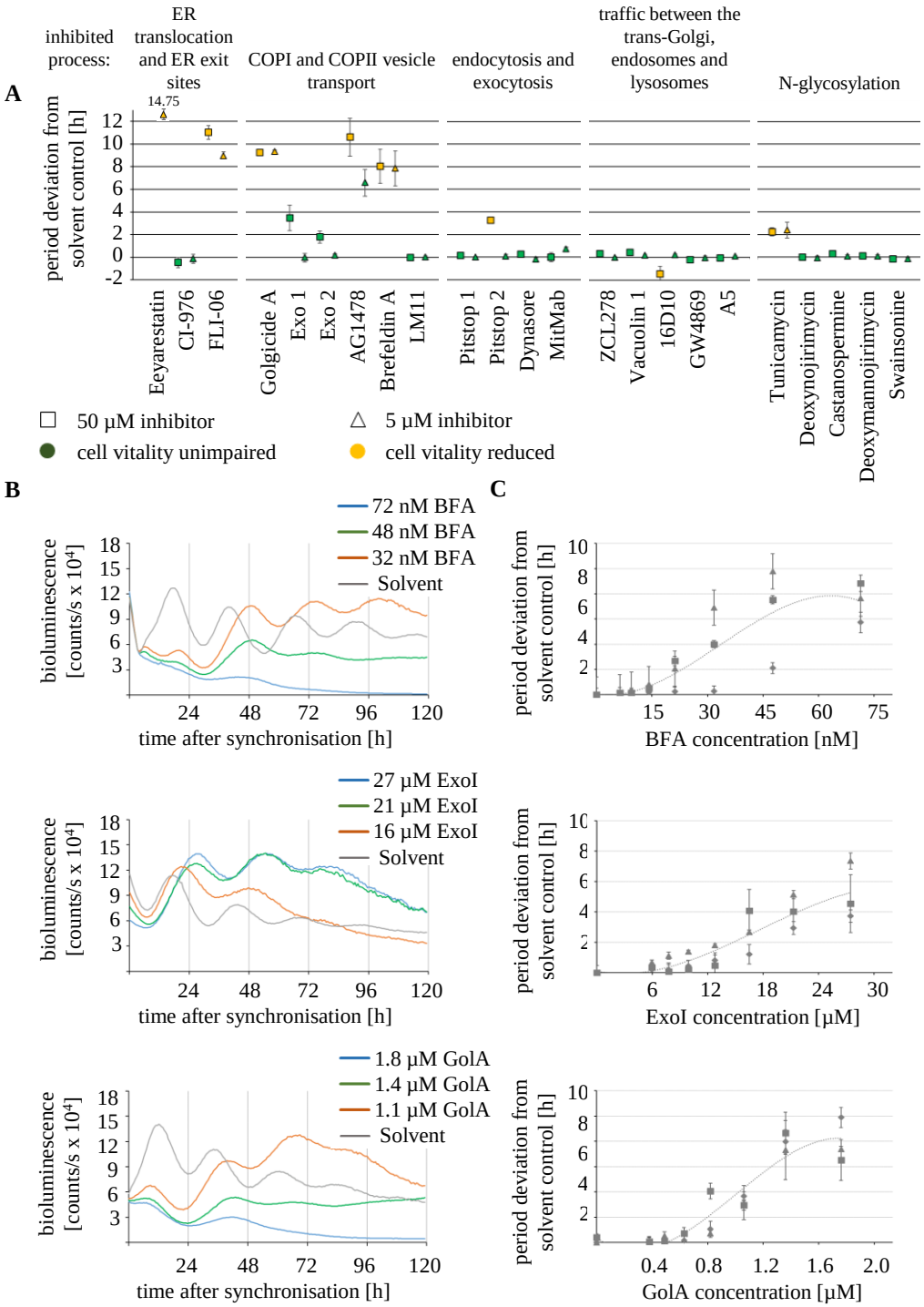

Figure 3-6: **Pharmacological perturbation of the early vesicular protein transport pathway lengthened the circadian period of human osteosarcoma cells in a dose dependant manner.** U-2 OS cells harbouring a *Bmal1*-promotor driven *luciferase* reporter construct were synchronised and then treated with either solvent or pharmacological inhibitors blocking different steps in the vesicular protein transport or N-glycosylation pathway prior to bioluminescence recordings over seven days. Bioluminescence data were fitted to sine waves, using chronostar2.0 and the circadian parameters were assessed. **A)** Depicted are the circadian period deviations relative to solvent controls for all tested inhibitors at two different concentrations (n = 3 individual recordings with 4 biological replicates, mean ± SD). **B and C)** Brefeldin A (BFA), Exo I and Golgicide A (Gol A) have been described to act at the cis-Golgi membrane and were applied at increasing concentrations. Depicted are representative bioluminescence recordings and the period deviation from solvent controls (n = 3 individual recordings with 4-6 biological replicates, mean ± SD, the dotted lines indicate the third-degree polynomial fit through the mean values of the three data sets).

Therefore, we had a closer look at these inhibitors and conducted experiments to identify their ideal working concentrations. For this purpose, the selected inhibitors were applied at individual concentrations to confluent U-2 OS reporter cells harbouring a *Bmal1*-promotor driven *luciferase* construct after synchronisation with dexamethasone. The bioluminescence was measured for five days and the datasets were fitted to sinewaves using chronostar2.0.

Three out of seven inhibitors could successfully be titrated down to non-toxic working concentrations, showing robust period lengthening effects with limited cell vitality issues (see **Figure 3-6B** and **Figure 3-6C**). Brefeldin A prolonged the circadian cycle up to 7.3 hours in a dose-dependent fashion over an inhibitor concentration range from 15 nM to 72 nM. The cell vitality was reduced when the highest concentration of 72 nM was applied, but was unaffected in all other tested concentrations. Exo I lengthened the circadian period dose-dependently up to 4.12 hours. The optimal working concentrations ranged from 12.78 µM to 27.45 µM. The cell vitality was not impaired at all tested concentrations. Golgicide A showed a dose-dependent period lengthening effect of up to 8.20 hours. The working concentration was in a range of 0.63 µM to 1.76 µM. The cell vitality was reduced in the highest concentration of 1.76 µM, but not in the other tested concentrations. In contrast, four inhibitors did show no period lengthening at non-toxic working concentrations. Exo II showed no dose-dependent period lengthening effect and the observed effects could not be uncoupled from the cell vitality. The previously observed effects of AG1478 could not be reproduced in two independent experiments, leaving the circadian period unaltered even at concentrations as high as 60 µM. Pitstop II and Tunicamycin both showed the previously observed lengthening of the circadian cycle but the effect was tightly coupled with cell vitality.

In conclusion, Brefeldin A, Exo I and Golgicide A dose-dependently lengthen the circadian period with unimpaired cell vitality. All three inhibitors were known to block vesicular protein transport events between the ER and the Golgi, providing further evidence that this part of the transport machinery is of immense importance for normal circadian clock function. Furthermore, the application of Pitstop II and Tunicamycin as well as Eeyarestatin and FLI-06 suggested that cargo sorting in the ER, N-glycosylation, exo- as well as endocytosis might play a role for the circadian clock but their phenotype is accompanied by reduced cell vitality.

3.2.2 RNA interference and pharmacological inhibitors impinged on the same process in vesicle biogenesis

Collected evidence from the genetic perturbation assay and the pharmacological perturbation assay hinted towards the importance of vesicular trafficking events between the ER and the Golgi for the circadian clock. Since the shRNA as well as the inhibitors were described to act on proteins involved in the same process, we raised the question if the observed phenotypes were additive or non-additive. In the former case one could argue, that shRNA and inhibitor acted on different targets or processes, leading to two different phenotypes adding up to an even longer period. In the latter case, one could claim, that shRNA and inhibitor share a common target or process, leading to an inhibition that could not be pushed any further. To address this question, we combined genetic and pharmacological perturbation in U-2 OS reporter cells and monitored the bioluminescence analysing the effect on the circadian period. Briefly, we transduced U-2 OS cells harbouring a *Bmal1*-promotor driven *luciferase* construct with either non-silencing control or shRNA constructs targeting *TMED10*. After selection and synchronisation of the reporter cells we applied increasing non-toxic concentrations of the three selected inhibitors Brefeldin A, Exo I and Golgicide A. The bioluminescence was recorded for five to seven days and the circadian parameters were assessed using the chronostar2.0 software.

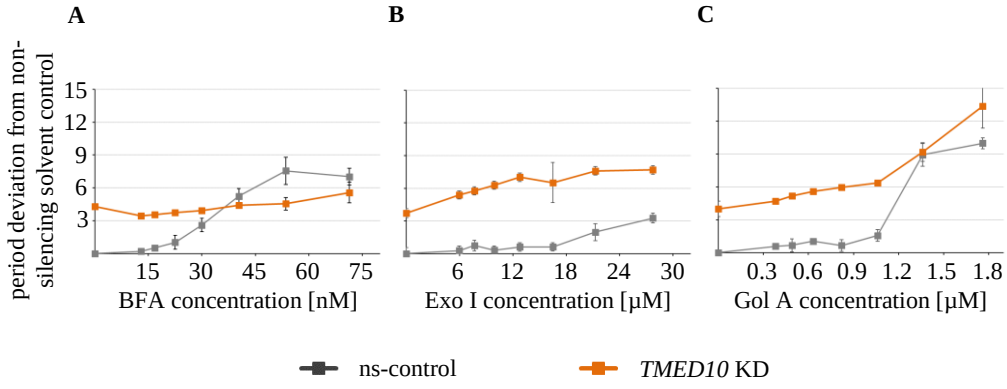

Figure 3-7: Transport inhibitors Exo I and Golgicide A but not Brefeldin A showed an additive effect of period lengthening on top of the RNAi phenotype. U-2 OS cells harbouring a *Bmal1*-promotor driven *luciferase* reporter construct were transduced with either a non-silencing control plasmid or an RNAi construct targeting *TMED10*. After synchronisation with dexamethasone the cells were treated with the solvent or increasing concentrations of transport inhibitor **A)** Brefeldin A, **B)** Exo I or **C)** Golgicide A and bioluminescence was measured for seven days. The data were fitted to sine waves, using chronostar2.0 and the depicted period deviation from ns solvent treated control was calculated (representative dataset selected from n = 2 recordings with 4-6 biological replicates, mean ± SD, additional dataset see **Supplemental Figure A 5**).

The application of the three inhibitors, known to act on COPI and COPII vesicular protein transport between the ER and the Golgi to the culture medium of U-2 OS non-silencing control cells, resulted in similar dose-dependent period lengthening effects as observed in previous experiments (see **Figure 3-6C** and **Figure 3-7**, dataset in grey and **Supplemental Figure A 5**). Shortly, supplementing the cell culture medium with Brefeldin A, Exo I or Golgicide A in concentrations ranging from 15 nM to 72 nM, 12.78 µM to 27.45 µM or 0.63 µM to 1.76 µM lengthened the circadian period by 7.0 hours, 3.3 hours and 10.0 hours, respectively. The *TMED10* depleted cells treated with the solvent showed in all three experiments the known knockdown phenotype, prolonging the circadian cycle by 4.3 hours, 3.7 hours and 4.0 hours (see **Figure 3-7**, orange dataset from left to right and **Supplemental Figure A 5**). Supplementing the cell culture medium with increasing concentrations of Brefeldin A, lengthened the circadian period by an additional 90 minutes up to a total of 5.6 hours in the highest concentration of 75 nM. The addition of the inhibitor Exo I in increasing concentrations to the cell culture medium resulted in a rapid increase in circadian period, reaching a plateau around 7.5 hours at concentrations between 12.78 µM to 27.45 µM. The previously observed period lengthening of 3.2 hours at an inhibitor concentration of 27.45 µM and the circadian *TMED10* knockdown phenotype of 3.7 hours added up to a combined circadian period lengthening effect of over seven hours. Golgicide A lengthens the circadian cycle slightly at concentrations between 0.36 µM and 1.08 µM and stronger at concentrations between 1.36 µM and 1.76 µM. The effect was additive at the concentration of 1.76 µM but not at 1.36 µM to the circadian *TMED10* knockdown phenotype, resulting in combined prolonged circadian period of 13.4 hours for 1.76 µM. In the second dataset (see **Supplemental Figure A 5**) Golgicide A addition to cells with reduced *TMED10* expression did not result in additive effects.

In conclusion, the period lengthening effects of the reduced *TMED10* transcripts and Brefeldin A as well as Golgicide A were non-additive. Since the shRNA-mediated knockdown did not lead to a complete inhibition, Brefeldin A probably inhibited the residual activity, leading to a slight increase in circadian period. Therefore, we speculate that Brefeldin A and the shRNA against *TMED10* acted on the same process in the COPI/ COPII pathway, highlighting its importance for normal circadian clock function. We propose a similar scenario for Golgicide A, as well. At lower concentrations, Golgicide A inhibited the remaining activity of COPI/ COPII-vesicle-mediated transport that remained unaffected by the shRNA-mediated knockdown of *TMED10* transcript level. At

higher concentrations, the Golgicide A-mediated period lengthening effects reached a plateau. The combined effect of the shRNA and Golgicide A showed the maximal inhibition and especially in the second dataset no additional period lengthening effect was detectable, using a concentration higher than 1.36 µM.

On the other hand, the addition of Exo I resulted in additive period lengthening effects. Additionally, the data suggested that the reduction of *TMED10* expression sensitised the cells for Exo I, resulting in a longer period at lower concentrations. Thus, we speculate that Exo I and the shRNA against *TMED10* probably acted on different targets which were dependent on each other to allow the sensitisation.

3.3 Unimpaired COPII vesicular protein transport was necessary for normal clock function

So far, our findings suggest the requirement of an unimpaired early vesicular protein transport, more precisely the COPI and COPII machinery. Therefore, we wondered, whether the anterograde protein transport using the COPII machinery or the retrograde protein transport using the COPI machinery played the most important role for the clock. Since both processes were highly interlocked, approaching this question turned out to be complicated[341]. Interfering with the ER export was described to induce ER stress responses, altering various cellular processes culminating in possible cell death or reduced cell vitality[342]. Inhibiting the COPI machinery at the Golgi interface was known to block inter-Golgi transport and retrograde protein transport leading to a collapse of the Golgi and therefore negative feedback to the ER transport machinery.

Our first approach to identify the role of the COPI protein transport machinery for the circadian clock involved the ectopic overexpression of dominant-negative *ARF1* mutants, described to interfere with the COPI vesicle biogenesis (see **Figure 3-8**). Using site-directed mutagenesis, we altered the coding sequence of wild-type *ARF1* to exchange specific amino acid residues in the ARF1 protein and cloned the corresponding sequences into lentiviral expression plasmids, exploiting the TOPO-cloning and Gateway techniques.

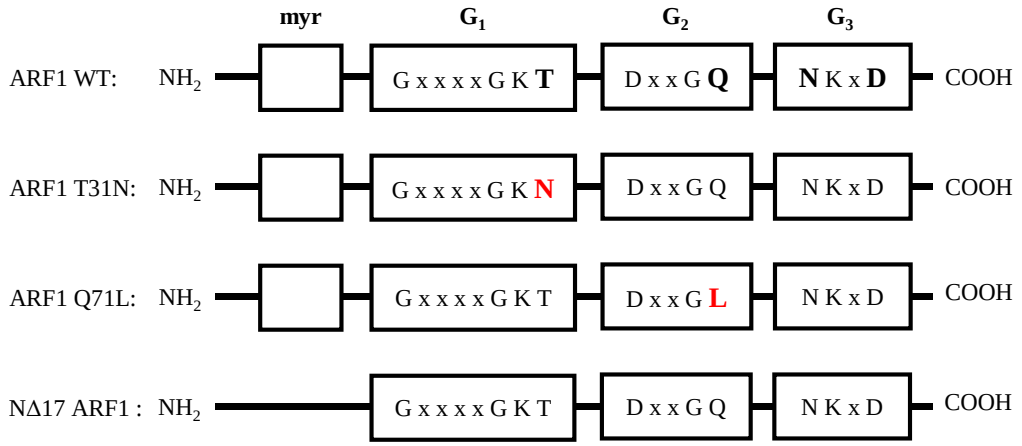

Figure 3-8: Schematic design of the generated ARF1 variants displaying either altered affinities to GDP/GTP or incapability of membrane insertion. The scheme outlines the organisation of ARF1's post-translational myristoylation as well as the three GTP-binding domains (G_1-G_3) for the wild type protein and the three altered variants. The highlighted amino acids in bold are known to be important for the GDP/GTP binding and were exchanged to the indicated amino acids in red. The myristoylation modification is necessary to insert ARF1 into the membrane and was missing in the truncated protein lacking the first 17 amino acids.

The first generated variant was Arf1 Q71L, known to possess a reduced intrinsic GTP hydrolytic activity, rendering ARF1 in a constitutively active form[343,344]. Thus, the coatomer protein complex is recruited to the membrane decorating the membrane with numerous coated budding vesicles, which are uncoated after fission with much slower rates. Additionally, it is speculated that the inactive vesicles at the membrane might interfere with docking COPII vesicles. The second mutant was the Arf1 T31N variant, known to preferentially bind to GDP and the associated GEF staying in the inactivated form. Due to its binding affinity, ARF1 T31N sequesters the available GEFs, consequently, blocking COPI vesicle formation[343,344]. Finally, the third variant was ARF1 NΔ17, lacking the first 17 amino acids N-terminally. This truncated ARF1 protein has been described to be no longer myristoylated and, therefore, to be precluded to insert into the Golgi membrane[343]. Consequently, the COPI vesicle biogenesis is highly impaired. Subsequently, we lentivirally transduced U-2 OS cells harbouring a *Bmal1*-promotor driven *luciferase* construct with either one of the generated *ARF1*-mutant expression plasmids. Synchronisation with dexamethasone and bioluminescence recordings over five consecutive days were scheduled but could not be carried out due to substantial cell death after day two. These results suggested that perturbation of the ARF1-mediated initiation of the COPI coat assembly was necessary for cellular survival and not suited for investigating the role of the retrograde transport machinery for the circadian clock.

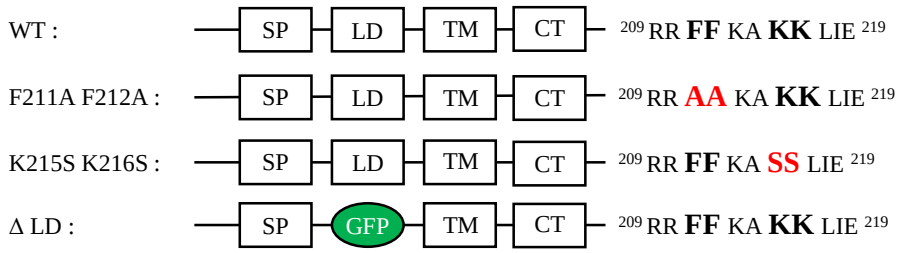

Figure 3-9: Schematic design of the generated TMED10 variants lacking cytoplasmic COPI/COPII specific transport signals or the luminal domain thought to be important for protein-protein interaction. The scheme outlines the organisation of the different TMED10 domains for the wild type protein and three versions with double amino-acid exchanges: SP – ER translocation signal peptide, LD – luminal domain, GFP – *green fluorescent protein*, TM – transmembrane domain, CT – cytoplasmic tail containing important transport signals highlighted in bold. The mutated amino acids are indicated in red.

In our second approach, we focused on two different transport signals in the C-terminus of TMED10 as well as TMED10's luminal domain in the process of cargo sorting and their role for the circadian clock. For this purpose, we designed three mutated *TMED10* versions using site directed mutagenesis (see **Figure 3-9**). Subsequently, the mutated *TMED10* sequences were shuttled into expression vectors.

The two phenylalanine residues at position 211 and 212 in the TMED10 protein are described to function as anterograde transport signals binding to SEC23[214]. In addition, they have been described to contribute to the binding of the F sub-complex of COPI consisting of β-, γ- and ζ-COP in some p24 protein family members[239]. The degree of their contribution on F sub-complex binding in TMED10 is still under debate and has not been fully enlightened, yet. The exchange of the two phenylalanine to alanine has been described to disrupt SEC23 binding completely and to slow down ER to Golgi transport drastically compared to cells expressing wild-type TMED10[214,263]. The two lysine residues at position 215 and 216, however, are part of the C-terminal ER retrieval signal KKXXX. It is well described to bind COPI subunits of the B complex consisting of α-, β'- and ε-coatomer and, therefore, to function primarily in the retrograde transport machinery[214,239,261,345,346]. The exchange of the two lysine to serine decreases the overall COPI binding and redistributes TMED10 to the trans-Golgi and the plasma membrane whereas it is predominantly found at the cis-Golgi and the ER in wild-type cells[214]. TMED10's luminal domain facilitates protein-protein interaction and is believed to be responsible for the hetero-oligomerization with other p24-family members[347]. Furthermore, studies implicate that the luminal domain might be involved in cargo sorting processes and the retention of TMED10 in the ER-Golgi-trafficking machinery by introducing a trafficking delay, allowing the proper organisation into vesicles. The

exchange of the luminal domain into a Gfp protein abolishes the interaction with other members of the p24-family, thus, inducing destabilization of the TMED10 protein, weakened retention in the Golgi, and an altered overall cellular TMED10 distribution. Since the modifications of the TMED10 protein were not dominant negative, we performed rescue experiments in cells with reduced *TMED10* expression or control cells to investigate the function of TMED10's cytoplasmic transport signals and TMED10's luminal domain. To this end, the expression plasmids containing the mutated *TMED10* sequences were lentivirally transduced into *TMED10* depleted or non-silencing control U-2 OS reporter cells. After synchronisation with dexamethasone, the cellular bioluminescence was recorded over five consecutive days (see **Figure 3-10**, first column) following cell lysis, total RNA extraction, and qRT-PCR to assess endogenous *TMED10* mRNA levels as well as *TMED10* mRNA levels upon overexpression (see **Figure 3-10**, second column).

The overexpression of the TMED10 wild-type protein as well as the TMED10 K215S K216S protein in the *TMED10* knockdown background could restore normal circadian rhythms with periods similar to the ones observed in non-silencing control cells (see **Figure 3-10**, third column). In more detail, the depletion of *TMED10* resulted in the previously observed period lengthening of 3.4 ± 0.9 hours compared to the control. To rescue the period phenotype, we overexpressed the wild-type protein (compare **Figure 3-2**, first column) and reduced the period lengthening to 0.6 ± 0.1 hours. The qRT-PCR data confirmed the knockdown of the endogenous *TMED10* mRNA down to 12% through amplification of a sequence in the 3'UTR and the successful rescue through ectopic overexpression of the *TMED10* ORF, increasing *TMED10* mRNA level 73-fold. Normal circadian rhythmicity was also restored overexpressing the TMED10 K215S K216S mutant 49-fold, resulting in a period lengthening of 0.0 ± 0.3 hours.

In contrast, neither the overexpression of the TMED10 F211A F212A mutant nor the overexpression of the TMED10 ΔLD rescued the circadian phenotype of *TMED10* depletion. Although the *TMED10* F211A F212A mutant's mRNA level were elevated 67-fold, the circadian period was 3.2 ± 1.0 hours longer than in control cells. Moreover, the circadian cycle was lengthened by 0.8 ± 0.2 hours when the mutant was overexpressed in the non-silencing background. These findings imply that the mutated *TMED10* interferes and negatively influences the transport processes even in the presence of the wild-type TMED10 protein.

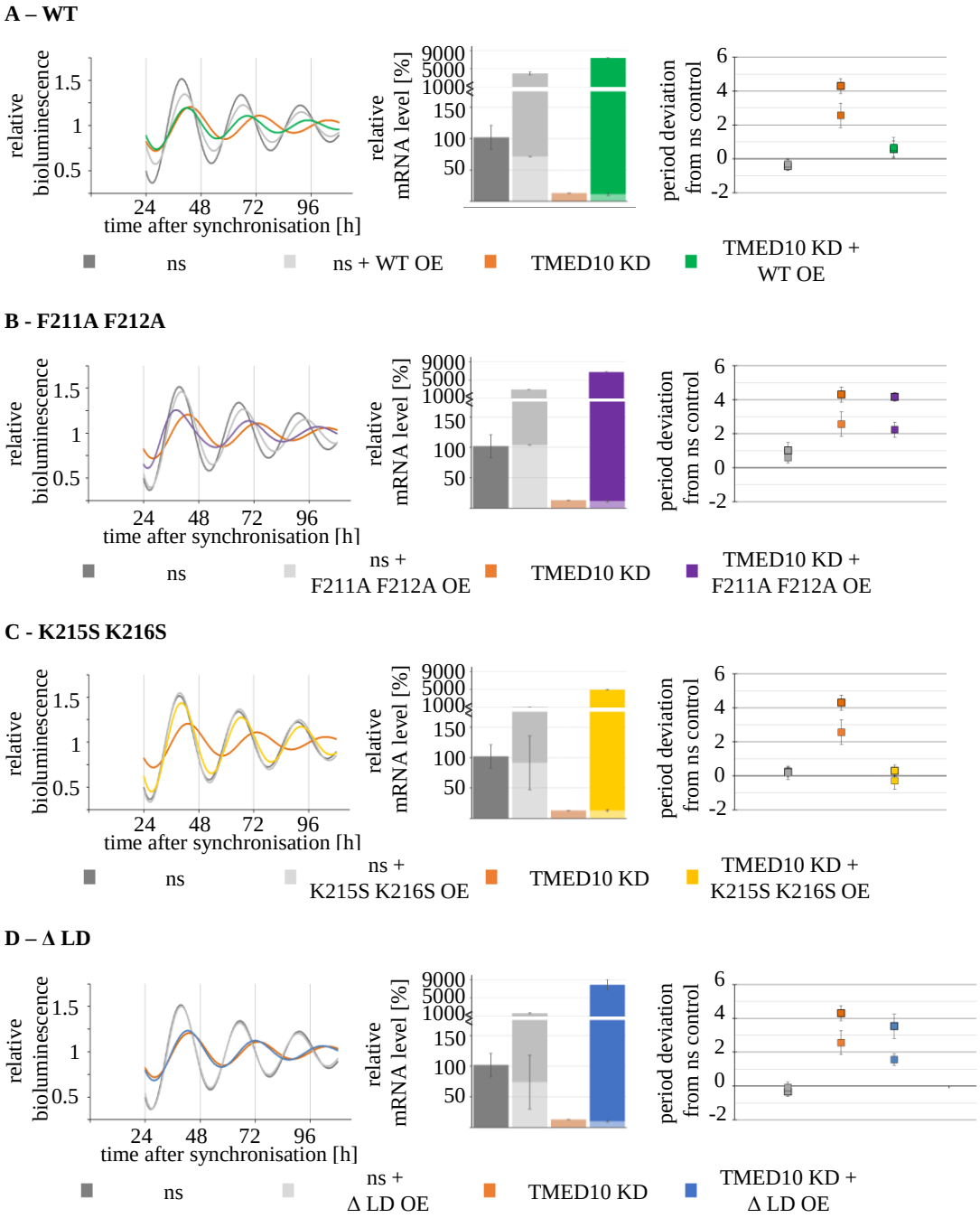

Figure 3-10: TMED10's luminal domain and the anterograde transport signals encoded in the cytoplasmic domain were necessary for normal circadian function. U-2 OS cells harbouring a *Bmal1*-promotor driven *luciferase* reporter construct were transduced with a **A)** wild-type (WT)-, **B)** F211A F212A-, **C)** K215S K216S- or **D)** ΔLD-*TMED10* overexpression (OE) construct, followed by a second transduction with either a non-silencing control plasmid or an RNAi construct targeting *TMED10* (KD). Cells were synchronized with dexamethasone and bioluminescence was recorded for five days. The time series were fitted to sine waves and circadian parameters were assessed, using chronostar2.0. Depicted are representative normalized and detrended bioluminescence data of the four rescue experiments, the corresponding endogenous (light colours) and overexpression (dark colours) *TMED10* mRNA level [%] (mean ± SD), and the period deviations from non-silencing controls [h] (n = 2 individual recordings with 3-8 biological replicates, mean ± variance).

The *TMED10* ΔLD mutant displayed a 79-fold overexpression and a slightly shorter period of 2.5 ± 1.0 hours compared to the *TMED10* depleted cells. This partial rescue might result from the intact di-phenylalanine motive but due to the missing luminal domain the TMED10 protein had impaired dimerization capacity and was destabilized. Therefore, one could speculate that normal vesicular transport dynamics could not be established to rescue the circadian phenotype.

Taken together, the second approach collected valuable data on the connection between vesicular protein transport and the clock. TMED10 wild-type protein as well as the TMED10 K215S K216S protein restored normal rhythmicity and rescued the shRNA-mediated *TMED10* knockdown period phenotype, suggesting that the retrograde protein transport was of minor importance for the circadian clock. Consequently, the COPII-mediated anterograde protein transport had to be functional and unperturbed for the cell to display normal circadian rhythmicity. This hypothesis was supported by the failed rescue attempts, using the *TMED10* F211A F212A and the *TMED10* ΔLD mutant overexpression plasmids described to lack SEC23 binding properties, escaping the ER-Golgi-machinery and destabilizing 24-family members, thus, slowing down COPII vesicle machinery.

3.4 Unfolded protein response was not responsible for the period lengthening effect

The previous experiments suggested the importance of the COPII machinery, the unperturbed anterograde vesicular protein transport from the ER to Golgi, and normal Golgi morphology to be crucial for normal clock function. As it was described by de Galarreta et al and reviewed by Ron and Walter that inference with this tightly regulated cellular process might lead to ER stress responses, we asked whether the circadian phenotype was caused by the ER overload coping mechanisms which involves changes in the transcription and translation machinery[348,349].

To answer this question, we chose two different assays to determine unfolded protein response (UPR) upon genetic and pharmacological perturbation. First, we analysed the IRE1α-dependent splicing of the X box-binding protein 1's (XBP1u) mRNA

to produce the active transcription factor (XBP1s)[350]. This transcription factor regulates the expression of genes involved in protein folding, ER-associated degradation (ERAD), protein quality control, and phospholipid synthesis. All these processes help the ER to cope with additional protein load. Additionally, IRE1α has been described to be involved in mRNA degradation through regulated IRE1-dependant decay (RIDD) and to induce alarm stress pathways. Secondly, we investigated the upregulation of UPR associated genes like *DNAJC3* also known as *P58IPK* and *HERPUD1* via qRT-PCR[350]. *DNAJC3* was known to function as a co-chaperone and regulator of *GRP78* in the ER promoting refolding of misfolded proteins and restoring ER homeostasis. Furthermore, it was described to modulate PIK function, re-allowing protein translation by blocking the PIK's kinase activity and, thus, the phosphorylation of serine 51 in eIF2α. HERPUD1 was described to be involved with the ERAD pathway. During ER stress *HERPUD1* was found to be highly upregulated in the ER membrane and being exposed to the cytosol, presumably interacting with the cytosolic components of the ERAD machinery.

To investigate, whether UPR-associated pathways get activated, we transduced U-2 OS reporter cells with shRNA constructs targeting *TMED2* and *TMED10* or with non-silencing control plasmids. Additionally, we treated cells with the compound Brefeldin A as a positive control, known to block early secretory transport processes and influence circadian oscillations. The cell culture medium was supplemented with three different concentrations ranging from 18 µM known to induce UPR, over 360 nM as an intermediate concentration, down to 72 µM which is the concentration used in the inhibitor screen, inducing a circadian period lengthening effect without an accompanied drastic reduction of cell vitality. U-2 OS cells were harvested on three subsequent days, total RNA was purified, and reversely transcribed to detect the spliced and unspliced form of *XBP1* as well as quantify the mRNA expression level of *P58IPK* and *HERPUD1*.

Neither the reduction of *TMED10* or *TMED2* transcript levels to under 10% compared to control cells (see **Figure 3-11B**) nor the addition of Brefeldin A in a concentration of 72 nM activated splicing of *XBP1* mRNA to generate the active transcription factor XBP1s (see **Figure 3-11A,** red arrowhead).

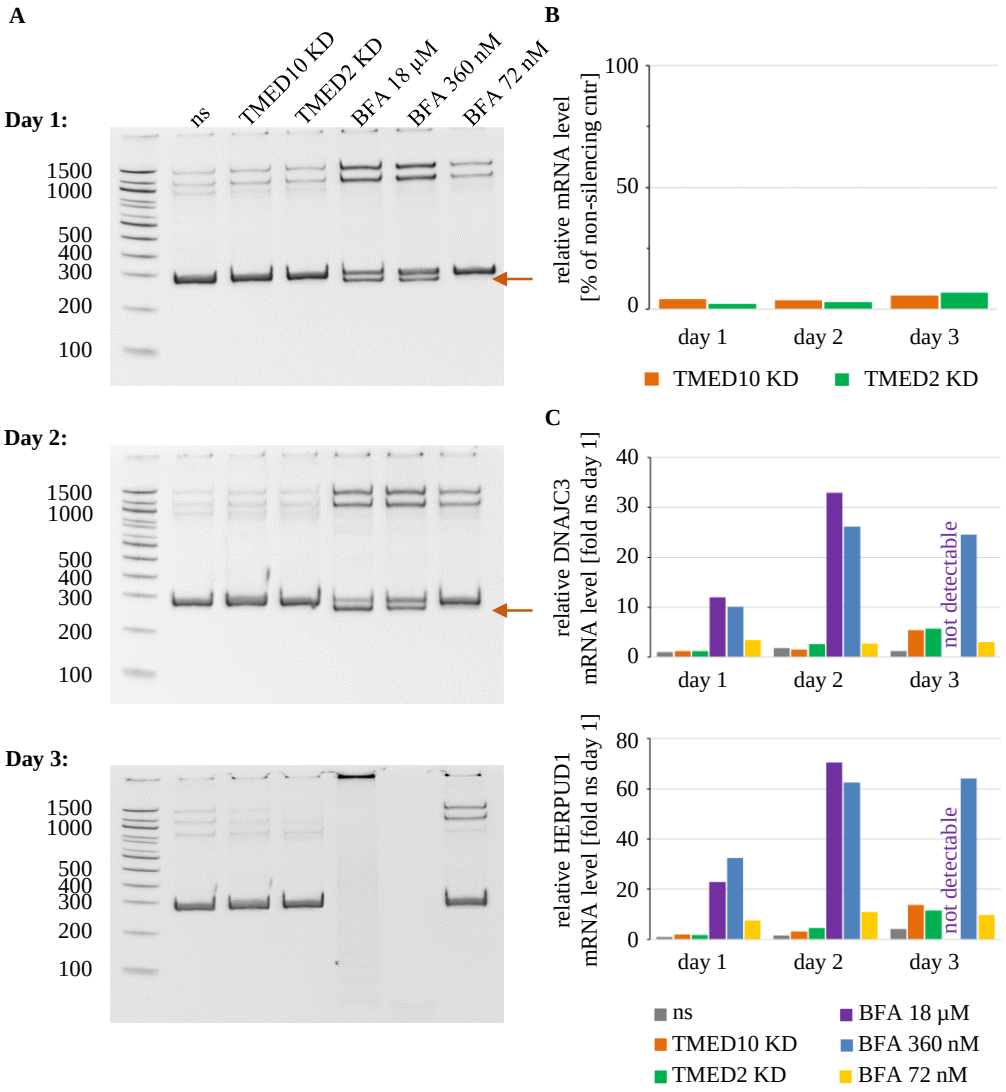

Figure 3-11: The RNAi-mediated knockdown of *TMED10* or *TMED2* transcripts did not trigger unfolded protein response (UPR) in human osteosarcoma cells. U-2 OS cells harbouring a *Bmal1*-promotor driven *luciferase* reporter construct were transduced with non-silencing control plasmids, RNAi constructs targeting *TMED10* and *TMED2* or treated with decreasing concentrations of transport inhibitor BFA as a positive control before they were harvested on three constitutive days. **A)** Purified RNA was reversely transcribed to cDNA with oligo-dT primers and used as a template to amplify the 263 bp (short, UPR) and the 289 bp (long, no UPR) *XBP1* splice variants, the former indicating triggered UPR. Depicted are representative 12% polyacrylamide DNA gels showing the 263 bp *XBP1* splice variant in the BFA treated cells at higher concentrations at day 1 and 2 but not in the *TMED10* or *TMED2* depleted cells. **B)** *TMED2* and *TMED10* mRNA levels were measured using qRT-PCR, demonstrating a successful knockdown of both transcripts compared to non-silencing controls. **C)** Transcripts levels of *DNAJC3* and *HERPUD1* were analysed in all samples using qRT-PCR and normalized to the transcript levels of the ns control sample of day1 (A and B: n = representative of 2 individual experiments with one sample for each condition; C: n = 1 individual experiments with one sample for each condition).

We were unable to amplify the spliced 263 bp variant of *XBP1* and could only detect the 289 bp XBP1u in the corresponding cDNA samples of all three days. Therefore, we concluded that the RNAi-mediated knockdown of *TMED10* and *TMED2* as well as

the previously used concentration of 72 nM of Brefeldin A did not trigger unfolded protein response. In contrast, the cells treated with higher concentrations of Brefeldin A showed ER stress and upregulated IRE1α dependant splicing of *XBP1*u. For the first two days, we amplified both *XBP1* splice variants and, thus, detected two DNA bands corresponding to the 263 bp and the 289 bp *XBP1* splice forms. On the third day, overall purified mRNA concentrations were low which resulted in no *XBP1* amplification. We could detect none of the *XBP1* splice forms presumably due to UPR-induced cell death. The results were supported by the qRT-PCR data (see **Figure 3-11C**). On day one and two, *DNAJC3* was only slightly induced in *TMED10* and *TMED2* depleted cells as well as in the U-2 OS cells treated with 72 nM Brefeldin A compared to non-silencing cells on day one. On day three, the *DNAJC3* mRNA levels were elevated 5.4- and 5.7-fold upon decreased *TMED10* and *TMED2* expression and 3-fold for Brefeldin A. The samples that showed *XBP1* splicing, namely U-2 OS cells treated with Brefeldin A in concentrations of 18 µM and 360 nM exhibited 12.0- and 10.1-fold elevated *DNAJC3* mRNA levels on day one and 32.9- and 26.1-fold elevated *DNAJC3* mRNA levels on day two. On the third day, no mRNA levels could be determined in the 18 µM brefeldin A sample and 24.5-fold elevated mRNA level in the 360 nM brefeldin A sample, suggesting similar levels to day two. A similar result was obtained for analysis of the *HERPUD1* mRNA levels. Upon reduction of *TMED10* and *TMED2* expression levels and upon treatment with brefeldin A 72 nM cells showed only slight inductions over three days up to 13.7-, 11.6- and 9.7-fold respectively. In contrast, U-2 OS cells treated with higher concentrations of Brefeldin A exhibited *HERPUD1* mRNA level as high as 70.6- and 64.1-fold compared to non-silencing control cells on day one.

To summarize, the first assay analysing the activation of IRE1α dependent *XBP1* splicing clearly showed no indication for induction of unfolded protein response pathways upon decreases *TMED10* and *TMED2* expression. Also, we were unable to detect the *XBP1*s splice variant in cells supplemented with 72 nM of brefeldin A. The results of the second approach suggested an upregulation of two transcripts associated with UPR for the above-mentioned samples. In comparison to the positive controls the upregulation was minor, therefore we conclude that unfolded protein response was not a primary reason for the observed effect on the circadian clock. Nevertheless, the possibility remained that unfolded protein response might, although to minor extent, contribute to the observed period lengthening.

3.5 A secreted factor influenced circadian rhythms and induced phase shifts in U-2 OS reporter cells

Having identified that COPII-mediated anterograde vesicular protein transport between the ER and the Golgi was important for normal clock function, raised the question, how perturbances of this pathway impact circadian clock oscillations. It was established in numerous works that the secretory pathway played a fundamental role in organelle biogenesis, homeostasis of membrane lipids and proteins, constitutive secretion of signalling peptides, and transport as well as recycling of proteins and receptors to the plasma membrane. Interferences in the organelle biogenesis or the compositions of membranes would most likely have caused reduced cell vitality which was not found in our results (see **Figure 3-3**). Thus, we decided to focus our work on the secretion of signalling molecules. The literature provided multiple evidence that secreted factors of unknown entity synchronize peripheral cells and are responsible for intracellular coupling strengthening circadian rhythms[148,169,351]. Furthermore, it was suggested by Gerber et al. who investigated circadian synchronizing factors in the periphery that such factors might be proteins[141]. To test if cultured cells secreted signalling molecules influencing circadian dynamics, we purified and concentrated conditioned medium prior to application onto synchronised U-2 OS reporter cells. In more detail, we synchronised U-2OS cells harbouring a *Bmal1*- or *Per2*-promotor driven *luciferase* construct and recorded their bioluminescence. We harvested conditioned medium from U-2 OS wild-type cells and concentrated the conditioned medium or control medium on Amicon Ultra centrifugal filter units with molecular weight cut-off filter of 10 kDa. The 30x enriched eluates were applied to the reporter cells four to six hours after *Per2*-promotor driven *luciferase* peaked and the phase difference between conditioned medium and control medium treated cells was assessed over three consecutive days (see **Figure 3-12A, C, D and F**).

The application of purified and concentrated conditioned medium exhibited drastic effects on the circadian dynamics in two different U-2 OS reporter cell lines. These findings supported our hypothesis that secreted factors impinge on the circadian oscillator. First, conditioned medium application resulted in a phase shift by up to 5.1 hours in *Per2_luc* reporter cells and up to 2.7 hours in *Bmal1_luc* reporter cells compared to control medium. This effect was persistent over two consecutive days. Second, the application led to a slight acute induction of *Bmal1*- or *Per2*-promotor driven *luciferase*

expression followed by a long-lasting higher level of bioluminescence signal over the subsequent 48 hours. Since the *Per2_luc* and the *Bmal1_luc* reporter cell lines were synchronised at the same time and, therefore, oscillated antiphasic to each other, the stimulation time of the *Bmal1_luc* reporter cells was non-optimal. We applied the conditioned medium when the *luciferase* transcript levels were rising anyway and, thus, might have missed the full potential of the acute *Bmal1*-promotor driven *luciferase* induction. We speculated that the effect might be even more pronounced under optimal conditions, preferably four to six hours after the peak of *Bmal1*-promotor driven *luciferase* expression.

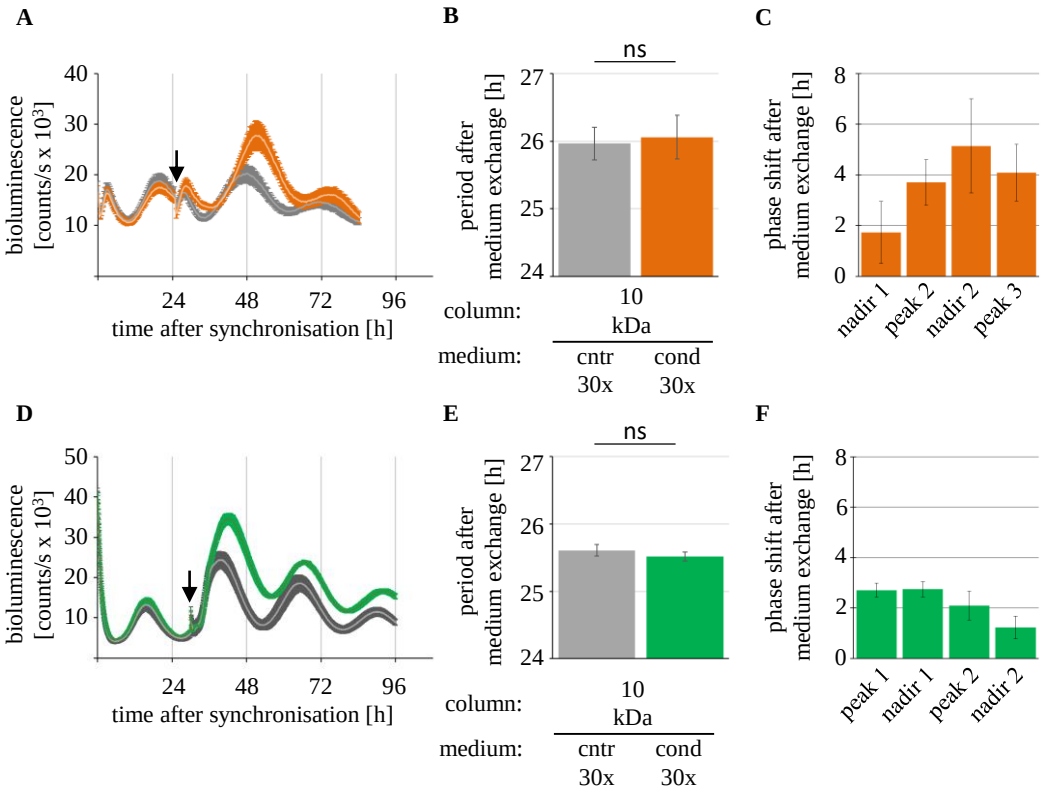

Figure 3-12: Conditioned medium induced a phase shift in synchronized human osteosarcoma cells. U-2 OS cells harbouring a (**A-C**) full length *Per2*-promotor driven *luciferase* reporter construct or a (**D-F**) *Bmal1*-promotor driven *luciferase* reporter construct were synchronized with dexamethasone and bioluminescence was recorded. Four to six hours after *Per2*-driven luciferase bioluminescence peak time, the cell culture medium was exchanged to either 30-fold concentrated control medium (cntr., grey) or 30-fold concentrated conditioned medium (cond., orange and green) from U-2 OS wildtype cells. **A and D)** Depicted are representative mean bioluminescence data before and after medium exchange with the standard deviation as a shaded area around the curve. **B and E)** The bioluminescence data after medium exchanged were fitted to sine waves and the circadian parameters were calculated using chronostar2.0. Shown are the circadian periods after medium exchange which did not significantly differ between control medium and conditioned medium treated cells (Student's T-Test: $p = 0.66$ and $p = 0.23$). **C and F)** The peaks and nadirs in the bioluminescence data of control medium and conditioned medium treated cells were analysed and the apparent phase shift was calculated for the first two peaks and nadirs (representative experiment selected from n = 2-3 individual recordings with 3-4 biological replicates; mean ± SD; Student's T-Test: * $p < 0.05$; ns: non- significant; additional dataset see appendix **Supplemental Figure A 6**).

To analyse whether the conditioned medium evoked additional effects on circadian oscillations, for example alterations in the period, we fitted sine waves to the times series after conditioned medium application using chronostar2.0 and assessed the circadian parameters (see **Figure 3-12B and E**).

The apparent phase shift induced by the treatment with conditioned medium was not due to changes in the circadian period. Cells harbouring a *Per2*-promotor driven *luciferase* exhibited a circadian period of 26.0 ± 0.2 hours when treated with control medium compared to 26.0 ± 0.3 hours when treated with conditioned medium. Thus, the periods were not significantly different (student's T-Test p = 0.66). The *Bmal1_luc* reporter cells showed a slightly shorter period than the *Per2_luc* reporter cells. Their circadian period averaged out at 25.6 ± 0.1 hours when treated with control medium compared to 25.5 ± 0.1 hours when treated with conditioned medium. Again, no significant difference was detected (student's T-Test p = 0.23).

To conclude, U-2 OS cells secrete soluble factors into the cell culture medium that induced a long-lasting phase shift by up to 5.1 hours in synchronised U-2 OS reporter cell lines. While the application of conditioned medium evoked a phase shift, the circadian periods of the reporter cells were not altered significantly and displayed a stable length of approximately 26.0 hours in *Per2_luc* reporter cells and 25.5 hours in *Bmal1_luc* reporter cells. We speculated at this point that the secreted factors add robustness to the circadian oscillator. Furthermore, they might cause severe alterations of circadian dynamics if they are not properly secreted, sensed by the corresponding signalling receptors, and internally processed.

3.6 Conditioned medium activated CRE-mediated but not SRE-mediated transcription

Since we discovered that conditioned medium induced phase-shifts in synchronized U-2 OS reporter cells we wondered which signalling pathways got activated and how they impinged on the molecular clockwork. The literature provided us with a profound understanding on how external, synchronising stimuli, particularly light, were processed in the superchiasmatic nucleus, culminating in the activation of immediate

early genes like *c-Fos, Erg1, Klf4, Per1* and *Per2*[73–75]. Promotor analysis have revealed that most of these immediate early genes contain a conserved CRE-promotor element. However, only little is known for in terms of signal processing in the periphery. Evidence suggests that in the periphery CRE-promotor elements as well as SRE-promotor elements might play an important role for the integration of timing information into the circadian oscillator[352]. To examine if CRE- or SRE-mediated transcription got upregulated upon conditioned medium application, we cloned reporter plasmids containing either one of the two enhancer sequences in front of a firefly luciferase (see **Figure 3-13A** and **D**) and conducted bioluminescence recordings. Specifically, we lentivirally transduced U-2 OS wild-type cells with the two reporter constructs and prepared them for bioluminescence recording without synchronization. One day after the start of measurement, the conditioned medium of separately cultured U-2 OS wild-type cells as well as the control medium were harvested, concentrated, and used to stimulate the reporter cells.

The application of conditioned medium to U-2 OS wild-type cells transduced with a 7x-CRE_*luciferase* reporter construct led to an immediate induction of the reporter and, thus, to a fast increase in luciferase activity (see **Figure 3-13B** and **C**). In the shown representative experiment, the addition of the conditioned medium resulted in a 14.1-fold induction of the reporter construct compared to a 1.2-fold induction caused by addition of the control medium. The increase in bioluminescence signal persisted for at least 19 hours, presumably longer, and peaked 14 hours after medium exchange.

The application of conditioned medium on U-2 OS cells transduced with a 7xSRE_*luciferase* reporter construct exhibited only minor induction and a comparatively short duration of the increase in bioluminescence (see **Figure 3-13E** and **F)**. Upon condition medium treatment, the reporter construct activation was 1.9-fold and the maximal luciferase activity was obtained two hours after medium exchange compared to a 1.2-fold induction after application of the control medium. Interestingly, the conditioned medium application led to a second activation of the reporter 12 hours later. Since the bioluminescence dataset resembled the shape of recently synchronized cells, we speculated if conditioned medium might work as a synchronizing agent.

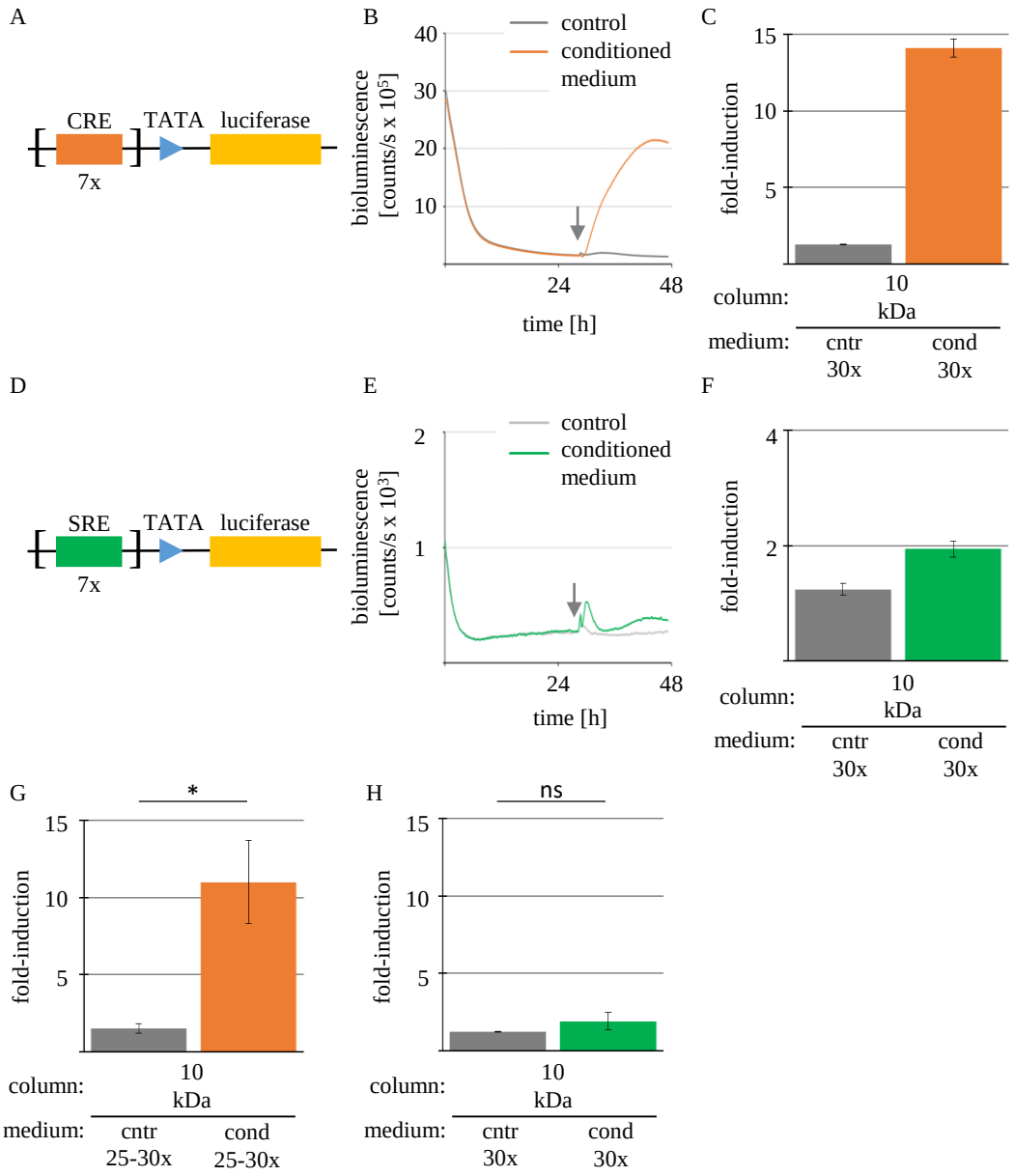

Figure 3-13: Conditioned medium elevated CRE- but not SRE-dependant gene expression. U-2 OS wild-type cells were transduced with either a 7x CRE or 7x SRE reporter construct. After approximately 24 hours of bioluminescence recording, when the minimum reporter activity was reached, medium was exchanged to 30-fold concentrated control or conditioned medium from U-2 OS wild-type cells. **A and D)** Schematic outline of the CRE- and SRE-reporter constructs containing seven tandem repeats of the corresponding enhancer sequence fused to a destabilized *luciferase*. **B and E)** Depicted are representative bioluminescence recordings of transduced and stimulated U-2 OS cells. Time of medium exchange is indicated by the grey arrowhead. **C and F)** Shown are the quantifications of the bioluminescence recordings (B and D) as fold-inductions (n = 1 with 6 biological replicates, mean ± SD). **G and H)** Depicted are the mean 7x CRE (Student's T-Test: p = 0.004) and 7x SRE (Student's T-Test: p = 0.118) activation as fold-induction (n = 3 individual recordings with 3-6 biological replicates, mean ± SD; Student's T-Test: * $p < 0.05$; ns: non- significant).

The observed difference in brightness between the two reporter constructs is most likely caused by the PEST sequence attached to the *luciferase* in the 7xSRE_*luc* reporter construct which destabilizes the luciferase. However, we exclude the possibility that the attached PEST sequence is responsible for the different transcriptional activation. As previously reported, the 7xSRE construct exhibits a fast and drastic increase in the bioluminescence signal upon serum application[141].

Taken together, conditioned medium activated a transcription factor and induced its binding to the CRE-promotor elements, thereby increasing *luciferase* expression. The addition of conditioned medium resulted in a 11.0 ± 2.7 -fold increase of luciferase activity (see **Figure 3-13G**). Furthermore, our results showed that the *SRF_luc* was only slightly upregulated upon conditioned medium treatment, increasing the luciferase activity 1.5-fold (see **Figure 3-13H**). Hence, we speculated that the factors in the conditioned medium led to the activation of a G-protein coupled receptor which stimulated activating transcription factors, presumably phosphorylated CREB, to bind to CRE-elements likely via a signalling cascade involving cAMP and proteinase K.

3.7 The CRE-signalling cascade was activated by molecules bigger than 30 kDa

Having revealed the existence of unidentified, soluble factors in conditioned medium that induce phase-shifts in U-2 OS reporter cells, presumably via a signalling cascade activating CRE, we aimed to find out more about its molecular properties. In the previous experiments, we used size exclusion filters that enriched molecules larger than 10 kDa. The strong induction suggested that the activating factors were highly enriched, thus, providing evidence that the secreted factors might be big proteins rather than a small peptide. To identify the specific molecular size of the stimulating molecules we harvested conditioned medium, enriched it by using distinct size exclusion filters ranging from 3 – 100 kDa, and monitored the bioluminescence of 7xCre_*luciferase* reporter cells after medium exchange.

The conditioned medium enriched by molecules bigger than 3 kDa exhibited the strongest effects on a 7xCre_*luciferase* reporter construct and led to a 4.7-fold induction

(see **Figure 3-14A**). With an increase in pore size, enriching molecules bigger than 10 kDa, 30 kDa, 50 kDa or 100 kDa, the activation of the 7xCRE_luciferase reporter decreased to 3.8-, 3.3-, 2.9- and 2.5-fold, respectively. This result could be explained by the residual retention of smaller molecules on the size exclusion filters of larger pore sizes or the existence of multiple activating factors of different molecular weights.

To test our hypothesis that the activating factors only got retained unintentionally on larger size exclusion filters, we harvested conditioned medium and enriched the medium by using distinct size exclusion filters ranging from 10 – 50 kDa. Next, the concentrated conditioned medium was separated on a bis-tris-polyacrylamide gel and the protein content was stained with Coomassie-blue to judge the enrichment of proteins by their molecular weight (see **Figure 3-14B**). The SDS polyacrylamide gel electrophoreses revealed the successful enrichment of a variety of proteins possessing different molecular weights, ranging from 10 kDa to more than 260 kDa. Although the 30 kDa size exclusion filter should only retain molecules bigger than 30 kDa (see **Figure 3-14B** lane 5 and 6) and the 50 kDa size exclusion filter should only retain molecules bigger than 50 kDa (see **Figure 3-14B** lane 7 and 8), smaller molecules were still detected even though to a lesser extent. These findings supported our hypothesis. To solve the problem of unintended retention, two additional washing steps were carried out in future experiments.

Since our stimulation with the conditioned medium enriched on the 3 kDa size exclusion filter evoked the strongest induction and declined with larger size exclusion filters, we speculated that the secreted soluble factors were rather small (3-30 kDa). Therefore, we expected to find the factor partially in the flow-through after enrichment of conditioned medium by a 30 kDa size exclusion filter. To challenge our assumption, we harvested conditioned medium and enriched the medium on a 30 kDa size exclusion filter, collecting the flow-through. Next, we applied the collected flow-through of the enrichment process as well as the flow-through of the additional washing steps on a 3 kDa column and stimulated 7xCRE_*luciferase* reporter cells with the concentrated conditioned medium, monitoring the bioluminescence.

Surprisingly, the stimulation of 7xCRE_*luciferase* reporter cells with the 15x enriched conditioned medium of a 30 kDa size exclusion filter resulted in a 14.9-fold induction of the bioluminescence signal (see **Figure 3-14C**). Therefore, we concluded that the activating factors of the CRE-signalling cascade were highly enriched on the 30 kDa size exclusion filter, suggesting that the factors possessed a bigger molecular weight than 30 kDa. The addition of the 15x enriched previously collected flow-through

exhibited negligible effects and resulted in a 1.7-fold increase in bioluminescence. This result indicated that the factors were enriched on the column and did not pass through the filter. Hence, we falsified our working hypothesis, collecting evidence for secreted factors with molecular weights bigger than 30 kDa. The signal decrease observed in **Figure 3-14A** was probably due to a loss of the factor, caused by slightly leaking filter units.

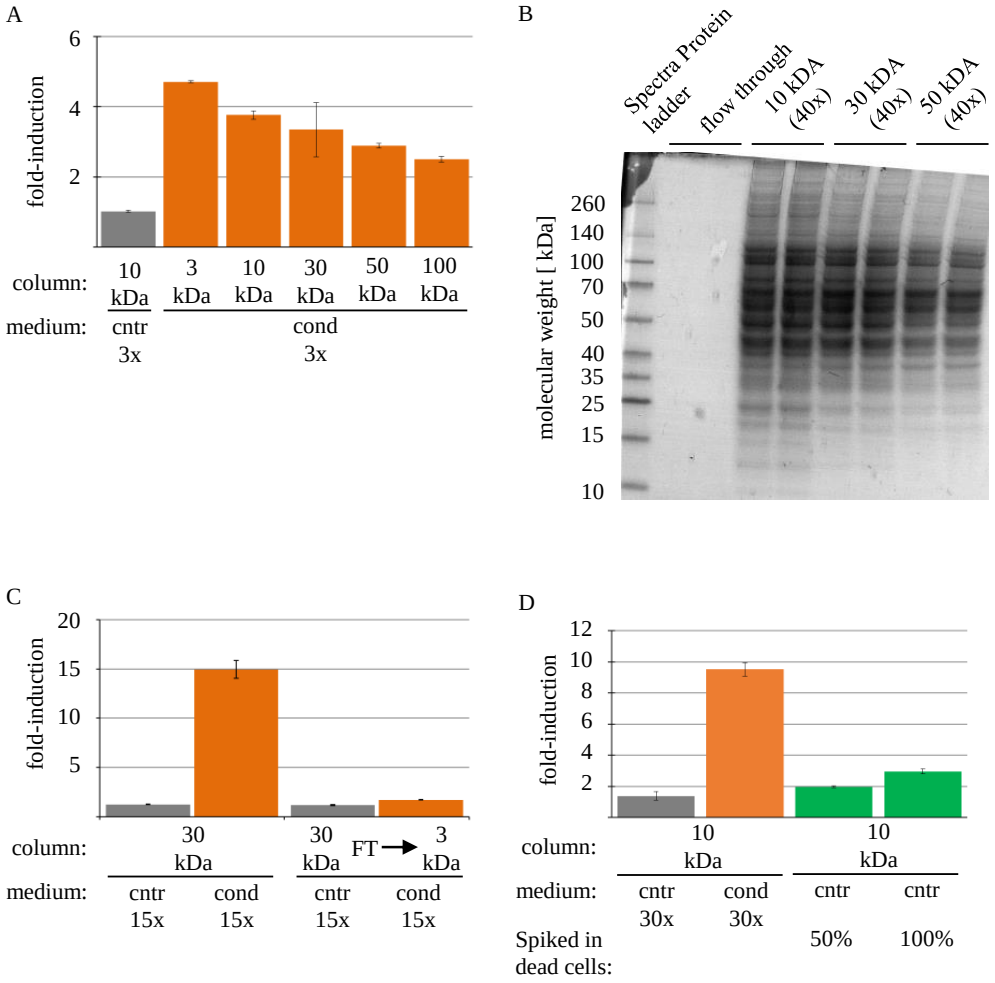

Figure 3-14: The CRE-signalling cascade activating factors were bigger than 30 kDa. U-2 OS wild-type cells were transduced with a 7xCRE_*luciferase* reporter construct. After 24 hours of bioluminescence recording, the reporter activity was minimal and the cell culture medium was exchanged to concentrated control or conditioned medium form U-2 OS wild-type cells. **A)** The harvested medium was concentrated on distinct size exclusion filters. Shown are the quantifications of the bioluminescence recordings as fold-inductions. **B)** The harvested conditioned medium was concentrated on distinct size exclusion filters, separated in an SDS-PAGE and then Coomassie stained. **C)** The harvested medium was concentrated on a 30 kDa exclusion filter. Meanwhile, the flow-through was collected and concentrated on a 3 kDa exclusion filter. Depicted are the quantifications of the bioluminescence recordings after stimulation as fold-inductions. **D)** Medium of dead U-2 OS wild-type cells cultured in PBS was spiked into control medium proportional to calculated dead cells in the conditioned medium and concentrated. Shown are the quantifications of the bioluminescence recordings as fold-inductions (representative experiments selected from n = 2-3 individual recordings with 3-5 biological replicates, mean ± SD).

One of our main concerns in this set of experiments was cell death during the conditioned medium production. We feared that cell death triggeres the degradation and disassembly of the outer cellular membrane, releasing the cytoplasm and its components into the cell culture medium. To test whether cytoplasmic components released upon cell death were responsible for the 7xCRE-driven *luciferase* expression, we supplemented control medium with cell culture medium from dead cells and monitored the bioluminescence of reporter cells after stimulation. In more detail, the preparation of the reporter cells and the production of the conditioned medium were carried out as described previously. Additionally, we counted dead cells in the cell culture medium during the conditioned medium production and extrapolated the total number of dead cells. Next, we detached a known number of U-2 OS wild-type cells from a cell culture flask, rinsed them twice with PBS and cultured them for 24 hours in serum-free PBS, known to prevent proper attachment and leading to cell death. A fraction of the "conditioned" PBS, matching 50% or 100% of the naturally occurring dead cells during conditioned medium production, was spiked into control medium, concentrated accordingly to the manual, and used to stimulate U-2 OS 7xCRE_*luciferas*e reporter cells. The effects on the bioluminescence signal were monitored.

The stimulation of U-2 OS 7xCRE_*luciferase* reporter cells with 30x concentrated conditioned medium resulted in a 9.5-fold induction of luciferase activity (see **Figure 3-14D**) and we counted less than one million dead cells per cell culture flask used for conditioned medium production. Therefore, we supplemented the control medium with a volume of PBS matching three million or six million dead cells as we used six cell culture flasks for conditioned medium production. The stimulation with this dead-cell-control-medium resulted in a 2.0- and 3.0-fold induction of luciferase activity, respectively. The results from our bioluminescence recordings suggested that only a small portion of the signal increase was caused by dead cells and their release of the cytoplasmic interior into the cell culture medium. Moreover, the result suggested the secretion of soluble factors from U-2 OS wild-type cells to account predominantly for the activation of CRE-mediated gene expression.

To conclude our findings, the size of the soluble secreted factor was estimated to be larger than 30 kDa. Since the size exclusion filter might unintentionally retain or leak the secreted factor a well-balanced enrichment protocol had to be established and executed. Furthermore, we collected evidence that secreted factors rather than unspecific

release of cytoplasmic proteins upon cell were responsible for 7xCRE-driven *luciferase* expression.

3.8 Circadian parameters were dependent on U-2 OS cell culture density

Under normal cell culture conditions, U-2 OS cells were exposed to a constitutively low secretion of the activating factor rather than a one-time high stimulation with the activating factor like in the previously described experiments. Therefore, we speculated that this factor might act in a paracrine fashion to sustain circadian rhythmicity as it obviously influenced circadian oscillations via the CRE-mediated transcriptional activation. This prediction was strengthened by our results from cells with decreased *TMED10* expression which were shown to suffer from a dispersed Golgi and, therefore, impaired vesicular protein transport. These cells showed severely reduced circadian amplitudes in the expression levels of multiple clock genes and drastically altered periods (see **Figure 3-5**). Furthermore, Welsh and colleagues reported that the strength of circadian rhythmicity as well as the observed circadian amplitude were highly dependent on the culture density in primary mouse fibroblasts, again, suggesting that paracrine signals from neighbouring cells might be beneficial to generate circadian rhythms[169,351]. To test our hypothesis that secreted factors acted as a paracrine signal, we aimed to decrease the signal's concentration in the cell culture medium through lowering the culture's density as David Welsh proposed. We expected a reduction in circadian rhythmicity and amplitude. Briefly, we seeded U-2 OS cells harbouring a *Per2*-promotor driven *luciferase* construct (see **Figure 3-15**) or U-2 OS cells harbouring a *Bmal1*-promotor driven *luciferase* construct (see **Supplemental Figure A 7**) in decreasing densities, ranging from 26.000 cells per cm^2 to 667 cells per cm^2. After synchronisation with dexamethasone the medium was exchanged to serum-free culture medium and the bioluminescence was recorded for six consecutive days. The data sets were fitted to sine waves, using the chronostar2.0 software, and the circadian parameters were assessed.

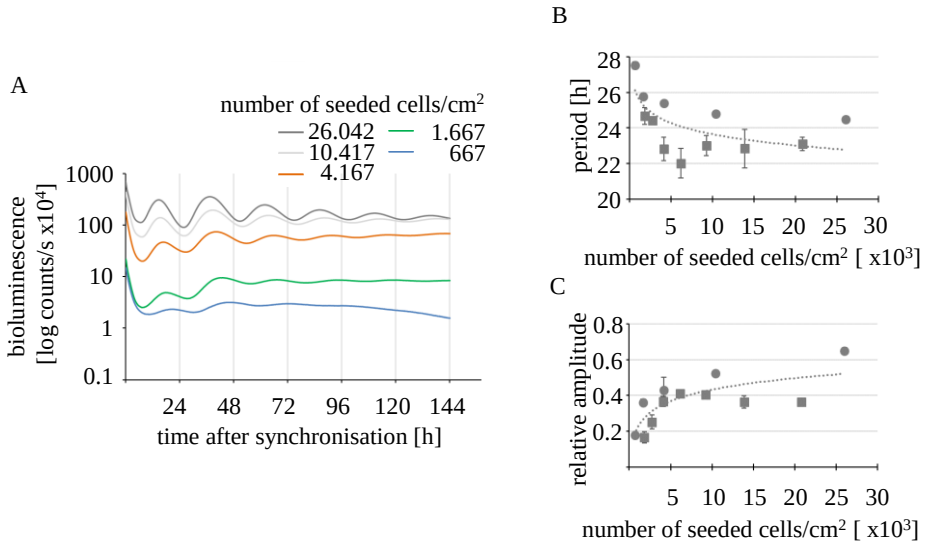

Figure 3-15: Circadian oscillations showed a longer period and a smaller amplitude with decreasing cell density. U-2 OS reporter cells harbouring a *Per2*-promotor driven *luciferase* construct were seeded in 9.6 cm^2 cell culture dishes in cell densities ranging from 26.042 down to 667 cells/cm^2, synchronized with dexamethasone, and bioluminescence was recorded for six days in serum free medium. Bioluminescence data were fitted to sine waves, using chronostar2.0, and the circadian parameters were assessed. **A)** Depicted are representative raw bioluminescence data. **B)** Shown are the calculated circadian periods [h] and **C)** the relative amplitudes (n = 2 individual recordings with 2 biological replicates, mean ± variance; the dotted line indicates the third-degree polynomial fit through the two data sets).

As expected, the detected bioluminescence counts per second reduced with decreasing numbers of U-2 OS reporter cells, nevertheless, the high-density as well as the low-density cells exhibited circadian rhythmicity over six days (see **Figure 3-15A**). The correlation coefficients of the sine waves fitted to the data set were all above 0.95 and did not statistically differ (data not shown). Interestingly, the data suggested a high correlation between cell culture density and the circadian parameters period and amplitude. The period lengthened from 23.1 hours up to 27.5 hours with decreasing cell numbers per cm^2. Additionally, the circadian amplitude decreased from 0.65 down to 0.17 in low-density cultures. This effect was observed in two independent experiments and was in accordance with our data (see **Figure 3-5**) and the effects described by Welsh and co-workers[169].

The obtained results partially supported our working hypothesis. Although we could not collect evidence for a reduced rhythmicity in low-density cultures, our results showed reduced circadian amplitudes and longer periods. Therefore, we concluded that lowering the cell density in cell cultures negatively affected the circadian oscillations likely due to a reduced concentration of beneficial paracrine signals. At that point, we

speculated that the paracrine signals helped to keep the cell culture in synchrony and, hence, sustained high-amplitude rhythms.

The reduced amplitude and longer periods were likely the result of a lower concentration of paracrine signals. To test if the lack of rhythmic or constitutive paracrine signals was indeed responsible for the effects, we supplemented the low-density cell culture of U-2 OS reporter cells with increasing numbers of non-bioluminescent U-2 OS feeder cells. Additionally, we examined the necessity of unimpaired vesicular protein transport by supplementing low-density cultures with non-bioluminescent non-silencing control cells or non-bioluminescent *TMED10* depleted cells. In more detail, U-2 OS reporter cells harbouring a *Per2*-promotor driven *luciferase* construct were co-cultured with increasing numbers of non-bioluminescent U-2 OS wild-type cells which were lentivirally transduced with either a non-silencing control or a shRNA targeting *TMED10*. After synchronization with dexamethasone, the bioluminescence was monitored over six consecutive days, the data set was fitted to sine waves, and the circadian parameters were assessed, using the chronostar2.0 software.

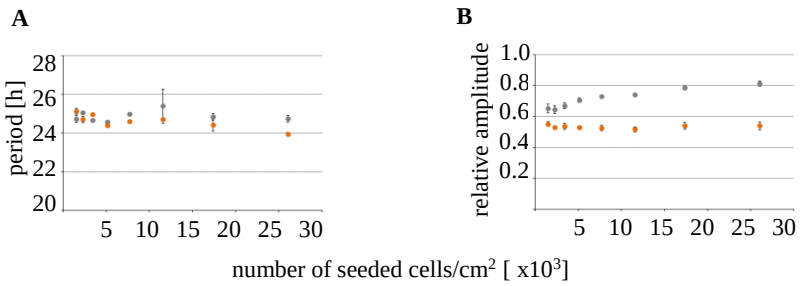

Figure 3-16: Non-bioluminescent human osteosarcoma cells with unimpaired vesicular protein transport rescued the reduced circadian amplitude of low-density cultures. 4.630 U-2 OS cells/cm^2 harbouring a *Bmal1*-promotor driven *luciferase* reporter construct were seeded in 9.6 cm^2 cell culture dishes with decreasing numbers of non-bioluminescent U-2 OS wild-type feeder cells that were either harbouring a non-silencing construct (grey) or a shRNA targeting *TMED10* (orange). Cells were synchronized with dexamethasone, bioluminescence was recorded for six days in serum free medium, and bioluminescence data were fitted to sine waves, using chronostar2.0. **A)** Shown are the calculated circadian periods [h] and **B)** relative amplitudes (representative experiment selected from n = 3 individual recordings with 2-6 biological replicates, mean ± SD; additional dataset, see **Supplemental Figure A 8**).

The co-cultivation of non-bioluminescent feeder cells with low-density U-2 OS reporter cells resulted in a robust circadian rhythmicity in all tested cultures, judged by the correlation coefficient of the sine fits (data not shown). The previously observed, lengthening of the circadian period in low-density reporter cell cultures was completely abolished (see **Figure 3-16**). Instead, the recorded cell cultures displayed normal periods

of approximately 24 hours with no distinction between the two supplemented feeder cell populations. Interestingly, the circadian amplitude of the recorded U-2 OS reporter cell rhythms increased continuously when co-cultured with non-bioluminescent control feeder cells (see **Figure 3-16B** and **Supplemental Figure A 9**). In the depicted experiment, the circadian amplitude improved from 0.65 to 0.81 with increment of overall cell density. In contrast, the amplitude of the recorded U2 OS reporter cells co-cultured with non-bioluminescent *TMED10* depleted feeder cells remained stable around 0.54 and did not improve.

To summarize, 4.630 bioluminescent U-2 OS reporter cells/cm^2 displayed a slightly longer period and a low-amplitude rhythm in the previous experiment (see **Figure 3-15B and C**). Therefore, we expected a shorter period and a higher amplitude in the samples supplemented with non-silencing feeder cells, compared to the feeder cells with decreased *TMED10* expression levels, if secreted paracrine signalling molecules were needed for the maintenance of robust circadian rhythm. The experimental results fulfilled our expectations, strengthening the hypothesis that paracrine factors are necessary for robust, high-amplitude circadian rhythms.

4 Discussion

The circadian clockwork is a hierarchical multi-oscillator network that regulates and influences almost every process in the mammalian organism and, therefore, has great implication in health and disease. Since the temporal and spatial organization of the circadian oscillator is of foremost importance, the scientific community still holds interest in gaining an even better understanding of the cellular and molecular mechanism of circadian rhythms, the transmission of input and output signal, and the maintenance of circadian rhythmicity in the SCN and in the periphery. In the past decade, genome-wide RNAi screens as well as small molecule screens have contributed greatly to the expanding picture of the core molecular clockwork with its intertwined transcriptional-translational feed-back loops, identifying dozens of important components and regulators. Advances in electrophysiology and imaging techniques have vastly expanded our knowledge about neuronal communication in the SCN and provided new insights into input and output pathways necessary for entrainment of the core oscillator and synchronisation of peripheral clocks. Especially the progress made in the identification of humoral and temperature-dependent transmission of time information from the brain to the periphery offers interesting future perspectives for pharmaceutical therapies against illnesses associated with shift work and jet lag. Fewer advances were made investigating the underlying mechanism for maintaining circadian rhythmicity in peripheral tissues. Living in our modern society, we are exposed to stochastic noise and non-reoccurring disturbances for the peripheral oscillator on a daily basis as we are more and more forced to live a life against our inner clock. For instance, the emerging concept of shift work leads to activity phases accompanied by core body temperature increase and food intake during our designated inactive phase which strongly influences the peripheral circadian clock and can desynchronise the peripheral from the SCN oscillators. As shown for the SCN neuronal network, coupling offers an interesting concept to slow down or even resist entrainment to conflicting signals. Although several studies reported substantial indication for existing coupling mechanism in peripheral organs and cell cultures, the general concept of coupling to achieve a stable period and phase coherence is still under debate. This thesis aims to shed some light on this topic and to provide further evidence for the existence of coupling mechanism that depend on the secretion of signalling

molecules by intracellular, vesicle-mediated transport mechanisms along the secretory pathway. To our knowledge, we are the first to demonstrate that anterograde transport from the ER to the Golgi and beyond, facilitated by COPII vesicles, is necessary for normal circadian oscillation *in vitro*. The shRNA-mediated knockdown experiments and the application of transport inhibitors, both targeting key steps along the secretory pathway, lead to strong period lengthening effects which are partly accompanied by a reduction in amplitude and higher damping. Strikingly, the observed circadian shRNA-mediated knockdown phenotype can be rescued by overexpressing mutated proteins that lack retrograde but not anterograde transport signals. Furthermore, the shRNA-mediated knockdowns directly induce rapid dispersion of the Golgi apparatus which alters and impairs the secretory pathway. We successfully excluded unfolded protein response and cell viability issues as the main cause for the observed circadian phenotypes, further strengthening our argument that anterograde vesicular protein transport is crucial for circadian dynamics.

To answer the question if the secretory pathway is important for the coupling mechanism in human cell cultures, we demonstrated that U-2 OS cells secrete soluble signalling molecules into the supernatant that are stable enough to be collected and enriched using size-exclusion columns. These as yet unidentified macromolecules directly impinge on the circadian oscillator when applied concentrated 30-fold or more by inducing phase shifts by up to five hours, at the same time leaving the circadian period unaltered. Attempts to identify the molecular nature of these factors in more detail revealed a molecular size bigger than 30 kDa and the release through either secretion along the secretory pathway or, to a minor degree, in the process of cell death. Furthermore, we gathered evidence suggesting the activation of signalling pathways by the secreted macromolecules, culminating in the binding of activating transcription factors to CRE-sites but not SRE-sites. The existence of secreted macromolecules that comprise synchronisation properties was proposed in the past especially in the context of communication between the SCN and peripheral tissues. Here, we are the first to present convincing data for a secreted paracrine-acting factor that directly affects the circadian oscillator through CRE-mediated transcriptional activation that is known to integrate circadian input signals, especially light, into the master clock - the SCN.

Finally, we present indications for a direct connection between cell culture density and the robustness of the circadian oscillator. Decreasing the density of cultured cells

results in longer periods, stronger damping and, consequently, in low amplitude oscillations, arguing for a reduction or loss of a beneficial synchronising factor.

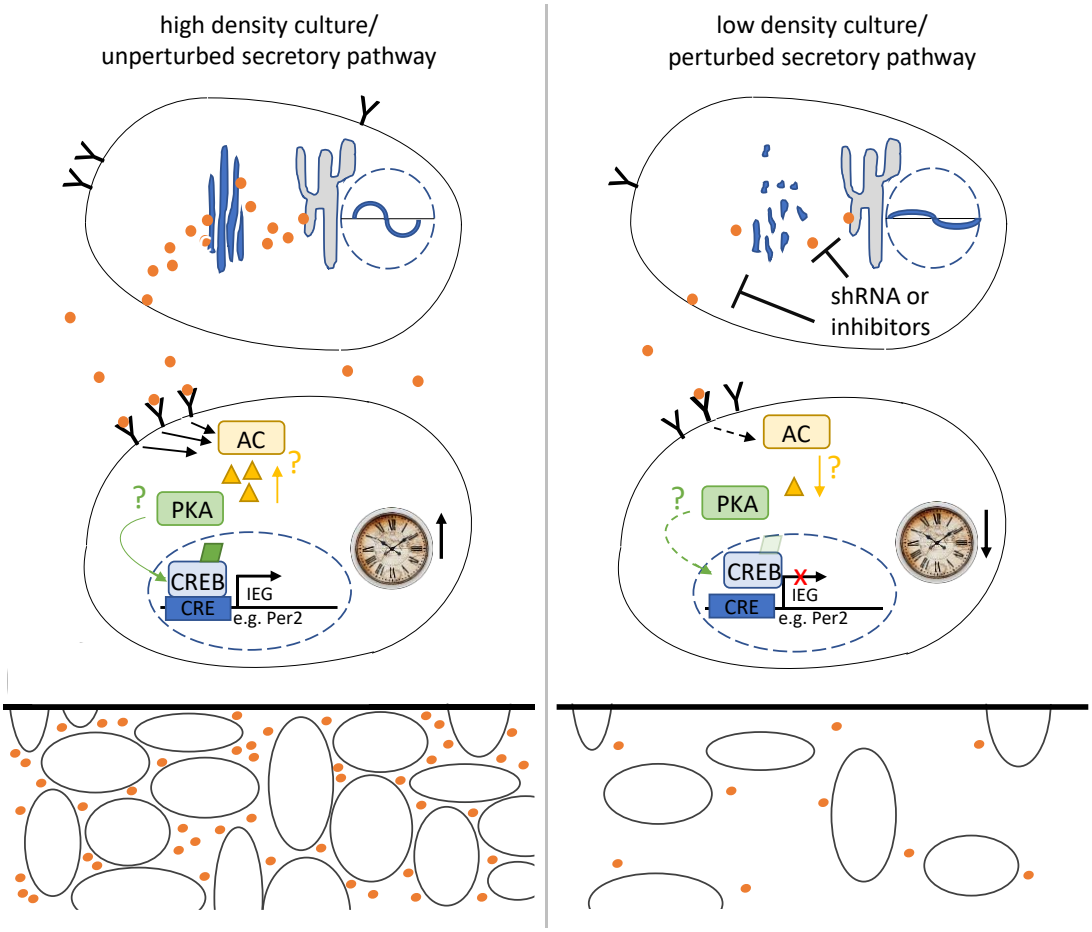

Figure 4-1: The secretory pathway and cell culture density influence circadian oscillations – a model. Left) U-2 OS cells with an unperturbed secretory pathway constantly or rhythmically secret a soluble, so far unidentified, paracrine acting molecule into the exterior of the cell whose concentration is directly dependent on cell culture density. Neighbouring cells as well as the secreting cell express signalling receptors at their plasma membrane which detect the paracrine factor and activate CRE-mediated transcription, presumably through activation of adenylate cyclase, increase of cAMP levels, stimulation of PKA, and ultimately the phosphorylation of activating transcription factors, e.g. CREB. CRE-mediated transcriptional activation leads to the expression of immediate early genes (IEG) like Per2. Bioluminescence rhythms of cultured U-2 OS cells exhibit 24-hour periods and high amplitude rhythms with progressive dampening over time. **Right)** U-2 OS cells with a genetically or pharmacologically perturbed secretory pathway exhibit a dispersed Golgi and decreased constant or rhythmic levels of secretion. Additionally, receptor levels at the cell surface are drastically reduced. Neighbouring cells as well as the secreting cell detect less or no secreted molecules and do not activate CRE-mediated transcription. Bioluminescence rhythms of the perturbed U-2 OS cells exhibit long circadian periods with lower amplitudes. In low density cultures, where the concentration of the secreted molecule is reduced due to the small number of cells, the bioluminescence rhythms of U-2 OS cells display long circadian periods and low amplitude rhythms with faster damping.

The circadian phenotype is rescued by supplementing the culture with non-bioluminescent wild-type U-2 OS cells, but not with non-bioluminescent U-2 OS feeder cells suffering from a genetically perturbed secretory pathway. These findings let us conclude that the secretory pathway is important for the secretion of a soluble synchronisation factor that promotes stable phase and period coherence.

To sum up and visualise our presented outcomes and their interpretations, we would like to propose a model to embed our findings into the existing view of the circadian clockwork and the idea of peripheral coupling (see **Figure 4-1**).

4.1 The secretory pathway and the circadian clock

In the last decades, our knowledge of circadian regulation and modification of physiology and metabolism in health and disease expanded rapidly through ambitious and laborious genome-wide screening projects and candidate driven studies[332,333,353,354]. In addition, forward and reverse genetic approaches led to the identification of key clock components that assemble into the interlocked transcriptional-translation feedback loops as we know them today (see **1.2.1**). On the other hand, the mechanism regulating the circadian on the hierarchical levels in the multi-oscillator network is only poorly understood. In our lab, Maier et al. used shRNA constructs to knockdown transcript levels of every known gene in human U-2 OS cells to identify potential circadian clock modulators[332]. Within this study, a group of genes associated with the Golgi apparatus and vesicular transport emerged which elicits drastic effects from the circadian oscillator (Bert Maier, unpublished data, personal communication). So far, the secretory pathway has not been implicated in the modulation of the circadian oscillator and, therefore, represents an interesting new level of circadian clock regulation. Furthermore, several studies investigating the concept of peripheral coupling speculated about the existence of a secreted paracrine factor that was important for stable phase and period coherences inside of primary cell cultures[169,170,351]. Along that line, the secretory pathway might play a significant role for coupling processes in the periphery. Consequently, we raised the question whether the secretory pathway is important for the maintenance of normal circadian oscillations. And if the secretory pathway turns out to be critical for cellular

circadian rhythmicity, to what degree do cell vitality and stress pathways like unfolded protein response contribute to the circadian phenotype upon perturbation?

4.1.1 The genetic perturbation of the COPI- and COPII-mediated vesicular transport and the implications for the circadian clockwork of U-2 OS cells as a model for peripheral tissues

Genetic perturbation of the early secretory pathway lengthens the circadian period

Using different shRNA constructs targeting *TMED10*, *TMED2*, *GBF1*, and *SEC13* key components of the COPI- and COPII-mediated vesicle transport pathway, while monitoring the bioluminescence rhythms of U-2 OS reporter cell, enabled us to characterise the impact of genetic perturbation of the secretory pathway on the circadian oscillator.

Our data reveals that the shRNA-mediated knockdowns of *TMED10*, *TMED2*, *GBF1*, and *SEC13* transcript levels significantly alter the parameters of circadian bioluminescence rhythms (see **Figure 3-1**). The most apparent effect is the period lengthening upon reduction of transcript levels by 1.5 ± 0.3 up to 5.0 ± 0.3 hours. These findings concur with the results from Zhang et al. reporting siRNA-mediated knockdown of *SEC13* transcript levels to result in dose-dependent period lengthening accompanied by a reduction in amplitude and higher damping of the recorded bioluminescence rhythms[333]. The effects of reduced *TMED10*, *TMED2* and *GBF1* transcript levels on the circadian clock have not been investigated before. But since our analysis of bioluminescence recordings show very similar effects for different knockdown constructs decreasing *TMED10*, *TMED2* and *GBF1* expression in several individual experiments, we feel that we carefully controlled for specificity and accuracy of the provided results. The conducted rescue experiments including *TMED10* and *TMED2* that exhibit normal circadian oscillations after substitution of the knocked-down transcripts by ectopic overexpression further preclude off-target effects of the shRNA constructs (see **Figure 3-2**). Unfortunately, we were unable to generate a *GBF1* or a *SEC13* overexpression construct without point mutations in important domains to perform rescue experiments for these two genes as well. A probable cause for the difficulties in generating these

overexpression constructs lies in their transcript length of 5569 and 1106 base pairs, compared to 659 base pairs for *TMED10* and 605 base pairs for *TMED2.*

Furthermore, the expression profiles of seven clock genes confirm the period lengthening effect upon *TMED10* knockdown independent of bioluminescence recordings (see **Figure 3-5**). Along this line, the shRNA-mediated knockdown of *TMED10* transcript levels results in the reduction of *REV-ERBα* and *DBP* transcript levels, an induction in *CRY1* transcript levels and in unchanged transcript levels of *CLOCK* and *PER2* which has been reported previously for the siRNA-mediated knockdown of *SEC13* transcript levels[333]. The authors speculate that the observed period lengthening effect and the accompanied changes in clock gene expression are a network effect rather than results of a direct interaction between SEC13 and a clock gene. We offer a different explanation, linking the circadian phenotype to the perturbation of the secretory pathway. Possible explanations for the obvious discrepancies between their results and ours regarding the *BMAL1* and *PER1* expression are the different knockdowns of genes associated with vesicular transport as well as the comparison of steady-state transcript levels versus transcript levels during a 36-hour time-series. However, it is feasible that interference with one of the COPII and COPI vesicular transport pathways directly affects the other due to their interdependent character[341]. Hence, similar effects on the circadian bioluminescence rhythms as well as the transcript levels of clock genes upon COPI or COPII disruption are expected.

Depletion of genes associated with vesicular transport causes dispersion of the Golgi apparatus

TMED10 and *SEC13* are described to fulfil functions in the mammalian cell despite their involvement in the secretory pathway. Several studies show *Tmed10* to play a role in the transport of the amyloid-β precursor protein (APP) in Alzheimer's disease, in the assembly of the presenilin γ-/ε- secretase complex, and in the modulation of autophagy[355–357]. None of these processes have been implicated to directly influence circadian dynamics so far. SEC13 interacts with NUP85 to form a part of the fence-like coat of the nuclear pore complex (NPC) involved in the protein transport across the nuclear envelope[358]. In contrast to TMED10, SEC13 and additional proteins forming the nuclear pore complex (NPC) were indeed previously identified in a shRNA screen

looking for clock modulating genes that were involved in nucleo-cytoplasmic translocation. At that time, the reduction of *SEC13* mRNA level showed a similar period lengthening phenotype (Sandra Korge, unpublished data, personal communication). Consequently, these findings raise the question if the observed *SEC13* phenotype in the present study is due to an impaired secretory pathway. Our results investigating the integrity of the Golgi apparatus upon shRNA-mediated knockdown *TMED10*, *TMED2*, *GBF1*, and *SEC13* transcript levels clearly indicate harmful effects on Golgi morphology and, therefore, disturbance of the secretory pathway (see **Figure 3-4** and **Supplemental Figure A 3**). These findings point to a direct link between the secretory pathway and the circadian phenotype. In more detail, reduction of transcript level leads to a dispersed Golgi in 60%, 67%, 69% and 44% of all analysed cells, respectively. These findings are overall in line with previously published results. Ong et al. report that the siRNA-mediated knockdown of *SEC13* transcript levels results in the dispersal of the Golgi in 25% of all HeLa cells[336]. Because siRNA-mediated knockdowns are often not as potent and long-lasting as shRNA-mediated knockdowns it is possible that the knockdown effects start to wear off after 72 hours, and that they might therefore underestimate the observed effects. An indication of the accomplished knockdown efficiency at the point of fluorescence microscopy would help to assess their work. Additionally, the rather small number of analysed cells (n = 15) raises concern that they draw conclusions from a non-representatively sized group. Other laboratories contradict our findings by reporting no dispersion of the Golgi upon reduction of *SEC13/Sec13* transcript levels in HeLa cells and primary lung fibroblasts[359,360]. Townley et al. used siRNA to deplete *SEC13* from HeLa cells and shows almost no detectable SEC13 protein in Western Blot analysis after 72 hours. Yet, they state that the Golgi only looks more densely packed but does not disperse. Examining the published immuno-fluorescence pictures there are “frazzled”-looking Golgi stacks detectable which might hint towards following Golgi dispersal. Moreira et al. generate a *Sec13*$^{H/-}$ mouse that expresses a low level of *Sec13*. In primary lung fibroblasts, the *Sec13* expression level is reduced to approximately 30% and no change in Golgi morphology is detectable. Since the level of transcript and the observed phenotype are often tightly linked in RNAi experiments, we speculate that the remaining *Sec13* transcript is sufficient to maintain the COPII-mediated vesicular transport. Two independent studies from Manolea et al. and Hansen et al. support our findings of Golgi dispersion upon *GBF1* depletion[337,338]. The former shows shRNA-mediated knockdown of *GBF1* transcript level under 10% and accompanied redistribution of cis-, medial-and

trans-Golgi marker proteins speaking for a Golgi collapse. The latter reports siRNA-mediated reduction of the *GBF1* expression down to 20% and an increased fragmentation of the Golgi apparatus. Furthermore, pharmacological inhibitors blocking the action of GBF1 at the Golgi membrane cause rapid dispersion of Golgi marker proteins, too, and provide evidence that the transport of membrane bound and secreted proteins is arrested upon GBF1 inhibition[361–363]. Luo et al. confirm Golgi dispersion upon *TMED2* depletion[339]. Using siRNA in HEK293 cells they reduce *TMED2* transcript levels to 40% of control cells and show that this reduction is sufficient to induce Golgi fragmentation. Apparently, we are the first to quantify the effect of *TMED10* depletion on Golgi morphology in terms of fragmentation or dispersion. Nevertheless, it is well known that *TMED10* expression is tightly regulated, as ectopic overexpression or complete knockouts severely compromise Golgi integrity and decrease overall cellular vitality during development[364–367]. In COS1 cells and in HeLa cells the overexpression of *TMED10* results in loss of co-expression with TMED2 and cis-Golgi marker ERGIC-53 and in apparent fragmentation of the cis-Golgi[364,367]. In primary neurons from the brainstem, but not the cortex or cerebellum, ectopic overexpression of *Tmed10* leads to altered Golgi morphology accompanied by severe fragmentation[366]. In liver and kidney cells from *Tmed10* heterozygous mice the Golgi saccules are flat and dilated, especially at the rims, and the number of vacuoles is significantly increased[365]. Since the overexpression of *Tmed10* leads to such severe effects on Golgi integrity it is plausible that the decrease of *TMED10* transcript levels leads to similar effects. Furthermore, homozygous *Tmed10*$^{-/-}$ suffer from severe developmental defects and die at early embryonic stages[365]. However, it should be mentioned that the deletion of all known p24 family members in *Saccharomyces cerevisiae* has little effect on the secretory pathway and does not change Golgi morphology[368]. Then again, UPR is activated in p24 family knockout yeast cells, indicating the induction of coping mechanisms to counter act the effects on the secretory pathway. Based on our results and the published literature, we conclude three things. First, the knockdown of *TMED10*, *TMED2*, *GBF1*, and *SEC13* transcript levels drastically impacts the circadian clock, most likely by inducing Golgi fragmentation and destabilising Golgi integrity, thereby slowing down or even arresting the secretory pathway. Second, the impact on Golgi morphology is highly dependent on the efficiency of transcript reduction and the cell line or tissue. Finally, members of the p24 family are dispensable in yeast cells but not in higher eukaryotes, and their depletion might lead to the activation of cellular stress pathways.

ARF1 *mutants are not suitable to discriminate which direction of vesicular protein transport is important for the circadian oscillator*

Since the early secretory pathway consists of the two interdependent COPI- and COPII-mediated vesicular transport machineries that facilitate antero- and retrograde protein transport we aimed to investigate which one is important for the circadian oscillator. Our study outcomes indicate that the use of *ARF1 T31N*, *ARF1 Q71L* and *ARF1 NΔ17* overexpression plasmids (see **Figure 3-8**) in U-2 OS reporter cells lead to rapid cell death between 48 and 72 hours which do not allow the long-time recording of bioluminescence oscillations. Given the knowledge on *Arf1* gained from the literature our results are consistent with the findings of previous studies[343,344,369]. ARF1 is a key molecule in the COPI biogenesis as it is directed to Golgi membrane by TMED10/TMED2 heterodimers, inserts its myristoylated amphipathic N-terminal helix into the Golgi membrane upon GDP to GTP exchange, deforms Golgi membranes and recruits the COPI protein coat (see **1.3.4** for more details). The dominant negative ARF1 T31N variant shows high affinity to GDP, sequesters the ARF1-GEF GBF1, does not insert the myristoylated amphipathic N-terminal helix into the Golgi membrane and, therefore, does not recruit COPI proteins. The ARF1 NΔ17 variant lacks the myristoylated amphipathic N-terminal helix and cannot be recruited and tethered to the Golgi membrane. Both mutants lead to COPI-mediated vesicle transport arrest by competing with wild-type ARF for effector proteins such as the guanine nucleotide exchange factor, which causes depletion of important receptors and co-factors needed for COPII vesicle biogenesis at the ER membrane and, eventually, the collapse of the Golgi into the ER[343,344,369]. Ultimately, the cell dies of this genetic perturbation, as GTP binding and an intact N-terminus are obviously required for the binding of ARF1 to the Golgi membrane and an unimpaired COPI vesicle transport. The ARF1 Q71L variant is known to possess a reduced intrinsic GTP hydrolytic activity, which leads to a constitutively active ARF1 at the Golgi membrane[343,344]. Thus, ARF1 Q71L is recruited to the Golgi membrane and binds the coatomer protein complex comparable to wild-type ARF1, covering the membrane with numerous coated vesicles. Since the intrinsic GTP hydrolytic activity is impaired, vesicle uncoating after the budding event is slowed down or arrested. Additionally, the increased number of budding vesicles blocks COPII tethering and fusion events. In the end, this leads to an impaired COPII and COPI vesicle-mediated transport that causes cell vitality issues and, over time, cell death. Accordingly,

the application of dominant-negative ARF1 mutants proved unsuitable to answer our initial question due to rapid cell death in the first 72 hours.

TMED10 *mutants reveal the importance of anterograde vesicular protein transport for the circadian oscillator*

Our second approach to discriminate whether the anterograde or the retrograde vesicular protein transport is important for the circadian oscillator involved the ectopic overexpression of either wild-type *TMED10* or *TMED10* mutants lacking important trafficking motifs in rescue experiments (see **Figure 3-9**). Both wild-type *TMED10* and *TMED10* carrying a mutated dilysine motif reported to function in the retrograde protein transport consistently restored normal circadian periods when overexpressed in a *TMED10* depletion background (see **Figure 3-10**). In contrast, overexpression plasmid of *TMED10* carrying a mutated diphenylalanine motif believed to function predominantly in the anterograde protein transport and *TMED10* lacking the luminal domain involved in protein-protein interaction failed to rescue the circadian phenotype when overexpressed in a *TMED10* depletion background. In more detail, the observed circadian period upon TMED10 transcript level knockdown in this was not restored to 24 hours but showed the lengthening by up to 3.4 ± 0.9 hours. Previous studies on TMED10's sorting signals all agree that the dilysine motif (in mammals -RRFFKA**KK**LIE) is directly involved in COPI binding and its interactions with the heterotetrameric B-subcomplex consisting of α-, β'- and ε-COP is well established today[214,239,253,261,345,346]. Interestingly, TMED10's dilysine motif does not only interact with COPI subunits in mammals but also in other eukaryotes, for instance in plants[370,371]. The binding of the COPI B-subcomplex by the dilysine motif of other mammalian p24 family members like TMED9 and TMED11 grant further credibility in these findings[253]. Therefore we speculate that the exchange of the conserved dilysine motif to a diserine motif destabilises the interaction between TMED10 and the COPI coat, which is supported by the work of Dominguez and co-workers[214]. It has to be noted though that there is evidence that the diphenylalanine motif might bind to the COPI heteroquatrameric F-subcomplex in the presence or absence of the dilysine motif[261–263]. Other studies oppose these findings, showing no binding of the F-subcomplex through the diphenylalanine motif, or only negligible amounts that probably represent cross-contaminations[214,239]. Possible explanations for the contradicting findings are the results'

high dependencies on the sample preparation and the co-immunoprecipitation conditions. Since both the wild-type *TMED10* and the *TMED10* carrying a mutated dilysine motif are able to restore 24-hour periods when expressed in the *TMED10* depletion background, we conclude that the dilysine motif-mediated interaction between TMED10 and COPI molecules in the retrograde vesicular protein transport is not mandatory for normal circadian function. The prevalent opinion in the literature still settles on the dilysine motif as the prominent retrieval signal in the COPI-mediated vesicle transport. Hence, we speculate that it is predominantly the anterograde protein transport that is necessary for normal circadian oscillations. This speculation is supported by the results from the rescue experiments using *TMED10* carrying a mutated diphenylalanine motif believed to function predominantly in the anterograde protein transport, which failed to restore circadian oscillations with a 24-hour period. Several studies agree that the diphenylalanine motif is involved in the binding COPII vesicle components and has important roles in vesicle biogenesis[214,218,263]. Dominguez et al. showed that the exchange of the diphenylalanine motif to a diarginine motif completely abolishes SEC23 interaction and leads to a redistribution of TMED10 and TMED2 (probably as a heterodimer) to the ER[214]. Belden and Barlowe showed not only an interaction between TMED10 and SEC23 but also a binding to SEC24, SAR1 and SEC13/SEC31-complexes. Consequently, they propose a regulatory role in COPII vesicle biogenesis[263]. TMED10's luminal domain contains the GOLD domain which is implicated to mediate protein-protein interactions that stabilize TMED10 as well as its interaction partner, particularly other p24 family members[372–374]. Overexpression of *TMED10* missing the luminal domain strongly destabilises other p24 family members and impairs their normal function in the transport machinery. Furthermore, Blum et al. report that the luminal domain retains the TMED10 protein in the early secretory pathway, probably due to its interaction with other p24 family members. Missing the luminal domain renders the protein unstable and promotes the transport of residual TMED10 proteins to the plasma membrane[347]. Hence, it is not surprising that the *TMED10* mutant lacking the luminal domain fails to rescue the *TMED10* depletion phenotype. Although the exact contribution of TMED10's individual transport signals in the COPI and COPII vesicle machinery has not been finally sorted, we are quite confident that unimpaired anterograde protein transport and a stable TMED10 protein with an intact luminal domain are necessary for an unperturbed circadian oscillator. To investigate the success of the different rescue approaches it seems

required to further analyse the integrity of the secretory pathway and the vesicular transport dynamics. A first step could be the examination of the Golgi morphology.

To summarize, our results from the genetic perturbation experiments exhibit three major findings that are largely in line with the literature and were therefore incorporated into our model (see **Figure 4-1**, upper cells):

1. An unperturbed COPI and COPII vesicle transport machinery is necessary for normal circadian functions. The reduction of transcript levels of *TMED10*, *TMED2*, *GBF1*, and *SEC13* leads to drastic period lengthening effects.
2. *TMED10*, *TMED2*, *GBF1*, and *SEC13* contribute to the integrity of the Golgi apparatus. Depletion of the transcripts of these four genes results in altered Golgi morphology and redistribution of Golgi markers.
3. The anterograde protein transport is the more likely transport route to be important for circadian dynamics based on our rescue experiments.

Taken together, these findings implicate a new cellular pathway involved in modulating the circadian oscillator. Since the secretory pathway is crucial for organelle organisation, the distribution of signalling molecules and the transport of secretory cargo, various levels of clock regulation are possible.

4.1.2 The pharmacological perturbation of the secretory pathway and the implications for the circadian clockwork of U-2 OS cells as a model for peripheral tissues.

Pharmacological interference with the secretory pathway confirms the importance of the early secretory pathway for circadian rhythmicity

In our pharmacological perturbation experiments, we used 18 out of 27 pharmacological compounds that are reported to inhibit endocytosis and exocytosis to strengthen our previous findings and search for additional steps along the secretory pathway that are important for the circadian oscillator[340]. The nine inhibitors that were precluded from our study were either not commercially available or too expensive in manufacturing. Out of the 18 compounds tested, three are shown to interfere with the

translocation of the nascent protein chain into the ER lumen or the vesicle budding event at ER exit sites; six are implicated in inhibiting either ARF1, GBF1, or other guanine nucleotide exchange factors of ARF1, or are speculated to prevent GTP hydrolysis after COPI vesicle budding; four are said to block clathrin dependent or independent endocytosis at the plasma membrane; and five exhibit effects on various transport routes between the TGN, endosomes and lysosomes[361,362,375–389]. In addition, we included five inhibitors that are reported to interfere with different steps along the N-linked glycosylation process[390–394]. N-linked glycosylation is implicated to play a role in proper protein folding and quality control mechanisms in the ER[395,396]. The 22 different compounds were tested at concentrations of 50 µM and 5 µM (see **Figure 3-6**). The use at non-toxic concentrations that leads to half-maximal inhibition for each compound would have been preferable. Unfortunately, the IC50 concentration for U-2 OS cells is unknown for most, if not all, inhibitors. Especially their optimal, non-toxic concentration for the use in long-term bioluminescence recordings over several days has never been studied before. Furthermore, pilot studies using two inhibitors showed that the published IC50 concentrations are different between different cell types and culture conditions (data not shown). Taking all of this into account, we decided to use rather high compound concentrations to accomplish complete target inhibition and deal with possible cell vitality issues as well as the determination of the ideal inhibitory concentration in subsequent studies. At this point, we cannot rule out that we missed effects that require compound concentrations higher than 50 µM to inhibit transport steps along the secretory pathway.

The outcomes of our pharmacological perturbation study indicate that predominantly interference with early stages of the secretory pathway leads to altered circadian oscillations, which is in line with the findings from our genetic perturbation experiments. Interestingly, six out of nine inhibitors that showed an effect on circadian oscillations interfere with the COPI or COPII vesicle pathway. Additionally, we identified Pitstop II, which blocks endocytosis and exocytosis at the plasma membrane, and tunicamycin, which inhibits initial steps of N-glycosylation and is reported to arrest the cell cycle and induce UPR to be harmful for normal circadian oscillations. Brefeldin A was previously identified to lengthen the circadian period by approximately nine hours when applied to primary mouse fibroblasts[397]. Nevertheless, the outcomes from Shende et al. should be handled with caution since they used a concentration eight times higher than we used on U-2 OS cells, which will most likely comprise cell vitality in long-term

bioluminescence recordings. The remaining compounds had not been tested for their ability to influence the circadian oscillator so far. Surprisingly, Dynasore, a potent inhibitor of dynamin which is known to be important for the circadian clock in *Drosophila melanogaster* as well as in murine SCN slices and primary fibroblasts, failed to perturb the oscillator in U-2 OS cells[397–399]. The concentration used on the SCN slices was 80 µM and the concentration used on the fibroblasts was 40 µM compared to our 50 µM on U-2 OS cells. We can only speculate that the differences between organ slices versus cell culture and primary cell culture versus immortalised cell are accountable for the deviating results. Testing Dynasore at an even higher concentration on U-2 OS cell might be necessary to accomplish stronger inhibition and detect a circadian phenotype. Nevertheless, dynamins' reported importance for the circadian oscillator and the identification of Pitstop II make endocytosis and exocytosis a crucial step for normal clock function. To which extent endocytosis and exocytosis events contribute to normal clock function requires further investigation. To our surprise, tunicamycin is the only compound that targets the N-glycosylation machinery to affect the circadian oscillator. Since N-glycosylation and the proper remodelling of the glycan-tree along the secretory pathway are essential quality control mechanisms for protein folding and vesicle packing, we expected severe transport issues upon perturbation leading to altered circadian oscillations. Our predictions are neither supported by our data on cell vitality nor by our data on changes of the circadian oscillator. This is in contrast to the results described by Hammond et al. that at least castanospermine and deoxynojirimycin, which inhibit glucosidases I and II, prevent the association with ER chaperons[396]. The concentrations used in their work exceeded ours by a factor of 20, which might explain the divergent results.

Inhibitors of the early secretory pathway lengthen the circadian period without compromising cell vitality

Since all compounds elicit similar period lengthening effects with decreased cell vitality at high concentrations, we were concerned about their specificity. Firstly, we excluded inhibitors that are known to alter other cellular processes than the vesical-mediated transport. For instance, tunicamycin locks dividing cells in the G1 phase and upregulates UPR[400,401]. Both the cell cycle and UPR are described to influence the

circadian clock by the regulation of *PER* and *CRY* transcript levels[402–404]. Therefore, it would be impossible to reveal the contribution of secretory pathway inhibition on clock modulation. Secondly, we titrated down three pharmacological inhibitors, Brefeldin A, Exo I and Golgicide A, to non-toxic concentrations and still observed drastic effects on the circadian period (see **Figure 3-6**). The half-maximal dosages for the effect on the circadian oscillator without cell vitality issues are approximately 32 nM for Brefeldin A, 16.5 µM for Exo I and 1.05 µM for Golgicide A. Thereby, they are all lower than the published IC50 value for the inhibition of transport events, which are reported to be between 360 nM and 72 nM for Brefeldin A, 20 µM for Exo I and 3.3 µM for Golgicide A[362,379]. While the published IC50 values were obtained using different cells and culture conditions, our findings suggest, nevertheless, that the effect on the circadian oscillator is apparent even before the protein transport is completely blocked, which speaks for a sensitive mechanism of clock regulation. In contrast, AG1478 and Pitstop II at non-toxic concentrations did no longer lead to a longer period. Especially for AG1478, which inhibits GBF1 by blocking the Sec7 domain, this loss of circadian phenotype is unexpected[361]. The inhibitory action of AG1478 mimics *GBF1* depletion, which we showed earlier to lengthen the period. It is possible that the application of high concentrations of AG1478 and Pitstop II in U-2 OS cell cultures completely inhibits GBF1 and exocytosis/endocytosis, respectively, which leads to impaired cell vitality and cell death. In contrast, at low concentrations AG1478 and Pitstop II fail to interfere with these processes effectively, losing the circadian phenotype. This needs to be investigated properly in follow-up studies. In conclusion, our data suggests that AG1478 and Pitstop II are not applicable to study the effect on the circadian oscillator in long-term bioluminescence recordings.

The combination of genetic and pharmacological perturbation suggests the inhibition of the same process

The combined applications of genetic and pharmacological perturbation were used to investigate whether both, compound and shRNA, act on the same target. We selected the reduction of *TMED10* transcript level for this study for two reasons. First, decrease in *TMED10* expression resulted in the most period lengthening in oscillating cells. Second, *TMED10* is equally implicated in COPI and COPII vesicle biogenesis and

potentially affects anterograde and retrograde transport. For the full picture, further experiments with *TMED2*, *GBF1* and *SEC13* in combination with the application of transport inhibiting drugs need to be carried out. Especially follow-up studies with *SEC13* and *GBF1*, which are either connected to the COPI or COPII vesicle biogenesis, might be interesting to address the question which transport route is important for the circadian oscillator. For our genetic and pharmacological interaction experiment, we hypothesised two possible outcomes:

1. Both, depletion of *TMED10* and the application of Brefeldin A, Exo I or Golgicide A, inhibit the same process in the early secretory pathway. Since the reduction of *TMED10* transcript levels alone already shows morphological changes of the Golgi, an impaired vesicular protein transport and a period lengthening effect, administration of pharmacological drugs does not inhibit the process any further. Possibly, the decrease in *TMED10* expression might inhibit the process only partially which sensitizes the cells, leading to period lengthening effects at lower drug dosages. However, the drug does not prolong the circadian period above an upper limit set by the maximal inhibition of either the shRNA-mediated knockdown or the compound and, hence, we detect no additive effects on the circadian oscillator.
2. Decreased *TMED10* expression level and the application of Brefeldin A, Exo I or Golgicide A inhibit different cellular processes or different stages of the early secretory pathway. The reduction of *TMED10* transcript levels leads to the above-mentioned impairments of the early vesicular protein transport or potentially interferes with an additional cellular process, resulting in an altered circadian oscillator. The administration of pharmacological compounds that act on the secretory pathway between ER and Golgi block secretion and modulate the circadian clock on their part. As a result, we detect two period lengthening effects that add up to a combined circadian phenotype.

Application of Brefeldin A on U-2 OS cell that are depleted of *TMED10* does not further lengthen the circadian period (see **Figure 3-7A** and **Supplemental Figure A 5A**). Hence, our results support the idea that Brefeldin A and shRNA-mediated knockdown of *TMED10* transcript levels interfere with the same process, presumably the early secretory

pathway. Brefeldin A is known to block GBF1-mediated activation of ARF1 at the Golgi membrane and induce tabulation of the Golgi leading to a complete collapse of the compartment into the ER[405,406]. TMED10 initiates COPI vesicle biogenesis and, upon *TMED10* depletion, altered Golgi morphology culminating in Golgi dispersal occurs. Both effects seem to complement each other, which may explain the non-additive circadian phenotype. Supplementing the cell culture medium of *TMED10* depleted U-2 OS cells with Golgicide A resulted in slightly divergent results (see **Figure 3-7C** and **Supplemental Figure A 5C**). While the period did not change at all after application of the drug in one experiment, the period lengthened dose-dependently in another. Yet, in both experiments the joint circadian phenotype of genetic and pharmacological perturbation resulted in the same circadian phenotype as seen upon administration of Golgicide A on control U-2 OS cells. Therefore, we hypothesise that in the second experiment the inhibition by TMED10 is incomplete and Golgicide A blocks the residual activity. We believe that Golgicide A interferes with an TMED10-associated process, leading to non-additive circadian period effects. Golgicide A inhibits GDP to GTP exchange in ARF1 molecules, blocking the initial step in vesicle biogenesis and induces Golgi tabulation[362]. As both compounds, Brefeldin A and Golgicide A, inhibit the same step in the COPI biogenesis, it is not surprising to obtain almost identical results further strengthening the hypothesis that the altered circadian oscillations are due to an impaired vesicular protein transport. Administration of Exo I on *TMED10* depleted U-2 OS led to additive, dose-dependent period lengthening in two individual experiments (see **Figure 3-7B** and **Supplemental Figure A 5B**). In the first experiment, Exo I was not applied in sufficient concentrations to hit saturation level onto control cells so the dose-dependent period lengthening did not reach the plateau phase. Therefore, we can only speculate whether reduction in *TMED10* transcript levels caused incomplete inhibition of the target process, allowing Exo I to block the residual activity. In this case, the results would argue for a non-additive inhibition through genetic and pharmacological perturbation. In the second experiment, the inhibitor was applied in the same concentrations but did hit the saturation level this time. Yet, the depletion of *TMED10* lengthened the period even further, indicating additive circadian effects. Interestingly, the use of Exo I on *TMED10* depleted cells causes lengthening of the circadian effect at low inhibitor concentrations that show no effect on control cells. This leads us to speculate that reduction in *TMED10* expression may sensitise the cells for the inhibition through Exo I. Our results clearly indicate that Exo I impinges on the circadian clock independent of TMED10s' role in the

secretory pathway. Feng et al. report that Exo I acts by a different mechanism from Brefeldin A and does not block ARF1 specific GEFs[379]. However, the dissociation of ARF1 from the membrane is still observed, and in higher concentrations even cis-Golgi dispersal. Feng et al. speculate that Exo I either accelerates the GTP hydrolysis rate of ARF1s bound GTP or that it stimulates ARFGAP activity. This would go along with our interpretation that the reduction of *TMED10* transcript levels sensitise the cells. Lower vesicle numbers are formed on the membrane due to missing TMED10 proteins, then the biogenesis of forming vesicles is disturbed by accelerated GTP hydrolyses caused by Exo I. In both cases, COPI vesicle biogenesis is slowed down and impaired. Additional off-target effects of Exo I on other cellular processes important for the clock are conceivable and need further careful investigation.

Taken together, the results from our pharmacological perturbation experiments neither contradict the little that is known from literature nor our previous findings from the genetic perturbation experiments and lead to the following conclusions:

1. The application of small molecules targeting vesicular protein transport or the initial step of N-linked glycosylation results in severe lengthening of the circadian period predominantly accompanied by cell vitality issues.
2. The three pharmacological inhibitors Brefeldin A, Exo I and Golgicide A impact the circadian oscillator at non-toxic concentrations.
3. Brefeldin A and Golgicide A interfere with same molecular process as *TMED10* depletion, which we presume to be COPI vesicle biogenesis, since we observe non-additive period lengthening on combined application of genetic and pharmacological perturbation.

Our outcome further strengthens the conclusions drawn from our genetic perturbation approach. We have collected strong evidence that anterograde and retrograde vesicular transport are inter-connected as well as highly dependent on each other and are of great importance for normal circadian function.

4.1.3 Genetic and pharmacological perturbation do not lead to cell toxicity or activation of unfolded protein response.

The minor decrease in cell vitality is not responsible for the observed circadian phenotype

Two of our biggest concerns throughout this study were the unspecific contribution of impaired cell vitality and the upregulation of the unfolded protein response due to inhibition of vesicular protein transport. Using U-2 OS cells with shRNA-mediated reduction of *TMED10*, *TMED2*, *GBF1* and *SEC13* transcript levels and monitoring their cell vitality over a course of five days did not reveal severe cell vitality reduction or even cell death (see **Figure 3-3**). In our study we used a Resazurin assay to determine cell vitality. The non-fluorescent Resazurin to the red-fluorescent Resorufin as a marker for unimpaired metabolic activity and redox potential as expected in vital cells. The measured red fluorescence never undercut 75% of the signal observed in control cells, which was considered as vital in our experiments. Nevertheless, it should be noted that the fluorescence signal was decreased to levels between 90-80% in all cells analysed. Using Brefeldin A in a concentration of 700 nM on U-2 OS cells, which is 10 times higher than the titrated non-toxic concentration, results in loss of red fluorescence, suggesting cell death after 24 hours to 48 hours. In conclusion, the metabolism and redox state was compromised slightly upon reduction of transcript levels of genes associated with vesicular protein transport. The number of dead cells cannot be calculated out of these results. The use of alternative cell vitality assays that do not depend on the metabolism or redox state is recommended to further investigate this issue. LIVE/DEAD cell vitality assays that use a green and a red fluorescent dye simultaneously to indicate living and dead cells in a culture are suitable. On one hand, the non-fluorescent dye calcein-AM is transported through the cell membrane into the cytoplasm where the acetomethoxy groups are removed by esterases that prevent calcein to bind calcium ions. Upon binding calcein emits a strong green fluorescent signal that can be detected by fluorescence microscopy or flow-cytometry. On the other hand, the non-fluorescent Ethidium-Homodimer-1 is internalised only when the cell membrane is compromised, as it is in dead or dying cells. There, it binds to the DNA and emits a strong red fluorescent signal that can be detected concurrent with the calcein-AM signal. Taken together, this assay would estimate the dead cells and allow conclusions if cells are dying due to reduced expression of genes associated with vesicular protein transport. The bioluminescence

signal intensity was a second read-out to determine cell vitality throughout our experiments, which is rapidly reduced in cultures with dying cells. Carefully monitoring the bioluminescence signal intensity, we very rarely observed any severe reductions upon *TMED10*, *TMED2*, *GBF1* and *SEC13* depletion in U-2 OS cells. Cells with shRNA-mediated reductions in transcript levels were vital in long-term cultures over at least three weeks, although we noticed impaired attachment to the cell culture flask after passaging the cells. We believe reduced transport of surface receptors and adhesion molecules to be responsible for the impaired attachment which was highly dependent on the knockdown efficiency of transcript levels. This could be reviewed by analysis of cell surface protein composition. Nevertheless, we cannot completely rule out the possibility that the reduction in cell vitality described above might influence the circadian oscillator.

Depletion of TMED2 and TMED10 does not activate UPR

Upon disruption of the secretory pathway, the cell often activates stress response pathways to deal with the overload of misfolded proteins and aggregated proteins that are not transported to the Golgi and beyond. This leads to an increase in chaperone transcript levels to promote proper folding of aggregated proteins and the activation of Endoplasmic-reticulum-associated protein degradation (ERAD)[342,348]. In our experiments, neither the reduction of *TMED10* and *TMED2* transcript levels nor the application of Brefeldin A at non-toxic concentrations did activate alternative splicing of *XBP-1*, indicating an absence of UPR (see **Figure 3-11**). These findings contrast with the observation made in *Saccharomyces cerevisiae* and *Arabidopsis thaliana*. Springer et al., Belden et al. and Pastor-Cantizano et al. report that UPR gets upregulated upon p24 family member depletion[368,407,408]. Since upregulation of UPR response was predominately observed in p24 family member knockout strains, we speculate that residual *TME10* and *TMED2* transcript levels in our study maintain sufficient levels of transport from the ER to the Golgi to prevent UPR induction. Gong et al. showed that overexpression of *TMED10* leads to Golgi dispersion and transport defects but does not activate ER stress pathways to deal with the interferences[366]. In contrast, administration of Brefeldin A in concentrations known to cause cell vitality issues shows upregulated alternative splicing of *XBP-1* during the first two days, indicating UPR and cell death on the third day. In line with our results, de Galarreta et al. report that application of 1 µg/ml

Brefeldin A over 24 hours leads to alternative splicing of *XBP-1*. Our second readout to evaluate UPR was the quantification of upregulation of UPR-induced transcripts that contain at least of one the following cis-acting response elements, namely ERSE, UPRE, or ERSE-II[350,409]. We chose *DNAJC3* and *HURPUD1* as our readout, which were shown to be induced upon UPR to varying level dependent on the cell line and the chosen stressor (Brefeldin A, tunicamycin, thapsigargin)[350,410–412]. We found only slight inductions of *DNAJC3* and *HURPUD1* upon reduction of *TMED10* and *TMED2* transcript level on day one and two and approximately 5-fold and 10-fold induction on day three, respectively. Compared to our positive controls, which showed 30-fold and 70-fold inductions respectively on day three, these inductions seem minor. In a study of H9c2 cells, a myoblast cell line obtained from rats, *Dnajc3* and *Hurpud1* transcript levels are induced 20-fold after treatment with thapsigargin[350]. Unfortunately, it is neither stated how long the cells were exposed to thapsigargin, nor is there mention of the concentration used in their study. Therefore, it is hard to directly compare the results. To further investigate the question if UPR is activated upon *TMED10* and *TMED2* depletion, the transcript levels of additional genes that are upregulated upon UPR should be assessed[350]. In addition, the mRNA and protein levels of the transcription factor C/EBP homologous protein (CHOP) are considered good indications for induction of UPR[413,414].

To summarize, we could detect a slight decrease in cell vitality but no indication for cell death upon depletion of *TMED2* and *TMED10* or upon the application of Brefeldin A at non-toxic concentrations in U-2 OS cells. The cells were vital in long-term cultures, which clearly indicates that cell vitality is not reduced to fatal levels. Unfolded protein response pathways are activated in this case, but only to a minor extent compared to the cells treated with toxic concentration of Brefeldin A. We recognize that we interfere with the secretory pathway - a crucial cellular process which is responsible for membrane integrity, distribution of signalling molecules and secretion of soluble proteins. Therefore, we cannot rule out completely the possibility that other cellular functions are affected and accountable, at least partially, for the phenotypes observed. Nevertheless, we believe that impaired cellular survival and UPR are not the main cause for the disturbance of the circadian oscillator. Our findings suggest that the secretory pathway contributes substantially to normal circadian rhythms and represents a new way of clock modulation.

4.2 Coupling in the periphery and the contribution of the secretory pathway

Coupling of peripheral oscillators is a controversial subject (see *Coupling in peripheral organs* for more detail). On one hand, Yamazaki et al. and Akhta et al. provide evidence that coupling in peripheral tissue does not exist due to strong damping of tissue bioluminescence and mRNA rhythms[22,147] On the other hand, Yoo et al., Tahara et al. and Saini et al. contradict these findings and support the idea of peripheral coupling by offering strong *ex vivo* and *in vivo* data on long-lasting, coherent bioluminescence rhythms in murine organs[148,166,167]. Thereby, the coupling of cells helps to maintain the high amplitude rhythms, probably by increasing phase coherence, but does not communicate any circadian period information[87,158,415]. In theory, intracellular coupling can be achieved in two ways – direct cell-cell communication via Gap junctions or paracrine signalling via soluble molecules that are secreted from neighbouring cells. In low density cultures, where cell-cell contact is negligible, conditioned medium can rescue low amplitude rhythms[169]. Furthermore, O'Neill and Hastings observe no disturbance of the circadian oscillator upon inhibition of Gap junction communication[351]. Both studies suggest the involvement of soluble paracrine factors. The biochemical properties and the corresponding receptor of such coupling factors have been elusive so far. Nevertheless, the secretion of paracrine factors would be highly dependent on the intracellular vesicular protein transport pathway, which might explain the lower amplitude and higher dampening that we observed upon interference with the secretory pathway. We therefore asked three main questions. Can we provide evidence for the secretion of a soluble factor that impinges on the circadian oscillator? Do we find indication for coupling in U-2 OS cell cultures, and does the secreted molecules play a role for the intercellular coupling? Does the density of a cell culture directly affect the robustness of circadian oscillations, and is this effect linked to a density-dependent concentration of secreted factors?

4.2.1 Conditioned medium and its effect on bioluminescence rhythms in U-2 OS cells

We harvested conditioned medium from U-2 OS wild-type cells cultured in serum free medium for 24 hours and concentrated it on Amicon Ultra centrifugal filter units with a molecular weight cut-off filter of 10 kDa prior to application on *Per2_luc* or *Bmal1_luc* U-2 OS reporter cells. The results show a phase shift of over five hours in the *Per2_luc* reporter cells and almost three hours in the *Bmal1_luc* reporter cells compared to the control medium and an acute as well as a long-lasting increase of the bioluminescence signal (see **Figure 3-12** and **Supplemental Figure A 6**). Interestingly, this phase shift is no accompanied by a change in circadian period, which is in line with the literature[87,158,415]. The different extent of phase shifts between *Per2_luc* and *Bmal1_luc* U-2 OS reporter cells is most likely the result of an unfavourable phase of conditioned medium application to the *Bmal1_luc* reporter cells. We believe that the application of conditioned medium four hours after the peak of bioluminescence would have resulted in comparable phase shifts. Together, these results suggest the existence of secreted signalling molecules which directly affects the circadian oscillator. We propose that the secreted molecules act like synchronizing factors that reset the cells in culture to the same phase when applied in high concentrations. Therefore, we see an overall phase shift and an increase in brightness of the bioluminescence signal. Further, we speculate that, if not applied in a highly concentrated single pulse, but continuously as paracrine signalling molecules in culture, the secreted molecules keep the cultured cells in synchrony – they are coupled - rather than induce acute phase shifts. Our hypothesis agrees with the findings from Noguchi et al. who showed that conditioned medium increases low-amplitude rhythms from low-density cultures[169]. It remains unknown whether these signalling molecules are effective when present at a tonic level or whether they contain timing information and must vary in a circadian manner. In contrast, we contradict the findings of Shende et al. who propose the secretion of micro RNA (miR) 142-3p and mIR-494 secretion into the cell culture supernatant which negatively regulates *Bmal1*-promotor driven *luciferase* expression[397]. We find no evidence for a miR-mediated reduction in *Bmal1_luc* bioluminescence signal in our study. Although we achieve comparable results as Noguchi and co-workers, it is important to highlight the differences of our studies. Our protocol for the preparation of conditioned medium differs severely from the procedure applied by Noguchi and coworkers[169]. First, we collected our

conditioned medium after 24 hours of serum starvation from U-2 OS wild-type cells, compared to a conditioned medium collection after seven to fourteen days of confluent fibroblast culture. We feel that the culture conditions applied by Noguchi et al. are questionable. To keep a confluent fibroblast cell culture on starvation for fourteen days drastically alters cellular physiology, which will most likely influence the secretory pathway and, therefore, the content of the conditioned medium. Second, we pooled the conditioned medium of multiple cell cultures and concentrated the medium 30- to 40-fold to enrich the secreted molecule, in comparison to the use of non-concentrated conditioned medium. Although we induce stronger effects through the higher concentration of the soluble factors, we are aware that we might miss metabolites and molecules smaller than 10 kDa. To test their influence on the circadian oscillator, the use of Amicon Ultra centrifugal filter units with molecular weight cut-off filter of 3 kDa is advised.

To summarize, we prepared conditioned medium which contained soluble molecules that acted on the circadian oscillator. This finding implies the secretion of paracrine factors that directly influence amplitude, phase and overall bioluminescence brightness. In accordance with the literature, we interpret this as first evidence for the existence of soluble coupling factors in human cell cultures as a model system for peripheral tissues. We incorporated these findings into our model (see **Figure 4-1**), stressing the importance of secreted factors through the secretory pathway and the increase of robustness of the circadian oscillator.

4.2.2 Paracrine signalling molecules bigger than 30 kDa in conditioned medium activate CRE-mediated but not SRE-mediated transcription in U-2 OS cells

Conditioned medium activates CRE-mediated transcription

We know from previous studies in SCN tissues and peripheral organs that circadian timing cues are often sensed by signalling receptors, resulting in the activation of immediate early transcription factors (IETFs)[141,416]. IETF activation is not accompanied by an upregulation of their encoding mRNA, therefore they cannot be detected by qRT-PCR. To address the question if paracrine signalling molecules impinge on the circadian oscillator by activation of IETF we used U-2 OS cells harbouring reporter

plasmids with IETF-binding sites fused to a firefly *luciferase*. Here, we report the more than 10-fold upregulation of CRE-mediated but not SRE-mediated transcription upon stimulation with enriched conditioned medium from U-2 OS wild-type cells (see **Figure 3-13**). The upregulation of CRE-mediated transcription suggests that the integration of the signal into the circadian oscillator of peripheral tissues, initiated by soluble factors in the conditioned medium, resembles the integration of light perceived through the retina of the eye into the circadian oscillator of the SCN. We speculate that the application of conditioned medium leads to the upregulation of immediate early genes (IEG), presumably *PER1* and *PER2*. Moreover, the findings imply a second input pathway at peripheral clocks in addition to the one proposed by Gerber et al. who has reported the activation of SRE-mediated transcription through blood-born circadian factors[141]. Preliminary experiments in our lab provide further evidence that G-protein coupled receptors and the activation of adenylate-cyclase as well as protein kinase A (PKA) may be involved (personal communication Anna-Marie Finger). Furthermore, we investigated additional cis-acting enhancer elements and their involvement in responses to conditioned medium exposure, but did not observe any acute induction on E-Box-, D-Box- and RRE-mediated transcription. However, application of conditioned medium induces rhythmic *luciferase* expression in unsynchronised U-2 OS cells when driven by E-Box-, D-Box- and RRE-enhancer elements that persist for at least two days (see **Supplemental Figure A 9**). In our study with the 7xSRE_*luc* reporter construct we observed similar rhythmic luciferase expression after administration of conditioned medium occasionally but not consistently. Under these culture conditions, the induction of rhythmic luciferase expression may be explained in two ways. First, the application of paracrine signalling molecules may synchronize the cell culture, like glucocorticoids, which leads to high-amplitude circadian oscillations with a strong phase coherence[137]. Second, the conditioned medium may provide a limiting molecule that, once replenished, enables circadian oscillations. Maywood and co-workers reported that paracrine factors of rhythmic SCN slices can restore circadian oscillations in co-cultured arrhythmic SCN slices through rhythmic signals emanating from the former[417]. In this study, they could not find any evidence that the secreted molecules replenish a limiting factor in the arrhythmic SNC. Therefore, it is tempting to speculate that paracrine signalling molecules have synchronized the cultured SCN slices and can fulfil similar roles in the periphery.

The secreted factor is bigger than 30 kDa and is actively secreted rather than released upon cell death

To get a better understanding about the nature of the secreted molecules in the conditioned medium we analysed it using size exclusion concentration. Here, we report that the secreted molecules which are responsible for the CRE-mediated transcriptional activation have a molecular weight above 30 kDa (see **Figure 3-14**). Although the conditioned medium enriched via Amicon Ultra centrifugal filter units with a molecular weight cut-off filter of 3 kDa leads to a stronger activation of luciferase transcription compared to the conditioned medium enriched on molecular weight cut-off filter of 10 kDa and 30 kDa, we were unable to enrich secreted factors that promote CRE-mediated transcriptional activation out of their collected flow-through. We believe that the bigger weight cut-off filter retained smaller molecules, unless extensively washed away, as indicated by the SDS-polyacrylamide gel electrophoreses and Coomassie staining. Nevertheless, molecules with a molecular weight below 30 kDa probably contribute to CRE_*luc* induction, although to a lower degree. Further, the SDS-PAGE confirms that during the preparation of the conditioned medium a variety of different molecules is collected (see **Figure 3-14**). That finding suggests that a complex interplay of activating and inhibitory molecules determines the final activation of CRE-mediated transcription. Further investigations regarding molecule sizes, biochemical properties and corresponding receptors are necessary to finally determine the intercellular signalling pathway and the interplay of activation and repression at the cell membrane. As a good example, in 2013 Gerber et al. conducted an elegant set of experiments and identified the main activating molecule of SRE-mediated transcription as a protein of approximately 65 kDa[141]. Interestingly, one third of the SRE-mediated transcriptional activity was detected in protein fractions with higher or lower molecular weight, which supports our hypothesis that multiple molecules are involved.

Finally, we address our major concern of this part of the study. We feared that the soluble molecules are released upon cell death in the donor culture and the CRE-mediated induction was an experimental artifact due to adverse culturing conditions. Here, we provide evidence that the major part of the activating signal is not released upon cell death but originates from cellular secretion (see **Figure 3-14**). We counted dead cells in the supernatant of the donor culture and extrapolated the number of dead cells in all pooled and concentrated culture supernatants. Of course, we cannot completely exclude non-

uniform culturing conditions, but we believe that we overestimated rather than underestimated the proportion of dead cells. Then, we spiked the supernatant of cells seeded in PBS rather than serum-containing culture medium into the control medium to mimic cell death and the release of cytosolic content into the medium. Since under these conditions U-2 OS cells do not attach to the cell culture flask and undergo programmed cell death, this procedure seems adequate. The use of damaging pharmacological compounds or chemicals is not applicable because they cannot be filtered out of the control medium and could potentially damage the acceptor cells upon stimulation.

In conclusion, we successfully demonstrated that paracrine signalling molecules in conditioned medium lead to the activation of CRE-mediated but not SRE-mediated transcription in U-2 OS cells. These findings are incorporated into our model (see **Figure 4-1**), including the hypothesised signalling pathway. We propose an additional circadian input pathway alongside the SRE-activating pathway reported by Gerber and co-workers. Furthermore, we present evidence that the paracrine factor has a higher molecular weight than 30 kDa and is actively secreted rather than released upon cell death. This finding further highlights the importance of the secretory pathway for the well-controlled release of paracrine factors involved in intercellular coupling in peripheral tissue. Identifying the paracrine factor(s) and the corresponding receptor(s) is the overall goal for the future.

4.2.3 Coupling in the circadian oscillator is dependent on cell culture density

Low-density cultures show compromised circadian rhythmicity

Seeding U-2 OS reporter cells at different densities and monitoring their bioluminescence rhythms led to the identification of a density-dependent circadian phenotype. Here, we report that the circadian period of U-2 OS reporter cell cultures lengthens and that the amplitude of bioluminescence rhythms reduces with decreasing numbers of cells per growth area (see **Figure 3-15** and **Supplemental Figure A 7**). These findings are in line with the published results from Noguchi et al. reporting cellular oscillations with slightly longer period and decreased amplitude in low-density fibroblast cultures compared to high-density cultures[169]. Although the observed differences were not significant in their experiments, the results clearly suggest a trend. In addition, they show that a smaller fraction of cells in low-density cultures stays rhythmic after

synchronisation compared to high-density cultures, which explains the observed effects. We identified two major differences between our study and the study of Noguchi and co-workers. First, the setup of the high and low-density culture is completely different. While we seeded a serial dilution with decreasing numbers of cells per growth area, Noguchi waited for several weeks until a high-density culture turned into a low-density culture due to accumulating cell death. We believe that the physiological state of the aged cultures which turned into low-density cultures over time is severely altered. Therefore, the physiological state might mask or induce effects on the circadian oscillator. Second, we look at the whole U-2 OS culture and their circadian properties. In contrast, Noguchi et al. identify rhythmic cells in the fibroblast culture as a first step and only analyse their circadian phenotype in single cell recordings. It will be interesting and necessary to study the effect of low-density culture conditions on a single cell level in U-2 OS cells to directly compare the outcomes to the findings in fibroblasts and asses the contribution of intercellular coupling in the U-2 OS culture to the robustness of the circadian oscillations. We speculate that the circadian phenotypes are caused by the lower concentrations of secreted molecules in low-density cultures. This destabilises the circadian oscillator and reduces intercellular coupling. As a result, we see decreased amplitudes and longer periods. To confirm our speculations, a low-density U-2 OS cell culture should be exposed to conditioned medium collected from high-density cultures before and during a bioluminescence recording. We predict a rescue of amplitude and period as proposed by Noguchi and colleagues[169].

Non-bioluminescent feeder cells can rescue the low-density culture circadian phenotype

In line with the previously described idea, we show that non-bioluminescent U-2 OS wild-type cells restore normal circadian period and amplitude when co-cultured with low-density U-2 OS reporter cell cultures (see **Figure 3-16** and **Supplemental Figure A 8**). Furthermore, we provide evidence that secreted molecules act as a coupling factors that increases the circadian amplitude in these co-cultures, since an approach with *TMED10* depleted U-2 OS cells fails to rescue the circadian phenotype of low-density cultures. In previous experiments, *TMED10* depleted cells were associated with an impaired secretory pathway, which likely prevents the release of soluble factors. We

exclude the possibility that different numbers of cells were seeded or that cells attached differently in the two different co-culture setups because we controlled for even cell numbers using microscopy. Also, Gap junction dependent communication was shown to be irrelevant for the rescue of the low-density culture in pharmacological inhibitor experiments by O'Neill and Hastings[351]. Single cell bioluminescence recordings in the two rescue approaches might deliver interesting data on intracellular circadian rhythms and how they are affected by the different co-culture conditions. In addition, we propose that exposure to conditioned medium from high-density cultures before and during a bioluminescence recording of co-cultures with *TMED10* depleted cells will rescue the circadian phenotype. To further strengthen our argument towards the secretion of paracrine signalling molecules we plan to conduct future experiments, in which the bioluminescent reporter cells are cultured independently from the non-bioluminescent feeder cells, separated through a diffusible membrane. We speculate that the feeder cells would still rescue the low-density culture phenotype.

To summarize, we find that robust, high-amplitude rhythms are strongly dependent on the culture's density. Lowering cell culture density lengthens the period and reduces the amplitude in U-2 OS reporter cells. This phenotype can be rescued by increasing cell culture density with U-2 OS wildtype cells but not U-2 OS cells with impaired vesicular traffic. Since Gap junction communication was shown to have no effect on coupling in fibroblast cultures we propose that the increasing concentration of a secreted factor contributes to the robustness of the circadian oscillations and promotes high-amplitude rhythms (see **Figure 4-1**).

4.3 Limitations of our study

Despite the earnest effort we made and the positive results we obtained during our study to answer the questions whether there is coupling in human U-2 OS cells as a model for peripheral tissues and how the secretory pathway is involved, we are aware that there are limitations in our work. As we discuss both our major concerns and the reasons for

our decisions, we would like to offer some solutions and propose future experiments to further address these issues and help to transfer our model to the *in vivo* situation.

4.3.1 Limitations of our model system and the use of RNAi

Although frequently used in circadian clock research, U-2 OS cells are an immortalised human cancer cell line with a severely transformed genome. According to the ATCC, U-2 OS cells are hyper-triploid, which might change mRNA and protein expression levels, thus not reflecting the *in vivo* situation[331]. Furthermore, evidence for coupling was mostly collected in primary cell cultures and murine tissue, which raises the question of transferability to an immortalised cancer cell line and whether U-2 OS cells need and display intercellular coupling comparable to complex peripheral organs. However, as chronobiologists we are limited in our choices of suitable research systems because we need a robust circadian clock to study their regulation and modulation. U-2 OS cells have several advantages over primary cells and murine organs:

1. They are easy to culture with no special nutritional requirements.
2. They are an immortalised cell line with a high proliferation rate.
3. They show contact inhibition, which allows long-term bioluminescence recordings.
4. They are easy to transduce.
5. They are a validated model system that is often used in circadian biology.

Alternative human cell lines that might be applicable are human colon cancer cells (HTC-116) and human keratinocytes (HaCat) which have been used in circadian studies before[418–420]. The HTC-116 cells require special medium composition and show a high proliferation rate without contact inhibition, which makes it difficult to monitor bioluminescence rhythms over several days. In our hands, HaCat cells are difficult to transduce with shRNA knockdown constructs, and the RNA interference is less efficient than in U-2 OS cells. Primary human fibroblasts and mononuclear blood cells possess a

robust circadian oscillator, too, but are hard to obtain in sufficient quantities on a weekly schedule and are probably hard to transduce based on observations on primary murine cells[421–423]. Since evidence for coupling is described for primary murine fibroblasts that do not grow in a three-dimensional network as well, we argue that U-2 OS cell are a suitable model to study coupling in human cell culture. As an advanced model system to study coupling in peripheral tissue, we propose the use of spheroids grown out of genetically modifiable U-2 OS cells. These three-dimensional miniaturized and simplified versions of tissues are much more representative of the *in vivo* environment. Preliminary results from our lab show high transduction efficiencies and satisfying bioluminescence rhythms. In the future, spheroids and organoids could be a promising tool to analyse peripheral coupling without the sacrifice of animals for scientific questions.

Nowadays, RNAi is a widely used tool to study the circadian oscillator and other behavioural and physiological processes[332,333]. This technique is based on RNA molecules that inhibit gene expression and translation through degradation of target mRNA molecules. One approach is the introduction of small interfering RNA molecules (siRNA) into the cell by transient transfection which leads to a decrease in transcript and protein levels. Since the siRNA molecules have a limited stability the RNA interference is most efficient within the first 72 hours after transfection. To ensure a long-lasting and efficient RNAi-mediated knockdown, we use short hairpin RNA (shRNA) in our lab. The RNA molecules are encoded on lentiviral expression plasmids which stably integrate at a random location in the genome and, therefore, are constitutively expressed for at least two weeks. Nonetheless, the decrease in transcript and protein levels is highly dependent on the transduction efficiency of the expression plasmid, the site of integration in the genome, the RNA-sequence (e.g. mismatches within the guide-RNA reduce the knockdown efficiency), and the protein stability. Although we frequently observe a decrease of mRNA level below 25 %, there is still the possibility that the remaining transcript level are sufficient to maintain circadian rhythmicity, making it hard to discriminate between right and false negatives. In addition, RNAi-mediated depletion of unintended transcripts due to tolerated mismatches in the guide-RNA is possible and should be controlled for. To overcome these obstacles, the use of genome editing tools like CRISPR/Cas9 to create a knockout cell line or the breeding of a transgenic knockout animal strain has been successful in the past[424,425]. Unfortunately, the use of CRISPR/Cas9 failed to generate a homozygous *TMED10*-knockout cell line, using for

different guide RNAs (data not shown). We observed a rapid decrease in cell number within the first 48 hours and the few remaining cells only exhibited a reduction of transcript levels down to approximately 50% and severely decreased growth rates. These results suggest, that heterozygous *TMED10*-knockdown cells are not lethal, but a complete gene knockout leads to cell death. This finding is supported by studies form Majewska and Denzel. They have reported that the complete knockout of *TMED10* or *TMED2* leads to early embryonic lethality or severe developmental defects in mice[365,426].

4.3.2 Limitations of the study and the transferability of our results to the *in vivo* situation

The early secretory pathway is a crucial cellular process for membrane maintenance, for the distribution of membrane-associated and integral membrane proteins, for and the secretion of soluble molecules. The cell activates stress pathways to deal with interferences and to cope with unfolded and retained proteins[342,348,427]. We are aware that genetic and pharmacological inhibition not only affects the targeted part of the secretory pathway but might have extensive repercussions on other levels of the protein transport. There is a chance that interference with early stages of the secretory pathway alters the membrane, as well as signalling receptor composition at the plasma membrane and other important intracellular organelles. The intertwined loops of retrograde and anterograde vesicular transport between the ER and the Golgi make it hard to discriminate between direct and indirect effects because of their highly interdependent character. Disruption of specific transport pathways at the trans-Golgi proves difficult because the transport events are far less understood. Nevertheless, we consider the secretory pathway to be an interesting regulator of the circadian clock. In particular, the secretion of soluble proteins and the surface expression of signalling receptors are believed to be of utmost importance and to function in a highly regulated temporal and spatial manner. In our opinion, we did our best to contradict the possibility of UPR and cell vitality dependent off-target effects and to control for the specificity of our perturbations. To what degree our findings in U-2 OS cells are applicable to the *in vivo* situation of cells or organs is hard to predict, but since the circadian oscillator is an omnipresent feature of almost every tissue in the body, we believe in the presence of similar regulatory mechanisms. With our

findings, we aim to drag the vesicular protein transport into the spotlight as an interesting contributor to the circadian oscillator and to lay the foundation for further work in this research area.

Coupling in the periphery is still under debate between the two camps that either believe or disbelieve in peripheral coupling events. Yet, we have found evidence for cellular coupling that is in line with the published results from Noguchi and O'Neill[169,351]. We present results that suggest a paracrine signalling pathway to directly affect the circadian oscillator, presumably through CRE-mediated transcription in U-2 OS cells. The influence of paracrine signalling in living animals, whose organs are exposed to serum in the blood stream at all times, is difficult to appraise. Furthermore, organs are composed of cells that form an interconnected three-dimensional network, where low-density culture conditions and decreasing paracrine signalling do not occur. To add more complexity to the issue, peripheral tissues *in vivo* are not only exposed so systemic signalling molecules, but also to temperature cycles and changes in nutrients that are integrated into the circadian oscillator[143,164]. Therefore, it proved difficult to assess the contribution of one signalling pathway to the steady-state phase of the circadian oscillator in the past. As we believe that the paracrine signalling molecules are important for coupling of cells in peripheral tissues and keeping them in synchrony, their loss would result in decreased resistance to external timing information. Once we identified potential candidate molecules, we propose to address the direct contribution of these signalling molecules by phase-shifting experiments in peripheral organs through inversed fasting-feeding cycles or inversed light-dark cycles in knockout animals. If the knocked-out signalling molecule were indeed a involved in peripheral coupling, we would expect an accelerated phase-shifting kinetic[428]. We are aware that we could not identify the secreted molecule that acts on the circadian oscillator, nor could we show that the factor is important for circadian timekeeping in peripheral tissues, and we acknowledge that other interpretations of our results are possible. Our data shows that the paracrine signalling increases the overall bioluminescence signal as well as the amplitude and, at the same time, decreases dampening of the oscillations. We found no evidence that circadian time information is transmitted and neither have other working groups (data not shown)[158,169]. Hence, it is possible that paracrine factors are a tonic rather than a rhythmic signal that boost circadian rhythms through the increase of internal *PER2* levels and prevent dampening. So far, it is not known how circadian oscillations arise during development. It might be that paracrine signalling plays a key role by initiating circadian time keeping

and maintains it over time. This hypothesis is supported by several studies, reporting a spontaneous and rapid increase in *PER2* transcript levels during development right before the circadian rhythms arise.

4.3.3 Future experiments and perspectives

In the future, it will be important to further strengthen our findings. The early secretory pathway greatly contributes to the generation of normal circadian rhythms, and we predict an involvement of paracrine signalling molecules which would connect the vesicular protein transport to coupling or maintenance of circadian oscillations in the periphery. To investigate the consequences of genetic or pharmacological interference on the vesicular protein transport we will use vesicular stomatitis virus G protein tagged with GFP (VSVG-GFP) and a luciferase fused to a signal tag targeting it for secretion. If the secretory pathway is really blocked, we expect no surface expression of VSVG-GFP and no detectable luciferase signal in the cell culture supernatant. Furthermore, we could compare the cell surface expression of signalling receptors between cells with impaired vesicular protein transport and control cells, as we predict less receptor expression at the cell surface and an altered composition upon depletion of genes associated with vesicular transport. Finally, the purification of cellular vesicles might help to identify transported cargo molecules that function as soluble paracrine signalling molecules or as receptors transmitting essential information for the circadian oscillator to effector molecules.

To provide additional evidence that a secreted factor is important for the robustness of circadian oscillations, it is important to exclude cell-cell contact and show an involvement of a soluble molecule. Hence, the use of semi-permeable membranes that separate the bioluminescent reporter cells and the non-fluorescent wild-type cells in co-cultures is an important first step. In line with this idea, we propose the use of conditioned medium from high-density cultures on low-density cells to rescue the observed circadian phenotype. Subsequently, the identification of the paracrine signalling molecule by mass-spectrometry will be a key step. Alternatively, we will design a set of molecular biology experiments to characterise if the paracrine molecule is a protein or DNA/RNA molecule,

analyse the size, investigate the chemical properties and identify potential bindings partners. Ultimately, the breeding of a transgenic animal that lacks the paracrine signalling factor either systemically or organ-specifically might provide further information on peripheral coupling or maintenance of circadian rhythmicity through phase shifting experiments. We expect altered phase shifting kinetics in transgenic animals lacking the synchronising factor when exposed to light-regimes or feeding-fasting cycles deviating from the circadian rhythms imposed by the SCN.

Bibliography

1. Kondo, T. *et al.* Circadian rhythms in prokaryotes: luciferase as a reporter of circadian gene expression in cyanobacteria. *Proc. Natl. Acad. Sci. U. S. A.* **90,** 5672–5676 (1993).

2. Bianchi, D. E. An Endogenous Circadian Rhythm in Neurospora crassa. *Microbiology* **35,** 437–445 (1964).

3. Nohales, M. A. & Kay, S. A. Molecular mechanisms at the core of the plant circadian oscillator. *Nat. Struct. Mol. Biol.* **23,** 1061–1069 (2016).

4. Whitmore, D., Foulkes, N. S., Strähle, U. & Sassone-Corsi, P. Zebrafish Clock rhythmic expression reveals independent peripheral circadian oscillators. *Nat. Neurosci.* **1,** 701–707 (1998).

5. Konopka, R. J. & Benzer, S. Clock mutants of Drosophila melanogaster. *Proc. Natl. Acad. Sci. U. S. A.* **68,** 2112–2116 (1971).

6. Mohawk, J. A., Green, C. B. & Takahashi, J. S. Central and peripheral circadian clocks in mammals. *Annu. Rev. Neurosci.* **35,** 445–462 (2012).

7. Pittendrigh, C. S. Temporal Organization: Reflections of a Darwinian Clock-Watcher. *Annu. Rev. Physiol.* **55,** 17–54 (1993).

8. Misra, H. S. & Tuli, R. Differential Expression of Photosynthesis and Nitrogen Fixation Genes in the Cyanobacterium Plectonema boryanum. *Plant Physiol.* **122,** 731–736 (2000).

9. Woelfle, M. A., Ouyang, Y., Phanvijhitsiri, K. & Johnson, C. H. The Adaptive Value of Circadian Clocks: An Experimental Assessment in Cyanobacteria. *Curr. Biol.* **14,** 1481–1486 (2004).

10. Bretzl, H. & Königliche Gesellschaft der Wissenschaften zu Göttingen. *Botanische forschungen des Alexanderzuges*. (Leipzig, B. G. Teubner, 1903).

11. de Mairan, J. Observation botanique. *Hist Acad Roy Sci* 35–36 (1729).

12. Monceau, D. du. *Phys. Arbres* **Vol.2,** 158–159 (1759).

13. Zinn, J. G. Vom Schlafe der Pflanzen. *Hambg. Mag.* **22,** 49–50 (1759).

14. M. C. Moore-Ede, Sulzman, F. & Fuller, C. A. The Clocks That Time Us. *Harv. Univ. Press Camb. MA* (1982).

15. De Candolle, A. P. Pflanzenphysiologie, oder Darstellung der Lebenskräfte und Lebensverrichtungen des Gewächse. *Stuttg. U Thübingen* 639–640 (1835).

16. Pfeffer, W. Die periodischen Bewegungen der Blattorgane. (1875).

17. Darwin, C. The Power of Movement in Plants. 407–408 (1880).

18. Kiesel, A. Untersuchungen zur Physiologie des facettierten Auges. *Sitzungsber Akad Wiss Wien* 97–139 (1894).

19. Halberg, F. & Stephens, A. N. Susceptibility to ouabain and physiologic circadian periodicity. *Proc Minn Acad Sci* **27,** 139–143 (1959).

20. Miller, B. H. *et al.* Circadian and CLOCK-controlled regulation of the mouse transcriptome and cell proliferation. *Proc. Natl. Acad. Sci. U. S. A.* **104,** 3342–3347 (2007).

21. Storch, K.-F. *et al.* Extensive and divergent circadian gene expression in liver and heart. *Nature* **417,** 78–83 (2002).

22. Akhtar, R. A. *et al.* Circadian cycling of the mouse liver transcriptome, as revealed by cDNA microarray, is driven by the suprachiasmatic nucleus. *Curr. Biol. CB* **12,** 540–550 (2002).

23. Buijs, R., Salgado, R., Sabath, E. & Escobar, C. Peripheral circadian oscillators: time and food. *Prog. Mol. Biol. Transl. Sci.* **119,** 83–103 (2013).

24. Damiola, F. *et al.* Restricted feeding uncouples circadian oscillators in peripheral tissues from the central pacemaker in the suprachiasmatic nucleus. *Genes Dev.* **14,** 2950–2961 (2000).

25. Dibner, C., Schibler, U. & Albrecht, U. The mammalian circadian timing system: organization and coordination of central and peripheral clocks. *Annu. Rev. Physiol.* **72,** 517–549 (2010).

26. Gekakis, N. *et al.* Role of the CLOCK protein in the mammalian circadian mechanism. *Science* **280,** 1564–1569 (1998).

27. Yamamoto, T. *et al.* Transcriptional oscillation of canonical clock genes in mouse peripheral tissues. *BMC Mol. Biol.* **5,** 18 (2004).

28. Brown, S. A. *et al.* PERIOD1-Associated Proteins Modulate the Negative Limb of the Mammalian Circadian Oscillator. *Science* **308,** 693–696 (2005).

29. Ye, R. *et al.* Dual modes of CLOCK:BMAL1 inhibition mediated by Cryptochrome and Period proteins in the mammalian circadian clock. *Genes Dev.* **28,** 1989–1998 (2014).

30. Shearman, L. P. *et al.* Interacting molecular loops in the mammalian circadian clock. *Science* **288,** 1013–1019 (2000).

31. Kume, K. *et al.* mCRY1 and mCRY2 are essential components of the negative limb of the circadian clock feedback loop. *Cell* **98,** 193–205 (1999).

32. Preitner, N. *et al.* The orphan nuclear receptor REV-ERBalpha controls circadian transcription within the positive limb of the mammalian circadian oscillator. *Cell* **110,** 251–260 (2002).

33. Forman, B. M. *et al.* Cross-talk among ROR alpha 1 and the Rev-erb family of orphan nuclear receptors. *Mol. Endocrinol. Baltim. Md* **8,** 1253–1261 (1994).

34. Sato, T. K. *et al.* A Functional Genomics Strategy Reveals Rora as a Component of the Mammalian Circadian Clock. *Neuron* **43,** 527–537 (2004).

35. Guillaumond, F., Dardente, H., Giguère, V. & Cermakian, N. Differential control of Bmal1 circadian transcription by REV-ERB and ROR nuclear receptors. *J. Biol. Rhythms* **20,** 391–403 (2005).

36. Akashi, M. & Takumi, T. The orphan nuclear receptor RORalpha regulates circadian transcription of the mammalian core-clock Bmal1. *Nat. Struct. Mol. Biol.* **12,** 441–448 (2005).

37. Reischl, S. *et al.* Beta-TrCP1-mediated degradation of PERIOD2 is essential for circadian dynamics. *J. Biol. Rhythms* **22,** 375–386 (2007).

38. Shirogane, T., Jin, J., Ang, X. L. & Harper, J. W. SCFβ-TRCP Controls Clock-dependent Transcription via Casein Kinase 1-dependent Degradation of the Mammalian Period-1 (Per1) Proteinm. *J. Biol. Chem.* **280,** 26863–26872 (2005).

39. Hirano, A. *et al.* FBXL21 regulates oscillation of the circadian clock through ubiquitination and stabilization of cryptochromes. *Cell* **152,** 1106–1118 (2013).

40. Yoo, S.-H. *et al.* Competing E3 Ubiquitin Ligases Determine Circadian Period by Regulated Degradation of CRY in Nucleus and Cytoplasm. *Cell* **152,** 1091–1105 (2013).

41. Abrahamson, E. E. & Moore, R. Y. Suprachiasmatic nucleus in the mouse: retinal innervation, intrinsic organization and efferent projections. *Brain Res.* **916,** 172–191 (2001).

42. Reghunandanan, V. & Reghunandanan, R. Neurotransmitters of the suprachiasmatic nuclei. *J. Circadian Rhythms* **4,** 2 (2006).

43. Herzog, E. D., Aton, S. J., Numano, R., Sakaki, Y. & Tei, H. Temporal precision in the mammalian circadian system: a reliable clock from less reliable neurons. *J. Biol. Rhythms* **19,** 35–46 (2004).

44. Welsh, D. K., Logothetis, D. E., Meister, M. & Reppert, S. M. Individual neurons dissociated from rat suprachiasmatic nucleus express independently phased circadian firing rhythms. *Neuron* **14,** 697–706 (1995).

45. Moore, R. Y., Speh, J. C. & Leak, R. K. Suprachiasmatic nucleus organization. *Cell Tissue Res.* **309,** 89–98 (2002).

46. Brown, T. M., McLachlan, E. & Piggins, H. D. Angiotensin II regulates the activity of mouse suprachiasmatic nuclei neurons. *Neuroscience* **154,** 839–847 (2008).

47. Cui, L. N., Coderre, E. & Renaud, L. P. Glutamate and GABA mediate suprachiasmatic nucleus inputs to spinal-projecting paraventricular neurons. *Am. J. Physiol. Regul. Integr. Comp. Physiol.* **281,** R1283-1289 (2001).

48. Moore, R. Y. & Speh, J. C. GABA is the principal neurotransmitter of the circadian system. *Neurosci. Lett.* **150,** 112–116 (1993).

49. Klein, D. C., Moore, R. Y. & Reppert, S. M. *Suprachiasmatic Nucleus: The Mind's Clock*. (Oxford University Press, 1991).

50. Kalsbeek, A. & Buijs, R. M. Output pathways of the mammalian suprachiasmatic nucleus: coding circadian time by transmitter selection and specific targeting. *Cell Tissue Res.* **309,** 109–118 (2002).

51. Watts, A. G. & Swanson, L. W. Efferent projections of the suprachiasmatic nucleus: II. Studies using retrograde transport of fluorescent dyes and simultaneous peptide immunohistochemistry in the rat. *J. Comp. Neurol.* **258,** 230–252 (1987).

52. Nakamura, W., Yamazaki, S., Takasu, N. N., Mishima, K. & Block, G. D. Differential Response of Period 1 Expression within the Suprachiasmatic Nucleus. *J. Neurosci.* **25,** 5481–5487 (2005).

53. Nagano, M. *et al.* An Abrupt Shift in the Day/Night Cycle Causes Desynchrony in the Mammalian Circadian Center. *J. Neurosci.* **23,** 6141–6151 (2003).

54. Stephan, F. K. & Zucker, I. Circadian Rhythms in Drinking Behavior and Locomotor Activity of Rats Are Eliminated by Hypothalamic Lesions. *Proc. Natl. Acad. Sci. U. S. A.* **69,** 1583–1586 (1972).

55. Moore, R. Y. & Eichler, V. B. Loss of a circadian adrenal corticosterone rhythm following suprachiasmatic lesions in the rat. *Brain Res.* **42,** 201–206 (1972).

56. Lehman, M. N. *et al.* Circadian rhythmicity restored by neural transplant. Immunocytochemical characterization of the graft and its integration with the host brain. *J. Neurosci. Off. J. Soc. Neurosci.* **7,** 1626–1638 (1987).

57. Ralph, M. R., Foster, R. G., Davis, F. C. & Menaker, M. Transplanted suprachiasmatic nucleus determines circadian period. *Science* **247,** 975–978 (1990).

58. Silver, R., LeSauter, J., Tresco, P. A. & Lehman, M. N. A diffusible coupling signal from the transplanted suprachiasmatic nucleus controlling circadian locomotor rhythms. *Nature* **382,** 810–813 (1996).

59. Moore, R. Y., Speh, J. C. & Patrick Card, J. The retinohypothalamic tract originates from a distinct subset of retinal ganglion cells. *J. Comp. Neurol.* **352,** 351–366 (1995).

60. Berson, D. M., Dunn, F. A. & Takao, M. Phototransduction by Retinal Ganglion Cells That Set the Circadian Clock. *Science* **295,** 1070–1073 (2002).

61. Foster, R. G. Shedding Light on the Biological Clock. *Neuron* **20,** 829–832 (1998).

62. Güler, A. D. *et al.* Melanopsin cells are the principal conduits for rod-cone input to non-image-forming vision. *Nature* **453,** 102–105 (2008).

63. Hattar, S. *et al.* Melanopsin and rod-cone photoreceptive systems account for all major accessory visual functions in mice. *Nature* **424,** 76–81 (2003).

64. Hamada, T. *et al.* Calbindin Influences Response to Photic Input in Suprachiasmatic Nucleus. *J. Neurosci.* **23,** 8820–8826 (2003).

65. Morin, L. P. & Allen, C. N. The circadian visual system, 2005. *Brain Res. Rev.* **51,** 1–60 (2006).

66. Michel, S., Itri, J., Han, J. H., Gniotczynski, K. & Colwell, C. S. Regulation of glutamatergic signalling by PACAP in the mammalian suprachiasmatic nucleus. *BMC Neurosci.* **7,** 15 (2006).

67. Meijer, J. H. & Schwartz, W. J. In search of the pathways for light-induced pacemaker resetting in the suprachiasmatic nucleus. *J. Biol. Rhythms* **18,** 235–249 (2003).

68. Hirota, T. & Fukada, Y. Resetting Mechanism of Central and Peripheral Circadian Clocks in Mammals. *Zoolog. Sci.* **21,** 359–368 (2004).

69. Crosio, C., Cermakian, N., Allis, C. D. & Sassone-Corsi, P. Light induces chromatin modification in cells of the mammalian circadian clock. *Nat. Neurosci.* **3,** 1241–1247 (2000).

70. Albrecht, U., Sun, Z. S., Eichele, G. & Lee, C. C. A Differential Response of Two Putative Mammalian Circadian Regulators, mper1and mper2, to Light. *Cell* **91,** 1055–1064 (1997).

71. Shigeyoshi, Y. *et al.* Light-Induced Resetting of a Mammalian Circadian Clock Is Associated with Rapid Induction of the mPer1 Transcript. *Cell* **91,** 1043–1053 (1997).

72. Morris, M. E., Viswanathan, N., Kuhlman, S., Davis, F. C. & Weitz, C. J. A Screen for Genes Induced in the Suprachiasmatic Nucleus by Light. *Science* **279,** 1544–1547 (1998).

73. Obrietan, K., Impey, S. & Storm, D. R. Light and circadian rhythmicity regulate MAP kinase activation in the suprachiasmatic nuclei. *Nat. Neurosci.* **1,** 693–700 (1998).

74. Coogan, A. N. & Piggins, H. D. Circadian and photic regulation of phosphorylation of ERK1/2 and Elk-1 in the suprachiasmatic nuclei of the Syrian hamster. *J. Neurosci. Off. J. Soc. Neurosci.* **23,** 3085–3093 (2003).

75. Kornhauser, J. M., Mayo, K. E. & Takahashi, J. S. Light, immediate-early genes, and circadian rhythms. *Behav. Genet.* **26,** 221–240 (1996).

76. Grewal, S. S., York, R. D. & Stork, P. J. Extracellular-signal-regulated kinase signalling in neurons. *Curr. Opin. Neurobiol.* **9,** 544–553 (1999).

77. Motzkus, D. *et al.* The human PER1 gene is transcriptionally regulated by multiple signaling pathways. *FEBS Lett.* **486,** 315–319 (2000).

78. Travnickova-Bendova, Z., Cermakian, N., Reppert, S. M. & Sassone-Corsi, P. Bimodal regulation of mPeriod promoters by CREB-dependent signaling and CLOCK/BMAL1 activity. *Proc. Natl. Acad. Sci.* **99,** 7728–7733 (2002).

79. Albrecht, U., Zheng, B., Larkin, D., Sun, Z. S. & Lee, C. C. MPer1 and mper2 are essential for normal resetting of the circadian clock. *J. Biol. Rhythms* **16,** 100–104 (2001).

80. Wakamatsu, H. *et al.* Additive effect of mPer1 and mPer2 antisense oligonucleotides on light-induced phase shift. *Neuroreport* **12,** 127–131 (2001).

81. Tischkau, S. A., Mitchell, J. W., Tyan, S.-H., Buchanan, G. F. & Gillette, M. U. Ca2+/cAMP Response Element-binding Protein (CREB)-dependent Activation of Per1 Is Required for Light-induced Signaling in the Suprachiasmatic Nucleus Circadian Clock. *J. Biol. Chem.* **278,** 718–723 (2003).

82. Akiyama, M. *et al.* Inhibition of light- or glutamate-induced mPer1 expression represses the phase shifts into the mouse circadian locomotor and suprachiasmatic firing rhythms. *J. Neurosci. Off. J. Soc. Neurosci.* **19,** 1115–1121 (1999).

83. Honma, S., Shirakawa, T., Katsuno, Y., Namihira, M. & Honma, K. Circadian periods of single suprachiasmatic neurons in rats. *Neurosci. Lett.* **250,** 157–160 (1998).

84. Liu, C., Weaver, D. R., Strogatz, S. H. & Reppert, S. M. Cellular Construction of a Circadian Clock: Period Determination in the Suprachiasmatic Nuclei. *Cell* **91,** 855–860 (1997).

85. Webb, A. B., Angelo, N., Huettner, J. E. & Herzog, E. D. Intrinsic, nondeterministic circadian rhythm generation in identified mammalian neurons. *Proc. Natl. Acad. Sci. U. S. A.* **106,** 16493–16498 (2009).

86. Yamaguchi, S. *et al.* Synchronization of cellular clocks in the suprachiasmatic nucleus. *Science* **302,** 1408–1412 (2003).

87. Liu, A. C. *et al.* Intercellular coupling confers robustness against mutations in the SCN circadian clock network. *Cell* **129,** 605–616 (2007).

88. Reppert, S. M. Pre-natal development of a hypothalamic biological clock. *Prog. Brain Res.* **93,** 119–132 (1992).

89. Bedont, J. L. & Blackshaw, S. Constructing the suprachiasmatic nucleus: a watchmaker's perspective on the central clockworks. *Front. Syst. Neurosci.* **9,** 74 (2015).

90. Schwartz, W. J., Gross, R. A. & Morton, M. T. The suprachiasmatic nuclei contain a tetrodotoxin-resistant circadian pacemaker. *Proc. Natl. Acad. Sci.* **84,** 1694–1698 (1987).

91. Bouskila, Y. & Dudek, F. E. Neuronal synchronization without calcium-dependent synaptic transmission in the hypothalamus. *Proc. Natl. Acad. Sci. U. S. A.* **90,** 3207–3210 (1993).

92. Shibata, S. & Moore, R. Y. Tetrodotoxin does not affect circadian rhythms in neuronal activity and metabolism in rodent suprachiasmatic nucleus in vitro. *Brain Res.* **606,** 259–266 (1993).

93. Card, J. P. & Moore, R. Y. The suprachiasmatic nucleus of the golden hamster: Immunohistochemical analysis of cell and fiber distribution. *Neuroscience* **13,** 415–431 (1984).

94. An, S. *et al.* A neuropeptide speeds circadian entrainment by reducing intercellular synchrony. *Proc. Natl. Acad. Sci.* **110,** E4355–E4361 (2013).

95. Glazer, R. & Gozes, I. Diurnal oscillation in vasoactive intestinal peptide gene expression independent of environmental light entraining. *Brain Res.* **644,** 164–167 (1994).

96. Takahashi, Y. *et al.* Vasoactive intestinal peptide immunoreactive neurons in the rat suprachiasmatic nucleus demonstrate diurnal variation. *Brain Res.* **497,** 374–377 (1989).

97. Cagampang, F. R. A., Sheward, W. J., Harmar, A. J., Piggins, H. D. & Coen, C. W. Circadian changes in the expression of vasoactive intestinal peptide 2 receptor mRNA in the rat suprachiasmatic nuclei. *Mol. Brain Res.* **54,** 108–112 (1998).

98. Couvineau, A. & Laburthe, M. VPAC receptors: structure, molecular pharmacology and interaction with accessory proteins. *Br. J. Pharmacol.* **166,** 42–50 (2012).

99. Harmar, A. J. *et al.* The VPAC2 Receptor Is Essential for Circadian Function in the Mouse Suprachiasmatic Nuclei. *Cell* **109,** 497–508 (2002).

100. Aton, S. J., Colwell, C. S., Harmar, A. J., Waschek, J. & Herzog, E. D. Vasoactive intestinal polypeptide mediates circadian rhythmicity and synchrony in mammalian clock neurons. *Nat. Neurosci.* **8,** 476–483 (2005).

101. Dardente, H. *et al.* Daily and circadian expression of neuropeptides in the suprachiasmatic nuclei of nocturnal and diurnal rodents. *Mol. Brain Res.* **124,** 143–151 (2004).

102. Van der Veen, D. R. *et al.* Circadian dynamics of vasopressin in mouse selection lines: Translation and release in the SCN. *Brain Res.* **1060,** 16–25 (2005).

103. Mahoney, M. M. *et al.* Daily rhythms and sex differences in vasoactive intestinal polypeptide, VIPR2 receptor and arginine vasopressin mRNA in the suprachiasmatic nucleus of a diurnal rodent, Arvicanthis niloticus. *Eur. J. Neurosci.* **30,** 1537–1543 (2009).

104. Yoshikawa, T. *et al.* Spatiotemporal profiles of arginine vasopressin transcription in cultured suprachiasmatic nucleus. *Eur. J. Neurosci.* **42,** 2678–2689 (2015).

105. Kalamatianos, T., Kalló, I. & Coen, C. W. Ageing and the Diurnal Expression of the mRNAs for Vasopressin and for the V1a and V1b Vasopressin Receptors in the Suprachiasmatic Nucleus of Male Rats. *J. Neuroendocrinol.* **16,** 493–501 (2004).

106. Schröder, H., Stehle, J. & Henschel, M. Twenty-four-hour pineal melatonin synthesis in the vasopressin-deficient Brattleboro rat. *Brain Res.* **459,** 328–332 (1988).

107. Brown, M. H. & Nunez, A. A. Vasopressin-deficient rats show a reduced amplitude of the circadian sleep rhythm. *Physiol. Behav.* **46,** 759–762 (1989).

108. Wideman, C. H., Murphy, H. M. & Nadzam, G. R. Vasopressin deficiency provides evidence for separate circadian oscillators of activity and temperature. *Peptides* **21,** 811–816 (2000).

109. Belenky, M. A., Yarom, Y. & Pickard, G. E. Heterogeneous expression of γ-aminobutyric acid and γ-aminobutyric acid-associated receptors and transporters in the rat suprachiasmatic nucleus. *J. Comp. Neurol.* **506,** 708–732 (2008).

110. Naum O, G., Fernanda Rubio, M. & Golombek, D. A. Rhythmic variation in γ-aminobutyric acidA-receptor subunit composition in the circadian system and median eminence of Syrian hamsters. *Neurosci. Lett.* **310,** 178–182 (2001).

111. Aguilar-Roblero, R. *et al.* Circadian rhythmicity in the GABAergic system in the suprachiasmatic nuclei of the rat. *Neurosci. Lett.* **157,** 199–202 (1993).

112. Gillespie, C. F., Mintz, E. M., Marvel, C. L., Huhman, K. L. & Albers, H. E. GABAA and GABAB agonists and antagonists alter the phase-shifting effects of light when microinjected into the suprachiasmatic region. *Brain Res.* **759,** 181–189 (1997).

113. Mintz, E. M., Jasnow, A. M., Gillespie, C. F., Huhman, K. L. & Albers, H. E. GABA interacts with photic signaling in the suprachiasmatic nucleus to regulate circadian phase shifts. *Neuroscience* **109,** 773–778 (2002).

114. Liu, C. & Reppert, S. M. GABA Synchronizes Clock Cells within the Suprachiasmatic Circadian Clock. *Neuron* **25,** 123–128 (2000).

115. Albus, H., Vansteensel, M. J., Michel, S., Block, G. D. & Meijer, J. H. A GABAergic Mechanism Is Necessary for Coupling Dissociable Ventral and Dorsal Regional Oscillators within the Circadian Clock. *Curr. Biol.* **15,** 886–893 (2005).

116. Evans, J. A., Leise, T. L., Castanon-Cervantes, O. & Davidson, A. J. Dynamic Interactions Mediated by Nonredundant Signaling Mechanisms Couple Circadian Clock Neurons. *Neuron* **80,** 973–983 (2013).

117. Lee, J. E. *et al.* Quantitative Peptidomics for Discovery of Circadian-Related Peptides from the Rat Suprachiasmatic Nucleus. *J. Proteome Res.* **12,** 585–593 (2013).

118. Shinohara, K., Tominaga, K., Isobe, Y. & Inouye, S. T. Photic regulation of peptides located in the ventrolateral subdivision of the suprachiasmatic nucleus of the rat: daily variations of vasoactive intestinal polypeptide, gastrin-releasing

peptide, and neuropeptide Y. *J. Neurosci. Off. J. Soc. Neurosci.* **13,** 793–800 (1993).

119. Karatsoreos, I. N., Romeo, R. D., McEwen, B. S. & Silver, R. Diurnal regulation of the gastrin-releasing peptide receptor in the mouse circadian clock. *Eur. J. Neurosci.* **23,** 1047–1053 (2006).

120. Gamble, K. L., Allen, G. C., Zhou, T. & McMahon, D. G. Gastrin-Releasing Peptide Mediates Light-Like Resetting of the Suprachiasmatic Nucleus Circadian Pacemaker through cAMP Response Element-Binding Protein and Per1 Activation. *J. Neurosci.* **27,** 12078–12087 (2007).

121. McArthur, A. J. *et al.* Gastrin-releasing peptide phase-shifts suprachiasmatic nuclei neuronal rhythms in vitro. *J. Neurosci. Off. J. Soc. Neurosci.* **20,** 5496–5502 (2000).

122. Brown, T. M., Hughes, A. T. & Piggins, H. D. Gastrin-releasing peptide promotes suprachiasmatic nuclei cellular rhythmicity in the absence of vasoactive intestinal polypeptide-VPAC2 receptor signaling. *J. Neurosci. Off. J. Soc. Neurosci.* **25,** 11155–11164 (2005).

123. Shinohara, K., Funabashi, T., Mitushima, D. & Kimura, F. Effects of gap junction blocker on vasopressin and vasoactive intestinal polypeptide rhythms in the rat suprachiasmatic nucleus in vitro. *Neurosci. Res.* **38,** 43–47 (2000).

124. Long, M. A., Jutras, M. J., Connors, B. W. & Burwell, R. D. Electrical synapses coordinate activity in the suprachiasmatic nucleus. *Nat. Neurosci.* **8,** 61–66 (2005).

125. Ueyama, T. *et al.* Suprachiasmatic nucleus: a central autonomic clock. *Nat. Neurosci.* **2,** 1051–1053 (1999).

126. Vujovic, N., Davidson, A. J. & Menaker, M. Sympathetic input modulates, but does not determine, phase of peripheral circadian oscillators. *Am. J. Physiol. Regul. Integr. Comp. Physiol.* **295,** R355-360 (2008).

127. Kalsbeek, A., La Fleur, S., Van Heijningen, C. & Buijs, R. M. Suprachiasmatic GABAergic inputs to the paraventricular nucleus control plasma glucose

concentrations in the rat via sympathetic innervation of the liver. *J. Neurosci. Off. J. Soc. Neurosci.* **24,** 7604–7613 (2004).

128. Kalsbeek, A. *et al.* Hypothalamic control of energy metabolism via the autonomic nervous system. *Ann. N. Y. Acad. Sci.* **1212,** 114–129 (2010).

129. Kaneko, M., Kaneko, K., Shinsako, J. & Dallman, M. F. Adrenal sensitivity to adrenocorticotropin varies diurnally. *Endocrinology* **109,** 70–75 (1981).

130. Cheng, M. Y., Bittman, E. L., Hattar, S. & Zhou, Q.-Y. Regulation of prokineticin 2 expression by light and the circadian clock. *BMC Neurosci.* **6,** 17 (2005).

131. Cheng, M. Y., Leslie, F. M. & Zhou, Q.-Y. Expression of prokineticins and their receptors in the adult mouse brain. *J. Comp. Neurol.* **498,** 796–809 (2006).

132. Cheng, M. Y. *et al.* Prokineticin 2 transmits the behavioural circadian rhythm of the suprachiasmatic nucleus. *Nature* **417,** 405–410 (2002).

133. Prosser, H. M. *et al.* Prokineticin receptor 2 (Prokr2) is essential for the regulation of circadian behavior by the suprachiasmatic nuclei. *Proc. Natl. Acad. Sci.* **104,** 648–653 (2007).

134. Li, J.-D. *et al.* Attenuated Circadian Rhythms in Mice Lacking the Prokineticin 2 Gene. *J. Neurosci.* **26,** 11615–11623 (2006).

135. Haus, E. Chronobiology in the endocrine system. *Adv. Drug Deliv. Rev.* **59,** 985–1014 (2007).

136. Cheifetz, P. N. The daily rhythm of the secretion of corticotrophin and corticosterone in rats and mice. *J. Endocrinol.* **49,** xi–xii (1971).

137. Balsalobre, A. *et al.* Resetting of circadian time in peripheral tissues by glucocorticoid signaling. *Science* **289,** 2344–2347 (2000).

138. Reddy, A. B. *et al.* Glucocorticoid signaling synchronizes the liver circadian transcriptome. *Hepatol. Baltim. Md* **45,** 1478–1488 (2007).

139. So, A. Y.-L., Bernal, T. U., Pillsbury, M. L., Yamamoto, K. R. & Feldman, B. J. Glucocorticoid regulation of the circadian clock modulates glucose homeostasis. *Proc. Natl. Acad. Sci. U. S. A.* **106,** 17582–17587 (2009).

140. Yamamoto, T. *et al.* Acute physical stress elevates mouse period1 mRNA expression in mouse peripheral tissues via a glucocorticoid-responsive element. *J. Biol. Chem.* **280,** 42036–42043 (2005).

141. Gerber, A. *et al.* Blood-Borne Circadian Signal Stimulates Daily Oscillations in Actin Dynamics and SRF Activity. *Cell* **152,** 492–503 (2013).

142. Abraham, U. *et al.* Coupling governs entrainment range of circadian clocks. *Mol. Syst. Biol.* **6,** 438 (2010).

143. Brown, S. A., Zumbrunn, G., Fleury-Olela, F., Preitner, N. & Schibler, U. Rhythms of mammalian body temperature can sustain peripheral circadian clocks. *Curr. Biol. CB* **12,** 1574–1583 (2002).

144. Reinke, H. *et al.* Differential display of DNA-binding proteins reveals heat-shock factor 1 as a circadian transcription factor. *Genes Dev.* **22,** 331–345 (2008).

145. Tamaru, T. *et al.* Synchronization of circadian Per2 rhythms and HSF1-BMAL1:CLOCK interaction in mouse fibroblasts after short-term heat shock pulse. *PloS One* **6,** e24521 (2011).

146. Gotic, I. *et al.* Temperature regulates splicing efficiency of the cold-inducible RNA-binding protein gene Cirbp. *Genes Dev.* **30,** 2005–2017 (2016).

147. Yamazaki, S. *et al.* Resetting Central and Peripheral Circadian Oscillators in Transgenic Rats. *Science* **288,** 682–685 (2000).

148. Yoo, S.-H. *et al.* PERIOD2::LUCIFERASE real-time reporting of circadian dynamics reveals persistent circadian oscillations in mouse peripheral tissues. *Proc. Natl. Acad. Sci. U. S. A.* **101,** 5339–5346 (2004).

149. Alvarez, J. D. & Sehgal, A. The thymus is similar to the testis in its pattern of circadian clock gene expression. *J. Biol. Rhythms* **20,** 111–121 (2005).

150. Liu, S., Cai, Y., Sothern, R. B., Guan, Y. & Chan, P. Chronobiological Analysis of Circadian Patterns in Transcription of Seven Key Clock Genes in Six Peripheral Tissues in Mice. *Chronobiol. Int.* **24,** 793–820 (2007).

151. DeBruyne, J. P., Weaver, D. R. & Reppert, S. M. CLOCK and NPAS2 have overlapping roles in the suprachiasmatic circadian clock. *Nat. Neurosci.* **10,** 543–545 (2007).

152. DeBruyne, J. P., Weaver, D. R. & Reppert, S. M. Peripheral circadian oscillators require CLOCK. *Curr. Biol. CB* **17,** R538-539 (2007).

153. Gachon, F., Olela, F. F., Schaad, O., Descombes, P. & Schibler, U. The circadian PAR-domain basic leucine zipper transcription factors DBP, TEF, and HLF modulate basal and inducible xenobiotic detoxification. *Cell Metab.* **4,** 25–36 (2006).

154. Lamia, K. A., Storch, K.-F. & Weitz, C. J. Physiological significance of a peripheral tissue circadian clock. *Proc. Natl. Acad. Sci.* **105,** 15172–15177 (2008).

155. Martelot, G. L. *et al.* REV-ERBα Participates in Circadian SREBP Signaling and Bile Acid Homeostasis. *PLOS Biol.* **7,** e1000181 (2009).

156. Marcheva, B. *et al.* Disruption of the clock components CLOCK and BMAL1 leads to hypoinsulinaemia and diabetes. *Nature* **466,** 627–631 (2010).

157. Guo, H., Guo, H., Brewer, J. M., Lehman, M. N. & Bittman, E. L. Suprachiasmatic regulation of circadian rhythms of gene expression in hamster peripheral organs: effects of transplanting the pacemaker. *J. Neurosci. Off. J. Soc. Neurosci.* **26,** 6406–6412 (2006).

158. Nagoshi, E. *et al.* Circadian Gene Expression in Individual Fibroblasts. *Cell* **119,** 693–705 (2004).

159. Dibner, C. *et al.* Circadian gene expression is resilient to large fluctuations in overall transcription rates. *EMBO J.* **28,** 123–134 (2009).

160. Stephan, F. K., Swann, J. M. & Sisk, C. L. Entrainment of circadian rhythms by feeding schedules in rats with suprachiasmatic lesions. *Behav. Neural Biol.* **25,** 545–554 (1979).

161. Krieger, D. T., Hauser, H. & Krey, L. C. Suprachiasmatic nuclear lesions do not abolish food-shifted circadian adrenal and temperature rhythmicity. *Science* **197,** 398–399 (1977).

162. Stokkan, K.-A., Yamazaki, S., Tei, H., Sakaki, Y. & Menaker, M. Entrainment of the Circadian Clock in the Liver by Feeding. *Science* **291,** 490–493 (2001).

163. Pezuk, P., Mohawk, J. A., Yoshikawa, T., Sellix, M. T. & Menaker, M. Circadian organization is governed by extra-SCN pacemakers. *J. Biol. Rhythms* **25,** 432–441 (2010).

164. Hara, R. *et al.* Restricted feeding entrains liver clock without participation of the suprachiasmatic nucleus. *Genes Cells* **6,** 269–278 (2001).

165. Pendergast, J. S. *et al.* Robust Food Anticipatory Activity in BMAL1-Deficient Mice. *PLOS ONE* **4,** e4860 (2009).

166. Tahara, Y. *et al.* In Vivo Monitoring of Peripheral Circadian Clocks in the Mouse. *Curr. Biol.* **22,** 1029–1034 (2012).

167. Saini, C. *et al.* Real-time recording of circadian liver gene expression in freely moving mice reveals the phase-setting behavior of hepatocyte clocks. *Genes Dev.* **27,** 1526–1536 (2013).

168. Landgraf, D., Achten, C., Dallmann, F. & Oster, H. Embryonic development and maternal regulation of murine circadian clock function. *Chronobiol. Int.* **32,** 416–427 (2015).

169. Noguchi, T., Wang, L. L. & Welsh, D. K. Fibroblast PER2 circadian rhythmicity depends on cell density. *J. Biol. Rhythms* **28,** 183–192 (2013).

170. Guenthner, C. J. *et al.* Circadian Rhythms of PER2::LUC in Individual Primary Mouse Hepatocytes and Cultures. *PLoS ONE* **9,** (2014).

171. Murat, D., Byrne, M. & Komeili, A. Cell Biology of Prokaryotic Organelles. *Cold Spring Harb. Perspect. Biol.* **2,** (2010).

172. Cannon, G. C. *et al.* Microcompartments in Prokaryotes: Carboxysomes and Related Polyhedra. *Appl. Environ. Microbiol.* **67,** 5351–5361 (2001).

173. Bonifacino, J. S. & Glick, B. S. The mechanisms of vesicle budding and fusion. *Cell* **116,** 153–166 (2004).

174. Rich, P. R. & Maréchal, A. The mitochondrial respiratory chain. *Essays Biochem.* **47,** 1–23 (2010).

175. Nufer, O., Kappeler, F., Guldbrandsen, S. & Hauri, H.-P. ER export of ERGIC-53 is controlled by cooperation of targeting determinants in all three of its domains. *J. Cell Sci.* **116,** 4429–4440 (2003).

176. Sato, K. & Nakano, A. Oligomerization of a cargo receptor directs protein sorting into COPII-coated transport vesicles. *Mol. Biol. Cell* **14,** 3055–3063 (2003).

177. Letourneur, F., Hennecke, S., Démollière, C. & Cosson, P. Steric masking of a dilysine endoplasmic reticulum retention motif during assembly of the human high affinity receptor for immunoglobulin E. *J. Cell Biol.* **129,** 971–978 (1995).

178. Margeta-Mitrovic, M., Jan, Y. N. & Jan, L. Y. A trafficking checkpoint controls GABA(B) receptor heterodimerization. *Neuron* **27,** 97–106 (2000).

179. Meyer, H. A. *et al.* Mammalian Sec61 is associated with Sec62 and Sec63. *J. Biol. Chem.* **275,** 14550–14557 (2000).

180. Barlowe, C. K. & Miller, E. A. Secretory Protein Biogenesis and Traffic in the Early Secretory Pathway. *Genetics* **193,** 383–410 (2013).

181. Wild, K., Halic, M., Sinning, I. & Beckmann, R. SRP meets the ribosome. *Nat. Struct. Mol. Biol.* **11,** 1049–1053 (2004).

182. Görlich, D., Prehn, S., Hartmann, E., Kalies, K. U. & Rapoport, T. A. A mammalian homolog of SEC61p and SECYp is associated with ribosomes and nascent polypeptides during translocation. *Cell* **71,** 489–503 (1992).

183. Prinz, A., Hartmann, E. & Kalies, K. U. Sec61p is the main ribosome receptor in the endoplasmic reticulum of Saccharomyces cerevisiae. *Biol. Chem.* **381,** 1025–1029 (2000).

184. Morrow, M. W. & Brodsky, J. L. Yeast ribosomes bind to highly purified reconstituted Sec61p complex and to mammalian p180. *Traffic Cph. Den.* **2,** 705–716 (2001).

185. Görlich, D., Hartmann, E., Prehn, S. & Rapoport, T. A. A protein of the endoplasmic reticulum involved early in polypeptide translocation. *Nature* **357,** 47–52 (1992).

186. Ng, D. T., Brown, J. D. & Walter, P. Signal sequences specify the targeting route to the endoplasmic reticulum membrane. *J. Cell Biol.* **134,** 269–278 (1996).

187. Shao, S. & Hegde, R. S. A calmodulin-dependent translocation pathway for small secretory proteins. *Cell* **147,** 1576–1588 (2011).

188. Ngosuwan, J., Wang, N. M., Fung, K. L. & Chirico, W. J. Roles of cytosolic Hsp70 and Hsp40 molecular chaperones in post-translational translocation of presecretory proteins into the endoplasmic reticulum. *J. Biol. Chem.* **278,** 7034–7042 (2003).

189. Dünnwald, M., Varshavsky, A. & Johnsson, N. Detection of transient in vivo interactions between substrate and transporter during protein translocation into the endoplasmic reticulum. *Mol. Biol. Cell* **10,** 329–344 (1999).

190. Plath, K., Mothes, W., Wilkinson, B. M., Stirling, C. J. & Rapoport, T. A. Signal sequence recognition in posttranslational protein transport across the yeast ER membrane. *Cell* **94,** 795–807 (1998).

191. Chirico, W. J., Waters, M. G. & Blobel, G. 70K heat shock related proteins stimulate protein translocation into microsomes. *Nature* **332,** 805–810 (1988).

192. Matlack, K. E., Misselwitz, B., Plath, K. & Rapoport, T. A. BiP acts as a molecular ratchet during posttranslational transport of prepro-alpha factor across the ER membrane. *Cell* **97,** 553–564 (1999).

193. Yabal, M. *et al.* Translocation of the C terminus of a tail-anchored protein across the endoplasmic reticulum membrane in yeast mutants defective in signal peptide-driven translocation. *J. Biol. Chem.* **278,** 3489–3496 (2003).

194. Schuldiner, M. *et al.* Exploration of the function and organization of the yeast early secretory pathway through an epistatic miniarray profile. *Cell* **123,** 507–519 (2005).

195. Abell, B. M., Pool, M. R., Schlenker, O., Sinning, I. & High, S. Signal recognition particle mediates post-translational targeting in eukaryotes. *EMBO J.* **23,** 2755–2764 (2004).

196. Rabu, C., Wipf, P., Brodsky, J. L. & High, S. A precursor-specific role for Hsp40/Hsc70 during tail-anchored protein integration at the endoplasmic reticulum. *J. Biol. Chem.* **283,** 27504–27513 (2008).

197. Stefanovic, S. & Hegde, R. S. Identification of a Targeting Factor for Posttranslational Membrane Protein Insertion into the ER. *Cell* **128,** 1147–1159 (2007).

198. Weihofen, A., Binns, K., Lemberg, M. K., Ashman, K. & Martoglio, B. Identification of signal peptide peptidase, a presenilin-type aspartic protease. *Science* **296,** 2215–2218 (2002).

199. Helenius, A. & Aebi, M. Intracellular functions of N-linked glycans. *Science* **291,** 2364–2369 (2001).

200. Schwarz, F. & Aebi, M. Mechanisms and principles of N-linked protein glycosylation. *Curr. Opin. Struct. Biol.* **21,** 576–582 (2011).

201. Helenius, A. & Aebi, M. Roles of N-linked glycans in the endoplasmic reticulum. *Annu. Rev. Biochem.* **73,** 1019–1049 (2004).

202. Strahl-Bolsinger, S., Gentzsch, M. & Tanner, W. Protein O-mannosylation. *Biochim. Biophys. Acta* **1426,** 297–307 (1999).

203. Bannykh, S. I. & Balch, W. E. Membrane Dynamics at the Endoplasmic Reticulum–Golgi Interface. *J. Cell Biol.* **138,** 1–4 (1997).

204. Bannykh, S. I., Rowe, T. & Balch, W. E. The organization of endoplasmic reticulum export complexes. *J. Cell Biol.* **135,** 19–35 (1996).

205. Barlowe, C. *et al.* COPII: a membrane coat formed by Sec proteins that drive vesicle budding from the endoplasmic reticulum. *Cell* **77,** 895–907 (1994).

206. Paccaud, J. P. *et al.* Cloning and functional characterization of mammalian homologues of the COPII component Sec23. *Mol. Biol. Cell* **7,** 1535–1546 (1996).

207. Tang, B. L., Kausalya, J., Low, D. Y. H., Lock, M. L. & Hong, W. A Family of Mammalian Proteins Homologous to Yeast Sec24p. *Biochem. Biophys. Res. Commun.* **258,** 679–684 (1999).

208. Shaywitz, D. A., Orci, L., Ravazzola, M., Swaroop, A. & Kaiser, C. A. Human SEC13Rp functions in yeast and is located on transport vesicles budding from the endoplasmic reticulum. *J. Cell Biol.* **128,** 769–777 (1995).

209. Tang, B. L. *et al.* Mammalian Homologues of Yeast Sec31p AN UBIQUITOUSLY EXPRESSED FORM IS LOCALIZED TO ENDOPLASMIC RETICULUM (ER) EXIT SITES AND IS ESSENTIAL FOR ER-GOLGI TRANSPORT. *J. Biol. Chem.* **275,** 13597–13604 (2000).

210. Futai, E., Hamamoto, S., Orci, L. & Schekman, R. GTP/GDP exchange by Sec12p enables COPII vesicle bud formation on synthetic liposomes. *EMBO J.* **23,** 4146–4155 (2004).

211. Nakańo, A. & Muramatsu, M. A novel GTP-binding protein, Sar1p, is involved in transport from the endoplasmic reticulum to the Golgi apparatus. *J. Cell Biol.* **109,** 2677–2691 (1989).

212. Bielli, A. *et al.* Regulation of Sar1 NH_2 terminus by GTP binding and hydrolysis promotes membrane deformation to control COPII vesicle fission. *J. Cell Biol.* **171,** 919–924 (2005).

213. Lee, M. C. S. *et al.* Sar1p N-Terminal Helix Initiates Membrane Curvature and Completes the Fission of a COPII Vesicle. *Cell* **122,** 605–617 (2005).

214. Dominguez, M. *et al.* gp25L/emp24/p24 Protein Family Members of the cis-Golgi Network Bind Both COP I and II Coatomer. *J. Cell Biol.* **140,** 751–765 (1998).

215. Miller, E. A. *et al.* Multiple Cargo Binding Sites on the COPII Subunit Sec24p Ensure Capture of Diverse Membrane Proteins into Transport Vesicles. *Cell* **114,** 497–509 (2003).

216. Miller, E., Antonny, B., Hamamoto, S. & Schekman, R. Cargo selection into COPII vesicles is driven by the Sec24p subunit. *EMBO J.* **21,** 6105–6113 (2002).

217. Mossessova, E., Bickford, L. C. & Goldberg, J. SNARE Selectivity of the COPII Coat. *Cell* **114,** 483–495 (2003).

218. Barlowe, C. Signals for COPII-dependent export from the ER: what's the ticket out? *Trends Cell Biol.* **13,** 295–300 (2003).

219. Nishimura, N. & Balch, W. E. A Di-Acidic Signal Required for Selective Export from the Endoplasmic Reticulum. *Science* **277,** 556–558 (1997).

220. Kappeler, F., Klopfenstein, D. R. C., Foguet, M., Paccaud, J.-P. & Hauri, H.-P. The Recycling of ERGIC-53 in the Early Secretory Pathway ERGIC-53 CARRIES A CYTOSOLIC ENDOPLASMIC RETICULUM-EXIT DETERMINANT INTERACTING WITH COPII. *J. Biol. Chem.* **272,** 31801–31808 (1997).

221. Sato, K. & Nakano, A. Emp47p and Its Close Homolog Emp46p Have a Tyrosine-containing Endoplasmic Reticulum Exit Signal and Function in Glycoprotein Secretion in Saccharomyces cerevisiae. *Mol. Biol. Cell* **13,** 2518–2532 (2002).

222. Appenzeller, C., Andersson, H., Kappeler, F. & Hauri, H.-P. The lectin ERGIC-53 is a cargo transport receptor for glycoproteins. *Nat. Cell Biol.* **1,** 330–334 (1999).

223. Nichols, W. C. *et al.* Mutations in the ER–Golgi Intermediate Compartment Protein ERGIC-53 Cause Combined Deficiency of Coagulation Factors V and VIII. *Cell* **93,** 61–70 (1998).

224. Bonnon, C., Wendeler, M. W., Paccaud, J.-P. & Hauri, H.-P. Selective export of human GPI-anchored proteins from the endoplasmic reticulum. *J Cell Sci* **123,** 1705–1715 (2010).

225. Takida, S., Maeda, Y. & Kinoshita, T. Mammalian GPI-anchored proteins require p24 proteins for their efficient transport from the ER to the plasma membrane. *Biochem. J.* **409,** 555–562 (2008).

226. Lederkremer, G. Z. *et al.* Structure of the Sec23p/24p and Sec13p/31p complexes of COPII. *Proc. Natl. Acad. Sci.* **98,** 10704–10709 (2001).

227. Presley, J. F. *et al.* ER-to-Golgi transport visualized in living cells. *Nature* **389,** 81–85 (1997).

228. Springer, S., Spang, A. & Schekman, R. A Primer on Vesicle Budding. *Cell* **97,** 145–148 (1999).

229. Cai, H. *et al.* TRAPPI tethers COPII vesicles by binding the coat subunit Sec23. *Nature* **445,** 941–944 (2007).

230. Cao, X. & Barlowe, C. Asymmetric Requirements for a Rab Gtpase and Snare Proteins in Fusion of Copii Vesicles with Acceptor Membranes. *J. Cell Biol.* **149,** 55–66 (2000).

231. Hay, J. C. *et al.* Localization, Dynamics, and Protein Interactions Reveal Distinct Roles for ER and Golgi SNAREs. *J. Cell Biol.* **141,** 1489–1502 (1998).

232. Lord, C. *et al.* Sequential interactions with Sec23 control the direction of vesicle traffic. *Nature* **473,** 181–186 (2011).

233. Ballensiefen, W., Ossipov, D. & Schmitt, H. D. Recycling of the yeast v-SNARE Sec22p involves COPI-proteins and the ER transmembrane proteins Ufe1p and Sec20p. *J. Cell Sci.* **111 (Pt 11),** 1507–1520 (1998).

234. Hsu, V. W. *et al.* A recycling pathway between the endoplasmic reticulum and the Golgi apparatus for retention of unassembled MHC class I molecules. *Nature* **352,** 441–444 (1991).

235. Semenza, J. C., Hardwick, K. G., Dean, N. & Pelham, H. R. ERD2, a yeast gene required for the receptor-mediated retrieval of luminal ER proteins from the secretory pathway. *Cell* **61,** 1349–1357 (1990).

236. Lewis, M. J. & Pelham, H. R. Ligand-induced redistribution of a human KDEL receptor from the Golgi complex to the endoplasmic reticulum. *Cell* **68,** 353–364 (1992).

237. Malhotra, V., Serafini, T., Orci, L., Shepherd, J. C. & Rothman, J. E. Purification of a novel class of coated vesicles mediating biosynthetic protein transport through the Golgi stack. *Cell* **58,** 329–336 (1989).

238. Waters, M. G., Serafini, T. & Rothman, J. E. 'Coatomer': a cytosolic protein complex containing subunits of non-clathrin-coated Golgi transport vesicles. *Nature* **349,** 248–251 (1991).

239. Fiedler, K., Veit, M., Stamnes, M. A. & Rothman, J. E. Bimodal interaction of coatomer with the p24 family of putative cargo receptors. *Science* **273,** 1396–1399 (1996).

240. Wegmann, D., Hess, P., Baier, C., Wieland, F. T. & Reinhard, C. Novel isotypic gamma/zeta subunits reveal three coatomer complexes in mammals. *Mol. Cell. Biol.* **24,** 1070–1080 (2004).

241. Moelleken, J. *et al.* Differential localization of coatomer complex isoforms within the Golgi apparatus. *Proc. Natl. Acad. Sci. U. S. A.* **104,** 4425–4430 (2007).

242. Donaldson, J. G., Cassel, D., Kahn, R. A. & Klausner, R. D. ADP-ribosylation factor, a small GTP-binding protein, is required for binding of the coatomer protein beta-COP to Golgi membranes. *Proc. Natl. Acad. Sci. U. S. A.* **89,** 6408–6412 (1992).

243. Gommel, D. U. *et al.* Recruitment to Golgi membranes of ADP-ribosylation factor 1 is mediated by the cytoplasmic domain of p23. *EMBO J.* **20,** 6751–6760 (2001).

244. Niu, T.-K., Pfeifer, A. C., Lippincott-Schwartz, J. & Jackson, C. L. Dynamics of GBF1, a Brefeldin A-sensitive Arf1 exchange factor at the Golgi. *Mol. Biol. Cell* **16,** 1213–1222 (2005).

245. Chardin, P. *et al.* A human exchange factor for ARF contains Sec7- and pleckstrin-homology domains. *Nature* **384,** 481–484 (1996).

246. Zhao, X., Lasell, T. K. R. & Melançon, P. Localization of large ADP-ribosylation factor-guanine nucleotide exchange factors to different Golgi compartments: evidence for distinct functions in protein traffic. *Mol. Biol. Cell* **13,** 119–133 (2002).

247. Antonny, B., Beraud-Dufour, S., Chardin, P. & Chabre, M. N-terminal hydrophobic residues of the G-protein ADP-ribosylation factor-1 insert into membrane phospholipids upon GDP to GTP exchange. *Biochemistry (Mosc.)* **36,** 4675–4684 (1997).

248. Beck, R. *et al.* Coatomer and dimeric ADP ribosylation factor 1 promote distinct steps in membrane scission. *J. Cell Biol.* **194,** 765–777 (2011).

249. Beck, R. *et al.* Membrane curvature induced by Arf1-GTP is essential for vesicle formation. *Proc. Natl. Acad. Sci. U. S. A.* **105,** 11731–11736 (2008).

250. Zhao, L. *et al.* Direct and GTP-dependent interaction of ADP ribosylation factor 1 with coatomer subunit beta. *Proc. Natl. Acad. Sci. U. S. A.* **94,** 4418–4423 (1997).

251. Zhao, L., Helms, J. B., Brunner, J. & Wieland, F. T. GTP-dependent binding of ADP-ribosylation factor to coatomer in close proximity to the binding site for dilysine retrieval motifs and p23. *J. Biol. Chem.* **274,** 14198–14203 (1999).

252. Sun, Z. *et al.* Multiple and stepwise interactions between coatomer and ADP-ribosylation factor-1 (Arf1)-GTP. *Traffic Cph. Den.* **8,** 582–593 (2007).

253. Béthune, J. *et al.* Coatomer, the coat protein of COPI transport vesicles, discriminates endoplasmic reticulum residents from p24 proteins. *Mol. Cell. Biol.* **26,** 8011–8021 (2006).

254. Beck, R., Rawet, M., Ravet, M., Wieland, F. T. & Cassel, D. The COPI system: molecular mechanisms and function. *FEBS Lett.* **583,** 2701–2709 (2009).

255. Munro, S. & Pelham, H. R. A C-terminal signal prevents secretion of luminal ER proteins. *Cell* **48,** 899–907 (1987).

256. Raykhel, I. *et al.* A molecular specificity code for the three mammalian KDEL receptors. *J. Cell Biol.* **179,** 1193–1204 (2007).

257. Aoe, T. *et al.* The KDEL receptor, ERD2, regulates intracellular traffic by recruiting a GTPase-activating protein for ARF1. *EMBO J.* **16,** 7305–7316 (1997).

258. Wilson, D. W., Lewis, M. J. & Pelham, H. R. pH-dependent binding of KDEL to its receptor in vitro. *J. Biol. Chem.* **268,** 7465–7468 (1993).

259. Jackson, M. R., Nilsson, T. & Peterson, P. A. Identification of a consensus motif for retention of transmembrane proteins in the endoplasmic reticulum. *EMBO J.* **9,** 3153–3162 (1990).

260. Eugster, A., Frigerio, G., Dale, M. & Duden, R. The alpha- and beta'-COP WD40 domains mediate cargo-selective interactions with distinct di-lysine motifs. *Mol. Biol. Cell* **15,** 1011–1023 (2004).

261. Sohn, K. *et al.* A major transmembrane protein of Golgi-derived COPI-coated vesicles involved in coatomer binding. *J. Cell Biol.* **135,** 1239–1248 (1996).

262. Goldberg, J. Decoding of sorting signals by coatomer through a GTPase switch in the COPI coat complex. *Cell* **100,** 671–679 (2000).

263. Belden, W. J. & Barlowe, C. Distinct roles for the cytoplasmic tail sequences of Emp24p and Erv25p in transport between the endoplasmic reticulum and Golgi complex. *J. Biol. Chem.* **276,** 43040–43048 (2001).

264. Yang, J.-S. *et al.* A role for BARS at the fission step of COPI vesicle formation from Golgi membrane. *EMBO J.* **24,** 4133–4143 (2005).

265. Yang, J.-S. *et al.* Key components of the fission machinery are interchangeable. *Nat. Cell Biol.* **8,** 1376–1382 (2006).

266. Yang, J.-S. *et al.* A role for phosphatidic acid in COPI vesicle fission yields insights into Golgi maintenance. *Nat. Cell Biol.* **10,** 1146–1153 (2008).

267. Adolf, F. *et al.* Scission of COPI and COPII Vesicles Is Independent of GTP Hydrolysis. *Traffic* **14,** 922–932 (2013).

268. Rambourg, A., Clermont, Y. & Marraud, A. Three-dimensional structure of the osmium-impregnated Golgi apparatus as seen in the high voltage electron microscope. *Am. J. Anat.* **140,** 27–45 (1974).

269. Opat, A. S., van Vliet, C. & Gleeson, P. A. Trafficking and localisation of resident Golgi glycosylation enzymes. *Biochimie* **83,** 763–773 (2001).

270. van Meer, G. Lipids of the Golgi membrane. *Trends Cell Biol.* **8,** 29–33 (1998).

271. Rothman, J. E. Mechanisms of intracellular protein transport. *Nature* **372,** 55–63 (1994).

272. Mironov, A. A., Weidman, P. & Luini, A. Variations on the intracellular transport theme: maturing cisternae and trafficking tubules. *J. Cell Biol.* **138,** 481–484 (1997).

273. Marsh, B. J., Volkmann, N., McIntosh, J. R. & Howell, K. E. Direct continuities between cisternae at different levels of the Golgi complex in glucose-stimulated mouse islet beta cells. *Proc. Natl. Acad. Sci. U. S. A.* **101,** 5565–5570 (2004).

274. Trucco, A. *et al.* Secretory traffic triggers the formation of tubular continuities across Golgi sub-compartments. *Nat. Cell Biol.* **6,** 1071–1081 (2004).

275. Farquhar, M. G. & Palade, G. E. The Golgi apparatus (complex)-(1954-1981)-from artifact to center stage. *J. Cell Biol.* **91,** 77s–103s (1981).

276. Bonfanti, L. *et al.* Procollagen traverses the Golgi stack without leaving the lumen of cisternae: evidence for cisternal maturation. *Cell* **95,** 993–1003 (1998).

277. Orci, L., Glick, B. S. & Rothman, J. E. A new type of coated vesicular carrier that appears not to contain clathrin: its possible role in protein transport within the Golgi stack. *Cell* **46,** 171–184 (1986).

278. Rothman, J. E. & Wieland, F. T. Protein sorting by transport vesicles. *Science* **272,** 227–234 (1996).

279. Orci, L. *et al.* Bidirectional transport by distinct populations of COPI-coated vesicles. *Cell* **90,** 335–349 (1997).

280. Martinez-Menárguez, J. A. *et al.* Peri-Golgi vesicles contain retrograde but not anterograde proteins consistent with the cisternal progression model of intra-Golgi transport. *J. Cell Biol.* **155,** 1213–1224 (2001).

281. Gilchrist, A. *et al.* Quantitative proteomics analysis of the secretory pathway. *Cell* **127,** 1265–1281 (2006).

282. Grasse, P. P. [Ultrastructure, polarity and reproduction of Golgi apparatus]. *Comptes Rendus Hebd. Seances Acad. Sci.* **245,** 1278–1281 (1957).

283. Glick, B. S. & Malhotra, V. The Curious Status of the Golgi Apparatus. *Cell* **95,** 883–889 (1998).

284. Lanoix, J. *et al.* Sorting of Golgi resident proteins into different subpopulations of COPI vesicles: a role for ArfGAP1. *J. Cell Biol.* **155,** 1199–1212 (2001).

285. Lanoix, J. *et al.* GTP hydrolysis by arf-1 mediates sorting and concentration of Golgi resident enzymes into functional COP I vesicles. *EMBO J.* **18,** 4935–4948 (1999).

286. Ishii, M., Suda, Y., Kurokawa, K. & Nakano, A. COPI is essential for Golgi cisternal maturation and dynamics. *J. Cell Sci.* **129,** 3251–3261 (2016).

287. Losev, E. *et al.* Golgi maturation visualized in living yeast. *Nature* **441,** 1002–1006 (2006).

288. Matsuura-Tokita, K., Takeuchi, M., Ichihara, A., Mikuriya, K. & Nakano, A. Live imaging of yeast Golgi cisternal maturation. *Nature* **441,** 1007–1010 (2006).

289. Cosson, P., Amherdt, M., Rothman, J. E. & Orci, L. A resident Golgi protein is excluded from peri-Golgi vesicles in NRK cells. *Proc. Natl. Acad. Sci. U. S. A.* **99,** 12831–12834 (2002).

290. Traub, L. M. & Kornfeld, S. The trans-Golgi network: a late secretory sorting station. *Curr. Opin. Cell Biol.* **9,** 527–533 (1997).

291. Hirschberg, K. *et al.* Kinetic analysis of secretory protein traffic and characterization of golgi to plasma membrane transport intermediates in living cells. *J. Cell Biol.* **143,** 1485–1503 (1998).

292. Kreitzer, G., Marmorstein, A., Okamoto, P., Vallee, R. & Rodriguez-Boulan, E. Kinesin and dynamin are required for post-Golgi transport of a plasma-membrane protein. *Nat. Cell Biol.* **2,** 125–127 (2000).

293. Jones, S. M., Crosby, J. R., Salamero, J. & Howell, K. E. A cytosolic complex of p62 and rab6 associates with TGN38/41 and is involved in budding of exocytic vesicles from the trans-Golgi network. *J. Cell Biol.* **122,** 775–788 (1993).

294. Kooy, J., Toh, B. H., Pettitt, J. M., Erlich, R. & Gleeson, P. A. Human autoantibodies as reagents to conserved Golgi components. Characterization of a peripheral, 230-kDa compartment-specific Golgi protein. *J. Biol. Chem.* **267,** 20255–20263 (1992).

295. Narula, N. *et al.* Identification of a 200-kD, brefeldin-sensitive protein on Golgi membranes. *J. Cell Biol.* **117,** 27–38 (1992).

296. Laird, V. & Spiess, M. A novel assay to demonstrate an intersection of the exocytic and endocytic pathways at early endosomes. *Exp. Cell Res.* **260,** 340–345 (2000).

297. Yoshimori, T., Keller, P., Roth, M. G. & Simons, K. Different biosynthetic transport routes to the plasma membrane in BHK and CHO cells. *J. Cell Biol.* **133,** 247–256 (1996).

298. Müsch, A., Xu, H., Shields, D. & Rodriguez-Boulan, E. Transport of vesicular stomatitis virus G protein to the cell surface is signal mediated in polarized and nonpolarized cells. *J. Cell Biol.* **133,** 543–558 (1996).

299. Stoops, E. H. & Caplan, M. J. Trafficking to the Apical and Basolateral Membranes in Polarized Epithelial Cells. *J. Am. Soc. Nephrol.* **25,** 1375–1386 (2014).

300. D'Souza-Schorey, C. & Chavrier, P. ARF proteins: roles in membrane traffic and beyond. *Nat. Rev. Mol. Cell Biol.* **7,** 347–358 (2006).

301. Christis, C. & Munro, S. The small G protein Arl1 directs the trans-Golgi–specific targeting of the Arf1 exchange factors BIG1 and BIG2. *J. Cell Biol.* **196,** 327–335 (2012).

302. Stamnes, M. A. & Rothman, J. E. The binding of AP-1 clathrin adaptor particles to Golgi membranes requires ADP-ribosylation factor, a small GTP-binding protein. *Cell* **73,** 999–1005 (1993).

303. Traub, L. M., Ostrom, J. A. & Kornfeld, S. Biochemical dissection of AP-1 recruitment onto Golgi membranes. *J. Cell Biol.* **123,** 561–573 (1993).

304. Wang, Y. J. *et al.* Phosphatidylinositol 4 phosphate regulates targeting of clathrin adaptor AP-1 complexes to the Golgi. *Cell* **114,** 299–310 (2003).

305. Collins, B. M., Watson, P. J. & Owen, D. J. The structure of the GGA1-GAT domain reveals the molecular basis for ARF binding and membrane association of GGAs. *Dev. Cell* **4,** 321–332 (2003).

306. Shiba, T. *et al.* Molecular mechanism of membrane recruitment of GGA by ARF in lysosomal protein transport. *Nat. Struct. Biol.* **10,** 386–393 (2003).

307. Hunziker, W., Harter, C., Matter, K. & Mellman, I. Basolateral sorting in MDCK cells requires a distinct cytoplasmic domain determinant. *Cell* **66,** 907–920 (1991).

308. Chen, W. J., Goldstein, J. L. & Brown, M. S. NPXY, a sequence often found in cytoplasmic tails, is required for coated pit-mediated internalization of the low density lipoprotein receptor. *J. Biol. Chem.* **265,** 3116–3123 (1990).

309. Hunziker, W. & Fumey, C. A di-leucine motif mediates endocytosis and basolateral sorting of macrophage IgG Fc receptors in MDCK cells. *EMBO J.* **13,** 2963–2969 (1994).

310. Deora, A. A. *et al.* The Basolateral Targeting Signal of CD147 (EMMPRIN) Consists of a Single Leucine and Is Not Recognized by Retinal Pigment Epithelium. *Mol. Biol. Cell* **15,** 4148–4165 (2004).

311. Kibbey, R. G., Rizo, J., Gierasch, L. M. & Anderson, R. G. W. The LDL Receptor Clustering Motif Interacts with the Clathrin Terminal Domain in a Reverse Turn Conformation. *J. Cell Biol.* **142,** 59–67 (1998).

312. Gonzalez, A. & Rodriguez-Boulan, E. Clathrin and AP1B: Key roles in basolateral trafficking through trans-endosomal routes. *FEBS Lett.* **583,** 3784–3795 (2009).

313. Lisanti, M. P., Caras, I. W., Davitz, M. A. & Rodriguez-Boulan, E. A glycophospholipid membrane anchor acts as an apical targeting signal in polarized epithelial cells. *J. Cell Biol.* **109,** 2145–2156 (1989).

314. Lisanti, M. P., Sargiacomo, M., Graeve, L., Saltiel, A. R. & Rodriguez-Boulan, E. Polarized apical distribution of glycosyl-phosphatidylinositol-anchored proteins in a renal epithelial cell line. *Proc. Natl. Acad. Sci. U. S. A.* **85,** 9557–9561 (1988).

315. Scheiffele, P., Peränen, J. & Simons, K. N-glycans as apical sorting signals in epithelial cells. *Nature* **378,** 96–98 (1995).

316. Alfalah, M. *et al.* O-linked glycans mediate apical sorting of human intestinal sucrase-isomaltase through association with lipid rafts. *Curr. Biol. CB* **9,** 593–596 (1999).

317. Gut, A. *et al.* Carbohydrate-mediated Golgi to cell surface transport and apical targeting of membrane proteins. *EMBO J.* **17,** 1919–1929 (1998).

318. Fiedler, K. & Simons, K. The role of N-glycans in the secretory pathway. *Cell* **81,** 309–312 (1995).

319. Matter, K. & Mellman, I. Mechanisms of cell polarity: sorting and transport in epithelial cells. *Curr. Opin. Cell Biol.* **6,** 545–554 (1994).

320. Duncan, M. C. & Payne, G. S. ENTH/ANTH domains expand to the Golgi. *Trends Cell Biol.* **13,** 211–215 (2003).

321. Legendre-Guillemin, V., Wasiak, S., Hussain, N. K., Angers, A. & McPherson, P. S. ENTH/ANTH proteins and clathrin-mediated membrane budding. *J. Cell Sci.* **117,** 9–18 (2004).

322. Habermann, B. The BAR-domain family of proteins: a case of bending and binding? *EMBO Rep.* **5,** 250–255 (2004).

323. McMahon, H. T. & Gallop, J. L. Membrane curvature and mechanisms of dynamic cell membrane remodelling. *Nature* **438,** 590–596 (2005).

324. Edeling, M. A., Smith, C. & Owen, D. Life of a clathrin coat: insights from clathrin and AP structures. *Nat. Rev. Mol. Cell Biol.* **7,** 32–44 (2006).

325. Tsujita, K. *et al.* Coordination between the actin cytoskeleton and membrane deformation by a novel membrane tubulation domain of PCH proteins is involved in endocytosis. *J Cell Biol* **172,** 269–279 (2006).

326. Cao, H. *et al.* Actin and Arf1-dependent recruitment of a cortactin-dynamin complex to the Golgi regulates post-Golgi transport. *Nat. Cell Biol.* **7,** 483–492 (2005).

327. Hinshaw, J. E. Dynamin and its role in membrane fission. *Annu. Rev. Cell Dev. Biol.* **16,** 483–519 (2000).

328. Danino, D., Moon, K.-H. & Hinshaw, J. E. Rapid constriction of lipid bilayers by the mechanochemical enzyme dynamin. *J. Struct. Biol.* **147,** 259–267 (2004).

329. Ungewickell, E. *et al.* Role of auxilin in uncoating clathrin-coated vesicles. *Nature* **378,** 632–635 (1995).

330. Schlossman, D. M., Schmid, S. L., Braell, W. A. & Rothman, J. E. An enzyme that removes clathrin coats: purification of an uncoating ATPase. *J. Cell Biol.* **99,** 723–733 (1984).

331. U-2 OS ATCC ® HTB-96™ Homo sapiens bone osteosarcoma. Available at: https://www.lgcstandards-atcc.org/products/all/HTB-96.aspx?geo_country=de. (Accessed: 10th May 2017)

332. Maier, B. *et al.* A large-scale functional RNAi screen reveals a role for CK2 in the mammalian circadian clock. *Genes Dev.* **23,** 708–718 (2009).

333. Zhang, E. E. *et al.* A Genome-Wide RNAi Screen for Modifiers of the Circadian Clock in Human Cells. *Cell* **139,** 199–210 (2009).

334. 293 [HEK-293] ATCC® CRL-1573™. Available at: https://www.lgcstandards-atcc.org/Products/All/CRL-1573.aspx. (Accessed: 10th May 2017)

335. 293T ATCC® CRL-3216™. Available at: https://www.lgcstandards-atcc.org/Products/All/CRL-3216.aspx. (Accessed: 10th May 2017)

336. Ong, Y. S., Tang, B. L., Loo, L. S. & Hong, W. p125A exists as part of the mammalian Sec13/Sec31 COPII subcomplex to facilitate ER-Golgi transport. *J. Cell Biol.* **190,** 331–345 (2010).

337. Manolea, F., Claude, A., Chun, J., Rosas, J. & Melançon, P. Distinct Functions for Arf Guanine Nucleotide Exchange Factors at the Golgi Complex: GBF1 and BIGs Are Required for Assembly and Maintenance of the Golgi Stack and trans-Golgi Network, Respectively. *Mol. Biol. Cell* **19,** 523–535 (2008).

338. Hansen, M. D. *et al.* Hepatitis C virus triggers Golgi fragmentation and autophagy through the immunity-related GTPase M. *Proc. Natl. Acad. Sci.* **114,** E3462–E3471 (2017).

339. Luo, W., Wang, Y. & Reiser, G. p24A, a type I transmembrane protein, controls ARF1-dependent resensitization of protease-activated receptor-2 by influence on receptor trafficking. *J. Biol. Chem.* **282,** 30246–30255 (2007).

340. Ivanov, A. I. Pharmacological inhibitors of exocytosis and endocytosis: novel bullets for old targets. *Methods Mol. Biol. Clifton NJ* **1174,** 3–18 (2014).

341. Gaynor, E. C., Graham, T. R. & Emr, S. D. COPI in ER/Golgi and intra-Golgi transport: do yeast COPI mutants point the way? *Biochim. Biophys. Acta BBA - Mol. Cell Res.* **1404,** 33–51 (1998).

342. Tsai, Y. C. & Weissman, A. M. The Unfolded Protein Response, Degradation from the Endoplasmic Reticulum, and Cancer. *Genes Cancer* **1,** 764–778 (2010).

343. Vasudevan, C. *et al.* The distribution and translocation of the G protein ADP-ribosylation factor 1 in live cells is determined by its GTPase activity. *J. Cell Sci.* **111,** 1277–1285 (1998).

344. Dascher, C. & Balch, W. E. Dominant inhibitory mutants of ARF1 block endoplasmic reticulum to Golgi transport and trigger disassembly of the Golgi apparatus. *J. Biol. Chem.* **269,** 1437–1448 (1994).

345. Jackson, L. P. *et al.* Molecular basis for recognition of dilysine trafficking motifs by COPI. *Dev. Cell* **23,** 1255–1262 (2012).

346. Popoff, V., Adolf, F., Brügger, B. & Wieland, F. COPI Budding within the Golgi Stack. *Cold Spring Harb. Perspect. Biol.* **3,** (2011).

347. Blum, R. & Lepier, A. The Luminal Domain of p23 (Tmp21) Plays a Critical Role in p23 Cell Surface Trafficking. *Traffic* **9,** 1530–1550 (2008).

348. Ron, D. & Walter, P. Signal integration in the endoplasmic reticulum unfolded protein response. *Nat. Rev. Mol. Cell Biol.* **8,** 519–529 (2007).

349. de Galarreta, M. R. *et al.* Unfolded protein response induced by Brefeldin A increases collagen type I levels in hepatic stellate cells through an IRE1α, p38 MAPK and Smad-dependent pathway. *Biochim. Biophys. Acta BBA - Mol. Cell Res.* **1863,** 2115–2123 (2016).

350. Samali, A., FitzGerald, U., Deegan, S. & Gupta, S. Methods for Monitoring Endoplasmic Reticulum Stress and the Unfolded Protein Response. *International Journal of Cell Biology* (2010). doi:10.1155/2010/830307

351. O'Neill, J. S. & Hastings, M. H. Increased Coherence of Circadian Rhythms in Mature Fibroblast Cultures. *J. Biol. Rhythms* **23,** 483–488 (2008).

352. Cochran, B. H. Regulation of immediate early gene expression. *NIDA Res. Monogr.* **125,** 3–24 (1993).

353. Chen, Z. *et al.* Identification of diverse modulators of central and peripheral circadian clocks by high-throughput chemical screening. *Proc. Natl. Acad. Sci. U. S. A.* **109,** 101–106 (2012).

354. Hirota, T. *et al.* Identification of small molecule activators of cryptochrome. *Science* **337,** 1094–1097 (2012).

355. Bromley-Brits, K. & Song, W. The role of TMP21 in trafficking and amyloid-β precursor protein (APP) processing in Alzheimer's disease. *Curr. Alzheimer Res.* **9,** 411–424 (2012).

356. St George-Hyslop, P. & Fraser, P. E. Assembly of the presenilin γ-/ε-secretase complex. *J. Neurochem.* **120 Suppl 1,** 84–88 (2012).

357. Xu, X., Gao, H., Qin, J., He, L. & Liu, W. TMP21 modulates cell growth in papillary thyroid cancer cells by inducing autophagy through activation of the AMPK/mTOR pathway. *Int. J. Clin. Exp. Pathol.* **8,** 10824–10831 (2015).

358. Debler, E. W. *et al.* A fence-like coat for the nuclear pore membrane. *Mol. Cell* **32,** 815–826 (2008).

359. Townley, A. K. *et al.* Efficient coupling of Sec23-Sec24 to Sec13-Sec31 drives COPII-dependent collagen secretion and is essential for normal craniofacial development. *J. Cell Sci.* **121,** 3025–3034 (2008).

360. Moreira, T. G. *et al.* Sec13 Regulates Expression of Specific Immune Factors Involved in Inflammation In Vivo. *Sci. Rep.* **5,** 17655 (2015).

361. Pan, H. *et al.* A Novel Small Molecule Regulator of Guanine Nucleotide Exchange Activity of the ADP-ribosylation Factor and Golgi Membrane Trafficking. *J. Biol. Chem.* **283,** 31087–31096 (2008).

362. Sáenz, J. B. *et al.* Golgicide A reveals essential roles for GBF1 in Golgi assembly and function. *Nat. Chem. Biol.* **5,** 157–165 (2009).

363. Citterio, C. *et al.* Unfolded protein response and cell death after depletion of brefeldin A-inhibited guanine nucleotide-exchange protein GBF1. *Proc. Natl. Acad. Sci. U. S. A.* **105,** 2877–2882 (2008).

364. Blum, R. *et al.* Intracellular localization and in vivo trafficking of p24A and p23. *J. Cell Sci.* **112,** 537–548 (1999).

365. Denzel, A. *et al.* The p24 family member p23 is required for early embryonic development. *Curr. Biol.* **10,** 55–58 (2000).

366. Gong, P. *et al.* Transgenic neuronal overexpression reveals that stringently regulated p23 expression is critical for coordinated movement in mice. *Mol. Neurodegener.* **6,** 87 (2011).

367. Rojo, M. *et al.* The transmembrane protein p23 contributes to the organization of the Golgi apparatus. *J. Cell Sci.* **113 (Pt 6),** 1043–1057 (2000).

368. Springer, S. *et al.* The p24 proteins are not essential for vesicular transport in Saccharomyces cerevisiae. *Proc. Natl. Acad. Sci.* **97,** 4034–4039 (2000).

369. Lee, M. H. *et al.* ADP-ribosylation factor 1 of Arabidopsis plays a critical role in intracellular trafficking and maintenance of endoplasmic reticulum morphology in Arabidopsis. *Plant Physiol.* **129,** 1507–1520 (2002).

370. Contreras, I., Ortiz-Zapater, E. & Aniento, F. Sorting signals in the cytosolic tail of membrane proteins involved in the interaction with plant ARF1 and coatomer. *Plant J. Cell Mol. Biol.* **38,** 685–698 (2004).

371. Contreras, I., Yang, Y., Robinson, D. G. & Aniento, F. Sorting signals in the cytosolic tail of plant p24 proteins involved in the interaction with the COPII coat. *Plant Cell Physiol.* **45,** 1779–1786 (2004).

372. Anantharaman, V. & Aravind, L. The GOLD domain, a novel protein module involved in Golgi function and secretion. *Genome Biol.* **3,** research0023 (2002).

373. Emery, G., Rojo, M. & Gruenberg, J. Coupled transport of p24 family members. *J. Cell Sci.* **113 (Pt 13),** 2507–2516 (2000).

374. Montesinos, J. C. *et al.* Coupled transport of Arabidopsis p24 proteins at the ER-Golgi interface. *J. Exp. Bot.* **63,** 4243–4261 (2012).

375. Cross, B. C. S. *et al.* Eeyarestatin I inhibits Sec61-mediated protein translocation at the endoplasmic reticulum. *J. Cell Sci.* **122,** 4393–4400 (2009).

376. Brown, W. J., Plutner, H., Drecktrah, D., Judson, B. L. & Balch, W. E. The lysophospholipid acyltransferase antagonist CI-976 inhibits a late step in COPII vesicle budding. *Traffic Cph. Den.* **9,** 786–797 (2008).

377. Krämer, A. *et al.* Small molecules intercept Notch signaling and the early secretory pathway. *Nat. Chem. Biol.* **9,** 731–738 (2013).

378. Boal, F. *et al.* LG186: An inhibitor of GBF1 function that causes Golgi disassembly in human and canine cells. *Traffic Cph. Den.* **11,** 1537–1551 (2010).

379. Feng, Y. *et al.* Exo1: a new chemical inhibitor of the exocytic pathway. *Proc. Natl. Acad. Sci. U. S. A.* **100,** 6469–6474 (2003).

380. Viaud, J. *et al.* Structure-based discovery of an inhibitor of Arf activation by Sec7 domains through targeting of protein-protein complexes. *Proc. Natl. Acad. Sci. U. S. A.* **104,** 10370–10375 (2007).

381. Fujiwara, T., Oda, K., Yokota, S., Takatsuki, A. & Ikehara, Y. Brefeldin A causes disassembly of the Golgi complex and accumulation of secretory proteins in the endoplasmic reticulum. *J. Biol. Chem.* **263,** 18545–18552 (1988).

382. von Kleist, L. *et al.* Role of the clathrin terminal domain in regulating coated pit dynamics revealed by small molecule inhibition. *Cell* **146,** 471–484 (2011).

383. Macia, E. *et al.* Dynasore, a cell-permeable inhibitor of dynamin. *Dev. Cell* **10,** 839–850 (2006).

384. Quan, A. *et al.* Myristyl trimethyl ammonium bromide and octadecyl trimethyl ammonium bromide are surface-active small molecule dynamin inhibitors that block endocytosis mediated by dynamin I or dynamin II. *Mol. Pharmacol.* **72,** 1425–1439 (2007).

385. Friesland, A. *et al.* Small molecule targeting Cdc42-intersectin interaction disrupts Golgi organization and suppresses cell motility. *Proc. Natl. Acad. Sci. U. S. A.* **110,** 1261–1266 (2013).

386. Cerny, J. *et al.* The small chemical vacuolin-1 inhibits Ca(2+)-dependent lysosomal exocytosis but not cell resealing. *EMBO Rep.* **5,** 883–888 (2004).

387. Nieland, T. J. F. *et al.* Chemical genetic screening identifies sulfonamides that raise organellar pH and interfere with membrane traffic. *Traffic Cph. Den.* **5,** 478–492 (2004).

388. Trajkovic, K. *et al.* Ceramide triggers budding of exosome vesicles into multivesicular endosomes. *Science* **319,** 1244–1247 (2008).

389. Duncan, M. C., Ho, D. G., Huang, J., Jung, M. E. & Payne, G. S. Composite synthetic lethal identification of membrane traffic inhibitors. *Proc. Natl. Acad. Sci. U. S. A.* **104,** 6235–6240 (2007).

390. Tkacz, J. S. & Lampen, O. Tunicamycin inhibition of polyisoprenyl N-acetylglucosaminyl pyrophosphate formation in calf-liver microsomes. *Biochem. Biophys. Res. Commun.* **65,** 248–257 (1975).

391. Pan, Y. T. *et al.* Castanospermine inhibits the processing of the oligosaccharide portion of the influenza viral hemagglutinin. *Biochemistry (Mosc.)* **22,** 3975–3984 (1983).

392. Saunier, B., Kilker, R. D., Tkacz, J. S., Quaroni, A. & Herscovics, A. Inhibition of N-linked complex oligosaccharide formation by 1-deoxynojirimycin, an inhibitor of processing glucosidases. *J. Biol. Chem.* **257,** 14155–14161 (1982).

393. Fuhrmann, U., Bause, E., Legler, G. & Ploegh, H. Novel mannosidase inhibitor blocking conversion of high mannose to complex oligosaccharides. *Nature* **307,** 755–758 (1984).

394. Tulsiani, D. R., Harris, T. M. & Touster, O. Swainsonine inhibits the biosynthesis of complex glycoproteins by inhibition of Golgi mannosidase II. *J. Biol. Chem.* **257,** 7936–7939 (1982).

395. Bieberich, E. Synthesis, processing, and function of N-glycans in N-glycoproteins. *Adv. Neurobiol.* **9,** 47–70 (2014).

396. Hammond, C., Braakman, I. & Helenius, A. Role of N-linked oligosaccharide recognition, glucose trimming, and calnexin in glycoprotein folding and quality control. *Proc. Natl. Acad. Sci. U. S. A.* **91,** 913–917 (1994).

397. Shende, V. R., Kim, S.-M., Neuendorff, N. & Earnest, D. J. MicroRNAs function as cis- and trans-acting modulators of peripheral circadian clocks. *FEBS Lett.* **588,** 3015–3022 (2014).

398. Kilman, V. L., Zhang, L., Meissner, R.-A., Burg, E. & Allada, R. Perturbing Dynamin Reveals Potent Effects on the Drosophila Circadian Clock. *PLoS ONE* **4,** (2009).

399. Deery, M. J. *et al.* Proteomic Analysis Reveals the Role of Synaptic Vesicle Cycling in Sustaining the Suprachiasmatic Circadian Clock. *Curr. Biol.* **19,** 2031–2036 (2009).

400. Ettlinger, C., Schindler, J. & Lehle, L. Cell-cycle arrest of plant suspension cultures by tunicamycin. *Planta* **168,** 101–105 (1986).

401. Wang, H. *et al.* Tunicamycin-induced unfolded protein response in the developing mouse brain. *Toxicol. Appl. Pharmacol.* **283,** 157–167 (2015).

402. Masri, S., Cervantes, M. & Sassone-Corsi, P. The circadian clock and cell cycle: interconnected biological circuits. *Curr. Opin. Cell Biol.* **25,** 730–734 (2013).

403. Bu, Y. & Diehl, J. A. Abstract A01: ER stress disrupts circadian rhythms via miR-211. *Cancer Res.* **76,** A01–A01 (2016).

404. Pluquet, O., Dejeans, N. & Chevet, E. Watching the clock: endoplasmic reticulum-mediated control of circadian rhythms in cancer. *Ann. Med.* **46,** 233–243 (2014).

405. Kano, F., Sako, Y., Tagaya, M., Yanagida, T. & Murata, M. Reconstitution of Brefeldin A–induced Golgi Tubulation and Fusion with the Endoplasmic Reticulum in Semi-Intact Chinese Hamster Ovary Cells. *Mol. Biol. Cell* **11,** 3073–3087 (2000).

406. Sciaky, N. *et al.* Golgi Tubule Traffic and the Effects of Brefeldin A Visualized in Living Cells. *J. Cell Biol.* **139,** 1137–1155 (1997).

407. Belden, W. J. & Barlowe, C. Deletion of yeast p24 genes activates the unfolded protein response. *Mol. Biol. Cell* **12,** 957–969 (2001).

408. Pastor-Cantizano, N., Bernat-Silvestre, C., Marcote, M. J. & Aniento, F. Loss of Arabidopsis p24 function affects ERD2 traffic and Golgi structure and activates the unfolded protein response. *J Cell Sci* jcs.203802 (2017). doi:10.1242/jcs.203802

409. Kokame, K., Kato, H. & Miyata, T. Identification of ERSE-II, a New cis-Acting Element Responsible for the ATF6-dependent Mammalian Unfolded Protein Response. *J. Biol. Chem.* **276,** 9199–9205 (2001).

410. van Huizen, R., Martindale, J. L., Gorospe, M. & Holbrook, N. J. P58IPK, a novel endoplasmic reticulum stress-inducible protein and potential negative regulator of eIF2alpha signaling. *J. Biol. Chem.* **278,** 15558–15564 (2003).

411. Yan, W. *et al.* Control of PERK eIF2alpha kinase activity by the endoplasmic reticulum stress-induced molecular chaperone P58IPK. *Proc. Natl. Acad. Sci. U. S. A.* **99,** 15920–15925 (2002).

412. Ma, Y. & Hendershot, L. M. Herp Is Dually Regulated by Both the Endoplasmic Reticulum Stress-specific Branch of the Unfolded Protein Response and a Branch That Is Shared with Other Cellular Stress Pathways. *J. Biol. Chem.* **279,** 13792–13799 (2004).

413. Wang, X. Z. *et al.* Signals from the stressed endoplasmic reticulum induce C/EBP-homologous protein (CHOP/GADD153). *Mol. Cell. Biol.* **16,** 4273–4280 (1996).

414. Wang, X. Z. & Ron, D. Stress-induced phosphorylation and activation of the transcription factor CHOP (GADD153) by p38 MAP Kinase. *Science* **272,** 1347–1349 (1996).

415. Welsh, D. K., Yoo, S.-H., Liu, A. C., Takahashi, J. S. & Kay, S. A. Bioluminescence imaging of individual fibroblasts reveals persistent, independently phased circadian rhythms of clock gene expression. *Curr. Biol. CB* **14,** 2289–2295 (2004).

416. Balsalobre, A., Damiola, F. & Schibler, U. A serum shock induces circadian gene expression in mammalian tissue culture cells. *Cell* **93,** 929–937 (1998).

417. Maywood, E. S., Chesham, J. E., O'Brien, J. A. & Hastings, M. H. A diversity of paracrine signals sustains molecular circadian cycling in suprachiasmatic nucleus circuits. *Proc. Natl. Acad. Sci. U. S. A.* **108,** 14306–14311 (2011).

418. Relógio, A. *et al.* Ras-Mediated Deregulation of the Circadian Clock in Cancer. *PLoS Genet.* **10,** (2014).

419. Spörl, F. *et al.* A circadian clock in HaCaT keratinocytes. *J. Invest. Dermatol.* **131,** 338–348 (2011).

420. Kiessling, S. *et al.* Enhancing circadian clock function in cancer cells inhibits tumor growth. *BMC Biol.* **15,** 13 (2017).

421. Brown, S. A. *et al.* The period length of fibroblast circadian gene expression varies widely among human individuals. *PLoS Biol.* **3,** e338 (2005).

422. Pagani, L. *et al.* Serum factors in older individuals change cellular clock properties. *Proc. Natl. Acad. Sci. U. S. A.* **108,** 7218–7223 (2011).

423. Keller, M. *et al.* A circadian clock in macrophages controls inflammatory immune responses. *Proc. Natl. Acad. Sci. U. S. A.* **106,** 21407–21412 (2009).

424. Jinek, M. *et al.* A programmable dual-RNA-guided DNA endonuclease in adaptive bacterial immunity. *Science* **337,** 816–821 (2012).

425. Korge, S., Grudziecki, A. & Kramer, A. Highly Efficient Genome Editing via CRISPR/Cas9 to Create Clock Gene Knockout Cells. *J. Biol. Rhythms* **30,** 389–395 (2015).

426. Jerome-Majewska, L. A., Achkar, T., Luo, L., Lupu, F. & Lacy, E. The Trafficking Protein Tmed2/p24β1 Is Required For Morphogenesis of the Mouse Embryo and Placenta. *Dev. Biol.* **341,** 154–166 (2010).

427. Samali, A., Fitzgerald, U., Deegan, S. & Gupta, S. Methods for monitoring endoplasmic reticulum stress and the unfolded protein response. *Int. J. Cell Biol.* **2010,** 830307 (2010).

428. Schibler, U. *et al.* Clock-Talk: Interactions between Central and Peripheral Circadian Oscillators in Mammals. *Cold Spring Harb. Symp. Quant. Biol.* **80,** 223–232 (2015).

Appendix

Supplemental figures

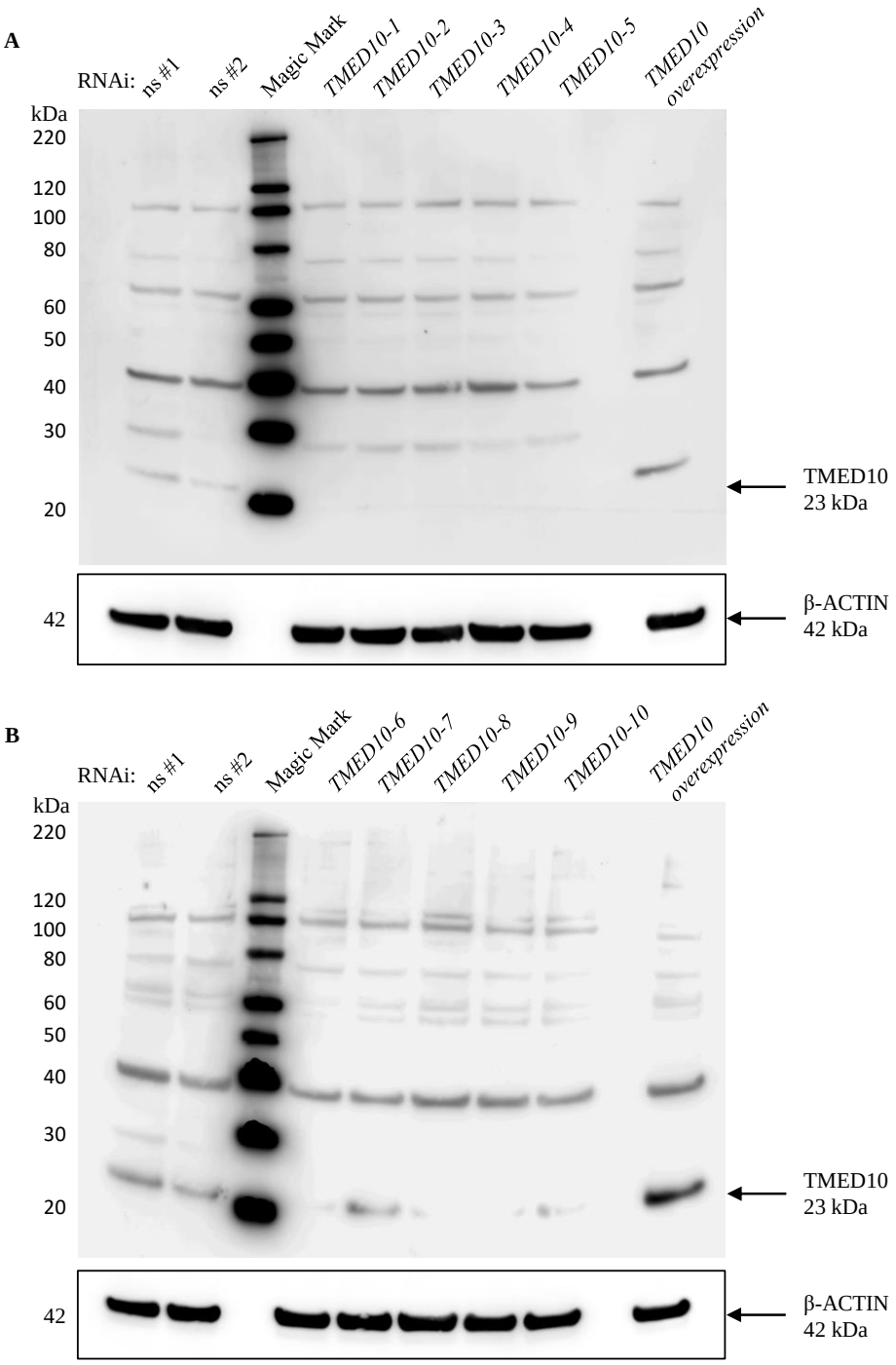

Supplemental Figure A 1: **RNAi-mediated knockdown of *TMED10* transcripts led to reduced protein levels in U-2 OS cells**. U-2 OS cells harbouring a *Bmal1*-promotor driven *luciferase* (BLH) reporter construct were transduced with either non-silencing control plasmids, RNAi knockdown plasmids targeting *TMED10* or *TMED10*-overexpression plasmids. Three days after transduction, cellular proteins were purified, run on a SDS-PAGE, and western blot was carried out. **A and C)** Depicted are TMED10 protein levels upon *TMED10* depletion or overexpression and the corresponding β-actin loading controls.

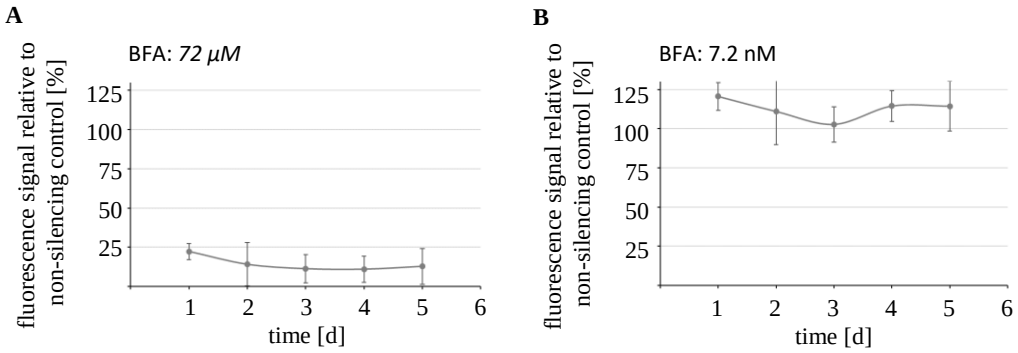

Supplemental Figure A 2: Application of 72 µM Brefeldin A but not of 7.2 nM Brefeldin A leads to cell death in U-2 OS cells. In five individual 96-well plates, U-2 OS cells harbouring a *Bmal1*-promotor driven *luciferase* reporter construct were exposed to A) 72µM or B) 7.2 nM Brefeldin A. After synchronisation with dexamethasone, cells were treated as cells prepared for bioluminescence recordings. Every 24 hours the cell culture medium of one plate was supplemented with 10 % Resazurin and incubated for four hours before the fluorescence signal was measured. Depicted are the fluorescence values relative to the untreated control cells of each individual plate (n = 1 individual recordings with 4 biological replicates).

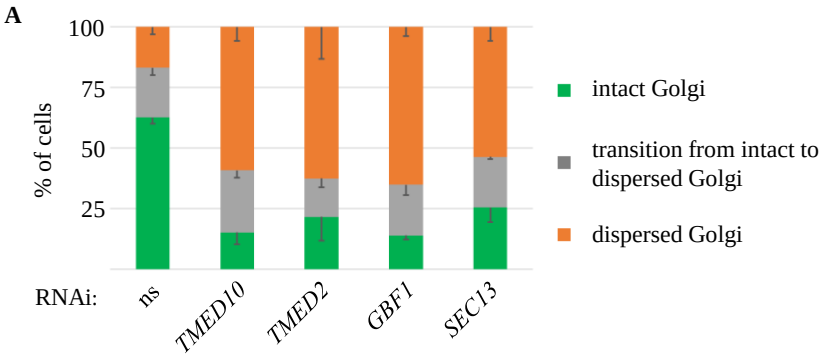

Supplemental Figure A 3: RNAi mediated knockdown of Golgi-associated genes disrupts Golgi integrity. U-2 OS cells harbouring a *Bmal1*-promotor driven *luciferase* reporter construct were lentivirally transduced with a non-silencing control plasmid or RNAi constructs targeting *TMED10*, *TMED2*, *GBF1* or *SEC13*. After selection, cells were stained with Hoechst solution and antibodies against GM130, labelling the nucleus and the Golgi, respectively. Fluorescence microscopy was used to analyse Golgi morphology. At least 40 cells per condition were imaged. Six people were asked to discriminate between the three different Golgi states: intact, transition from intact to dispersed and dispersed. **A)** Shown are the mean percentage of cells with Golgi morphology scored as intact (green), transition from intact to dispersed (grey) and dispersed (orange). (one experiment with 40-80 cells per condition, Golgi morphology scoring by six individuals with scientific background, mean ± SEM)

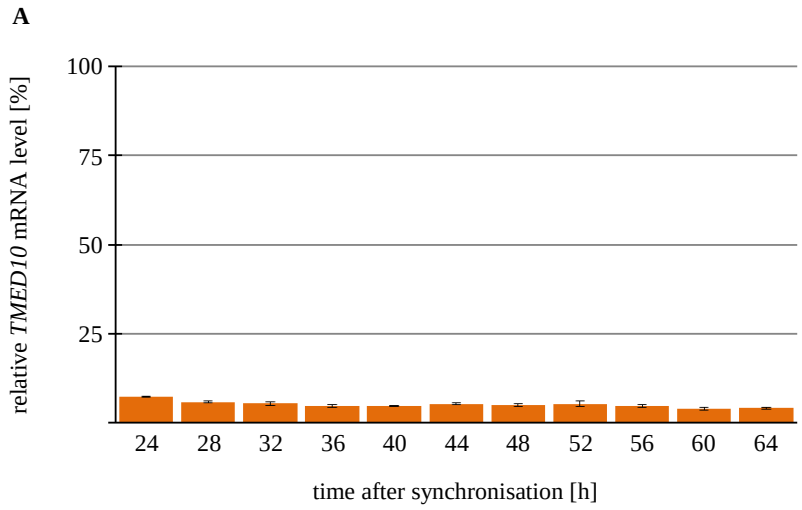

Supplemental Figure A 4: RNAi-mediated reduction of *TMED10* expression levels is consistent over 40 hours. U-2 OS cells harbouring a *Bmal1*-promotor driven *luciferase* reporter construct were transduced a non-silencing control construct or with an shRNA construct targeting *TMED10*. 24 hours after synchronization with dexamethasone cells were harvested in four-hour intervals over 40 hours and total RNA was extracted. **A**) Depicted are the *TMED10* expression levels relative to the corresponding non-silencing samples assessed through qRT-PCR. (n = 3 dishes per time point and condition, mean ± SD)

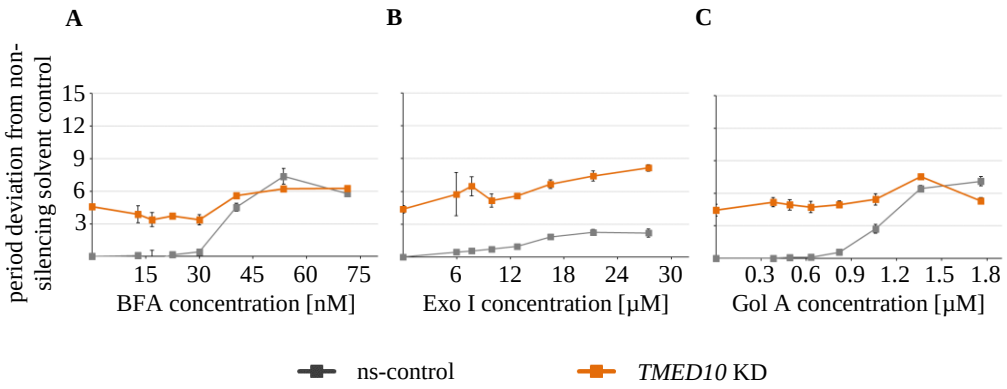

Supplemental Figure A 5: Transport inhibitor Exo I but not GolA and BFA show additive period lengthening on top of the RNAi phenotype. U-2 OS cells harbouring a *Bmal1*-promotor driven *luciferase* reporter construct were transduced with either a non-silencing control plasmid or an RNAi construct targeting *TMED10*. After synchronisation with dexamethasone the cells were treated with the solvent or increasing concentrations of transport inhibitor **A)** BFA, **B)** Exo I or **C)** Gol A and bioluminescence was measured for seven days. The data were fitted to sine waves using chronostar2.0 and the depicted period deviation from ns solvent treated control was calculated (representative dataset, 4-6 biological replicates, mean ± SD).

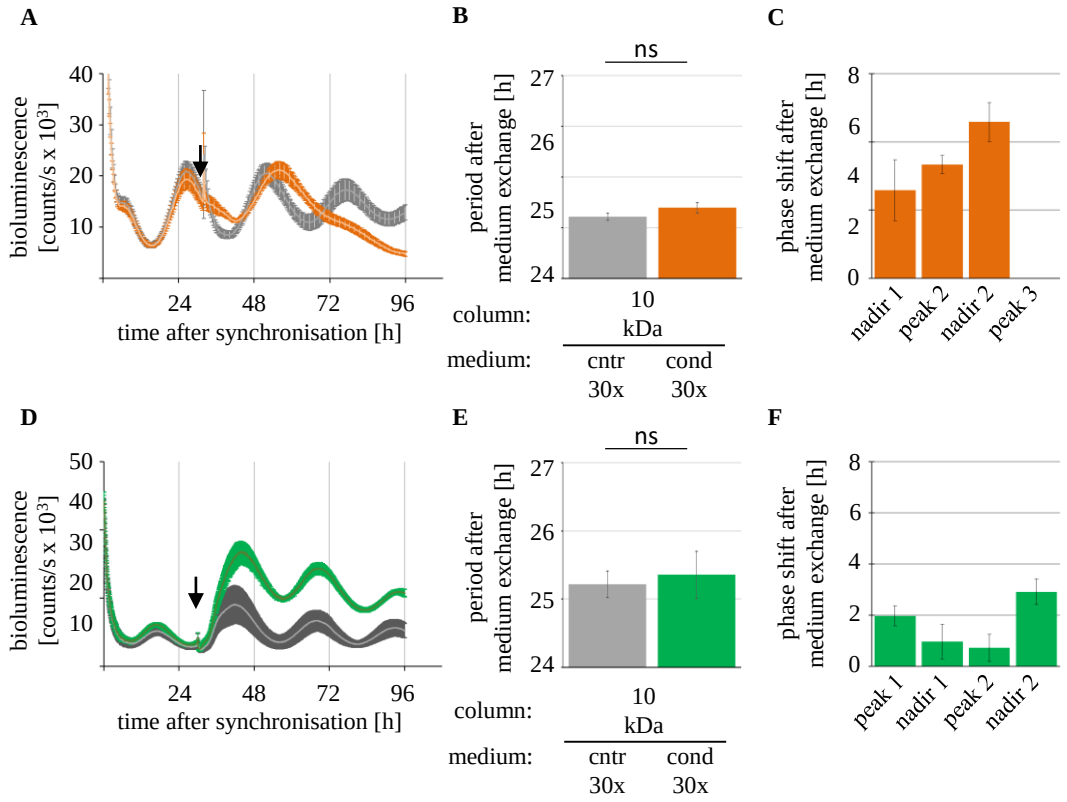

Supplemental Figure A 6: Conditioned medium induces a phase shift in synchronized U-2 OS cells. U-2 OS cells harbouring a (**A-C**) full-length *Per2*-promotor driven *luciferase* reporter construct or a (**D-F)** *Bmal*1-promotor driven *luciferase* reporter construct were synchronized with dexamethasone and bioluminescence was recorded. Four to six hours after the expression of full-length *Per2*-promotor driven *luciferase* peaked, the cell culture medium was exchanged to either 30-fold concentrated control medium (grey) or 30-fold concentrated conditioned medium (orange and green) from U-2 OS wild-type cells. **A and D)** Depicted are representative mean bioluminescence data before and after medium exchange with the standard deviation as a shaded area around the curve. **B and E)** The bioluminescence data after medium exchanged was fitted to sine waves and the circadian parameters were calculated using chronostar2.0. Shown are the circadian periods after medium exchange which did not significantly differ between control medium and conditioned medium treated cells (Student's T-Test: $p = 0.07$ and $p = 0.51$). **C and F)** The peaks and nadirs in the bioluminescence data of control medium and conditioned medium treated cells were analysed and the apparent phase shift was calculated for the first two peaks and nadirs. (additional dataset; individual recordings with 3-4 biological replicates; mean ± SD; Student's T-Test: * $p < 0.05$; ns: non-significant)

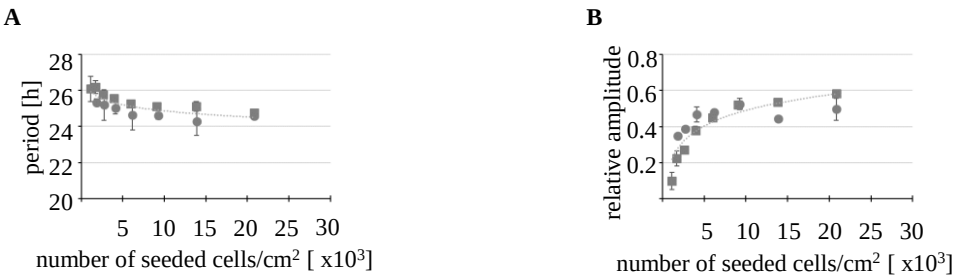

Supplemental Figure A 7: Circadian oscillations show a longer period and a smaller amplitude with decreasing cell density. U-2 OS cells harbouring a *Bmal1*-promotor driven *luciferase* reporter construct were seeded in 9.6 cm^2 cell culture dishes in cell densities ranging from 26.042 down to 667 cells per cm^2, synchronized with dexamethasone and bioluminescence was recorded for six days in serum free medium. Bioluminescence data were fitted to sine waves using chronostar2.0 and the circadian parameters were assessed. **A)** Shown are the calculated circadian periods [h] **(B)** and the relative amplitudes**.** (additional dataset; 2 biological replicates, mean ± variance)

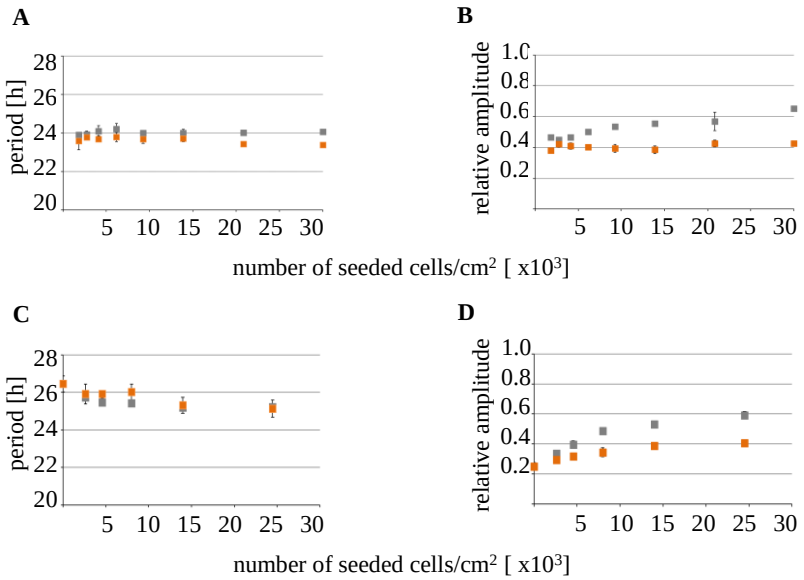

Supplemental Figure A 8: U-2 OS non-bioluminescent feeder cells with unimpaired vesicular protein transport rescued the reduced circadian amplitude of low-density cultures. 4.630 U-2 OS cells/cm^2 harbouring a *Bmal1*-promotor driven *luciferase* reporter construct were seeded in 9.6 cm^2 cell culture dishes with decreasing numbers of non-bioluminescent U-2 OS wild-type feeder cells that were either harbouring a non-silencing RNAi construct (grey) or a shRNA construct targeting *TMED10* (orange). Cells were synchronized with dexamethasone, bioluminescence was recorded for six days in serum free medium, and bioluminescence data were fitted to sine waves, using chronostar2.0. **A and C)** Shown are the calculated circadian periods [h] and **B and D)** relative amplitudes (two additional experiments with 2-3 biological replicates, mean ± SD).

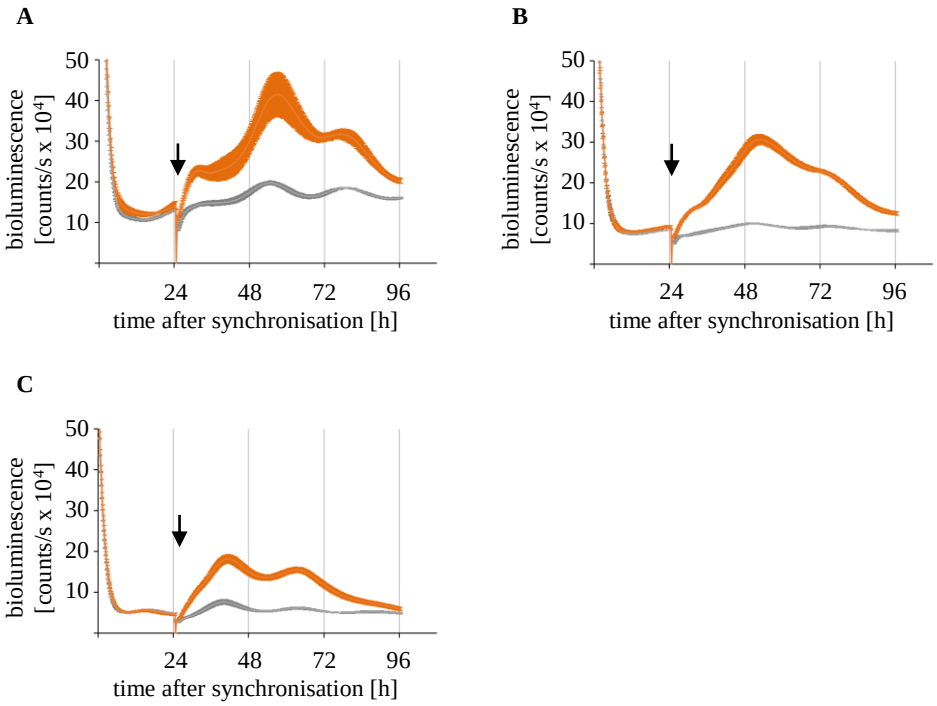

Supplemental Figure A 9: Conditioned medium induces rhythmic transcription of D-Box-, E-Box-, and RRE-driven luciferase. U-2 OS cells were transduced with either (**A**) D-Box-, (**B**) E-Box-, or (**C**) RRE-driven *luciferase* reporter plasmids. After 24 hours of bioluminescence recording when the minimum reporter activity was reached medium was exchanged to 30-fold concentrated control or conditioned medium from U-2 OS wild-type cells. Depicted are mean bioluminescence recordings of transduced and stimulated U-2 OS cells. Time of medium exchange is indicated by the grey arrowhead (n = 1 individual recording with 3-4 biological replicates; mean ± SD)

Vector maps

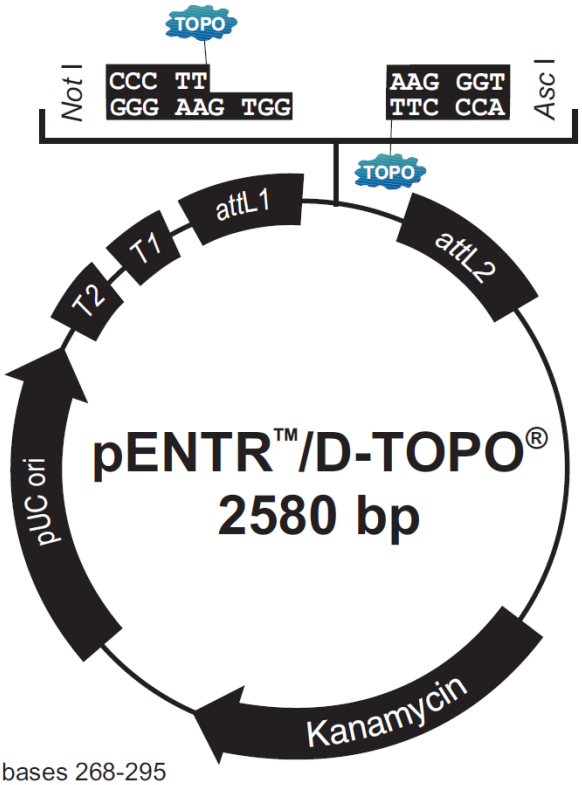

Comments for pENTR™/D-TOPO®
2580 nucleotides

*rrn*B T2 transcription termination sequence: bases 268-295
*rrn*B T1 transcription termination sequence: bases 427-470
M13 forward (-20) priming site: bases 537-552
*att*L1: bases 569-668 (c)
TOPO® recognition site 1: bases 680-684
Overhang: bases 685-688
TOPO® recognition site 2: bases 689-693
*att*L2: bases 705-804
T7 Promoter/priming site: bases 821-840 (c)
M13 reverse priming site: bases 845-861
Kanamycin resistance gene: bases 974-1783
pUC origin: bases 1904-2577

(c) = complementary sequence

Supplemental Figure B 1: Vector map pENTR/D-TOPO

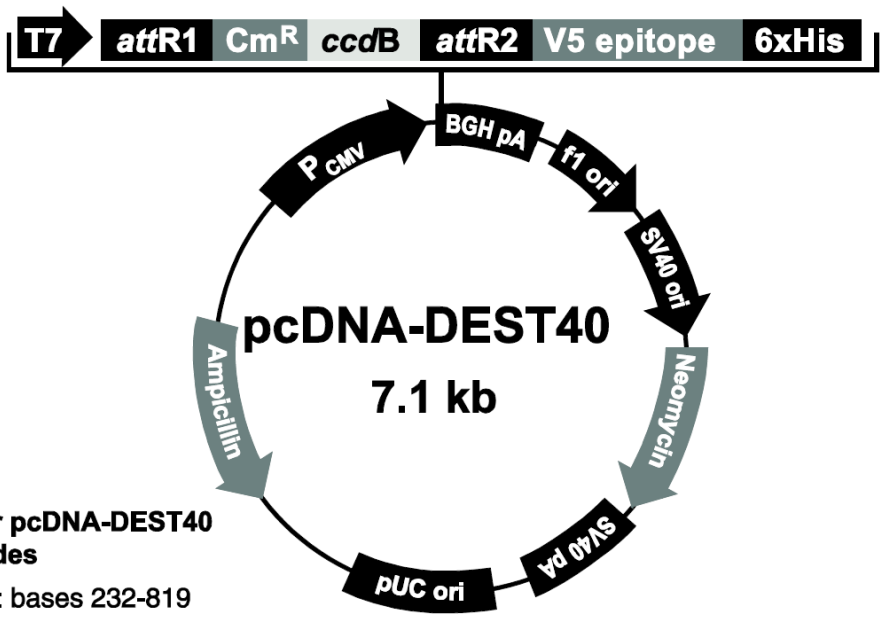

Comments for pcDNA-DEST40
7143 nucleotides

CMV promoter: bases 232-819
T7 promoter: bases 863-882
*att*R1 recombination site: bases 911-1035
Chloramphenicol resistance gene: bases 1144-1803
*ccd*B gene: bases 2145-2450
*att*R2 recombination site: bases 2491-2615
V5 epitope: bases 2641-2682
6xHis tag: bases 2692-2709
BGH polyadenylation region: bases 2735-2962
f1 origin: bases 3008-3436
SV40 early promoter and origin: bases 3463-3771
Neomycin resistance ORF: bases 3846-4640
SV40 early polyadenylation region: bases 4816-4946
pUC origin: bases 5329-6002
Ampicillin (*bla*) resistance ORF: bases 6147-7007 (complementary strand)
bla promoter: bases 7008-7106 (complementary strand)

Supplemental Figure B 2: Vector map pcDNA-Dest40

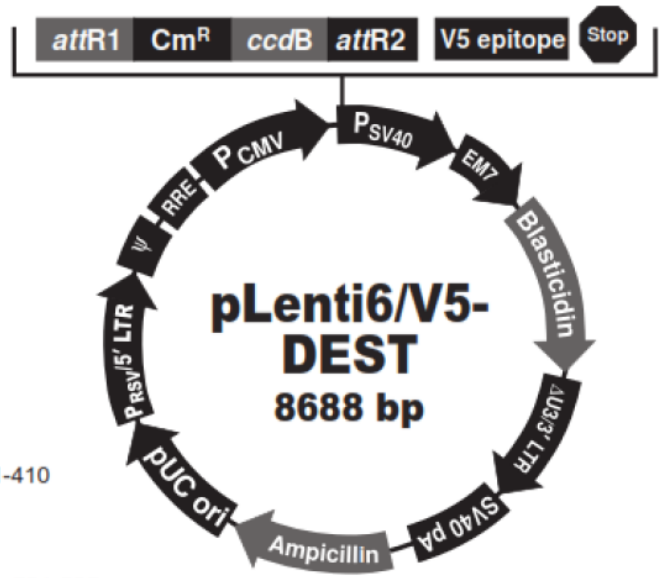

Comments for pLenti6/V5-DEST
8688 nucleotides

RSV/5′ LTR hybrid promoter: bases 1-410
RSV promoter: bases 1-229
HIV-1 5′ LTR: bases 230-410
5′ splice donor: base 520
HIV-1 psi (ψ) packaging signal: bases 521-565
HIV-1 Rev response element (RRE): bases 1075-1308
3′ splice acceptor: base 1656
3′ splice acceptor: base 1684
CMV promoter: bases 1809-2392
*att*R1 site: bases 2440-2564
Chloramphenicol resistance gene (Cm^R): bases 2673-3332
*ccd*B gene: bases 3674-3979
*att*R2 site: bases 4020-4144
V5 epitope: bases 4197-4238
SV40 early promoter and origin: bases 4293-4602
EM7 promoter: bases 4657-4723
Blasticidin resistance gene: bases 4724-5122
ΔU3/3′ LTR: bases 5208-5442
ΔU3: bases 5208-5261
3′ LTR: bases 5262-5442
SV40 polyadenylation signal: bases 5514-5645
bla promoter: bases 6504-6602
Ampicillin (*bla*) resistance gene: bases 6603-7463
pUC origin: bases 7608-8281

Supplemental Figure B 3: Vector map pLenti6/V5-Dest

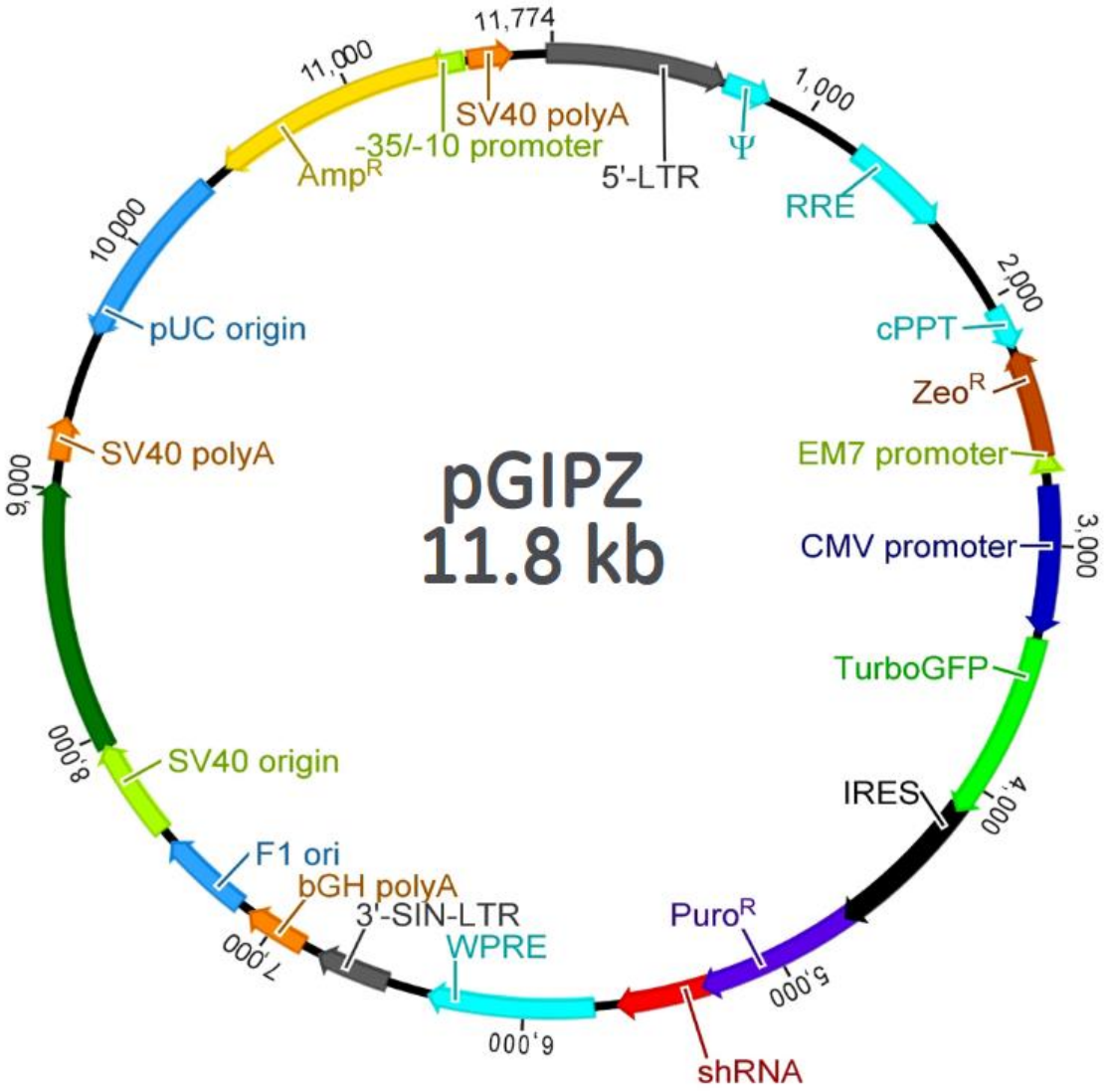

Supplemental Figure B 4: Vector map pGIPZ

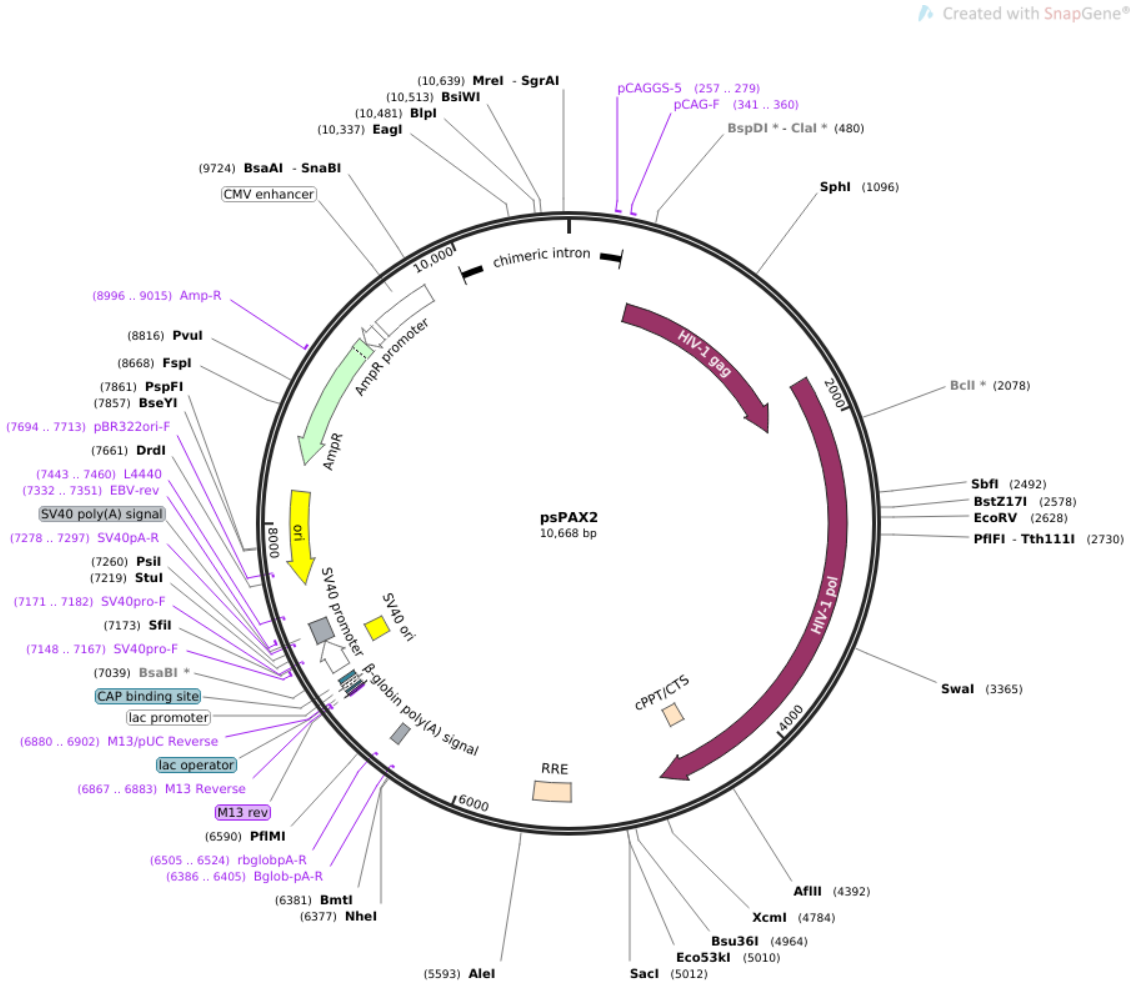

Supplemental Figure B 5: Vector map psPax

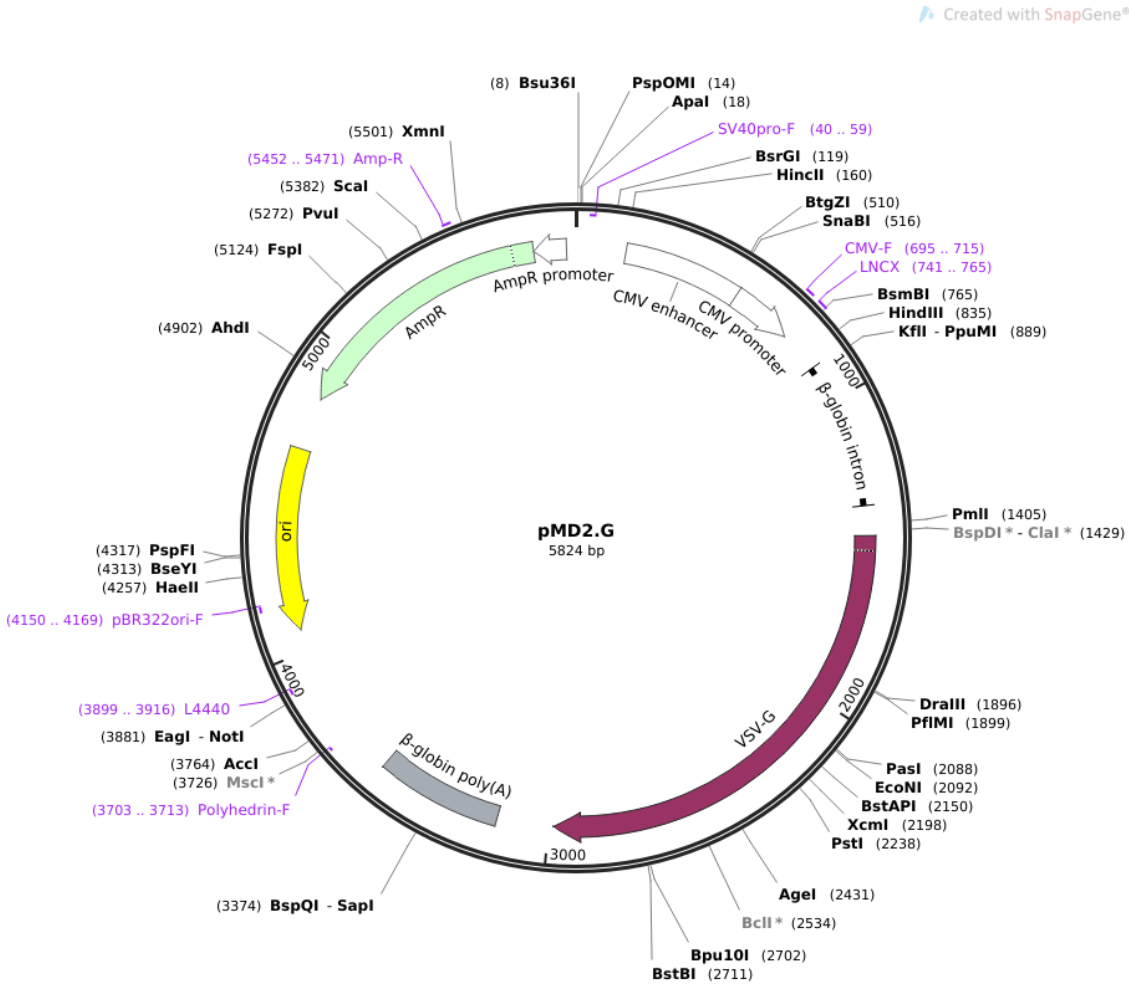

Supplemental Figure B 6: Vector map pMD2.G

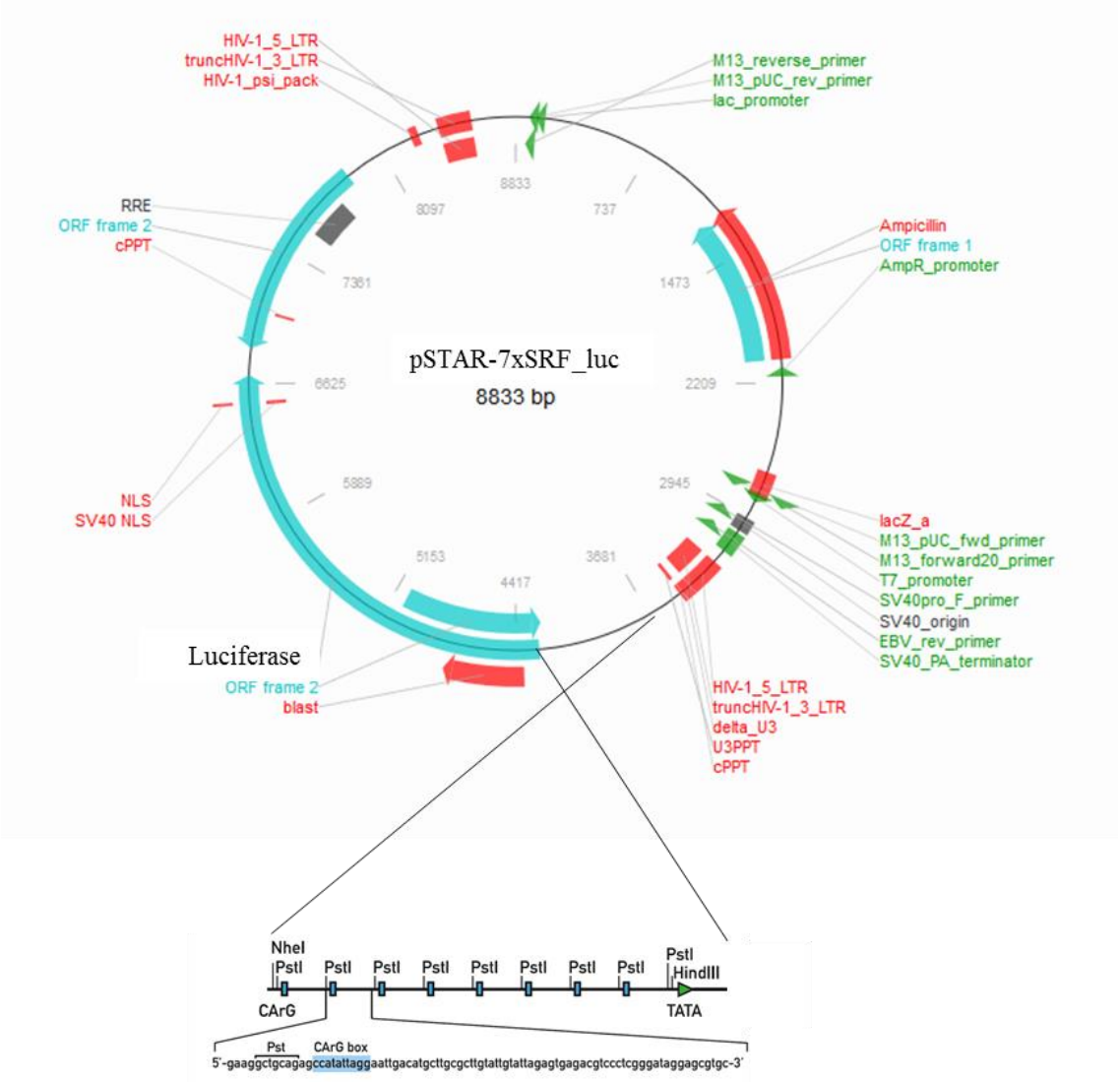

Supplemental Figure B 7: Vector map pSTAR-7xSRF_luc

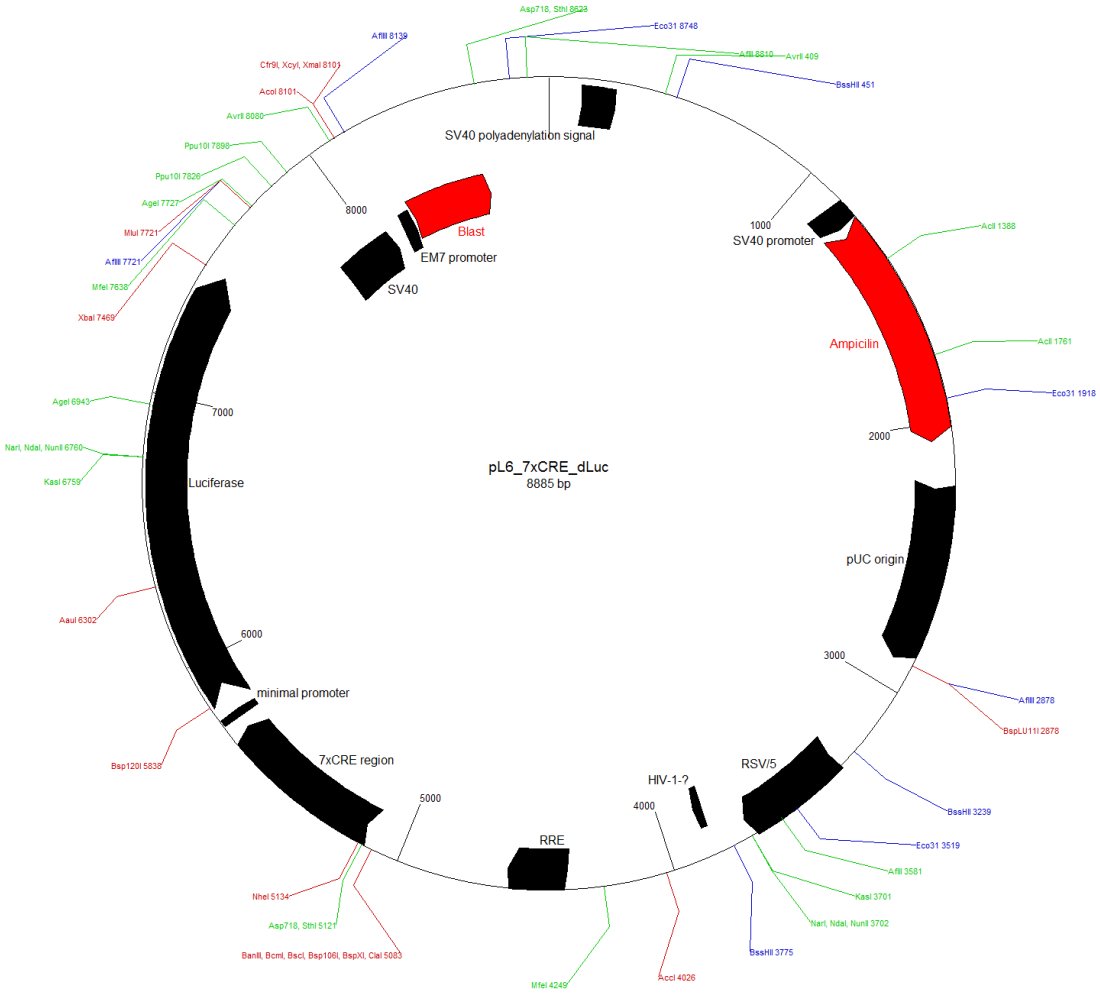

Supplemental Figure B 8: Vector map pLenti6-7xCRE_luc

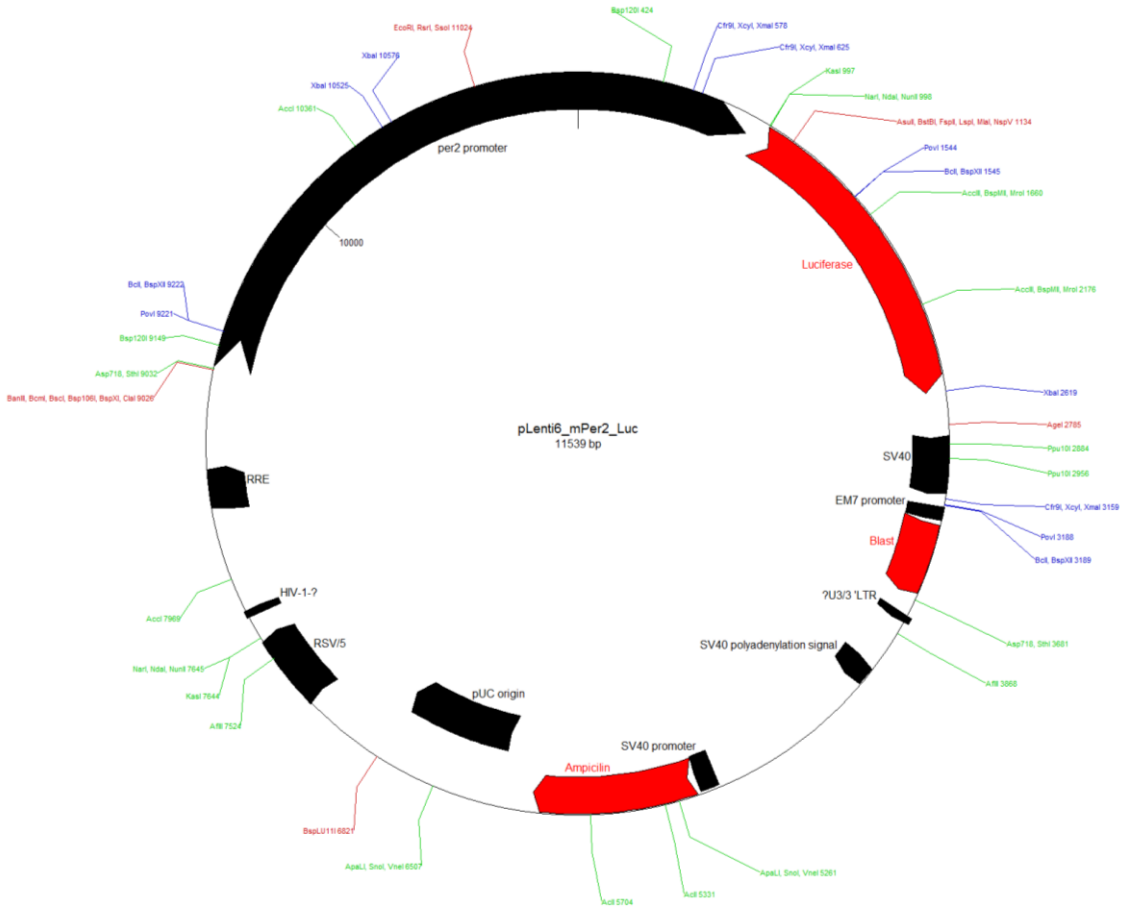

Supplemental Figure B 9: Vector map pLenti6-full-length mPer2_luc

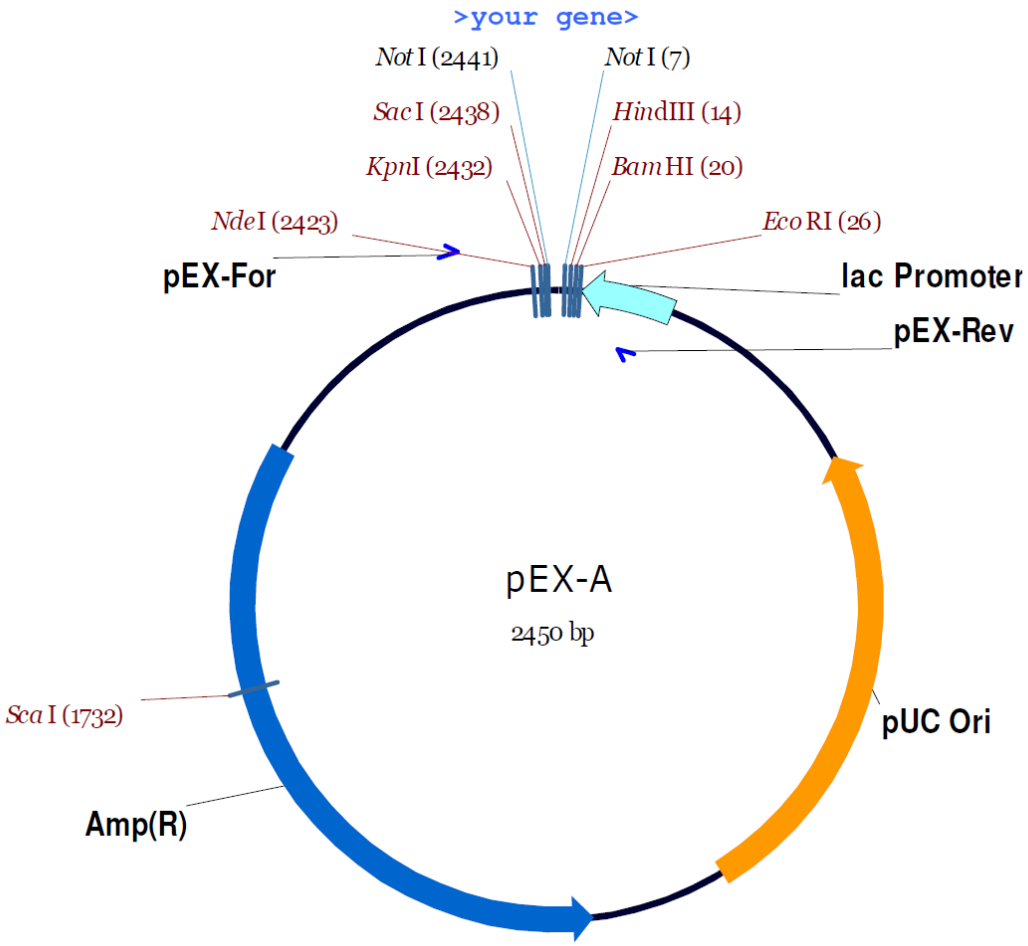

Supplemental Figure B 10: Vector map pEX-A

SOP Lentivirus production

Standard Operating Procedure
Lentivirus Production

Day 0

Seed HEK293T cells

Trypsinize an almost confluent 175cm^2 cell culture flask with HEK293T cells (culture time < 6 weeks) with Trypsin/EDTA (BIOCHROM AG #L2143) for ~5 min at 37 °C.
Seed 3 (7) 175 cm^2 (75 cm^2) flasks with HEK293T cells in equal parts in 25 ml (12.5 ml) culture media each.

Day 1

Transfection of HEK293T cells with packaging plasmid and lentiviral vector

Replace culture media of cells to be transfected.
Prepare one 1.5 ml eppendorf tube per transfection (flask): (A) Add 17.5 µg (8.4 µg) of your lentiviral expression plasmid, 12.5 µg (6 µg) psPAX and 7.5 µg (3.6 µg) pMD2G plasmid. Adjust volume to 1095 µl (526 µl) of plasmids with supplied H_2O (CalPhos™-Kit, BD-Biosciences™, #631312). Add 155 µl (74 µl) of supplied 2M Calcium solution.
Prepare one 15ml tube per transfection: (B) Ad 1250 µl (600 µl) 2xHBS (supplied with kit).
Mix both by carefully vortexing solution B while adding drop wise solution A. Incubate the transfection solution for 20 min at RT. Add 2.5 ml (1.2 ml) of each transfection solution to one 175 cm^2 (75 cm^2) flask. Incubate over night at cell culture conditions.

Day 2, morning

Replace Culture Media

Replace culture media of HEK293T cells (from day 1). Handle with care because cells only loosely stick to the plastic.

Day 3, afternoon

Harvest lentiviral supernatant I

Pour supernatant into 50 ml tube and let stand on ice over night. Refill flask with 25 ml (12.5 ml) culture media.

Day 4, morning

Harvest lentiviral supernatant II

Pour supernatant into corresponding 50 ml tube of day 3 and spin tube at 4100 x g for 15 min to remove cell debris. Pass supernatant through an 0.45 µm filter (SARSTEDT, # 83.1826).
Supernatant might either be used directly or frozen down to -80°C in working aliquots.

Laboratory of Chronobiology – Achim-Kramer Lab Version: 08.05.2009

Supplemental Figure C 1: SOP Lentivirus production

Abbreviations

°C	degree Celsius
µl	microliter
µM	micromolar
2D	two dimensional
3D	three dimensional
5HT	serotonergic tract
A	Alanine
ACTH	adrenocorticotropic hormone
Adv	adenovirus
AMP	adenosine monophosphate
amp	amplitude
amp	ampicillin
ANTH	AP180 N-terminal homology
AP	adapter protein
APP	amyloid precursor protein
APS	ammonium persulfate
aq	aqua
aqua dest.	aqua destillata
ARF1	ADP ribosylation factor 1
ArfGAP	ADP ribosylation factor GTPase activating protein
ASNA1	Arsenical pump-driving ATPase
ATCC	American Type Culture Collection
ATP	adenosine triphosphate
AVP	arginine vasopressin
BARS	BFA-induced ADP-ribosylation substrates
BB2	bombesin 2
BC	before Christ
BCA	bicinchoninic acid assay
BD	Becton Dickinson
beta-TRCP	beta-transducin repeat containing E3 ubiquitin protein ligase
BFA	Brefeldin A
BIG1/2	ADP ribosylation factor guanine nucleotide exchange factor 1/2
BiP	Binding immunoglobulin protein
BLH	*Bmal1-Luciferase-HygromycineB*
Bmal1	Brain and muscle aryl hydrocarbon receptor nuclear translocator-like protein 1
Bmal1_luc	*Bmal1*-promotor driven *luciferase*

bp	base pairs
C	Cysteine
calcein-AM	calcein-acetoxymethylester
cAMP	cyclic adenosine monophosphate
Cas9	CRISPR-associated 9
cDNA	complementary DNA
CDS	coding sequence
c-FOS	proto oncogene
CHOP	C/EBP homologous protein
CIP	calf intestinal alkaline phosphatase
CK	casein kinase
clock	circadian locomotor output cycles protein kaput
CM	complete medium
cntr	control
cps	counts per second
CO2	carbon dioxide
CO-IP	co-immuno precipitation
cond	conditioned
COPI	coat protein complex I
COPII	coat protein complex 2
cos	cosine
COS1	rat kidney fibroblast cell line, name derived from: CV-1 in Origin, carrying SV40;
CRE	cAMP response element
CREB	cAMP response element binding protein
CRH	corticotropin releasing hormone
CRISPR	Clustered Regularly Interspaced Short Palindromic Repeats
cry	cryptochrome
d	day
D	Aspartic acid
DNA	deoxyribonucleic acid
DAG	diacylglycerol
damp	damping
DAPI	4',6-diamidino-2-phenylindole
D-Box	enhancer element
DBP	D-box binding PAR BZIP transcription factor
ddH2O	double-distilled water
DEC1	Deleted in esophageal cancer 1
DMEM	Dulbecco's modified eagle's medium
DMSO	dimethyl sulfoxide
DNAJ3	DnaJ heat shock protein family (Hsp40) member C3
DNAse	deoxyribonuclease
dNTP	deoxyribose nucleoside triphosphate

DRN	dorsal raphe nucleus
DTT	Dithiothreitol
E	Glutamic acid
E. coli	*Escherichia coli*
E4BP4	nuclear factor, interleukin 3 regulated
E-Box	enhancer element
EDTA	Ethylenediaminetetraacetic acid
eGFP	enhanced green fluorescent protein
ENTH	Epsin N-terminal homology
ER	endoplasmic reticulum
ERAD	ER associated protein degradation
ERD2	KDEL endoplasmic reticulum protein retention receptor 1
ERES	ER exit site
ERGIC	ER-Golgi-intermediated compartment
ERK	Mitogen-cctivated protein kinase 1
et al.	and others
EtOH	ethanol
FBS	fetal bovine serum
FBXL	F-box and leucine rich repeat protein
F	Phenylalanine
FW	forward
g	gravity or gram
G	Glycine
GABA	gamma-aminobutyric acid
Gapdh	Glyceraldehyde 3-phosphate dehydrogenase
GBF1	Golgi-specific brefeldin A-resistance guanine nucleotide exchange factor 1
GDP	guanosine diphosphate
GEF	Guanine-nucleotide exchange factor
Get 1-3	Golgi to ER traffic protein 1
GFP	green fluorescent protein
GGA	Golgi-localising, γ-adaptin ear homology, ARF-bindning proteins
GHT	geniculohypothalamic tract
GIPZ	*GFP*-IRES-*Puromycin-Zeocin*
Glc	glucose
$GlcNAc_2$	N-acetylglucosamine
GmbH	Gesellschaft mit beschränkter Haftung
GolA	Golgicide A
GPI	glycosylphosphatidylinositol
GRP	gastrin releasing peptide
GRP78	Binding immunoglobulin protein
GTP	guanosine triphosphate

GTPase	guanosine triphosphate hydrolase
h	hour
H9c2	rat myoblast cell line
HaCat	human keratinocyte cell line
HBS	HEPES-buffered saline
HDEL	endoplasmic reticulum protein retention receptor 1
HEK293	human embryonic kidney cell line
HEK293T	human embryonic kidney cell line, stably expresses the SV40 large T antigen
HeLa	human cervical cancer cell line
HEPES	4-(2-hydroxyethyl)-1-piperazineethanesulfonic acid
HERPUD1	Homocysteine inducible ER protein with ubiquitin-like domain 1
HLF	HLF, PAR BZIP transcription factor
HPLC	high-performance liquid chromatography
HRP	horseradish peroxidase
HSC70	Heat shock protein family A (Hsp70) member 8
HSF1	Heat shock transcription factor 1
HTC-116	human colon cancer cell line
IC50	half maximal inhibitory concentration
IEG	immediate early genes
IETF	immediate early transcription factors
IgG	immunoglobulin G
ipRGC	intrinsically photosensitive retinal ganglion cells
IRE1	Endoplasmic reticulum to nucleus signaling 1
IRES	internal ribosome entry site
k	kilo
K	Lysine
Kar2	Binding immunoglobulin protein
kB	kilo bases
KD	knock-down
kDa	kilo Dalton
KDELR	KDEL endoplasmic reticulum protein retention receptor 1
Klf	Gut-enriched Krüppel-like factor
l	litre
L	Leucine
lat.	latin
LB	Luria-Bertani
LD	light/dark
LDLR	Low-density lipoprotein receptor
luc	*luciferase*
m	milli or meter
M	Mega or molar
Man	Mannose

MAPK	Mitogen-activated protein kinase 1
MDCK	canine kidney epithelial cell line
MeOH	methanol
miR	micro-RNA
ml	millilitre
MRN	median raphe nucleus
mRNA	messenger RNA
MRTF-beta	Myocardin-related transcription factor-B
n	number or nano
N	Asparagine
nM	nanomolar
nm	nanometre
nmol	nanomol
NPAS2	Neuronal PAS domain protein 2
NPC	nuclear pore complex
NR1D1	Nuclear receptor subfamily 1 group D member 1
ns	non-silencing or non-significant
OE	over-expression
oLD	ohne luminale domäne / without luminal domain
orf	open reading frame
OST	oligosaccharyltransferase complex
PA	phosphatic acid
PACAP	Pituitary adenylate cyclase-activating polypeptide
PAS	Per-Arnt-Sim
PBS	phosphate-buffered saline
PCR	polymerase chain reaction
per	period
Per2_luc	*Period2*-promotor driven *luciferase*
PER2::LUC	Fusion protein of PER2 and Luciferase
PEST	peptide sequence enriched in proline (P), glutamic acid (E), serine (S), and threonine
pH	potential of hydrogen
PI4P	phosphatidylinositol 4-monophosphat
PK2	Prokineticin 2
PLB	*Period-Luciferase-Blasticidin*
pM	pico molar
pmol	picomol
Pmts	Protein-O-mannosyltransferases
PVN-SCG	paraventricular nucleus superior cervical ganglia
Q	Glutamine
qPCR	quantitative polymerase chain reaction
qRT-PCR	real-time quantitative polymerase chain reaction
PAGE	polyacrylamide gel electrophoresis

RAS	Guanosine-nucleotide-binding protein, name derived from: Rat sarcoma
reverb	Nuclear receptor subfamily 1, group D, member 1
RHT	retinohypothalamic tract
RIDD	regulated IRE1-dependant decay
RIPA	radioimmunoprecipitation assay
RNA	ribonucleic acid
RNAi	RNA interference
ROR	RAR-related orphan receptors
RRE	ROR response elements
RT	reverse transcription
RV	reverse
S	Serine
SAR1	Secretion associated Ras related GTPase 1A
SCF	Skp, Cullin, F-box containing complex
SCN	suprachiasmatic nucleus
SD	standard deviation
SDS	Sodium dodecyl sulfate
SEC	SECretory protein
SEM	standard error of the mean
Ser	Serine
shRNA	short-hairpin RNA
siRNA	small interfering RNA
SNARE	Soluble N-ethylmaleimide-sensitive-factor attachment receptor
SOP	standard operating procedure
SRE	serum response element
SRF	serum response factor
SRP	signal recognition particle
SYBR-green	cyanine dye
t	time
t	temperature
T	Threonine
TBS	Tris-buffered saline
TEF	Thyrotroph embryonic factor
TEMED	Tetramethylethylenediamine
tGFP	turbo green fluorescent protein
TGN	trans-Golgi network
Thr	Threonine
TMED	Transmembrane p24 trafficking proteins
TRAM	translocating chain-associated membrane protein
TRC40	Transmembrane domain recognition complex 40 KDa ATPase
TTX	tetrodotoxin
U-2 OS	human osteosarcoma cell line

UGGT	UDP-glucose:glycoprotein glucosyltransferase
UPR	unfolded protein response
UTR	untranslated region
UV	ultra violet
V	Valine or volume
v/v	volume/volume
VIP	Vasoactive intestinal polypeptide
VPAC2	Vasoactive intestinal polypeptide receptor 2
VSVG	Vesicular stomatitis virus G protein
WT	wild-type
XBP1	X-box binding protein 1

Danksagung

An dieser Stelle möchte ich all jenen Menschen in meinem Leben meinen aufrichtigen Dank und meine tiefste Verbundenheit aussprechen, die mich durch die arbeitsintensive, schwere, traurige, lustige, manchmal auch verrückte, aber nie langweilige Phase der Promotion begleitet haben.

Ein besonderer Dank gilt hier Prof. Dr. Achim Kramer, der mir diese großartige Chance gab, meine Promotion in seiner Arbeitsgruppe anzufertigen. Die Chronobiologie ist mir in meinem Studium früh begegnet und mich seitdem nicht mehr losgelassen. Er schaffte es durch seine Begeisterung für die Chronobiologie dieses Interesse am Leben zu erhalten und mich stets auf wissenschaftlicher aber auch auf persönlicher Ebene zu fördern und zu fordern. Dabei stand er mir die vergangenen Jahre immer mit einem offenen Ohr zur Seite und ich bin Ihm mehr als dankbar für die vielen konstruktiven Gespräche, die intensive Betreuung, sein Verständnis für meine schwere Situation am Anfang der Schreibphase, seine Fähigkeit mich auch bei Schreibblockaden immer wieder zu motivieren und das Interesse an meiner Arbeit.

Prof. Dr. Florian Heyd möchte ich dafür danken, dass er sich auf meiner ersten internationalen Konferenz in Mitten der laufenden Poster-Präsentation dazu bereit erkläre, die Begutachtung meiner Doktorarbeit zu übernehmen und schon damals ehrliches Interesse an meiner Arbeit zeigte. Die Diskussionen und Anregungen, die wir in den letzten Jahren austauschten, habe ich mir sehr zu Herzen genommen. Darüber hinaus möchte ich mich noch einmal dafür bedanken, dass er es mir ermöglichte die Golgi-Färbungen in seinem Labor durchzuführen und zu analysieren. An dieser Stelle auch ein herzliches Dankeschön an Alexander Neumann, der mich dabei mir Rat und Tat unterstützte und mir mit seinem Wissensschatz eine großartige Hilfe war; sowie den restlichen Mitgliedern der Arbeitsgruppe Heyd, die mich mehr als freundlich in Empfang nahmen und mir hilfsbereit zur Seite standen, wenn ich im fremden Labor verloren wirkte.

Bei allen Mitgliedern der Arbeitsgruppe „Chronobiologie“ - sowohl bei den alten Hasen als auch den jungen Hüpfern und den ehemaligen Mitgliedern, die im Laufe der letzten 5 Jahre kamen und gingen - möchte ich mich herzlich für ihren Beistand, ihre Hilfe und ihre konstruktiven Diskussionen bedanken. Insbesondere die wunderbare Hilfe von Annette Hayungs in allen administrativen Belangen und sonstigen Lebenslagen sowie ihre kontinuierliche Versorgung der Arbeitsgruppe mit Keksen und Gummibärchen ist dabei besonders hervor zu heben. Vielen Dank auch an Bharath Ananthasubramaniam, Bert Maier, Nicole Wittenbrink, Silke Reischl und Thomas Wallach, die stets ein offenes Ohr auf dem Flur hatten, wenn man eine spontane Frage hatte, über Statistik plaudern wollte oder unter einer „ernsten“ Sinneskriese litt. Ute Abraham möchte ich meine tiefste Verbundenheit ausdrücken für ihre einzigartige Hilfe im Serum-Projekt und die vielen großen und kleinen Diskussionen über die Jahre. Ein großer Dank geht auch an das vorherige Semester an Doktoranden: Katja Schellenberg, Manjana Saleh, Jeannine Mazuch, Sabrina Klemz und Veronika Lang, die mich damals bei meiner Ankunft im Labor durch ihre alltägliche Hilfe sehr unterstützten. Zu guter Letzt möchte ich Anna

Finger meinen Dank aussprechen, die an diesem Projekt mit sehr viel Herzblut weiterarbeitet und tolle Ideen einbringt. Ich bin mir sicher, dass mein „Baby“ bei dir in guten Händen ist.

Bei Marja Kornhuber, Narges Molavi und Joanna Trzmiel möchte ich mich für ihre großartige Arbeit und ihre Begeisterung bedanken, mit der sie dieses Projekt unterstützten. Ihr ward die besten Praktikanten, die man sich wünschen kann!

Ein besonderer Dank gilt Astrid Grudziecki, Barabara Koller, Neta Tuvia und Sandra Korge. Sie waren nicht nur im Labor-Alltag eine große Hilfe und seelische Stütze (wenn mal wieder alles schieflief), sondern haben darüber hinaus auch mein privates Leben sehr bereichert. Ich bin sehr froh, euch kennen gelernt zu haben!

Auch möchte ich mich bei Lea Ehrhardt, Sandra Korge, Silke Reischl und Svenja Rosenberger bedanken, die mir mit Rat und Tat beim Verfassen dieser Arbeit zur Seite standen. Marco Fritz, es war klasse mit dir die verschiedenen juristischen Bibliotheken unsicher zu machen um in Ruhe und mit voller Motivation zu arbeiten!

Zu guter Letzt möchte ich all meinen Freunden und meiner Familie meinen tiefempfunden und herzlichen Dank aussprechen, die ihr mich auf meinem Weg begleitet habt. Karolina Woznicka, Johannes Fischer, Narmin Wielgosz, Sandra Korge und Tina May – ihr seid die Besten! Mama und Papa, Harald und Regine, und natürlich Martin, vielen Dank, dass ihr all die Jahre für mich da ward, mich immer unterstützt habe, mir geholfen habt und meine Entscheidungen immer bedingungslos akzeptiert habt. Euch allen widme ich diese Arbeit, in Liebe.

Statement of Authorship

I hereby declare that I am the sole author of this thesis with the title “The role of the secretory pathway for the mammalian circadian clock” and that I have not used any sources other than those listed in the bibliography and identified as references. I further declare that I have not submitted this thesis at any other institution in order to obtain a degree.

Berlin, 4th of October 2017	Sebastian Jäschke
(Place, Date)	(Name)